

**Investigation of the mechanism that underlies MS32
minisatellite instability in cells that use the Alternative
Lengthening of Telomeres pathway**

Thesis submitted for the degree of

Doctor of Philosophy at the University of Leicester

by

Clara Patrícia Lopes Novo

Department of Genetics, University of Leicester, September 2009

ABSTRACT

Cancer cells escape senescence by activating a telomere maintenance mechanism (TMM) to elongate telomeres and continue dividing. The most common TMM is the enzyme telomerase that adds telomeric repeats. However, some cancer cells activate the Alternative Lengthening of Telomeres (ALT), a recombination-based mechanism to extend shortened telomeres. One of the most peculiar features of ALT⁺ cells is the instability at the MS32 minisatellite (D1S8), especially as six other minisatellites remained stable in these cells. As MS32 instability correlates with activation of the ALT mechanism, it is likely that the underlying process depends, at least in part, on the same proteins. Thus, a better understanding of the molecular mechanism that underlies ALT may be gained through knowing how and why the MS32 minisatellite becomes unstable in ALT⁺ cells.

Several hypotheses that might explain MS32 instability in ALT⁺ cells were investigated. In this study it was shown that the instability is restricted to the minisatellite itself and no transcriptional or copy-number changes distinguish this region between ALT⁺ and non-ALT cells. Interestingly, changes in the DNA methylation-status adjacent to one end of the minisatellite were found, which might indicate that ALT⁺ cells have a different chromatin conformation around the MS32 minisatellite. Additionally, the mutant molecules arising at MS32 in ALT⁺ cells seem to derive from intra-allelic processes. Also, EXO1 expression was higher in ALT⁺ compared to ALT⁻ cells. Thus, our current model proposes that a protein (perhaps hEXO1) involved in lagging-strand synthesis and DNA repair is preferentially recruited to the telomeres in ALT⁺ cells and this may cause the accumulation of unprocessed 5' DNA flaps at MS32 during replication. Subsequent DNA repair at MS32, by error-prone processes, may underlie the instability seen in ALT⁺ cells.

ACKNOWLEDGMENTS

First of all, I have to thank the person without whom this thesis would have not been possible, my supervisor Dr. Nicola Royle. Thank you for your insightful discussions, knowledgeable input but especially for your support and enthusiasm that inspired me along when things were not working.

I also have to thank Dr. Tim Gant and his research group, whom patiently supervised me throughout the microarray procedure and analysis.

Another key person was Professor Sir Alec Jeffreys, whom shared valuable information about the MS32 minisatellite region and gave essential feedback for this project.

Finally, big thank you to Rita Neumann, the “PCR Queen” for always “guessing” the perfect PCR conditions and giving her time for problem-solving.

Many people contributed to make my PhD years such an enjoyable experience. Jennie Jeyapalan, my tutor and bay colleague, for teaching me so much, from the wonders of single-molecule PCR to laughing with and about science. Thank you Jenny, “We’ve seen the minisatellite!” Jenny Foxon, for always having a smile, a word and finding time to help with the most bureaucratic things. To Aaron, (sorry, Dr. Aaron now) and Jon, the “little-genious” thank you for your constant support and feedback but especially for making it so easy to work together. The telomere group rules! One of the best memories I will carry with me is the harmony of working in lab G19/G18. Everything is shared, from equipment and reagents to knowledge. Everyone carries a constant smile. Special people, great scientists, a community that I will miss and will always remember as what a “perfect lab” should be. To all G18/G19 members, thank you so much!

To my friends outside the lab, especially the Leicestersians Alfonso, Barbara, Carla, David, Ines, Koustov, Lenny, Luisa, Mattias and my old friends from home Andreia, Catarina, Claudia, Heini, Marisa, Mario, Marta, Susa, Veronica (we’ll always have Christmas!), thank you for keeping my sanity, for your constant enthusiasm and motivation.

To Ewan, it has been a pleasure doing this adventure side by side. Thank you for your patience, love and motivation and for not running away during the writing-up months.

Finally, I would like to thank my Papis and my Su. Without your support, love and motivation I could not have made it. Thank you for being always present, even if it was behind a camera or at the other end of the phone.

TABLE OF CONTENTS

Abstract.....	1
Aknowledgments	3
List of figures.....	7
List of tables.....	10
List of Abbreviations	11
1. Chapter 1: Introduction	1
1.1 Telomeres.....	1
1.1.1 Telomere structure	2
1.2 telomere function	3
1.2.1 Shelterin complex.....	3
1.2.2 Replication at telomeres	5
1.2.3 Telomeric Chromatin	7
1.3 Telomere maintenance mechanism	9
1.3.1 Telomerase	10
1.3.2 Alternative Lengthening of Telomere - ALT	12
1.3.3 Proteins and ALT	20
1.4 From yeast to humans	22
1.5 Minisatellites	24
1.5.1 Minisatellite structure.....	24
1.5.2 Minisatellite Biology.....	25
1.5.3 Minisatellite stability.....	27
1.5.4 From Yeast to humans	30
1.6 MS32 minisatellite	31
1.6.1 MS32 minisatellite structure	31
1.6.2 Region around MS32 minisatellite.....	32
1.6.3 MS32 mutation mechanism in germ-line	34
1.6.4 MS32 mutation mechanism in yeast	35
1.6.5 MS32 Minisatellite and ALT	36
1.7 Project aims.....	37
CHAPTER 2: Material and Methods	38
2.1 Materials.....	38
2.1.1 Chemicals and general reagents	38
2.1.2 Buffers and solutions.....	39

2.1.3 Oligonucleotides, enzymes and radiolabelled reagents.....	39
2.1.4 Cell-lines	39
2.2 Cell culture.....	40
2.2.1 conditions for culture of Cell-lines.....	40
2.2.2 Cell cloning.....	40
2.3 DNA and RNA extraction.....	41
2.3.1 DNA.....	41
2.3.2 RNA	42
2.4. DNA-restriction digestion.....	42
2.5 cDNA synthesis.....	43
2.6 Polymerase Chain Reaction (PCR)	43
2.6.1 Small-Pool and single-molecule PCR.....	46
2.6.2 Minisatellite Variant Repeat (MVR)-PCR.....	47
2.6.3 TCA reaction.....	48
2.6.4 qPCR.....	49
2.6.5 MLPA.....	50
2.7 Sequencing.....	51
2.7.1 Exo/SAP Cleaning	52
2.8 Agarose gel electrophoresis.....	52
2.8.1 Isolation of DNA from gel.....	52
2.8.2 2D-Gel electrophoresis.....	53
2.9 Southern blotting.....	53
2.9.1 probe labelling.....	54
2.9.2 Hybridisation and washing.....	55
2.10 Methylation-status analysis.....	56
2.11 Microarray.....	58
2.11.1 Array preparation	58
2.11.2 sample labelling with fluorescence probes.....	58
2.11.3 Hybridization.....	60
2.11.4 Array washing	60
2.12 Dot blotting.....	61
2.13.1 Probe labelling	61
3. CHAPTER 3:Genome instability in ALT-expressing cells	63
3.1 Background	63

3.2 Aims	65
3.3 Results.....	66
3.3.1 Extent of MS32 locus instability.....	66
3.3.2 Screen for other putative instable loci.....	72
3.4 Discussion	82
CHAPTER 4: Gene expression across the MS32 region	86
4.1 Background	86
4.1.1 Genes around MS32.....	86
4.2 AIMS.....	88
4.3 Results.....	89
4.3.1 GENE expression in ALT+ vs. Tel+ cells	89
4.3.2 Gene expression around MS32	99
4.3.3 Conclusion	119
4.4 Discussion	121
CHAPTER 5: MS32 instability and the ALT mechanism	127
5. 1 Background	127
5.2 Aims	129
5.3 Results.....	129
5.3.1 Mutation mechanism at MS32 in ALT+ cells.....	129
5.3.2 from yeast to humans – FEN1 analysis.....	141
5.3.3 MS32 extrachromosomal sequences	152
5.4 Discussion	170
CHAPTER 6:MS32 minisatellite loci in ALT+ vs. non-ALT cells.....	178
6.1 AIMS.....	178
6.2 Results.....	178
6.2.1 copy-number analysis.....	178
6.3.2 Methylation around MS32	202
6.4 Discussion	217
Chapter 7: Conclusion and future work	223
Appendices.....	231
Bibliography.....	239

LIST OF FIGURES

Figure 1.1: Telomere capping structure.....	3
Figure 1.2: Shelterin complex.....	4
Figure 1.3: Replication at telomeres.	6
Figure 1.4: Telomere length along time.....	10
Figure 1.5: Unequal sister-chromatic exchange at telomeres.	17
Figure 1.6: T-loop excision and extension by RTE	18
Figure 1.7: BIR-elongation of telomeres.	19
Figure 1.8: MS32 minisatellite structure.....	32
Figure 3.1: MSNID minisatellite locus.	66
Figure 3.2: Amplification of MSNID minisatellite by SP-PCR in ALT+ cell-lines.....	68
Figure 3.3:SP-PCR amplification of MSNID minisatellite in JFCF6T.IJ/11C (Tel+) and JFCF6T.IJ/11E (ALT+).	68
Figure 3.4: STR locus.	69
Figure 3.5: PCR amplification of STR.....	70
Figure 3.6: Amplification of STR by SP-PCR.....	71
Figure 3.7: Progenitor allele-sizes of MS32 minisatellite in the SUSM-1 clones.	77
Figure 3.8: DNA fingerprinting with 33.15 probe	78
Figure 3.9: DNA fingerprinting with 33.6 probe.	79
Figure 3.10: Aligment of MS32 sequence with DNA fingerprint probes.....	80
Table 1: Order of genes in the vicinity of MS32 minisatellite and their function.....	87
Figure 4.1: Amplification of IMAGE clone containing cDNA of genes from around MS32.....	92
Figure 4.2: Global LOWESS normalization.	94
Figure 4.3: Plot of the expression fold-changes of the Tel+ against the ALT+ cell-line.....	96
Figure 4.4: Global LOWESS normalization for the 2nd design.	97

Figure 4.5: Gene distribution around MS32.....	99
Figure 4.6: Scheme of the qPCR experiment.....	100
Figure 4.7: G3PDH expression and statistical analysis.....	104
Figure 4.8: ACTB expression and statistical analysis.....	105
Figure 4.9: TBP expression and statistical analysis.	106
Figure 4.10: Diagram representing NID1 gene.....	107
Figure 4.11: Validation of NID1 qPCR amplification.	108
Figure 4.12: NID1 expression levels.....	109
Figure 4.13: LYST diagram.	111
Figure 4.14: Validation of LYST qPCR amplification.	111
Figure 4.15: LYST expression levels.....	112
Figure 4.16: GPR173B diagram.....	114
Figure 4.17: Validation of GPR137B qPCR.....	114
Figure 4.18: GPR137B expression.....	115
Figure 4.19: Diagram of pseudogene ACO2.....	118
Figure 5.1: Determination of the size of progenitor MS32 alleles in SUSM1 clones.....	131
Figure 5.2: Identification of SUMS1 clones with highest MS32 mutation frequency.....	133
Figure 5.3: Methodology used for mutant identification and analysis.....	136
Figure 5.4: Size distribution of mutants and breakpoints for mutational events in each allele.....	137
Figure 5.5: Alignment of MS32 length mutants with progenitor alleles.....	138
Figure 5.6: Schematic representation of hFEN1 gene.....	143
Figure 5.7: hFEN1 qPCR assay optimization.	143
Figure 5.8: hFEN1 expression analysis in ALT+ and non-ALT cell-lines.	144
Figure 5.9: Schematic representation of hEXO1 gene.....	149
Figure 5.10: hExo1 qPCR assay optimization.	150
Figure 5.11: hEXO1 expression analysis.	151

Figure 5.12: Scheme of the migration pattern of DNA structures in 2D-gels.....	154
Figure 5.13: Optimization of 2D-gel electrophoresis.....	155
Figure 5.14: Telomeric DNA in SUSM1 cell-line.....	156
Figure 5.16: Variant telomeric repeat detection in circular DNA.....	Error! Bookmark not defined.
Figure 5.15: Detection of telomeric variants in extrachromosomal circular DNA in ALT+ cells..	158
Figure 5.17: T-circle origin model.....	160
Figure 5.18: MS32 detection by 2D-gel.....	162
Figure 5.19: Optimixzation of T-circle amplification by TCA.....	164
Figure 5.22: TCA-input sensitivity	167
Figure 5.20: Amplification of extrachromosomal circular DNA by TCA.....	168
Figure 5.21: TCA efficiency and sensitivity	169
Figure 5.22: Model for the three types of MS32 mutations identified.....	174
Figure 6.1: Diagram representing the MLPA reaction.....	182
Figure 6.3: MLPA results per cell-line.....	191
Figure 6.4: <i>Alu</i> distribution around MS32 minisatellite.....	193
Figure 6.5: Selected <i>AluY</i> for copy-number analysis around MS32 minisatellite.....	197
Figure 6.6: Representation of a dot-blot for the <i>Alu</i> copy-number analysis.....	198
Figure 6.7: Dot-blot for <i>Alu</i> copy-number analysis.....	200
Figure 6.8: <i>Alu</i> dot-blotting analysis.....	201
Figure 6.6: MS32 minisatellite flanking region.....	205
Figure 6.7: Methylation levels at each CpG site of each analysed clone per cell-lines.....	210
Figure 6.8: Methylation-status of the regions flanking MS32 minisatellite.....	211
Figure 6.10: <i>AluI</i> and methylation-sensitive MS32 digestion.....	215

LIST OF TABLES

Table 4-1: Order of genes in the vicinity of MS32 minisatellite and their function.	87
Table 4-2: I.M.A.G.E. clones used to improve the gene representation of the MS32 region on the expression microarray.	91
Table 4-3: Experimental design.	92
Table 4-4: 2 nd experimental design for the expression microarray experiment.	97
Table 4-5: Sequencing data to confirm pseudogene template for PCR reaction.....	118
Table 5-1: MS32 mutation frequencies obtained by Small-Pool PCR (PD20).....	133
Table 5-2: Screening for hFEN1 point mutations.	147
Table 6-1: MLPA kit X-104 probemix.	187
Table 6-2: MLPA summary of results.	188
Table 6-3: AluY elements with highest sequence identity to the one near MS32.	194
Table 6-4: Specificity of the primers designed for the <i>Alu</i> copy-number study.	196
Table 6-5: Genotyping of the upstream region of MS32 minisatellite.....	206
Table 6-6: Percentage of methylation per CpG dinucleotide on each cell-line.....	212
Table 6-7: Statistical analysis of the methylation-status between ALT+ and non-ALT cells.....	213
Table 6-8: MS32 mutation frequencies.	220

LIST OF ABBREVIATIONS

2D two-dimensional	NHEJ non-homologous end-joining fusion
Aa amino acid	ORC origin-recognition complex
ALT Alternative Lengthening of Telomeres	ORF open-reading frame
APC adenomatous polyposis coli	PCR polymerase-chain reaction
bp base pairs	PD population doubling
Ct threshold cycle	qPCR quantitative PCR
CN copy number	RNA ribonucleic acid
CNA copy number alterations	SP-PCR small-pool PCR
CNV copy number variation	SM-PCR small-molecule PCR
DNA deoxy-ribonucleic acid	SDSA synthesis-dependent single strand annealing
dNTP deoxy-nucleotide	shRNA short-hairpin RNA
DSB double-strand breaks	SNP single-nucleotide polymorphism
dsDNA double-stranded DNA	spcDNA small polydispersed circular DNA
ECTR extrachromosomal circular telomeric repeats	ssDNA single-stranded DNA
EM electronic microscopy	TCA telomeric-circle amplification
HR homologous recombination	Tel+ telomerase positive cells
kb kilobases	t-circle telomeric circles
MLPA multiplex-ligation probe amplification	t-loop telomeric loop

1. CHAPTER 1: INTRODUCTION

1.1 TELOMERES

Telomere: from the Greek nouns telos (τέλος) "end" and meros (μερος) "part".

Telomeres first drew the attention of Muller and McClintock, who found that natural chromosome-ends had unique “non-sticky” properties, which prevented end-to-end fusions (Muller 1938, McClintock 1939). Later, with the discovery of DNA and the mechanisms underlying its semi-conservative replication, the function and molecular structure of these natural ends was again questioned. DNA polymerases can only synthesize in a 5’ to 3’ direction and require a primer (RNA or DNA). When the last primer is removed from the lagging-strand, attrition occurs at the DNA sequences present at the very end of chromosomes. As predicted by Olovnikov and later by Watson, if no other mechanism acted on these ends, a natural consequence of the semi-conservative replication mechanism would be the loss of genetic information that could prevent cells from continuing to divide, a state later called by senescence (Olovnikov 1971, 1973; Watson 1972).

Also, McClintock had noticed that, without its natural ends, chromosomes fused allowing cycles of breakage-fusion-bridge events to occur, which results in genetic rearrangements. Currently, such genetic rearrangements are believed to be able to confer a tumourigenic potential to cells that manage to evade telomere-attrition and persist on dividing.

1.1.1 TELOMERE STRUCTURE

Telomeres are nucleoprotein structures assembled at the end of each chromosome and essential for the maintenance of genome stability as they “cap” chromosome ends preventing their recognition as double-strand breaks, end-to-end fusion and illegitimate recombination (Zakian et al 1995, Kurenova et al 1997).

Telomeres are formed by two major components: the telomeric DNA and its associated proteins. Telomeric DNA sequences are highly conserved amongst eukaryotes and, in vertebrates, comprise tandem repeats of TTAGGG. The double-stranded telomeric DNA extends for 10-20 kb in the human germ-line but is shorter in somatic cells where it varies between 2-20 kb between different chromosomes within a cell and also between cells and tissues. The most proximal region of the telomeric DNA is characterized by an interspersion of the consensus telomeric repeat (TTAGGG) with variant repeats (TTGGGG; TCAGGG; TGAGGG; etc) whereas the distal region is formed by a homogeneous array of the consensus repeat (Allshire et al. 1989, Varley et al. 2002). At the distal end, telomeric DNA ends with a 150-200 nucleotide 3' single-stranded DNA overhang on the G-rich strand (de Lange 2002). The 3'-overhang can be “hidden” from cellular activities, such as DNA repair or nucleases activity, by the formation of a t-loop structure in which the overhang folds back invading the double-stranded region of the telomere forming a t-loop and creating a displacement loop (D-loop) at the point of insertion, as demonstrated by electron microscopy (Fig. 1.1) (Griffith et al. 1999, Nikitina et al 2004). This “cap” structure is dynamic suffering dramatic changes during the cell

cycle, particularly during S-phase, when telomeres undergo replication (Blackburn 2001, Vega, Mateyak et al 2003, van Steensel et al 1998).

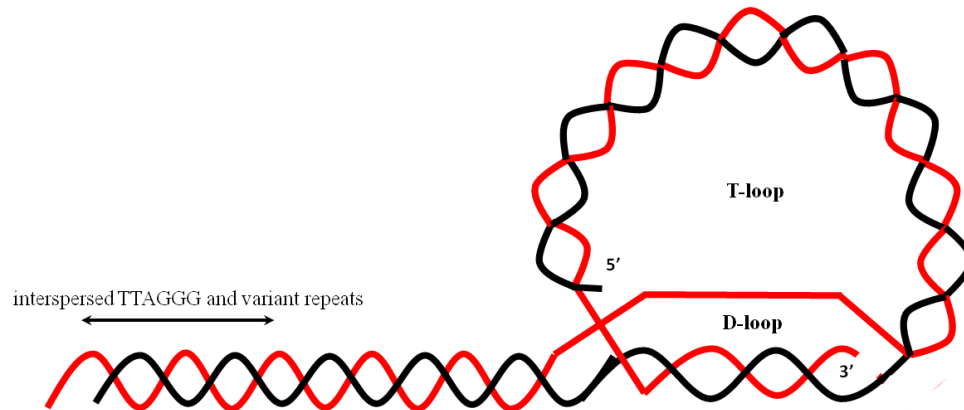


Figure 1.1: Telomere capping structure.

The 3' G-rich overhang on the end of a linear chromosome can loop back, invading a proximal double-stranded region and forming a displacement, the D-loop structure. The resulting cap structure, known as t-loop, protects the telomere from being recognized as a double-strand break. The proximal region of the telomere (marked by an arrow) is composed of an interspersion of sequence variants and TTAGGG units, whilst the distal region is composed of a tandem array of the TTAGGG units.

1.2 TELOMERE FUNCTION

1.2.1 SHELTERIN COMPLEX

Mammalian telomeres are bound by a protein complex known as Shelterin (de Lange 2002). The Shelterin complex is formed by the binding of the Telomeric Repeat binding Factors 1 and 2 (TRF1 and TRF2, respectively) to the double-stranded telomeric DNA and the single-stranded overhang to the Protection of Telomeres 1 (POT1) protein. TRF1 and TRF2 bind as homodimers to the telomeric DNA via their Myb domain (Palm et al 2008), whereas POT1 binds to the single-strand portion with two OB (oligonucleotide/oligosaccharide-binding) domains (Baumann et al 2001). These three

telomere binding proteins recruit three additional proteins: TRF2 recruits the Repressor Activator Protein 1 (RAP1), TRF1-Interacting Nuclear factor 2 (TIN2) associates with both TRF1 + 2 and TPP1 (a POT1-binding partner) is recruited by POT1 and also interacts with TIN2 (Palm et al 2008).

The main function of the shelterin complex is to protect chromosome ends from being recognized as double-strand breaks. Thus, the shelterin complex promotes and maintains the t-loop structure of telomeres and prevents non-homologous end-joining (NHEJ) activity through the TRF2/RAP1 complex (Bae et al 2007, Sarthy et al. 2009). Additionally, the shelterin complex can regulate telomere length by inhibiting telomerase access to telomeres. In fact, long telomeres have enough bound shelterin complex to ensure the formation of t-loop structures and thus, repress the access of telomerase to the chromosome ends (Marcand et al. 1997). In contrast, short telomeres are bound to less shelterin complexes, which may jeopardize the maintenance of the closed structure and allow access to telomerase.

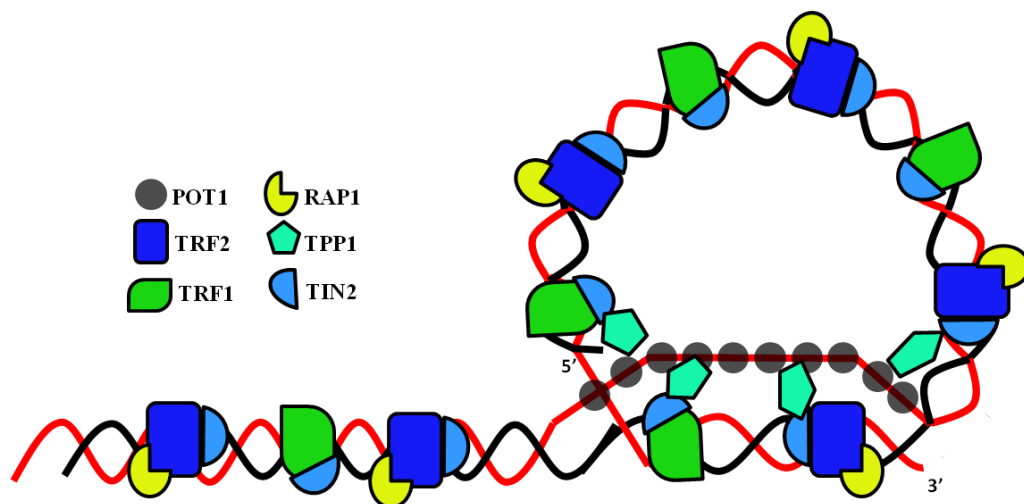


Figure 1.2: Shelterin complex.

The diagram represents a t-loop stabilized by the shelterin complex formed by the direct binding of TRF1, TRF2 and POT1 to the telomeric repeats and consequent recruitment of RAP1 (TRF2), TPP1 (POT1) and TIN2 (TRF1, TRF2 and TPP1).

1.2.2 REPLICATION AT TELOMERES

The semi-conservative replication mechanism poses a problem for the complete replication of telomeres due to the “end-replication problem”. At every replication cycle, removal of the very last RNA-primer of the nascent-strand leaves a gap in the lagging strand, which causes a successive shortening of telomeres with cell divisions. The Origin of Replication Complex (ORC) has been shown to locate and contribute to telomere maintenance in cells with different telomere maintenance mechanisms. ORC2, one of the essential core ORC proteins, was shown to bind specifically to telomeric repeats in a TRF2-dependent manner and its depletion caused telomere attrition and formation of extrachromosomal telomeric circles, a phenotype similar to the overexpression of the TRF2 Δ B (TRF2 mutant that lacks the amino-terminal domain inducing telomere dysfunction) (Deng et al. 2007; McCarroll, et al 1988). In budding yeast, telomeres are late replicating (McCarroll et al 1988) and seem to be able to delay the origin firing (Ferguson et al 1992). Also, yeast telomeres were shown to replicate from subtelomeric origins of replication, by a bidirectional replication fork that moves towards the ends of telomeres (Wellinger et al. 1993). In humans, however, it still remains to be clarified whether the ORC complex activates an origin of bidirectional replication within the telomeres or in the adjacent subtelomeric region. Nonetheless, due to the conserved directionality of the telomeric repeats the telomeric G-strand is replicated by lagging-strand synthesis whilst the C-strand by leading-strand synthesis. Thus, the 3' overhang on the leading-nascent strand is thought to result from direct 5'-3' resection of the C-strand template, whilst the 3' overhang of the lagging-nascent strand is thought to arise by conventional DNA replication by resection after the removal of the last Okazaki fragment (Chai et al. 2006) (Fig. 1.3).

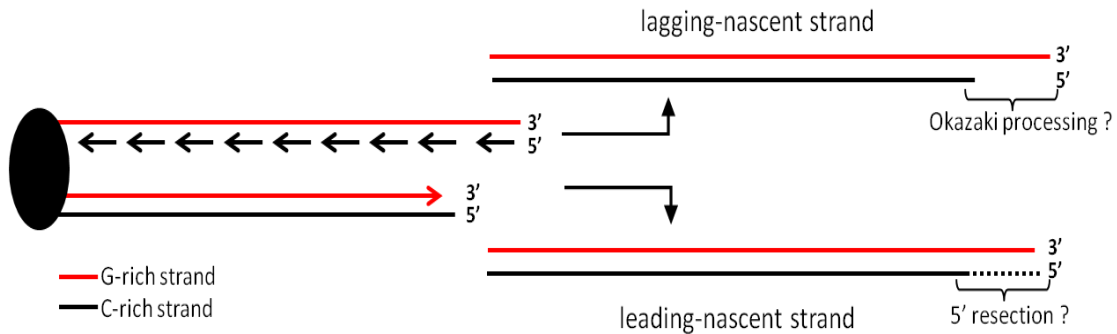


Figure 1.3: Replication at telomeres.

Due to the conserved directionality of telomeres, the C-rich nascent strand is replicated by lagging-strand synthesis and the 3' overhang of the nascent strand is most likely initiated by conventional DNA replication, by the removal of the last Okazaki fragment followed by 5' resection. The G-rich nascent strand is synthesized by leading-strand synthesis and 5' resection of the template C-strand may generate a 3' overhang.

In addition to the end-replication problem, some sequences like repeated DNA pose a challenge for the DNA replication machinery and may be prone to errors that can lead to genomic instability. The repetitive nature of telomeres has been shown to cause replication forks to stall (Gilson et al 2007) especially the G-strand, which has the potential to form G-quadruplexes (G4) structures (Sundquist et al 1989; Wang SS et al. 1989, Wang Y, et al 1993). G4 structures are formed by the interaction of four G residues by Hoogsteen base pairing, which confers an extreme stability to these structures and a possible barrier to a replication fork's progression. Indeed, DNA replication at telomeres is believed to facilitate G4 formation when the G-rich single-strand is transiently exposed and intra or intermolecular G4 structures may form between the newly synthesized and/or the parental G-rich strand (Bichara, et al 2006, Zahler et al. 1991, Zauget al. 2005). Finally, the t-loop structure itself may pose a topological barrier to the replication fork progression, since the shelterin binding most likely prevents t-loop rotation causing an accumulation of

supercoiling (Amiard et al. 2007). Stalled replication forks are usually tolerated at most genomic sites, since a fork arriving from the opposite direction will eventually replicate the region. At telomeres however, replication is thought to be uni-directional resulting in any stalled fork having to be restarted by molecular mechanisms.

Although telomeres seem to be prone to replication-derived errors that could lead to genomic instability, a vast and complex network of proteins involved in DNA replication and repair are recruited by the shelterin complex to ensure an accurate telomere replication. Amongst those proteins, Bloom (BLM) and WRN (Werner) RecQ helicases seem to be essential to stabilize and/or resolve stalled replication forks at telomeres, since both associate with telomeres during S-phase (Lillard-Wetherell et al. 2004, Opresko PL. et al. 2004) and WRN was shown to be essential for efficient lagging-strand replication on the telomeric G-strand (Crabbe L. et al. 2004). The current model proposes that TRF2 and POT1 recruit WRN and BLM to release the invading 3' overhang strand (forming the D-loop) to allow the replication fork to proceed. In addition, RecQ helicases might resolve any secondary structures (like G4) formed during the replication fork progression, which is then followed by POT1 binding and stabilization of the exposed G-strand (Zaug AJ et al. , Lillard-Wetherell et al. 2004 , Mohaghegh et al. 2001, Opresko et al. 2005, Londoño-Vallejo et al 2009).

1.2.3 TELOMERIC CHROMATIN

Telomeres have long been classified as constitutive heterochromatic domains since they are rich in epigenetic modifications characteristic of transcriptional repression, like histone H3 trimethylated at lysine 9 (H3K9m3), histone H4 trimethylated at lysine 20

(H4K20m3), histone hypoacetylation and accumulation of various isoforms of heterochromatin protein 1(HP1). Although telomeric repeats, unlike centromeric, do not contain CpG dinucleotides susceptible to methylation by DNMTs, the subtelomeric regions are composed of highly methylated cytosines in CpG dinucleotides in human somatic cells (Benetti, et al 2007, Ottaviani, et al 2008, Tilman G et al. , Ng LJ et al. 2009).

The heterochromatic state of telomeres is thought to contribute to chromosome positioning and movement within the nucleus and also to the regulation of telomerase. Alterations to the telomeric chromatin state were associated to severe telomere loss, suggesting crucial roles of this structure during telomere replication (Michishita et al. 2008; Yehezkel et al. 2008). Another long known property of the heterochromatic telomeric state is its silencing function. The insertion of reporter genes in subtelomeric regions undergoes gene silencing, a conserved characteristic known as Telomere Position Effect (TPE) first described in *D. melanogaster* (Hazelrigg, et al 1984, Levis R et al. 1985) but also observed in yeast (Gottschling et al. 1990, Pryde et al 1999, Baur et al. 2001, Koering CE et al. 2002), in humans (Wright et al 2001) and in mouse (Murnane et al 2006).

The heterochromatic state of telomeres together with the TPE silencing has led to the assumption that telomeric regions were transcriptionally silenced and that this silencing extended to subtelomeric regions. Thus, it was surprising when different groups reported that mammalian telomeres are transcribed into Telomeric Repeat containing RNA (TERRA) molecules ranging from 100 bases to around 9 kb and present in nuclear fractions only. The C-rich strand is transcribed from transcription sites within subtelomeric regions, thus, TERRA molecules are composed of UUAGGG repeats and subtelomeric sequences (Azzalin et al. 2007, Schoeftner, et al 2008). The exact function of TERRA is still under investigation but it adds another level of complexity to telomere maintenance.

1.3 TELOMERE MAINTENANCE MECHANISM

In 1961, Hayflick and Moorhead noticed that normal human diploid fibroblasts could not grow indefinitely in culture. After 60-80 populations, somatic cells stop dividing and enter a state phenotypically characterized by large and flat cells, with vacuolated morphology and inability to synthesize DNA. The progressive telomere shortening in these cells eventually results in structural telomere changes that can induce the P53- and P16/retinoblastoma protein (P16/pRB)-dependent replicative senescence (Harley CB et al. , Shay, et al 1991, Karlseder, et al 2002). At this stage, cells stop dividing and enter a replicative-senescent state or mortality stage 1 - M1, which is characterized by their inability to divide despite being metabolically active and therefore, alive (Olovnikov et al 1973). This limit for the proliferative potential of somatic cells is also known as Hayflick limit. The inactivation of the senescence-dependent pathways P53 and/or RB pathways by some viral oncogenes and other agents allow the cell to bypass this replication checkpoint, leading to a continuous telomere shortening and consequent compromise of the genetic stability. Therefore, at mortality stage 2 – M2, telomeres are extremely short, which triggers an increase in chromosomal rearrangements and genome instability, a state also known as crisis. Almost all cells that undergo crisis die but some rare cells may acquire infinite replicate potential emerging from crisis through the activation of one of the Telomere Maintenance Mechanism (TMM) (Fig. 1.4).

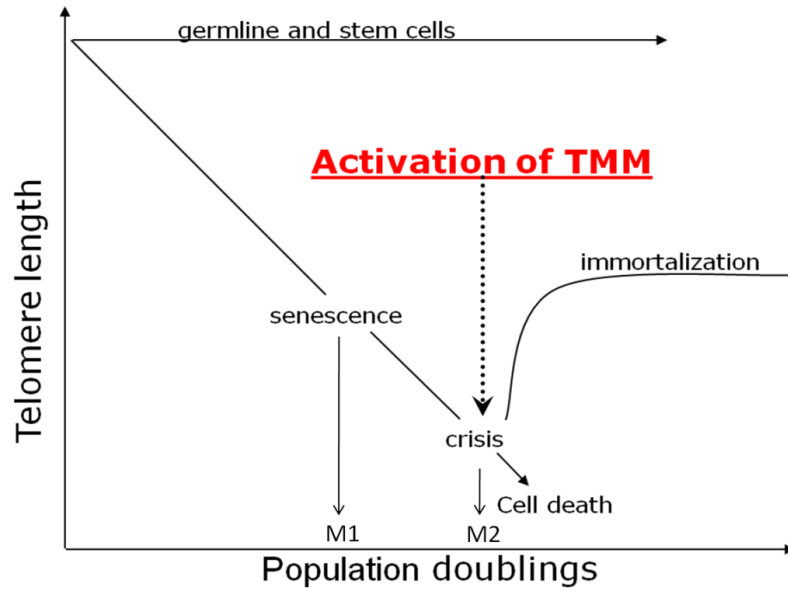


Figure 1.4: Telomere length along time.

Telomeres shorten with each cell cycle, which functions as a mitotic clock that limits the number of divisions a cell can undertake. When telomeres reach a critical length, senescence happens. At M1, if some checkpoints are compromised, cells can escape senescence and keep dividing. Telomere dysfunction results in massive chromosome aberrations leading to cell death (crisis). Immortal cells activate a TMM to maintain the length of telomeres, escaping to the crisis.

1.3.1 TELOMERASE

1.3.1.1 TELOMERASE STRUCTURE

The discovery of telomerase in the ciliate *Tetrahymena thermophila* by Greider and Blackburn, in 1985 revolutionized telomere biology. The holo-enzyme telomerase is a reverse transcriptase composed of a catalytic protein subunit (TERT) and a RNA component (TERC) (Greider, et al 1985). The TERT component recognizes the free telomeric 3' end as primer site and uses its TERC component as template for reverse-transcription of one nucleotide at a time onto the 3' end of the telomeric G-rich strand. The

complementary strand is synthesized by the conventional DNA polymerases (Blackburn 2001; Collins et al 2002).

1.3.1.2 TELOMERASE FUNCTION

In human adults, telomerase is active in the germ-line, stem cells and some differentiated somatic cells (Collins 2000), probably due to the highly methylated region present around the *hTERT* locus in somatic cells (Zhu et al. 2004). Nonetheless, cells under telomere-induced crisis have the ability to express hTERT, activating telomerase to bypass crisis and become immortal (Zhu J et al. 1999, Shay, et al 1989, Maser, et al 2002). A large proportion (85%) of all human tumours and a high percentage of immortalized cell lines reactivate telomerase preventing critical telomere shortening and facilitating cell proliferation which favours growth of the tumour (Bryan, et al 1997). Cells expressing telomerase often present short and length-homogeneous telomeres. Transcription of the hTERT component of telomerase is the limiting factor for telomerase activity (Aisner, et al 2002), since the TERC subunit is highly expressed in many normal and cancer cells (Blasco et al. 1996). Furthermore, hTERT ectopic expression stabilized telomeres, bypassing senescence without causing neoplastic transformation (Bodnar et al. 1998, Jiang XR et al. 1999).

Several different mechanisms have been proposed to induce hTERT expression, from transcription initiation by the binding of c-MYC (Wang et al. 1998, Greenberg et al. 1999) or the viral oncoprotein E6 of some human papillomaviruses (Klingelutz et al. 1996, Veldman et al. 2003, Xu et al. 2008) to the *hTERT* promoter; to chromosome rearrangements where the *hTERT* gene is translocated to heterologous loci, evading the tight repressive chromatin state (Zhao et al. 2009).

1.3.2 ALTERNATIVE LENGTHENING OF TELOMERE - ALT

Certain tumours, however, seem to preferentially activate the Alternative Lengthening of Telomeres (ALT) pathway. It remains to be elucidated what triggers one or the other mechanism. Most ALT-positive (ALT+) tumours are from mesenchymal-derived tissues, mainly sarcomas (osteosarcomas and glioblastoma multiforme), which show a tighter telomerase repression at chromatin level that may facilitate ALT activation (Ulaner et al. 2003, Hakin-Smith et al. 2003). Generally, 30-40% of human immortalized cell lines and 10-15% of tumours lack telomerase activity and maintain or elongate their telomeres (Bryan et al. 1997, Henson et al. 2002) and they would not be responsive to anti-telomerase drug therapies.

Grobelny demonstrated that both TMM can be activated in the same cell (Grobelny, et al 2001), though it seems that telomerase becomes dominant towards the ALT pathway, since these cells have homogeneous-length telomeres. Moreover, ALT+ primary tumours are able to progress to Tel+ secondary tumours and the opposite has also been observed (Henson et al. 2002). Thus, it was suggested that either ALT is switched off in presence of telomerase or the two mechanisms compete for the same molecular components and/or to the telomeric DNA access (Henson et al. 2002).

1.3.2.1 ALT FEATURES

The phenotype of ALT+ cells has been widely characterised, facilitating their distinction from normal and Tel+ cells. The most commonly used ALT-marker is the presence of specialized promyelocytic leukaemia (PML) bodies (known as ALT-associated PML bodies or APBs), as they are only formed upon ALT activation and disappear when ALT is repressed (Dunham et al. 2000). APBs are defined as PML bodies containing

telomeric DNA, shelterin and other proteins involved in DNA repair, DNA synthesis and DNA recombination (Nabetani, et al 2004, Tarsounas et al. 2004). APBs are predominantly present during G2 phase of the cell-cycle, which coincides with the phase where telomeres seem to be elongated by the ALT mechanism (Grobelny et al 2000). The percentage of APBs varies greatly between cell-lines, ranging from 0.5 to 50% (Yeager et al 1999; Tarsounas et al 2004). The MRE11/RAD50/NBS1 MRN complex appears to be essential for APBs formation. In fact, formation of APBs seems to require NBS1, which recruits MRE11 and RAD50 (to form the MRN complex) into these structures (Wu et al. 2003, Wei-Qin et al. 2005, Wu et al. 2003). Also, if one of the main components of PML bodies, SP100, is over-expressed to sequester the MRN complex, APBs formation in ALT+ cells is inhibited, causing the disruption of ALT features, including rapid disappearance of telomere length heterogeneity accompanied by telomere shortening as seen in normal cells (Henson et al. 2005). The role of APBs in the ALT mechanism is still under investigation. Some evidence suggests that APBs are highly involved in the ALT process, as they constitute sites for telomere elongation. In fact, APBs were shown to be the site where telomeres converged and colocalized with the recombination-protein RAD51 and the replication-protein RPA (Draskovic et al. 2009). However, APB formation seems to require HP1-mediated chromatin compaction, which is likely to repress recombination, and APBs were also detected in cells entering senescence after P53 activation (Jiang et al. 2009). Thus, another model proposes that APBs might instead be repositories for by-products of telomere elongation by ALT or sites where proteins required by ALT are held until needed.

ALT-positive cells can also be recognized by their highly heterogeneous telomeres, ranging from undetectable to 50 Kb, the presence of extrachromosomal telomeric DNA (ECTR), both in linear and circular forms (Yeager et al. 1999, Cesare, Griffith 2004).

Another characteristic of ALT⁺ cells is the increase sister-chromatid exchange exclusively at telomeres, known as telomeric sister-chromatic exchange (T-SCE), even though they could derive from non-sister chromatids or from extrachromosomal telomeric DNA (Bailey, et al 2004, Bechter et al. 2003, Londono-Vallejo et al. 2004). Finally, the extreme instability at the MS32 minisatellite was only found at ALT⁺ cells, providing another molecular marker for these cells (Jeyapalan et al. 2005).

1.3.2.2 THE ALT MECHANISM

The telomeres in ALT⁺ cells shorten gradually until they undergo a sudden and rapid elongation of many kb of DNA. Thus, it is very likely that the ALT mechanism is based on a single extension event (Murnane et al. 1994, Wang, et al 2004, Li et al 1996). To determine the molecular mechanisms underlying the ALT pathway, Dunham et al. incorporated a tag into ALT⁺ telomeres and, after several population doublings, observed that the tag had been copied to previously untagged telomeres (Dunham et al. 2000). Accordingly, studies on the mutational processes occurring at telomeres showed that, in normal and telomerase-positive cells, mutations are dominated by simple intra-allelic events whilst telomeres elongated by ALT show complex mutations likely to have arisen by inter-telomeric exchange. In fact, single-telomere analysis, which allows the mapping of the interspersed pattern of the variant and normal telomeric repeats within a single telomere, showed that a small proportion of ALT⁺ progenitor telomeres underwent partial replacement with new repeats that come from elsewhere in the genome. The progenitor allele was truncated (within the proximal 1 kb) and distal to the breakpoint a novel interspersed pattern of TTAGGG and sequence-variant repeats was observed. Interestingly, no similar complex mutations were observed in normal, pre-crisis or telomerase-positive cell-

lines (Varley et al. 2002). Simple insertions and deletions were also observed in ALT+ telomeres, suggesting that intra-allelic events are also contributing to rearrangements mutations in the telomeric DNA in these cells. Accordingly, a recent study demonstrated that intratelomeric (intramolecular and/or telomeric sister-chromatid) recombination also occurs at ALT+ telomeres (Muntoni A et al. 2009). Furthermore, the presence at APBs of several proteins involved in recombination at ALT telomeres, like RAD50, RAD51, RAD52, MRE11, NBS1, BLM and WRN, represents indirect evidence for an ALT recombination-based mechanism (Henson et al. 2002, Henson et al. 2002). Accordingly, the high T-SCE exclusively in ALT+ cells also supports a recombination-based model for the ALT-mechanism. Finally, the presence of extrachromosomal telomeric circles (t-circles) has also been proposed to result from recombination processes at telomeres, specifically intra-allelic recombination events. In the absence of a functional TRF2 (under expression of the dominant negative allele TRF2 Δ B that lacks the basic domain), t-loops seem to be resolved by homologous-recombination (HR) involving NBS1 and XRCC3 proteins, resulting in a shortened telomere and a free t-circle (Wang et al 2004). Supporting the HR-dependent t-circle formation via t-loop resolution, RNAi knockdown of XRCC3 or NBS1 or inhibition of the latter via over-expression of SP100 in ALT+ cells resulted in a decrease of t-circles, suggesting that these structures derive from on-going HR-dependent t-loop resolution (Jiang et al. 2005, Compton et al. 2007).

Therefore, there is clear evidence for telomere recombination in ALT+ cells, at least as three distinct forms: HR-dependent telomere copying; post-replicative telomere exchanges (T-SCE) and t-loop resolution in ALT+ cells. Hence, ALT must be a recombination-like mechanism involving intra and/or inter-telomeric copying, although the precise template for the newly elongated telomeres remains unclear. Several models have

been proposed and all agree that after crisis, DNA repair machinery might interpret critically short telomeres as double-strand breaks, which might activate a recombination-mediated process leading to elongation of the short telomere (McEachern et al 1996). The repair might involve strand invasion into a homologous DNA sequence, followed by replication until the chromosome end. The resulting crossover structure could be resolved by a nuclease generating a recombinant molecule and/or unwind and rewind processes may result in a non-recombinant molecule (Bryan et al. 1997). Though, the various models for ALT-recombination mechanism differ in the template for the copying events and on the exact processes involved.

1.3.2.2.1 UNEQUAL SISTER-TELOMERE EXCHANGE (T-SCE)

A specific inter-telomeric recombination mechanism is Telomeric Sister Chromatid Exchange (T-SCE). T-SCE occur spontaneously and at high rate in ALT+ cells compared to normal cells or tel+ cells (Bailey et al 2003). The factors required for the high rate of T-SCE in ALT+ cells have not yet been found. Cells from BLM-syndrome patients (lack a functional BLM helicases) show no elevation of telomeric exchanges, though the SCE rate across the genome is 10-12 fold higher than normal cells (Londono-Vallejo et al. 2004), suggesting a different mechanism for T-SCE than normal SCE. Also, this model presents no net gain in telomere length, since one sister-telomere would be elongated at the expense of another (Fig. 1.5). To overcome this problem, a bias on the segregation of chromatids with elongated telomeres to the same daughter cell that could confer a higher replicative potential to that daughter-cell compared to the other, was proposed and confirmed by mathematical modelling (Bailey et al 2004, Muntoni et al 2005, Blagoev et al 2008).

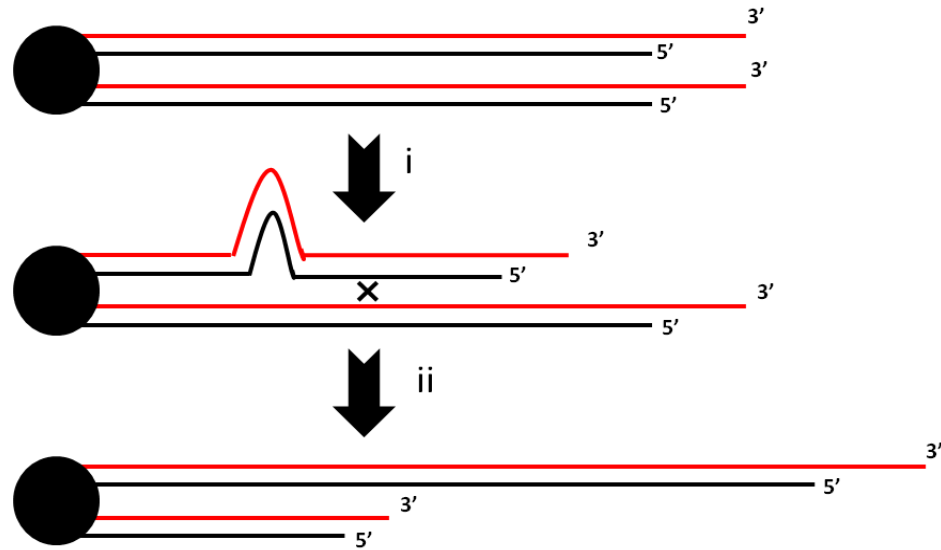


Figure 1.5: Unequal sister-chromatid exchange at telomeres.

If recombination happens between telomeric sister-chromatids aligned out of register (i), one telomeric sister-chromatid will be elongated at the expense of the donor one, resulting on a long and a short telomeric sister-chromatid (ii).

1.3.2.2.2 T-LOOP EXCISION AND ROLLING-TELOMERIC ELONGATION (RTE)

Besides preserving the telomeres from degradation, t-loops have also been proposed as the perfect structure for the elongation and shortening of ALT-telomeres, as they resemble a recombination-dependent replication structure. T-loop resolution could explain the rapid reduction in telomere length (Murnane et al 1994) as well as extrachromosomal telomeric circles generation (Dunham et al 2000), both of which are features of ALT+ cells (Henson et al 2002). D-loop resolution by XRCC3 and NBS1 would result on extrachromosomal telomeric circles and a shortened telomere with a 3' overhang that, depending on the length, could form another t-loop structure or be the substrate for telomere copying (Fig. 1.6-a) (de Lange 2004). Additionally, replication could initiate within the D-loop, with extension of the 3' G-strand. Progression of the replication fork round the t-loop, by rolling-circle amplification or rolling-telomeric elongation (RTE)

would generate extension of the telomere by an intramolecular process (Fig. 1.6-b) (Cesare et al 2004, Wang, et al 2004, Tomaska et al. 2000). Indeed, studies in *Kluyveromyces lactis* (Natarajan, et al 2002) and the mitochondria of the yeast *Candida parapsilosis* that contain a linear genome capped by telomeres maintained exclusively in the absence of telomerase (Nosek J et al. 2005) show evidence for telomeric rolling-circle amplification. However, this model cannot occur by itself since it fails to explain how telomeric sequences move from one chromosome to other.

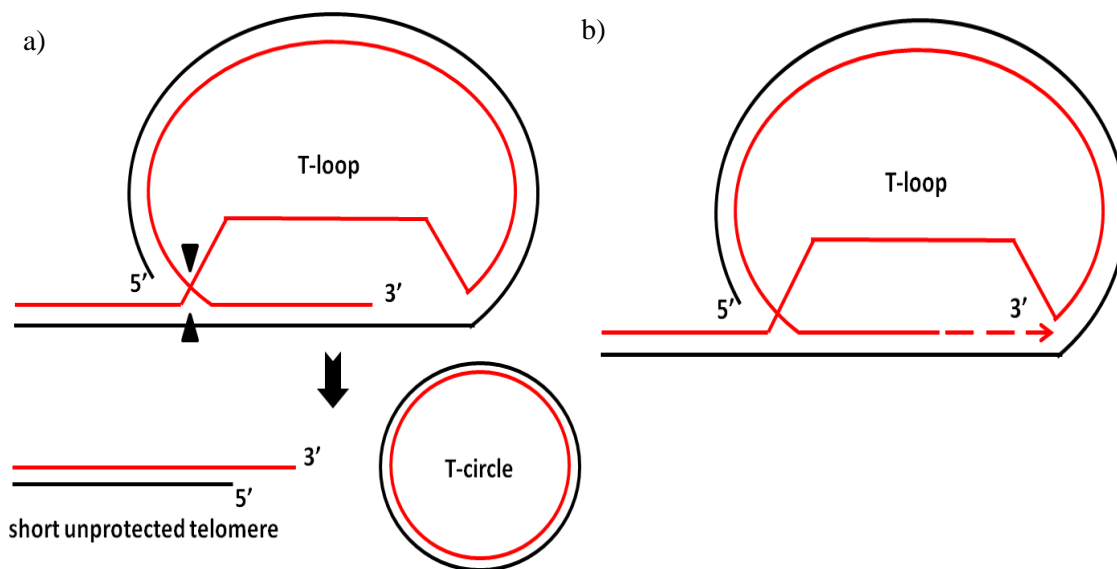


Figure 1.6: T-loop excision and extension by RTE

a) The HR-dependent resolution of the t-loop would originate a shortened telomere, with a 3'-free end passive for further copying and a t-circle. b) Telomere copying initiated within the D-loop could proceed along the loop, generating new telomeric DNA.

1.3.2.2.4 BREAK-INDUCED REPLICATION (BIR)

The 3' single-stranded end of the G-strand on short and consequently deprotected telomeres (d'Adda di Fagagna et al. 2003, Takai, et al 2003) can invade a double-stranded DNA at another telomeric template (other chromosome, t-circles or sister-chromatid),

forming a D-loop structure and using the donor C-strand for telomere copying. The resolution of the D-loop structure would result on an elongated telomere without loss of telomeric repeats from the donor sequence, which could be the end of another chromosome and/or a sister-chromatid (McEachern et al 2006, Lydeard et al. 2007). The different products of BIR at telomeres are represented in Fig. 1.7.

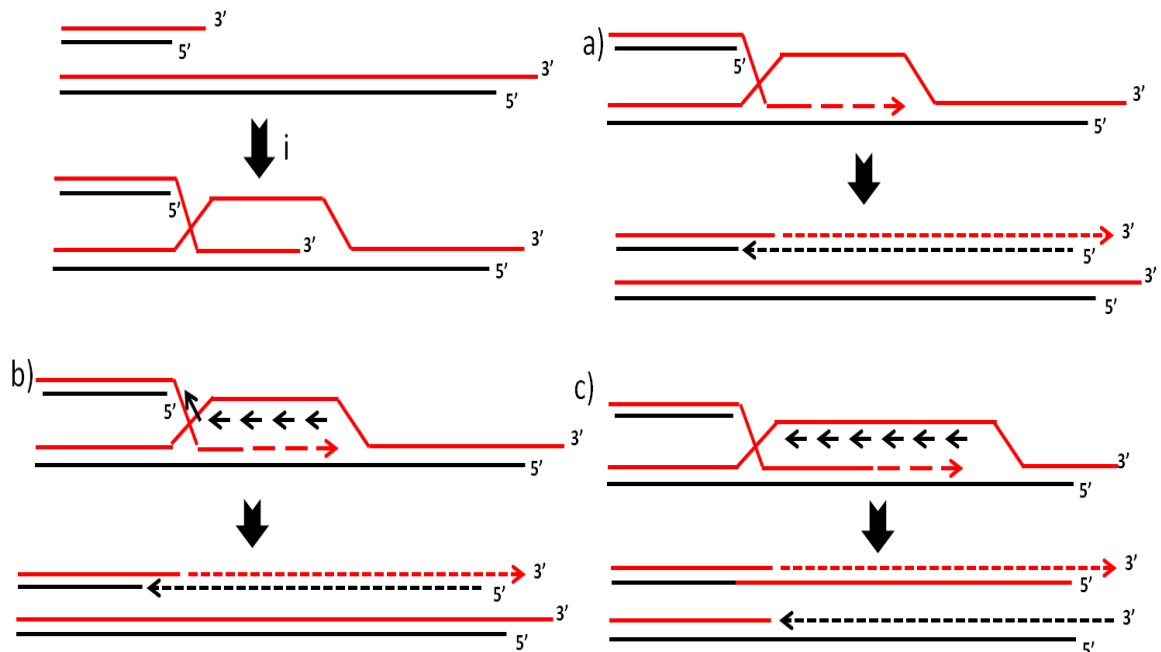


Figure 1.7: BIR-elongation of telomeres.

The 3'-end of a shortened telomere invades a donor telomere (i) (on another chromosome, sister-chromatid or t-circle) forming a D-loop. The telomere can be elongated by either copying one strand and the complement will be synthesized by normal DNA replication (a) or copying of both strands of the template (b). In both cases, a branch migration of the Holliday junction will displace two newly synthesized strands resulting on an elongated telomere and an unaltered donor telomere. Alternatively, if a unidirectional replication fork is formed, the copying process extends till the end of the template and the resolution of the Holliday junction leaves two semi-conservative replicated products (c). This process could also be perceived by sister-chromatid exchange.

1.3.2.3 ALTERNATIVE ALT

An alternative ALT mechanism has been reported in a cell-line derived from a Werner syndrome (WS) patient. This cell-line (AG11395, SV40-transformed Werner mutant fibroblast) shows telomeres with heterogeneous lengths that undergo rapid length changes, a typical ALT-telomere dynamics but lack APBs, the ALT-associated nuclear aggregates. Additionally, the telomeres of these cells are composed of non-telomeric DNA (SV40 derived sequences) interspersed with telomeric DNA sequences. The interspersion pattern observed resembles type I yeast survivors (see section 1.4) that are dependent on RAD51 whereas type 2 survivor depends on RAD50 and SGS1, the yeast homologue of *WRN* and *BLM* gene helicases and their telomeres are characterized by a simple telomeric array with heterogeneous lengths (reminiscent of human ALT). The finding of this peculiar ALT cell-line suggests that ALT might be underlined by more than one mechanism, one of them arising by the absence of a functional *WRN* protein (Marciniak et al. 2005, Fasching, et al 2005).

1.3.3 PROTEINS AND ALT

Although several proteins have been implicated in the ALT mechanism, very few have been shown to be required for telomere elongation by ALT. Thus, the list for candidate “ALT proteins” is still extensive. The MRN complex has been shown to be required for APB formation (see section 1.3.2.1) since NBS1 recruitment by SP100 overexpression inhibited APB formation and, consequently, the ALT phenotype was lost (Jiang et al. 2005). Another piece of evidence for ALT deregulation via inhibition of APBs came from studies with the structural maintenance of chromosomes (SMC5/6) recombination complex. The SMC5/6 complex was shown to be present at APBs, but more

interesting was the finding that the SUMOylation of several shelterin-proteins by the E3 SUMO-protein ligase (MMS21) component of the SMC5/6 complex was required for APB formation (Potts, Yu 2007). The authors proposed that the MMS21-induced shelterin SUMOylation may trigger telomere deprotection, allowing the ALT-recombination like processes to access and elongate telomeres in ALT+ cells. More recently, topoisomerase III α (TOP3A) was implicated in ALT since its depletion resulted in loss of the G-strand overhangs and reduction of cell viability (Temime-Smaali et al. 2008). Interestingly, TOP3A forms a complex with TRF1, TRF2 and the heat shock protein 90 (HSP90) to localize the BLM helicase to telomeres in ALT+ cells (Bhattacharyya et al. 2009). Furthermore, Bloom-syndrome patients show cancer-predisposition and elevated SCE (Londono-Vallejo et al. 2004) but no T-SCE, suggesting that BLM might have a role in telomere elongation by ALT. Another protein shown to be essential for ALT+ cells viability through regulation of telomere recombination is the endonuclease MUS81. Since its depletion resulted in the reduction of ALT-specific telomere recombination and lead to proliferation arrest of ALT cells (Zeng, et al 2009). A similar effect on the ALT mechanism was also observed after depletion of either FANCD2 or FANCA, components of the Fanconi anemia (FA) complex. Its depletion was associated to a decrease in T-SCE and with a drastic loss of detectable telomeres exclusively in ALT+ cells, suggesting that the FA pathway might participate in telomeric recombination and/or control the resolution of recombinational events at telomeres in ALT+ cells (Fan et al. 2009). Many other proteins are known to have an effect in telomere function, for example the telomere dysfunction seen in cells with a defect in the DSB repair BRCA1 protein (Al-Wahiby et al 2005, Cabuy et al 2008), may be also found to play an active role in the ALT mechanism. Despite all

these advances, the identification of the proteins involved in ALT activation and/or suppression have not yet been identified.

1.4 FROM YEAST TO HUMANS

A considerable amount of the telomere biology already elucidated has come from studies in the budding yeast *Saccharomyces cerevisiae*. The *S. cerevisiae* telomeric DNA consists of an array of 350 +/- 75 bp TG₁₋₃ and, internally to this repeat track, repetitive DNA elements known as X and Y` (Zakian et al 1995). The double-stranded telomeric DNA is bound by RAP1, while the single-stranded 3' overhang is bound by the trimeric CDC13/STN1/TEN1 complex (Alexander et al 2003, Hug et al 2006). Interestingly, RAP1P regulates telomerase function at telomeres by the recruitment of both negative telomerase regulators RIF1 and RIF2 (Marcand, et al 1997, Hardy, et al 1992) and a complex responsible for establishing the heterochromatin-like state in the subtelomeric regions (Moretti et al. 1994, Marcand et al. 1996). This *cis*-acting negative regulation of telomerase access to the telomere is controlled by the number of negative regulators bound to the telomeric DNA, which is directly associated to the length of the telomere (Marcand, et al 1997; Cooper et al. 1997; Maringele et al 2004 and 2005). However, *S. cerevisiae* strains deficient in telomerase can survive crisis by the activation of recombination-based pathways dependent on RAD52 (Lundblad et al 2002). The type-I survivors depend on RAD52 and the RAD51-pathway genes (RAD55 and RAD57). Their telomeres are composed of a variable copy number of the Y' subterminal repeats (Y' element interspersed with telomeric repeats) terminated by a very short array of telomeric repeats (Chen et al 2001). These yeast cells are slow growing and can convert to type II survivors (Chen et al 2001). Type II survivors are dependent on RAD52, RAD50 and the SGS1

genes, since *SGS1* Δ telomerase-negative mutants give rise to type I survivors only (Johnson et al 2001). Type-II survivors have telomeres with highly heterogeneous-length telomeres, with a similar pattern of shortening and sudden elongation observed in human ALT cells (Lundblad et al 2002; Teng et al 2000). Finally, *S. cerevisiae* telomerase-negative cells (*TLC1* Δ *RAD52* Δ *EXO1* Δ) also utilize a recombination-independent survival pathway that involves repair of DNA double-strand breaks by palindromic DNA structures (Maringele et al 2004 and 2005).

Interestingly, the exonuclease 1 seems to be essential for the initiation of recombination in telomerase-negative survivors, since *TLC1* Δ *EXO1* Δ survivors arise much later than *TLC1* Δ only survivors (Maringele et al 2004). Also, the nonessential subunit of DNA POL δ required for BIR, POL32, was shown to be required for the generation of both types of survivors (Lydeard et al 2007).

Regardless of the different possibilities of recombination-based *TLC1* Δ survivors, the type-II survivors clearly resemble human ALT the most. The human proteins that bear a conserved function with *SGS1*, required for the activation of type II yeast survivors, are Bloom (BLM) and Werner (WRN) (REQ4 helicases). BLM complemented *SGS1* function in *SGS1* mutants (Lillard-Wetherell et al 2005). WRN can also promote the resolution of recombination intermediates (Swanson et al. 2004). Furthermore, it is located on chromosome 8, a chromosome that has been implicated with ALT activation by LOH just seen in ALT (Shigeeda et al. 2003). However, an ALT phenotype similar to the type I yeast survivors (variant with tandem array telomeres) has been described in another WRN deficient cell line (Henson et al 2003; Bryan et al 1997). Thus, it is tempting to speculate that, similar to yeast lacking telomerase activity, humans also have two pathways for telomere elongation that might have different RecQ requirements.

1.5 MINISATELLITES

It was back in late 1960s that the discovery of repetitive DNA as part of mammalian genomes was highlighted by the re-association kinetic experiments (COT curves) (Britten et al 1968). However, it has not been until quite recently that the various genome-sequencing projects have uncovered the extent to which repetitive DNA composes mammalian genomes (Venter et al. 2001, Lander et al. 2001). Repetitive DNA in the human genome can be classified in different categories: dispersed elements (transposons, retrotransposons, tDNAs, etc), tandem repeats (satellites, minisatellites, microsatellites and rDNAs) that include elements like telomeres and centromeres. Almost half of the euchromatic genome sequence (45%) is composed of transposable elements (Wang et al. 2005; Nishihara, et al 2002). Copy number variants, including deletions and duplication of large regions (1-200 kb long) have recently been considered to constitute 10% of the human genome (Iafate et al. 2004). Tandem repeats, which are composed of an array of the same repeat units, are thought to constitute 3% of euchromatic DNA. According to the size of the repeat units, tandem repeats can be further divided in microsatellites (1-10 bp), minisatellites (10-100 bp) and satellites (above 100 bp).

1.5.1 MINISATELLITE STRUCTURE

Minisatellites were first described in humans, by Wyman and White (Wyman, 1980) and ever since minisatellites have been described in many organisms, including bacteria (Jeffreys *et al.* 1985). Minisatellites are composed of 6-100 bp repeats, organized on a tandem array that can range from 0.5 to many kilobases in length. Generally, minisatellites are GC rich and, in humans, cluster in subtelomeric regions (Royle et al. 1988). Most G-rich minisatellites described share a core sequence of 10-15 bp

(GGAGGTGGGCAGGARG) similar to the χ sequence, a recombination signal in *E. coli* (Jeffreys et al 1985). AT-rich minisatellites, although not as frequent, have also been characterized, like the first haploid minisatellite described MSY1 (Jobling, et al 1998).

1.5.2 MINISATELLITE BIOLOGY

Minisatellites were first used for individual identification in DNA fingerprinting, a technique based on minisatellites length polymorphisms that reflect repeat number variation and on their capacity to cross-hybridize to several other loci throughout the genome (Nakamura *et al.* 1987). Following this application, highly polymorphic minisatellites were used as the first multiallelic markers for linkage studies (Nakamura *et al.* 1987). Since then, minisatellites have been implicated in genome function through a variety of different mechanisms like transcriptional regulation, imprinting control and proper chromosomal segregation (see below). Especially, alterations in minisatellites have been linked to changes in transcription levels of nearby genes and to human disease phenotypes, including oncogenesis.

Several studies provide evidence for direct protein binding to certain minisatellites and, even though the function of most identified proteins is still not known, some transcription factors have been characterized. The insulin-linked polymorphic region (ILPR) is a minisatellite located in the 5' region of the insulin gene with affinity to the transcription factor PUR-1. *In vitro*, this affinity controls the expression of the insulin gene since the longer the allele the higher the affinity to PUR-1 (Kennedy, et al 1995). A reduction in the transcription of the *cystatin B* gene has been associated with the expansion of a minisatellite located within its promoter region, which is thought to be the underlying cause of the myoclonic epilepsy of the Unverricht–Lundborg type (Joensuu et al. 2007).

More recently, a minisatellite located within the promoter region of X-ray repair cross-complementing 5 (*XRCC5*) was also implicated in the regulation of gene expression due to its affinity to the transcription factor SP1, which may be evidence for direct contribution of a polymorphic minisatellite to susceptibility to bladder cancer (Wang et al. 2008). Another minisatellite, 6-16, is composed of repeat units with a similar sequence to the mammalian splicing donor consensus sequence. When located within an intronic sequence was shown to provide functional splice donor sites, originating different spliced transcripts (Turri et al 1995). Also, minisatellites have been associated with imprinting control, as minisatellites were found at imprinted loci (Chaillet et al 1994). Furthermore, minisatellites have been proposed as sites for chromosome fragility, like FRA10B and FRA16B, both amplified AT-rich minisatellite repeats (Yu et al. 1997, Debrauwere et al. 1997). Finally, the most recent application for minisatellites relies on its sensitivity to genotoxic agents. Minisatellites have been proposed as biomarkers for genotoxicity as ionizing radiation was shown to affect hypermutable minisatellite stability in mouse (Dubrova et al 1993) and in humans exposed to radioactive material released after the Chernobyl explosion (Dubrova et al. 1996). However, it is not clear if the target of genotoxic agents is the tandem array, a flanking DSB hotspot or the replication machinery itself and further investigations in yeast models are underway. Thus, minisatellites seem to be involved in a wide range of human genome biology, participating in processes as different as gene regulation, fragile sites and imprinting as well as providing insights into meiotic recombination and being biomarkers for genotoxicity.

1.5.3 MINISATELLITE STABILITY

Minisatellites are the genomic regions with higher tendency for instability, especially when the genome is exposed to genotoxic agents and ionising radiation, which might be a consequence of the repetitive and phenotypically-neutral nature. A better understanding of the factors that interfere with minisatellite stability may shed light onto molecular mechanisms responsible for genome rearrangements. Particularly minisatellites have been associated with various human diseases, thus the identification of the causes of minisatellite instability might prove helpful for the development of more efficient therapies.

Studies in human minisatellites have allowed the proposition of several models for the mechanisms underlying minisatellite instability in both germline and soma. Several techniques were developed for this purpose, facilitating the detection of mutant alleles directly from the genomic DNA. Small-pool PCR (SP-PCR) is based on the amplification of multiple pools of genomic DNA containing a minimum number of minisatellite molecules that, by gel electrophoresis resolution, allow the identification of length-mutant minisatellite molecules (Jeffreys et al. 1994). SP-PCR allowed the reliable estimation of mutation rates above 1×10^{-3} per progenitor allele (Jeffreys et al. 1994, Jeffreys et al. 1990), although the addition of a size enrichment step (recovery of multiple size-fractions excluding the progenitor alleles after gel electrophoresis resolution) prior to the SP-PCR reaction can lower the mutation rate estimation to 1×10^{-4} - 1×10^{-6} (Jeffreys, et al 1997). The characterization of the internal structure (interspersions of the repeat unit sequence variation along the array) by Minisatellite Variant Repeat (MVR)-PCR facilitates the elucidation of the molecular mechanism responsible for the instability (Jeffreys et al. 1991). Therefore, the application of these methodologies to the analysis of several hypermutable human GC-

rich minisatellites has elucidated differences on the mechanisms responsible for the instability in germ line and somatic cells.

In the soma, blood DNA analysis revealed that minisatellite length alterations usually derive from rare simple insertions and/or deletions of repeat units, rearrangements that can be explained by unequal sister chromatid exchange, intramolecular recombination or perhaps replication slippage (Jeffreys, et al 1997). In tumours, minisatellite instability might increase, as instability was observed at the H-RAS minisatellite in human clonal tumour cell-populations and during tumour progression (Kiaris et al. 1995, Kiaris, et al 1996). However, this minisatellite changes in tumours may reflect general genome instability and the mechanisms involved might differ from the normal somatic instability.

In contrast, the germ-line shows extreme minisatellite instability, which accounts for the large number of alleles of different lengths within the human population and suggests that the stability of these tandem repeats in the human germ-line is more relaxed than in soma. In fact, during meiosis, minisatellites can be the substrate for recombination events, as seen at the highly unstable minisatellite MS32, where a base transversion in the DNA sequence adjacent to one end of the MS32 repeat array (for more detail see section 1.6.3) is associated with rare stable alleles that seems to suppress instability (Monckton et al. 1994). Furthermore, the presence of a meiotic recombination hotspot adjacent to one end of highly variable minisatellites, like CEB1, MS31a and MS32 (Jeffreys 1997, Alec J. Jeffreys, et al. 1994), suggests that minisatellites might have evolved as byproducts of localized meiotic recombination hotspots in the human genome. The germline rearrangements in the GC-rich minisatellites are believed to arise from complex process involving the copying and transfer of blocks of repeats from one allele to the other. In the MS31A, MS32, and MS205 minisatellites the mutations arise mainly by gene conversion-

like transfers of repeat units between alleles that are largely restricted to only one of the ends of the array (polarized mutations) and do not involve exchange of flanking markers (Jeffreys et al. 1993, Jeffreys et al. 1994, May, et al 1996). CEB1 shows polar interallelic conversion but also has complex and nonpolar intra-allelic rearrangements that still appear to be meiotic in origin (Buard, et al 1994 and 1998). Some alleles of the AT-rich minisatellite (3' end of the apolipoprotein B gene) were shown to be in linkage disequilibrium with flanking polymorphisms, an indication that intramolecular recombination events may predominate, like unequal sister chromatid exchange (Ellsworth et al 1995). These observations support a model where the instability of a minisatellite might depend on its DNA sequence, more precisely on its ability to form secondary structures. In fact, GC-rich minisatellites that might form more stable secondary structures compared to the AT-rich ones seem to be more prone to instability than the former. Accordingly, the exceptionally unstable AT-rich minisatellites FRA10B and FRA16B associated with fragile-sites, are formed by short inverted repeats, which enable the formation of hairpin structures (Debrauwere et al. 1997), which might underlie their instability.

Despite this evidence, the mechanisms underlying minisatellite instability in the soma remain unknown. The only insight to potential participants was reported in tumour cells deficient in the mismatch repair that showed MS1 instability (Hoff-Olsen et al 1995). However, dysfunction in the mismatch repair has been associated with microsatellite instability (Aaltonen et al. 1993, Parsons et al. 1993) thus, the observed MS1 instability might be a consequence of its short unit repeat (9 bp), instead of a function of mismatch repair on minisatellite stability.

1.5.4 FROM YEAST TO HUMANS

Thus far, the only model organism used to dissect the molecular basis of mutation events at minisatellites has been *Sacharomyces cerevisiae*. In addition to allow meiotic studies through tetrad analysis, yeast models provide a platform for mitotic studies and pathway dissection. Several human minisatellites have been integrated near defined meiotic hotspots for DSBs so that their repair by recombination events extends to the repeat array causing mutations at the minisatellite.

Studies performed in yeast models have shown that, during meiosis, minisatellite stability depends on the meiotic recombination-initiation protein – Spo11p – and on the DNA loop mismatch repair activity – Rad1p (Jauert et al. 2002). Additionally, during mitosis minisatellite stability can be compromised by mutations affecting genes involved in DNA replication, like Rad27p (a FEN1-like endonuclease responsible for processing of Okazaki fragments), proliferating cell nuclear antigen - PCNA or DNA polymerase III – Pol3 (Lopes et al. 2002, Maleki, et al 2002). An interesting study has found that a minisatellite tract in *S. cerevisiae* can be destabilized during stationary-phase by mutation of zinc homeostasis genes, in a rad50-dependent manner (Kelly et al. 2007). Particularly mutations in genes encoding the high-affinity zinc transporter –ZRT1 and the zinc-dependent transcription factor ZAP1 specifically destabilize minisatellites, since microsatellites and simple insertions were not affected. The authors propose an interesting model where loss of the ZRT1 (directly or through loss of its transcriptional factor ZAP1) reduces the cellular zinc-intake, which can consequently compromise several cellular processes dependent on proteins that use zinc as cofactor. One of those proteins, rad50, which binds to zinc (Hopfner et al. 2002, Wiltzius et al. 2005) and was shown to be

Sequence of the four MS32 repeat types:

E	TGACTCAGAATGGAGCAGGT TGGCC AGGGG
e	TGACTCAGAATGGAGCAGG CGG CCAGGGG
Y	TGACTCAGAATGGAGCAGGT GACC AGGGG
y	TGACTCAGAATGGAGCAGG CGACC AGGGG

Figure 1.8: MS32 minisatellite structure

The diagram shows the MS32 unit repeat sequence and the position of the two polymorphic sites, with the respective base transversions. The table shows the individual sequence of each of the four MS32 repeats and each polymorphism is emphasized in bold.

1.6.2 REGION AROUND MS32 MINISATELLITE

The region around MS32 minisatellite has been well characterized (Jeffreys, et al 1998). Most human minisatellites form clusters in subtelomeric positions but the minisatellite closest to MS32 is 57 kb downstream. Another peculiarity is the high level of *Alu* elements; *Alus* are found throughout the genome, but the region surrounding MS32 locus has a four times higher incidence than the rest of genome. Also, due to its high G/C content, MS32 is refractory to thermal denaturation (probability of DNA helix to open determined for three different temperatures per locus on the basis of overall base composition for each locus) but there is a DNA region showing propensity to opening 4 kb upstream the minisatellite (Murray et al. 1999). However, this region is probably too far away to affect the minisatellite stability, since the O1G/C transversion, responsible for a cis-suppression of the initiation of recombination in and near the minisatellite in germline (see below), does not affect the denaturation observed. Nonetheless, the O1G/C transversion seems to influence the ability of this region to bend, since it decreases the curvature propensity (Murray et al. 1999). A change in flexibility could affect the

nucleosome positioning and, consequently, the chromatin structure, since curved DNA is more easily wrapped around a histone octamer. Finally, according to a database compiling all the predicted G-quadruplexes formed across the genome (www.quadruplex.org), the MS32 locus cannot form G-quadruplexes and only one could be formed approximately 1kb downstream the minisatellite. This was further supported by G4 formation experiments with the MS32 sequence that failed to form the structures (Mergny J., personal communication).

MS32 is situated in a 77 kb non-coding region between genes NID and TM7SF1. Several meiotic hotspots were detected in this region: four in and near the NID gene and three between MS32 and GPR173B gene (Jeffreys et al 2005). A simple tandem-repeat (STR) composed of short unit repeats is located 1080 bp downstream MS32. The STR is 50-52% GC-rich and is flanked upstream by an Alu element. MSNID is a small minisatellite composed of seven repeats of 34 bp palindromic AT-rich sequence (Fig. 1.9). The MSNID germ-line mutation rate was estimated as 3×10^{-5} per gamete, low heterozygosity and is flanked by two meiotic recombination hotspots (Jeffreys et al 2005).

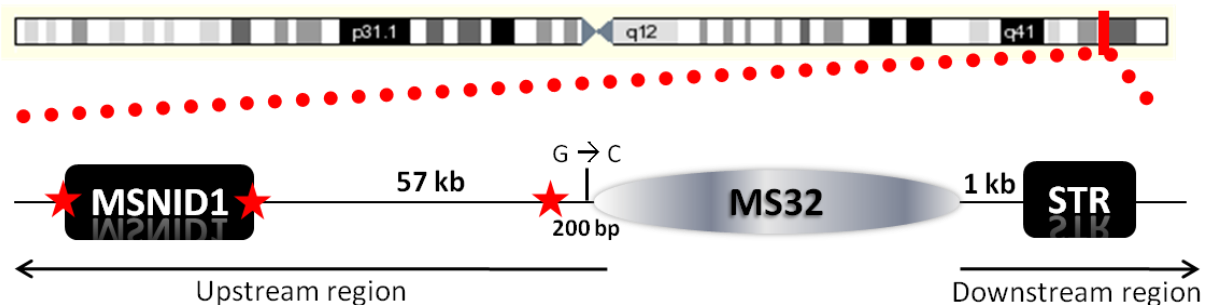


Figure 1.9: MS32 minisatellite region.

The MS32 minisatellite is flanked by the MSNID1 minisatellite at 57 kb and a STR at 1 kb. There are three hotspots in the region (red stars), one 200 bp from MS32 and the other flanking MSNID1. The O1G/O1C base locates between the hotspot and MS32. The region located on the hotspot-side of MS32 is usually referred to as upstream whilst the other side is considered the downstream region of the minisatellite.

1.6.3 MS32 MUTATION MECHANISM IN GERM-LINE

In somatic blood cells, rare somatic MS32 mutants were detected after genomic size-fractioning and SP-PCR, with a mutation frequency of 0.004% per haploid genome, that most likely arise by unequal sister-chromatid exchange and/or intramolecular recombination (Jeffreys, et al 1997). In contrast, SP-PCR in gametic DNA (germ-line) revealed a high instability at MS32 (0.81% per sperm per generation) with a mutational pattern much more complex than somatic cells. MVR-PCR analysis showed polar mutations in the germline, since the changes observed were largely restricted to one end of the MS32 array (Jeffreys et al. 1991, Tamaki et al. 1993). This polarity was also observed in two other human minisatellites, MS31 (D7S21) and MS205 (D1 6S309) (Jeffreys et al. 1993, Monckton et al. 1993). In addition, the germline mutations frequently involve the transfer of repeat units from one allele to another via a complex gene conversion process (Jeffreys et al. 1994). One working model is that minisatellite mutation is driven by cis-acting elements which lie adjacent to the repeat array and introduce double-strand breaks into the 5' end of the repeat unit array (Monckton et al. 1993). In fact, the analysis of the DNA flanking the highly unstable MS32 minisatellite (*DIS8*) by crossover linkage studies revealed a meiotic hotspot centred 200 bp upstream of the array (on the end where the germline mutations predominantly occur). Therefore, a direct effect of the meiotic hotspot on the MS32 minisatellite provides a simple explanation for the polarity observed at this minisatellite. Additionally, a base transversion, known as O1G→ O1C and located 48 bp from the MS32 minisatellite on the hotspot side, directly affects the minisatellite instability since it was associated with the suppression of mutational events in germ-line. Furthermore, the suppression was observed in a variety of MS32 lengths, suggesting that

the single base change is responsible for the suppression of the instability (Jeffreys, et al 1994). In summary, the mutations in germ-line cluster to the 5' end and are mainly complex, polar inter-allelic exchanges (crossovers and conversion-like events). Thus, meiotic recombination is the most plausible mutation mechanism to be affecting MS32 stability, whereas unequal sister chromatid exchange/intramolecular recombination are more likely to cause MS32 mutations in somatic cells (Jeffreys, et al 1994).

1.6.4 MS32 MUTATION MECHANISM IN YEAST

MS32 minisatellite was integrated in yeast and the mutation profile observed in yeast correlated with the previously described in humans: very sporadic mutations in mitotic cells but high instability during meiosis derived by both simple intra-allelic events and more complex inter-allelic events (Appelgren, et al 1997). However, the meiotic mutation rate in yeast was 10x higher than in humans, mutations occurred in both ends of the array, in contrast to the 5' polarity observed in humans and the proportion of inter-allelic events in yeast (around 30%) was lower than in humans (80%) (Jeffreys et al. 1994). MS32 stability has also been analysed in a RAD27 Δ haploid yeast strain and, like other minisatellites (CEB1, MS1) was more unstable than in wild-type, suggesting that RAD27 (yeast flap-endonuclease homologue of hFEN1 and hEXO1) stabilizes minisatellites, probably by processing of replication intermediates. Although the spectrum of mutations of MS32 was not analysed, CEB1 mutations observed in RAD27 Δ haploid yeast has been reported (Lopes, et al 2006). Complex contraction events are frequently accompanied by duplications and depend on the integration position on the genome (the level of destabilization between two integration sites differed).

1.6.5 MS32 MINISATELLITE AND ALT

Attempting to determine the degree of tandem repeat instability in ALT⁺ cells, in loci other than telomeres, Jeyapalan *et al* found that one particular minisatellite, MS32, was ~2000 fold more unstable in these cells than in tel⁺ or normal cells (Jeyapalan et al 2005). In ALT⁺ cells, the MS32 mutation mechanism is not understood but it seems to be far more complex than simple deletions or duplications (as seen in normal somatic DNA). In addition, there is some evidence that it differs from the inter-allelic exchanges seen in the germ-line (Jeyapalan, et al 2005). Since ALT⁺ cells have a high level of inter-telomeric exchange, sister-chromatid exchange events could be promoting the high mutation rate at MS32 minisatellite as well. However, genome-wide sister-chromatid exchange is not increased in ALT⁺ cells compared to Tel⁺ or normal cells and the increase in sister-chromatid exchanges in ALT⁺ cells is restricted to telomeres (Bechter et al 2003). Furthermore, six other minisatellites (MS1, MS31, CEB1, MS205, B6.7 and DXY14) remain stable after ALT activation. Thus, the relaxation of general repression of recombination-like processes in tandem repeats, by ALT activation, does not underlie the instability of MS32, suggesting that other factors may be participating. MS32 instability was also observed *in vivo*, in samples from soft tissue sarcomas and in liposarcomas, hence the instability associated to ALT is not a culture artefact (Jeyapalan et al 2005; Jeyapalan et al 2008).

1.7 PROJECT AIMS

More than a decade after the first descriptions of the ALT pathway, little is still known about its underlying mechanism. One of the markers for the ALT activation is the extreme instability at the hypervariable minisatellite MS32 (Jeyapalan et al. 2005). MS32 is one of the most well studied minisatellites and the mutational mechanisms affecting its stability in both germ-line and soma have already been analysed and described (Jeffreys et al. 1994, Jeffreys, et al 1997), respectively. Nonetheless, the relationship between ALT activation and consequent MS32 instability remains unclear and deciphering it might enlighten some of the molecular processes involved in the ALT process.

Since the reasons triggering MS32 instability in ALT+ cells are not obvious (no similarities with telomeric repeats, no subtelomeric location, etc), several different hypothesis can be raised. This project aims to:

1. Determine whether the MS32 minisatellite is the only minisatellite affected by ALT activation and determine the extent of the instability in the MS32 region.
2. Detect potential gene expression alterations around MS32 minisatellite that could elicit chromatin alterations exposing MS32 minisatellite to the mechanism(s) responsible for its instability in ALT+ cells.
3. Determine the mutational spectrum resulting from the MS32 instability in ALT+ to facilitate the identification of the molecular mechanism involved.
4. Identify other alterations in the MS32 minisatellite region that could explain its instability in ALT+ cells.

CHAPTER TWO: MATERIAL AND METHODS

2.1 MATERIALS

2.1.1 CHEMICALS AND GENERAL REAGENTS

The chemicals were obtained from Cambrex Biowhittaker Molecular Applications (BMA) (Rockland, USA), Fisher Scientific (Loughborough, UK), Flowgen (Ashby de la Zouch, UK) and Sigma-Aldrich Company Ltd (Poole, UK).

Molecular biology reagents were obtained from ABgene (Epsom, UK), Ambion, Inc. (Austin, USA), Amersham Biosciences (Little Chalfont, UK), Applied Biosystems (Warrington, UK), Biogenesis (Poole, UK), Bio-Rad (Hemel Hempstead, UK), Bio Wittaker Molecular Applications (BMA) (Rockland, USA), Dynal Ltd (Merseyside, UK), Invitrogen UK (Paisley, UK), Millipore (Watford, UK), New England Biolabs (NEB) (Hitchin, UK), Perkin Elmer LAS Ltd (Bucks, UK), Promega (Southampton, UK), Qiagen Ltd (Crawley, UK), Raymond A Lamb Ltd (East Sussex, UK), ResGen (Division of Invitrogen Ltd, Paisley, UK), Roche Molecular Biochemicals (Mannheim, Germany), Sigma-Aldrich Company Ltd (Poole, UK), and Stratagene (Amsterdam, The Netherlands).

Specialised equipment was obtained from Applied Biosystems (Warrington, UK), Becton Dickinson-Pharmingen (Oxford, UK), Bio-Rad (Hemel Hempstead, UK), Cecil Instruments (Cambridge, UK), Eppendorf (Hamburg, Germany), Fisher Scientific (Loughborough, UK), Genetic Research Instrumentation (GRI) (Braintree, UK), Helena Biosciences (Sunderland, UK), Heraeus Instruments (Hanau, Germany), Labtech International Ltd (East Sussex), Life Sciences (Cambridge, UK), Perkin-Elmer applied biosystems (Beaconsfield, UK), MJ Research (Waltham, USA) and Walker safety cabinets Ltd (USA).

2.1.2 BUFFERS AND SOLUTIONS

The solutions used throughout all experimental procedures are listed on Appendix-1 and were stored at room temperature, except when indicated.

2.1.3 OLIGONUCLEOTIDES, ENZYMES AND RADIOLABELLED REAGENTS

Primers were designed according to the DNA sequences obtained from the NCBI database (<http://www.ncbi.nlm.nih.gov>) and obtained from Sigma-Aldrich Company Ltd (Poole, UK). A list of all oligonucleotides used on this thesis is shown in Appendix-3.

Restriction enzymes were supplied by New England Biolabs (NEB) (Hitchin, UK). Taq polymerase was supplied by ABgene (Epsom, UK). Pfu polymerase was supplied by Stratagene (Amsterdam, The Netherlands). Proteinase K and RNase A were supplied by Sigma-Aldrich Company Ltd (Poole, UK). γ -³²P-ATP (10mCi/ml) and α -³²P-dCTP (3000Ci/mmol) were supplied by Amersham Pharmacia Biotech (Amersham, UK).

2.1.4 CELL-LINES

The cell-lines used in this PhD thesis are outlined on Appendix-2. The JFCF6T.IJ/11C, JFCF6T.IJ/11E and IICF/a2 cell-lines were a kind gift from Dr. R. Reddel (Cancer research unit, Children's Medical Research Institutes, Sydney, Australia). SuSM1 cell-line was kindly given by Professor O. M. Pereira-Smith (Worcester Polytechnic Institute, USA). SaOS and U2OS cell-lines were a gift from Dr. P. Salomini (MRC, Leicester, UK). WI38, WI38VA13/2RA and NT2D1 were obtained from the European collection of Cell Cultures (ECACC). HT1080, MRC5, GMO3798 were obtained from the American Type Culture Collection (ATCC).

The DNA from Centre d'Etude du Polymorphism Humain (CEPH) family were obtained from Professor H. Cann and Dr. J. Dausset (Paris, France).

The cDNAs for the genes around MS32 minisatellite were obtained from Geneservice Ltd (Cambridge, UK).

2.2 CELL CULTURE

2.2.1 CONDITIONS FOR CULTURE OF CELL-LINES

Table 2.1:

Cell-line	Cell type	Specific medium
SUSM-1	Fibroblast	MEM ¹ + 10% FCS ²
JFCF6T.IJ/11C	Fibroblast	DMEM ³ + 15% FCS + 1% NEAA ⁴
JFCF6T.IJ/11E	Fibroblast	DMEM + 15% FCS
GM03798	Lymphoblastoid	RPMI+10% FCS

¹Minimum Essential Medium (Gibco RBL)

²Foetal Calf Serum (Gibco RBL)

³Dulbecco's Modified Eagles Medium (Gibco RBL)

⁴ non essential aminoacids (Gibco RBL)

All cell-work was performed in a suitable category II laminar flow hood (Walker safety cabinets Ltd). Cells were incubated at 37° C, in saturated humid atmosphere under 5% CO₂ with the specific growing-medium (table 2.1). Sub-culturing was performed when cells reached confluence: the cells were washed with trypsin, trypsinized (1 ml) and diluted into fresh medium in a new flask.

2.2.2 CELL CLONING

The medium of actively growing SUSM1 cells was removed when they were confluent and kept to be used as conditioned medium (contains nutrients produced by cells that are essential to promote growth). The cells were trypsinized to obtain a single-cell

suspension, counted and recovered by centrifugation (1100 rpm, 8 min). The cell pellet was suspended in the conditioned medium and a final concentration of 8 cells/ml was reached after successive dilutions. Each well of a 96-well plate was seeded with approximately 100 μ l in order to obtain 0,8 cells/well. Some visible colonies derived from a single cell were selected for clonal expansion into 25 cm² and the cloned cells were harvested and counted after 20, 30 and 40 population doublings.

2.3 DNA AND RNA EXTRACTION

2.3.1 DNA

Genomic DNA was extracted from frozen cell-pellets, by phenol/chloroform extraction. Firstly, the medium from populations that had reached confluence was removed and the cells trypsinized. The cell-suspension was transferred to a tube with 9 ml of medium + 10% FCS and cells were counted with a haemocytometer. Then, the cell-suspension was centrifuged at 1100 rpm for 8 min., the pellet was washed by resuspension in 4 ml 1X PBS and cells recovered with an additional centrifugation. The obtained cell-pellet was resuspended in 100-250 μ l 1X SSC and stored at -80° C until required.

To isolate DNA from the cell-pellets, cells were lysed with Lysis Buffer and the RNA degraded by addition of RNase (final concentration of 10 mg/ml) at room temperature, for 20 min. Then, proteinase K (final concentration of 20 mg/ml) was added to digest proteins at 55°C, for 6 hours. After the incubation, 1 ml phenol/chloroform/isoamyl alcohol (25:24:1) added in 2 ml phase lock tubes, the mixture was emulsified by gently inverted to minimize DNA shearing and centrifuged at 13000 rpm for 5 min. The DNA-containing aqueous phase (upper) was separated from the phenol and proteins organic phase (lower). DNA was ethanol-precipitated by adding 1 ml of isopropanol and 100 μ l 3M

NaAc (pH 5.5). The tubes were inverted to precipitate the DNA, which was transferred to 1 ml 70% (v/v) ethanol (EtOH). Finally, DNA was again precipitated by centrifugation for 10 minutes at 3000rpm, the EtOH was removed and the pellet air dried. According to the pellet size, DNA was re-suspended in 50-200 ul ddH₂O (nuclease-free water) and stored at 4°C.

2.3.2 RNA

Total RNA was extracted from adherent cells (JFCF6T.IJ/11C and JFCF6T.IJ/11E) and suspension cells (GM03798) using TRI Reagent (SIGMA). This reagent is a mixture of guanidine thiocyanate and phenol that effectively lyses the cells and dissolves DNA, RNA and proteins into a homogeneous lysate. Adding chloroform to this lysate and centrifuging, the mixture separates in 3 phases: an upper aqueous phase containing RNA, an interphase composed of DNA and a lower organic phase formed by proteins. The purified RNA was quantified measuring the absorbance at 260 nm. In water, an absorbance of 1 unit at 260 nm corresponds to 40 mg of RNA per ml ($A_{260} = 1 = 40 \text{ mg/ml}$) and the ratio 260/280 should be higher than 1.70.

2.4. DNA-RESTRICTION DIGESTION.

All the enzymes used for DNA (genomic, plasmid or PCR product) digestion were supplied by New England Biolabs (NEB) (Hitchin, UK) and Fermentas (UK). Digestion conditions and buffer used were as recommended by the supplier. BSA was also added to the reaction when recommended. The incubation time varied from 5 min. to overnight periods. The glycerol concentration (<5%), enzyme concentration and pH (>8) were kept at recommended levels, to avoid star activity.

2.5 CDNA SYNTHESIS

The cDNA synthesis was performed with the Verso[™] cDNA kit (Thermo Fisher Scientific). 1 µg of RNA was denatured for 5 min at 70°C and 9 µl of previously prepared reaction mix (1x cDNA synthesis buffer [Thermo Scientific], 500 µM each dNTP, 1 µl of random hexamers, RT enhancer [DNA degradation] and 1 µl of Verso enzyme mix). The reverse transcription was performed at 42°C for 30 minutes and the reaction was stopped by heat inactivation at 95°C for 2 minutes. To the final reaction, 80 µl of dH₂O were added to obtain a final working concentration of 100 ng/µl.

2.6 POLYMERASE CHAIN REACTION (PCR)

The regions of interest throughout the development of this thesis were amplified by PCR. To minimize the contamination risk, all PCR reaction from genomic DNA and PCR mixes for plasmid or previously PCR-amplified templates were prepared in a category II laminar-flow hood with equipment exclusively used for PCR purposes. The latter templates were then added to the PCR mix on the bench.

The PCR reactions were prepared in 0.2ml sterile tubes and performed on Peltier Thermal Cycler (PCT)-200 engine thermal-cycler (MJ research). Generally, 10 ng of DNA was amplified in a 10µl reaction containing: 1x 11.1x-buffer (to obtain the final concentrations: 45mM Tris-HCl [pH 8.8], 11mM ammonium sulphate, 4.5mM magnesium chloride, 0.045% 2-mercaptoethanol, 4.4µM EDTA pH 8.8 at 25°C, 1mM of each dNTP, and 13 µg/ml BSA), 0.3-0.4 µM of each primer, 40 mM of Tris and 0.07 U of Taq polymerase (ABgene, Epsom, UK). When it was necessary to increase the PCR fidelity, Pfu polymerase (1:20 (U/U)) was added to the reaction. The PCR conditions were specific to each reaction, accordingly to the primer annealing temperature and fragment size, but

usually common on the following steps: 1 min. of denaturation at 96°C, followed by 20-38 cycles of: 20 sec. of denaturation at 96°C, 30 sec. at the appropriate annealing temperature followed by a size-dependent (usually 1 min. per 1 kb of region to be amplified) elongation step at an appropriate temperature. The tables below represent the PCR mix and conditions used for each DNA target amplified during the development of this thesis.

The PCR products were resolved by, unless differently stated, 1.2% agarose gel electrophoresis (see section 2.8).

Tables 2.2:

PCR mix for STR amplification		Conditions for STR amplification		
Final conc.	Reagent (stock concentration)	Temperature	Time	Cycles
40 mM	1M Tris	96°C	1 min.	x5 cycles
0.07 U	0.5 U/μl Taq	96°C	1 min.	
0.4 μM	32+1.4F primer	68°C	1 min.	
0.4 μM	32+0.6R primer	70°C	2 min.	x33 cycles
1x	11.1x buffer	96°C	1 min.	
		67°C	1 min.	
		70°C	2 min.	

Tables 2.3:

PCR mix for MSNID amplification		Conditions for MSNID amplification		
Final conc.	Reagent (stock concentration)	Temperature	Time	Cycles
40 mM	1M Tris	96°C	1 min.	x33 cycles
0.07 U	0.5 U/μl Taq	96°C	20 sec.	
0.3 μM	M-59.0F primer	57°C	30 sec.	
0.3 μM	M-57.7R primer	61°C	5 min.	
1x	11.1x buffer			

Tables 2.4:

PCR mix for IMAGE clones amplification		Conditions for IMAGE clones amplification		
Final conc.	Reagent (stock concentration)	Temperature	Time	Cycles
40 mM	1M Tris	96°C	1 min.	x30 cycles
0.07 U	0.5 U/μl Taq	96°C	20 sec.	
0.4 μM	T7 or M13 primer	59°C	30 sec.	
0.4 μM	T3 or M13rev. primer	70°C	3 min.	
1x	11.1x buffer			

Tables 2.5:

PCR mix for MS32 amplification		Conditions for MS32 amplification		
Final conc.	Reagent (stock concentration)	Temperature	Time	Cycles
12 mM	1M Tris	96°C	1 min.	x25 cycles
0.05 U	0.5 U/μl Taq	96°C	20 sec.	
0.0025 U	0.05 U/μl pfu	59°C	30 sec.	
0.2 μM	32B primer	70°C	10 min.	
0.2 μM	32E primer	56 °C	1 min.	
1x	11.1x buffer	70 °C	10 min.	

Tables 2.6:

PCR mix for MS32 probe amplification		Conditions for MS32 probe amplification		
Final conc.	Reagent (stock concentration)	Temperature	Time	Cycles
12 mM	1M Tris	96°C	1 min.	x36 cycles
0.07 U	0.5 U/μl Taq	96°C	20 sec.	
0.015 U	0.05 U/μl pfu	66°C	30 sec.	
0.4 μM	32D2 primer	68°C	2 min.	
0.4 μM	32E primer			
1x	11.1x buffer			
1 μl	DNA Ceph member 104.5 (25 ng/μl)			

Tables 2.7:

PCR mix for STR probe amplification		Conditions for STR probe amplification		
Final conc.	Reagent (stock concentration)	Temperature	Time	Cycles
12 mM	1M Tris	96°C	1 min.	x5 cycles
0.07 U	0.5 U/μl Taq	96°C	1 min.	
0.015 U	0.05 U/μl pfu	68°C	30 sec.	
0.4 μM	32+1.4NNF primer	70°C	1.5 min.	
0.4 μM	32+0.6F2NR primer	96°C	1 min.	
1x	11.1x buffer	65°C	30 sec.	x34 cycles
1 μl	HT1080 DNA (20 ng/μl)	70°C	1.5 min.	

Tables 2.8:

PCR mix for 33.15 and 33.6 probes amplification		Conditions for 33.15 and 33.6 probes amplification		
Final conc.	Reagent (stock concentration)	Temp.	Time	Cycles
12 mM	1M Tris	96°C	1 min.	x33 cycles
1x	11.1x buffer	96°C	20 sec.	
0.07 U	0.5 U/μl Taq	57°C	30 sec.	
0.015 U	0.05 U/μl pfu	70°C	1.5 min.	
0.15 μM	T7 primer			
0.15 μM	T3 primer			
1 μl	33.15 pBlueScript (2 ng/μl) 33.6 pBlueScript (1.2 ng/μl)			

2.6.1 SMALL-POOL AND SINGLE-MOLECULE PCR

Small-pool and Single-Molecule PCR (SP-PCR and SM-PCR, respectively) are alternatives to the PCR technique where aliquots from serially diluted genomic DNA containing approximately 20 (SP-PCR) or a single molecule (SM-PCR) are amplified. The subsequent resolution of the PCR products by gel electrophoresis allows the identification (and isolation in SM-PCR) of abnormal-length molecules. Approximately 6 pg of DNA will contain 1 molecule consequently, to amplify 20 molecules per reaction, 120 pg of DNA should be added to each PCR tube. The aimed dilutions were achieved by serial dilutions from a 10 ng/μl *Mbo*I-digested genomic DNA stock with a carrier tRNA buffer. The SP-PCR or SM-PCR mixes and conditions used for each amplicon are shown in the tables in section 2.2.2.1, except for the DNA input (120 pg or 20 pg of DNA per SP-PCR or SM-PCR reactions, respectively) and the addition of the carrier tRNA to a final concentration of 1 ng/μl.

The quantification of the number of amplifiable DNA molecules present in the limiting dilutions of genomic DNA by Poisson analysis permits the direct measurement of mutation frequencies. For the Poisson analysis, serial dilutions of the DNA were performed

with tRNA buffer, so that a final concentration of 20 pg/μl was achieved for the amplification of 0.2-1.5 molecules per reaction (a total of 10 reactions were performed for each nr. molecules trial). A correction factor $[-\ln(\text{negative tracks}/\text{total reactions})]$ was multiplied by the ratio of final DNA input in SP-PCR and Poisson reactions to determine the total number of amplifiable molecules per reaction. Consequently, the total number of molecules amplified on the SP-PCR experiment was calculated, which determined the mutation frequency or mutation rate, if the population divisions were known.

The SP-PCR and SM-PCR products were resolved on 1.2% agarose gel electrophoresis (Tables 2.5, section 2.8) and detected by Southern-hybridization (see section 2.9) with a radioactive-labelled MS32 probe (see section 2.9.1).

2.6.2 MINISATELLITE VARIANT REPEAT (MVR)-PCR

Minisatellite-variant repeat PCR (MVR-PCR) is another PCR amplification that takes advantage of the natural repeat variation within minisatellites to map the interspersed pattern of each of those variant repeats along the array. The alignment of MVR-PCR maps of mutant-length with the progenitor (most common) alleles facilitates the analysis of the processes underlying minisatellite instability. In this study, a forward and reverse four-state MVR-PCR (Tamaki et al. 2004) methodology was used to determine complete maps of the mutant-length molecules identified by SM-PCR (see section 2.4.2.2).

The MS32 amplification master-mix specified in section 2.6 was divided into four separate MVR-PCR reactions and a variant-repeat specific primer added to each one of them (3.6 nM primer TAG-E, TAG-e or TAG-y and 7 nM of TAG-Y). The isolated SM-

PCR products were diluted 1:20 in dH₂O and 0.5 µl were added as template for the each of the four MVR-PCR mixes on the bench, to avoid PCR-contamination.

The MVR-PCR products were resolved by agarose gel electrophoresis (see section 2.8) and detected by Southern-hybridization (see section 2.9) with a radioactive-labelled MS32 probe (see section 2.9.1).

Tables 2.9:

PCR master-mix for MVR-PCR		Conditions for MVR-PCR		
Final conc.	Reagent (stock concentration)	Temp.	Time	Cycles
12 mM	1M Tris	96°C	1 min.	
1x	11.1x buffer	96°C	20 sec.	x4 forward x5 reverse cycles
0.05 U	0.5 U/µl Taq	64°C	30 sec.	
0.0025 U	0.05 U/µl pfu	70°C	3 min.	
0.2 µM	TAG primer	96°C	20 sec.	x13 forward x19 reverse cycles
0.2 µM	32HIC primer (forward MVR) 32E primer (reverse MVR)	62°C	30 sec.	
0.5 µl	SM-PCR product (1:20)			
		70°C	3 min.	

2.6.3 TCA REACTION

A reaction mix was prepared with 1 µg of *ExoV*-digested genomic DNA, 1 µM of the respective primer (telomere or MS32-specific) and 1x annealing buffer (see appendix-1). the reaction was denatured for 5 minutes at 96°C and the annealing of the primer to the DNA was achieved by letting the reaction cool down to 25°C for approximately 1 hour. The DNA was precipitated with sodium acetate and ethanol and resuspended in 20 µl dH₂O. The annealed-DNA solution was divided into two tubes: the positive and a negative reaction (with or without Ø29 polymerase, respectively). To both tubes 9.25 µl of premix (final 2x Ø29 buffer, 0.5 mM dNTP mix and 6.25 µl dH₂O) and 7.5 U of Ø29 polymerase

(+ reaction) or 0.75 μl dH_2O (- reaction) were added. The amplification reaction was carried out at 30°C for 12 hours and stopped by heat inactivation at 65°C for 20 minutes.

To the final products, 5 μl of loading buffer (100 μl 6x LBI, 3 μl NaOH [10M] and 1.2 μl EDTA [0.5M]) were added and the mixture was loaded into a denaturing gel (0.8% agarose [HGT], 50 mM NaOH, 1 mM EDTA) for electrophoresis resolution at 2V/cm, under alkaline conditions (50 mM NaOH, 1 mM EDTA). After resolution, gel was washed 7 minutes in depurinating solution, 30 minutes in denaturing solution and 30 minutes in neutralizing conditions and Southern-hybridized as usual (section 2.9).

2.6.4 QPCR

All qPCR reactions were performed with the MESA GREEN qPCR Master Mix Plus (Eurogentec). The reactions were prepared in a final volume of 20 μl with 1x reaction buffer, 300nM of forward and reverse primers (unless otherwise stated) and 2 μl of cDNA (100 ng/ μl). The amplification was carried out under the following conditions (see table 2.10), on a DNA Engine Opticon 2 system (MJ Research). After the amplification, a melting curve was performed between 45°C to 96°C, with a 1 second hold every 0.5°C, followed by a plate read.

Table 2.10:

Conditions for qPCR amplification		
Temperature	Time	Cycles
95°C	5 min.	
95°C	15 sec.	x40 cycles
58-60°C	20 sec.	
72°C	40 sec.	
Plate read		

2.6.5 MLPA

The MLPA reactions were performed with the X-014 test MLPA kit (MRC-Holland) that includes all the PCR reaction reagents, as well as the probemix. Genomic DNA was diluted to a working stock of 30 ng/ul using dH₂O and 150 ng were denatured for 5 min at 98°C. To each DNA sample 1.5 µl MLPA buffer and 1.5 µl probemix were added when the sample-reaction reached the 25 °C. The mixture was incubated for 1 minute at 95 °C and left overnight for 60 °C, to ensure hybridization of the probemix to the target sequences. The reaction was lowered to 54 °C and 32 µl of ligase buffer mix (3 µl Ligase-65 buffer A, 3 µl Ligase-65 buffer B and 25 µl water) were added and mixed by pipetting up and down. The reaction was incubated for 15 minutes at 54 °C, followed by 5 minutes at 98 °C. The ligation products were stored at 4 °C until used.

In a new PCR tube, 15 µl of PCR buffer mix (2 µl SALSA PCR buffer, 13 µl water) and 5 µl of ligation product were mixed and placed at 60 °C in a PCR machine. 5 µl of PCR mix (1 µl SALSA primers, 1 µl SALSA enzyme dilution buffer, 2.75 µl water and 0.25 µl SALSA polymerase) were added to the reaction and a PCR cycling was performed as follows:

Table 2.11:

Conditions for MLPA amplification		
Temperature	Time	Cycles
95°C	30 sec.	x35 cycles
60°C	30 sec.	
72°C	1 min.	
72°C	20 min	

Following the PCR reaction, 3 µl of PCR product were mixed with 10 µl of internal size standard (20 µl LIZ 500 [ABI] and 1 ml formamide) and denatured for 3 min at 95 °C before placed on ice.

The products were resolved by electrophoresis ABI 3100 Genetic Analyzer (Applied Biosystems) with 16 36cm-long capillaries according to the following settings: run at 60 °C, POP-7 polymers, capillary fill volume 6500, pre-run voltage 15 kV for 180 sec, injection voltage 3 kV for 23 sec and run at 15 kV with a data delay time of 1 sec. The run was performed for 1500 sec.

2.7 SEQUENCING.

The PCR products were either cleaned by EXO/SAP reaction (see section 2.6.1) or recovered after resolution from the agarose gel (Qiagen extraction kit [Qiagen]), according to the manufacturer's instructions. 20-40 ng/kb of PCR products were mixed with 1 µl of Big dye mix version 3.1 (Applied Biosystems), 1.5 µl 5x sequencing buffer and 3.2 µmol of the sequencing primer. The reactions were cycled for 10 sec. at 96°C, 5 sec. at 50°C and 4 min. at 60°C for 27 cycles. After cycling, 10 µl dH₂O and 2 µl 2.2% SDS were added to the reactions and heated at 98°C for 5 min, followed by a 10 minute incubation at 25°C. Performa DTR Gel filtration columns were prepared by centrifugation at 3.4*1000 rpm for 3 min in a Eppendorf 5415. The columns were placed in clean tubes and the samples applied directly to the gel bed. Finally, samples were eluted by centrifugation (as above) and submitted to the Protein and Nucleic Acid Chemistry Laboratory (PNACL, University of Leicester, UK). The sequence data was analysed and edited with the Factura™ Release 1.2.0 (Applied Biosystems, Warrington, UK) and sequences were aligned with reference sequences obtained from the NCBI site (<http://www.ncbi.nlm.nih.gov/>) and edited in Autoassembler Release 1.4.0 (Applied Biosystems, Warrington, UK).

2.7.1 EXO/SAP CLEANING

PCR products were cleaned by adding 1.5 U of shrimp alkaline phosphatase SAP [Roche] and 10U exonuclease I (ExoI) [NEB]. The reactions were incubated at 37°C for 1 hour and stopped by heat inactivation at 85°C for 15 minutes.

2.8 AGAROSE GEL ELECTROPHORESIS.

DNA fragments were separated by horizontal agarose gel electrophoresis. Agarose gels (0.4-4.0% (w/v)) were prepared by boiling agarose in 1xTBE (which contained Ethidium Bromide when required) and cast in sealed gel trays. Gel combs were used to generate wells of desired volume and gels were left to solidify at room temperature. DNA samples were mixed with DNA loading dye and loaded in the wells next to the appropriate DNA size markers. The 1Kb, 100bp [supplied by New England Biolabs (NEB) (Hitchin, UK)], ϕ X174/HaeIII or λ DNA/HindIII DNA ladders were used, supplied by ABgene (Epsom, UK). Ethidium bromide-stained DNA was visualised under UV light using a UV-transilluminator (UVP life sciences, Cambridge, UK).

2.8.1 ISOLATION OF DNA FROM GEL.

PCR purification/DNA fragment isolation was carried out using the QIAquick gel extraction kit [Qiagen Ltd (Crawley, UK)]. Resolved DNA fragments were excised from a 1-1.5% (w/v) low melting point agarose [Invitrogen (Paisley UK)] gel prepared with 1xTAE and stained with Ethidium bromide. Low melting point agarose gels melt at 50°C, which is well below the DNA melting point. DNA was extracted using the QIAquick gel extraction kit according to the manufacturer's protocol. Essentially, excised gel fragments were melted at 50°C and the solution was passed through a column. DNA was bound on

the QIAquick silica membrane, washed and purified. Following the removal of residual contaminants DNA was eluted and fragment size was confirmed by agarose gel electrophoresis.

2.8.2 2D-GEL ELECTROPHORESIS

2-dimensional gel electrophoresis was used to detect circular DNA. The first dimension was performed by loading 10 µg of digested genomic DNA on a 0.4% agarose gel (Seakem HGT agarose in 1x TBE with no ethidium bromide) and resolving the DNA at 1 V/cm, for 18 hours. The gel made measured 20 x 20 cm and the wells were made with combs of 4 mm per 2 mm dimension. For the second dimension, a 1 % agarose gel (Seakem HGT agarose in 1x TBE + ethidium bromide) gel was prepared and cooled to 55°C. The DNA track from the 1st dimension gel was cut with a sterile scalpel blade and placed in a new gel tray (flipped 90° to the right). The 1% gel was poured in the tray so that the DNA track was completely covered. After solidifying, the second dimension was run at 5 V/cm for 5.5 hours. The gel was photographed with a UV transilluminator and Southern-hybridized as mentioned in section 2.9.

2.9 SOUTHERN BLOTTING.

After adequate gel electrophoresis resolution, the agarose gels were prepared for blotting by removing the excess gel with a sterile scalpel. Each gel was washed, unless differently stated, under the following conditions: 2x 5 min in depurinating solution (0.25M HCl), 2x 15 min in denaturing solution (0.5M NaOH, 1M NaCl) and 2x 20 min in neutralizing solution (0.5M TRIZMA Base, 3M NaCl). In the meantime, the blotting device was set-up by filling a deep tray with 20x SSC, a glass was placed over the tray and one

sheet of Whatmann 3MM paper was placed over the glass with the edges sank on the 20x SSC of the tray, so that the paper remains soaked in the solution. After the washes, the gel was placed upside down onto the soaked Whatmann paper and covered by a membrane previously cut-to-fit the size of the gel (MAGNA nylon transfer membrane, GE Healthcare). On top, two Whatmann paper sheets soaked in 2x SSC and also fitting the gel-size were placed and a glass pipette used to remove any air-bubble present between the different layers. Finally, the Whatmann sheets were topped by piles of paper towels and, covering the blotting device, another glass on top of which an appropriate weight was rested. The paper towels were changed a few times for the first hour, to maximize the soaking process, and the blotting apparatus was left between of five hours-overnight.

After blotting, the nylon membrane was rinsed in 2x SSC to remove any debris, dried at 80°C for 10 minutes and exposed to UV light (70 mJ/cm²) to covalently link the DNA to the membrane. The membrane was stored at room temperature unless immediately used.

2.9.1 PROBE LABELLING

Double-stranded DNA probes were labelled with α -32P-dCTP (3000 Ci/mmol) in 30 μ l reactions. 15 ng target-specific PCR-amplified or 2.5 ng of the markers (λ HindI and Φ X174/HaeIII) was denatured by boiling for 5 minutes. After DNA denaturation, 6 μ l 5x Oligo Labelling buffer (OLB), 1.2 μ l BSA (0.4 μ g/ μ l stock), 7.5 U of Klenow and α -32P-dCTP (20 μ Ci for locus-specific probes or 5 μ Ci for marker DNA) were added to the reaction and incubated at either 37°C for at least 5 hours or at room-temperature overnight.

After the labelling, the probe reaction was transferred to a glass tube and 50 μ l of oligo-stop solution (OSS), 35 μ l high molecular weight salmon (*E.coli* 3 mg/ml for 33.15

and 33.6 pokes), 25 μ l 2M sodium acetate and 470 μ l 100% ethanol were added. The DNA probe was precipitated by gentle tube agitation. After ethanol removal, the pelleted probe was washed with 500 μ l of 70% ethanol and re-suspended in 500 μ l dH₂O. Before hybridization, probe was denatured at 100°C for 3 minutes.

2.9.2 HYBRIDISATION AND WASHING

The membrane was soaked in dH₂O, rolled between hybridization-meshes and transferred into a hybridisation bottle containing ~20 ml of the hybridisation solution (modified Church buffer pre-heated to 65°C) and pre-hybridised for at least 30 minutes at 60-65°C (dependent on the probe used). After pre-hybridisation, the solution was replaced by another 20 ml of modified Church buffer and the denatured and labelled probe was added to the bottle and hybridised overnight at 60-65°C.

After hybridization, the excess probe was removed by washing the membrane with the washing solutions (see Table for specific conditions. After excess liquid had been removed, the membrane was wrapped in saran-wrap and exposed to a phosphorimager screen between 5-48 hours.

To enable re-hybridisation membranes were stripped by immersing in boiling 0.1xSSC, 0.1% (w/v) SDS for 10-20 minutes. The procedure was repeated if the radioactivity detected with a Geiger counter exceeded 5counts/second. Stripped membranes were placed against a phosphorimager screen to check for any remaining radioactivity. If no background signal was detected, the membrane was re-used.

Table 2.12:

Probe	Hyb + wash temp.	Washing conditions
Telomere (TTAGGG)	65°C	0.1x SSC, 0.1 SDS for 10 min
MS32 + MSNID (PCR products)	65°C	40mM NaHPO ₄ , 0.5% SDS for 5 min x1 0.2x SSC, 0.1% SDS for 10 min. x2
MS32 (genomic)	65°C	0.5x SSC, 0.1% SDS x2
STR	60°C	0.5x SSC, 0.1% SDS for 10 min. x2
33.15 and 33.6	65°C	2x SSC, 0.1% SDS for 10 min. x2 1.5x SSC, 0.1% SDS for 10 min. x1
Tel G (TGAGGG) Tel K (TCAGGG) Tel J (TTGGGG)	65°C	0.5x SSC, 0.1 SDS for 10 min. x3

2.10 METHYLATION-STATUS ANALYSIS

1 µg of genomic DNA was *Bam*HI-digested (20-40 U in a total 10 µl reaction) for 4 hours at 37°C. The digestion was confirmed by resolving 200 ng in a 0.8% agarose gel electrophoresis (see section 2.6). The digested genomic DNA was sodium-bisulfite treated using the EpiTect kit (Qiagen, Crawley, UK) according to the manufacturer's protocol, except for a modified cycling program (developed by Rita Neumann, Department of Genetics, University of Leicester), for maximum conversion of unmethylated cytosine residues. The treated DNA was cleaned without the addition of carrier RNA to the buffer BL. The pure treated-DNA was eluted from the spin columns in 20 µl of buffer EB and used as template for the primary PCR reactions mentioned on the tables below. The primary-products were then used for a secondary-PCR reaction (1 µl) as template and the products resolved by 1% agarose gel electrophoresis (see section 2.8). After Exo/SAP cleaning, the products were sequenced and submitted for analysis.

Tables 2.13:

Bisulfite-treatment cycling conditions:		
Temperature	Time	Cycles
99°C	3 min.	
96°C	30 sec.	x 25 cycles
55°C	20 min.	
20°C	∞	

Primary-PCR mix for 5'-end analysis		
Final	Reagent (stock conc.)	
12 mM	1M Tris	
0.07 U	0.5 U/μl Taq	
0.025 U	0.05 U/μl pfu	
0.2 μM	32-1.4btF primary primer 32-0.9btF secondary primer	
0.2 μM	32-0.16btR primary primer 32-0.18btR secondary primer	
1x	11.1x buffer	
1 μl	eluted DNA	
Primary conditions for 5'-end		
Temperature	Time	Cycles
95°C	30 sec.	x 1 cycle
57°C	1 min.	
68°C	3 min.	
96°C	20 sec.	x 38 cycles
57°C	30 sec.	
68°C	1.3 min.	
68°C	15 min.	
Secondary conditions for 5'-end		
Temperature	Time	Cycles
96°C	1 min.	x 38 cycles
96°C	20 sec.	
58°C	30 sec.	
68°C	1 min.	

Primary-PCR mix for 3'-end analysis		
Final	Reagent (stock conc.)	
12 mM	1M Tris	
0.07 U	0.5 U/μl Taq	
0.025 U	0.05 U/μl pfu	
0.2 μM	32+01btF primary primer 32+02btF secondary primer	
0.2 μM	32+05btR primary primer 32+04btR secondary primer	
1x	11.1x buffer	
1 μl	eluted DNA	
Primary conditions for 3'-end		
Temperature	Time	Cycles
95°C	30 sec.	x 1 cycle
58°C	1 min.	
68°C	3 min.	
96°C	20 sec.	x 38 cycles
58°C	30 sec.	
68°C	1.3 min.	
68°C	15 min.	
Secondary conditions for 3'-end		
Temperature	Time	Cycles
96°C	1 min.	x 38 cycles
96°C	20 sec.	
55°C	30 sec.	
68°C	1 min.	

2.11 MICROARRAY

2.11.1 ARRAY PREPARATION

Prior to array printing, poly-L-lysine coated slides were prepared by placing the slide-carriers into chambers covered by cleaning solution (70g NaOH, 420 ml 95% ethanol in final volume of 700 ml) and rocked for 2 hours. The cleaned slides were quickly transferred to dH₂O to avoid air exposition and rinsed in 4x dH₂O. The liquid was removed by centrifugation for 5 min at 500 rpm and slides were transferred to a poly-L-lysine solution (70 ml poly-L-lysine [Sigma] and 70 ml PBS in 560 ml dH₂O) and rocked up to 1 hour (this step was carried out in polypropelene boxes). The slides were transferred to fresh dH₂O and rinsed in 5x dH₂O, followed by centrifugation for 5 min at 500 rpm. The slides were transferred to a vacuum oven and dried for 10 min at 45°C. The slides were labelled with a batch number and stored in a closed box for a minimum of 2 weeks. Before printing, the hydrophobic ability of the slides was checked to ensure full coating.

2.11.2 SAMPLE LABELLING WITH FLUORESCENCE PROBES

20 µg of previously dried RNA sample was dissolved in 13 µl dH₂O and 1µl of oligo Tanchor (dT25 8µg/µl) and 1µl of hexamers (3 µg/µl). The mix was heated for 5 min at 95°C and for 10 min at 70°C, followed by quickly ice-cooling for 1 minute. The cDNA synthesis was carried out by adding 14 µl of the labelling mix (0.01M DTT, 1x first strand buffer [Invitrogen], 0.3 mM aadUTP [Ambion], 0.2mM dTTP and 0.5mM of the three other dNTP [Amersham Biosciences]) and 1 µl of Superscript III (Invitrogen) and incubated at 50°C overnight.

After first-strand cDNA synthesis, the RNA was hydrolysed by adding 0.5M EDTA and 1N of NaOH and incubation for 15 min at 65°C, followed by addition of 1M HEPES pH 7.0.

The cDNA was purified using Microcon 30 filters (Milipore) by adding the sample into 375µl water previously putted in the filter and spinning at 12K rpm for 7 min. Another 450 µl of water were added to the column and discard by repeating the centrifugation. The column was inverted and placed into a new collection tube and the cDNA was recovered by repeating the centrifugation conditions. At this stage, the cDNA product was quantitated on a nanospec. The aminoallyl cDNA was stored at -20°C until needed.

The Alexa dyes (fluor 555 and fluor 647 [Molecular probes]) were prepared by adding 4 µl of DMSO and stored at -20°C in dark conditions. The cDNA sample was dried and resuspended in 0.5 µl of carbonate buffer (1M HCl pH 9.0) and 3.5 µl water. 1 µl of the DMSO + Alexa dye were added to the mixture and incubated at room temperature for 1 hour in the dark. 4.5 µl of hydroxylamine (4M) were added and the reaction was incubated for another 15 minutes in the dark. The labelled-samples to be hybridized together were combined and the labelled cDNA was cleaned using qiagen columns (Qiagen). Briefly, 250 µl of buffer PB were added to the combined sample and the mixture placed in a Qiagen Quick Spin PCR column and spinned for 1 min at 13K rpm. 750 µl buffer PE was used for washing, followed by two similar centrifugations to remove the washing buffer. The labelled-combined sample was eluted with 60 µl of EB buffer, by collecting the volume after spinning at 13K rpm for 1 minute. The labelling was checked with the nanospec.

2.11.3 HYBRIDIZATION

The labelled-combined samples were mixed with 1 μ l of polyA (1 μ g/ μ l), 10 μ l human Cot1 (1 mg/ml) and 1 μ l tRNA (4 mg/ml [Gibco]) and dried. The human Cot1 avoids non-specific binding of Alu fragments to the target sequences. The probes were re-suspended in 24.5 μ l of the hybridization buffer (5 ml deionized formamide, 500 μ l 50x Denhardtts, 1 ml water and 500 μ l 10% SDS filtered through a 0.45 μ syringe filter) and 10.5 μ l of 20x SSPE (3M NaCl, 10mM NaH₂PO₄, 20 mM EDTA). The mixture was denatured at 95°C for 2 min and incubated at 42°C for up to 1 hour.

2.11.3.1 PRE-HYBRIDIZATION ARRAY PREPARATION

The array coverslips were washed in 1% SDS for 30 minutes, followed by 5x 5 minutes water washes. Before use, coverslips were dried by spinning at 1000 rpm for 5 min. The DNA in the printed arrays was denatured by heating the slide to 100°C for 2 minutes and washed in 0.2% SDS for 2 minutes, before drying by centrifuging at 1500 rpm for 4 min.

2.11.3.2 SETTING UP MICROARRAY

The labelled-combined sample was placed on the left of the array and covered by a coverslip. 25 μ l of water were placed in the bottom of the hybridization chamber before placing the array slide. The lids were screwed tight and placed in a 50°C water bath overnight.

2.11.4 ARRAY WASHING

The inverted slides were placed in 1x SSC, 0.03% SDS for 10 min. To remove the SDS, slides were washed in 0.2x SSC for 5 mi, before a final wash of 0.05x SSC. The

liquid was removed by maximum possible centrifugation and slides kept on a box until scanned.

2.12 DOT BLOTTING.

Before blotting, two 13 x 9.5 cm pieces of Whatmann 3MM paper and 12.5 x 9cm of Hybond nylon membrane (Amersham) were prepared by soaking in water. The two Whatmann paper sheets were placed on the dotblot device, followed by the nylon membrane and the dotblot apparatus was assembled. The vacuum-water line was attached.

After PCR amplification, 160 μ l of denaturing mix (0.5M NaOH, 2M NaCl, 25 mM EDTA with bromophenol blue powder) were added to each sample and the mix was blotted onto the membrane (under vacuum). Each dot was washed with 120 μ l of 2x SSC to neutralise the DNA and, after dismantling the apparatus, the membrane was dried for 5 min at 80 °C and the DNA UV-crosslinked to the membrane.

2.13.1 PROBE LABELLING

The Alu-probe (7 μ g/ml) was denatured for 3 min at 100 °C. γ -32P-ATP was incorporated in a labelling reaction containing: 1 μ l 10x kinase mix (700 mM Tris-HCl pH7.5, 100mM MgCl₂, 50mM spermidine trichloride and 30mM dithiothreitol), 0.35 μ l T4 Polynucleotide Kinase (stock: 10U/ml) and 0.12 μ l γ -32P-ATP (stock: 10mCi/ml) and the denatured Alu-probe. T4 kinase catalyses the transfer of a phosphate group from the γ position of the ATP molecule to the 5' hydroxyl terminus of the probe. The reaction was incubated at 37 °C for 2 hours. In the meantime, the dot-blot membrane was pre-hybridized with modified Church buffer for 10 min. Prior to hybridisation, 20 μ l of kinase stop solution (25mM diNa EDTA, 0.1% SDS and 10mM ATP) were added to inactivate the T4 kinase

enzyme. The labelled-probe was hybridized to the membrane with modified Church buffer, at 48 °C for 4 hours.

After hybridization, excess probe was removed by washing membrane with boiling 1% SDS solution until Geiger counter detected less than 5 cps. The membrane was then rinsed in 2x SSC, the excess liquid removed and, after wrapping in saran wrap, exposed to a phosphorimager screen overnight.

3. CHAPTER 3: GENOME INSTABILITY IN ALT+ CELLS

3.1 BACKGROUND

Although the ALT mechanism is not fully understood, evidence that recombination underlies the telomere elongation has been demonstrated (Dunham et al. 2000; Varley et al. 2002). ALT-telomeres have also been reported to undergo progressive shortening followed by sudden elongation events (Murnane et. al 2004). The observed telomere dynamics in ALT+ cells is proposed to cause critically short telomeres prone to be recognized as DSB, which can trigger initiation of the recombination process (McEachern et al 1996). Thus, a break-induced replication process might occur by the invasion of the shortened telomere of a template with telomeric repeats, followed by the copying of the donor sequence to the invading telomere. These ALT-recombination events seem to occur exclusively at telomeres, since the overall genomic homologous recombination has been shown to be identical to that in Tel+ cells, suggesting that the high frequency of recombination at ALT-telomeres does not extend to subtelomeric or other regions within the genome (Wright et al. 2003). In fact, no differences in sister chromatid exchange rates at interstitial locations were detected between ALT+ and Tel+ cells and the high telomeric sister-chromatid exchange observed in ALT+ cells was not observed in non-ALT Bloom syndrome cells, which are characterized by very high general sister-chromatid exchange rates (Reddel et al 2004). Thus, ALT events seem to be triggered by a specific telomere signal (perhaps the extreme short size of some telomeres), initiating recombination-like processes that are thought to be naturally blocked in normal and Tel+ cells. The occurrence of TTAGGG variants, such as TGAGGG or TCAGGG, at the base of the telomeres and sequences sharing great

homology between different chromosomes, might behave as hot-spots for recombination in ALT+ cells (Allshire et al., 1989; Baird et al., 1997; Varley et al., 2002).

Although the current evidence suggests an exclusive role of the ALT-mechanism at telomeres, a potential effect on other repeated genomic loci has not been fully investigated. Microsatellite instability (MSI) has been associated with the disruption of mismatch repair mechanism - MMR (Liu et al 1995) and in yeast, MMR disruption, especially *MSH2*, increases the proliferation of telomerase-negative survivors. Furthermore, MMR-defective colon cancer cells showed some ALT-markers (T-SCE but no APBs), when telomerase was inhibited by the expression of a double-mutant hTERT, indicating that an ALT-like mechanism may arise when telomerase is inhibited in conjunction with an *MSH6* defect (Bechter et al 2004). Together, these studies suggested that the ALT-mechanism might be activated on a MMR-defective background and thus ALT+ cells could show MSI. However, tumours with and without MMR mutations showed similar frequencies of telomerase and ALT activation (de Caceres, I. et al. 2004), suggesting that a MMR-defect is not required for the ALT activation. Furthermore, MSI in MMR-defective cells also leads to the instability of a repeat intronically located in the *MRE11* gene, which creates an alternative-spliced dysfunctional MRE11 and is accompanied by a reduction of the MRN complex expression (Giannini et al., 2002. As a functional MRN complex seems to be essential for APB formation (Reddel et al 2005) and for ALT-telomere elongation, a major MMR-defect causing general microsatellite instability should not be expected to occur at ALT+ cells. Indeed, no MSI evidence was detected in telomerase and P53-negative Li-Fraumeni Syndrome-derived cells, a background that most ALT+ cell-lines share showing an ALT-phenotype (Tsutsui et al 2003).

In contrast, the same study showed minisatellite instability (Barret, J.C. et al., 2003). DNA fingerprints on telomerase-negative clones derived from single-cell expansions of the Li-Fraumeni fibroblast cell-line showed gain of new bands, variability in telomere length, dicentric chromosomes and double-minute chromosomes (DMs), features associated with gene amplification and genomic rearrangements (Tsutsui. et al. 2003). However, only clones derived by aflatoxin B1 immortalization showed DNA fingerprints variation, since clones derived from spontaneously-immortalized telomerase-negative cells did not show minisatellite instability. Furthermore, as aflatoxin B1 is a powerful inducer of mitotic recombination events (Sengstag C et al., 1994), the mutagen used for cell-immortalization could be the underlying cause for the minisatellite instability observed and not the TMM.

Surprisingly, high levels of instability were later detected at a particular locus in ALT+ cells. Indeed, the activation of the ALT pathway seems to affect directly the stability of MS32 minisatellite, located in 1q43. Furthermore, the analysis of six other minisatellites, located both in subtelomeric (MS31, CEB1, MS205, B6.7 and DXY14) and interstitial loci (MS1) demonstrated that they remain stable in ALT+ cells, suggesting that MS32 might be the only locus affected by the ALT activation (Jeyapalan, J. et al. 2005).

3.2 AIMS

Understanding the relationship between MS32 minisatellite stability and the activation of the ALT-pathway might indirectly highlight some aspects of the ALT-mechanism that have not yet been elucidated. This chapter analyses the extent of instability around MS32 and in other minisatellites that have not been analysed previously in ALT+ and in Tel+ cell-lines.

3.3 RESULTS

3.3.1 EXTENT OF MS32 LOCUS INSTABILITY

To verify the extent of destabilization of tandem-repeat sequences in the D1S8 locus, two other repeat sequences near the MS32 minisatellite were analysed. Contrary to most minisatellites that cluster at subtelomeric regions (Royle et al., 1988), MS32 locates at an interstitial position of chromosome 1, distant from other minisatellites. The closest tandem repeats are MSNID minisatellite, 57 Kb upstream MS32 and a single-tandem repeat - STR - located 1Kb downstream.

3.3.1.1 MSNID ANALYSIS

MSNID is a small minisatellite composed of a short array of 34 bp AT-rich repeat units and located 57 kb upstream the MS32 minisatellite, at the intron 4 of the Nidogene 1 – *NID1*. Interestingly, MSNID minisatellite might have evolved from a ~300 bp AT-rich region, located just before the NID hotspot (Fig. 3.1) (Jeffreys A. et al. 2005).



Figure 3.1: MSNID minisatellite locus.

The diagram shows the region comprising the MSNID minisatellite. A variable array of the 34 bp repeats is located ~300 bp of the exon 5 of NID gene. An AT-rich region is located between the NID hotspot (red star) and MSNID. The primers used for MSNID amplification are shown.

MSNID has very short alleles (2-7 repeats) and a palindromic structure, as shown by sequence analysis. Since the heterozygosity inferred from population diversity studies at

MSNID is low, the predicted MSNID mutation rate is 3×10^{-5} per gamete (Jeffreys A. et al. 2005).

As MSNID is the closest minisatellite to MS32 and is flanked by a very active hotspot with a peak activity similar to the MS32 flanking hotspot (70 cM/Mb^{-1} (Jeffreys A. et al. 2005) and 50 cM/Mb^{-1} (Jeffreys et al 1994), respectively), its stability was assessed in ALT+ cells. A Small-Pool PCR (SP-PCR) study was undertaken. SP-PCR is a powerful technique that relies on a succession of DNA dilutions to control the number of amplifiable molecules in each reaction, which facilitates the detection of rare or infrequent length mutant molecules. When combined with a Poisson analysis of single molecule dilutions to estimate the overall number of amplifiable molecules analysed, this methodology allows the calculation of mutation frequencies. As this region had not been previously analysed in ALT+ cells, a preliminary study on two tumour-derived ALT+ cell-lines was performed to determine whether the MSNID was unstable in these cell-lines. As seen in Figure 3.2, U2OS cell-line is homozygous for MSNID, with allele lengths of 1.1 kb. SaOS cell-line seems to be heterozygous, with MSNID alleles of 1.1 and 2Kb. However, no evidence for instability in MSNID minisatellite could be observed (Fig. 3.2).

However, since the mutation rate in the germ-line was estimated to be very low (3×10^{-5}) (Jeffreys et al 2005), an extensive SP-PCR analysis was performed to investigate if ALT activation caused at least the same degree of instability observed in the germ-line, as observed in the MS32 minisatellite. Cell-lines JFCF6T.11C (Tel+) and JFCF6T.11E (ALT+) were used as they derive from the same parental cell-line, differing exclusively in the activated telomere maintenance mechanism. As expected, since both cell-lines share the same parental cell-line, they are heterozygous for the same MSNID alleles' length. In total,

8760 (JFCF6T.11C) and 4584 (JFCF6T.11E) molecules were analysed (Fig. 3.3) and only one mutant allele (red arrow) was detected in the ALT+ cell line.

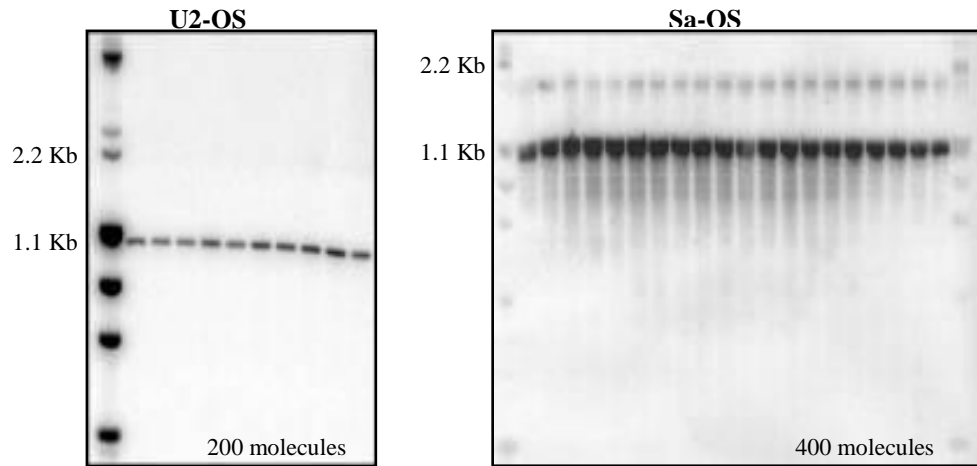


Figure 3.2: Amplification of MSNID minisatellite by SP-PCR in ALT+ cell-lines. Southern-hybridization of SP-PCR products resolved on an agarose gel electrophoresis and detected with MSNID probe. Each lane shows the resolution of PCR products derived from MSNID amplification with M59.0F and M57.7R primers, from 20 molecules input per tube.

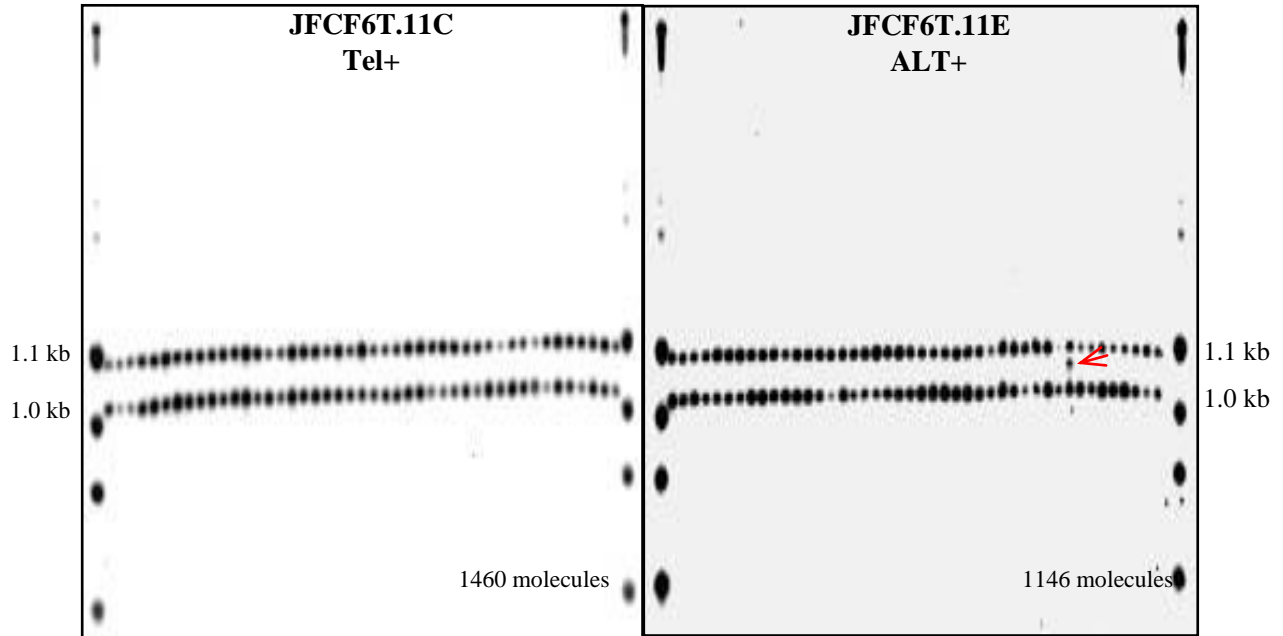


Figure 3.3: SP-PCR amplification of MSNID minisatellite in JFCF6T.IJ/11C (Tel+) and JFCF6T.IJ/11E (ALT+). Both cell-lines are heterozygous for MSNID with length alleles of 1.0 and 1.1 kb. The total number of amplified molecules in each blot is shown (derived from 20 molecules per tube) and the red arrow highlights the mutant-allele detected.

The mutation frequency (2.2×10^{-5} ; $0-1.2 \times 10^{-4}$ low and upper confidence intervals, respectively) observed in the ALT+ compared to the Tel+ cell-line (not significant difference $p = 0.34$, according to Fisher's Exact 2-tail test), is similar to the estimated for the germline, suggesting that the extreme MS32 instability does not extend to the MSNID minisatellite in ALT+ cells. Indeed, MS32 is so unstable in JFCF6T.IJ/11E cells that determining the progenitor alleles proved to be very difficult in a previous study, due to the frequency of mutant length MS32 molecules (Jeyapalan et al., 2005). Therefore, the extraordinary instability observed at MS32 in ALT+ cells does not seem to extend to the MSNID minisatellite, 70 kb from MS32 minisatellite.

3.3.1.2 STR ANALYSIS

On the other side of the MS32 minisatellite, the closest tandem repeat is a STR (Simple-tandem repeat), located 1 kb from MS32. This STR is 50-52% GC-rich and is composed of a tandem array of ~6 bp repeat units (variations of AAGGAA). A 350 bp long *Alu* element immediately flanks the STR (Fig. 3.4).

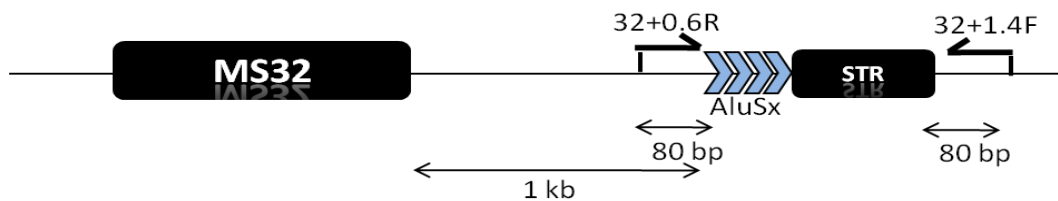


Figure 3.4: STR locus.

A simple tandem repeat locates 1 kb downstream MS32 minisatellite and is flanked by an *Alu* element. The primers used for the STR amplification are shown in the diagram.

As with the MSNID minisatellite, the STR stability was also analysed in cell-lines with different telomere maintenance mechanisms (Fig. 3.5). The product arising from the STR PCR-amplification comprises the STR itself and an *Alu* sequence just upstream the STR, which might be masking any STR instability. To overcome this technical problem a double-enzymatic digestion with the *HinfI* and *HaeIII* enzymes following the PCR amplification was performed and the parental STR-allele sizes determined.

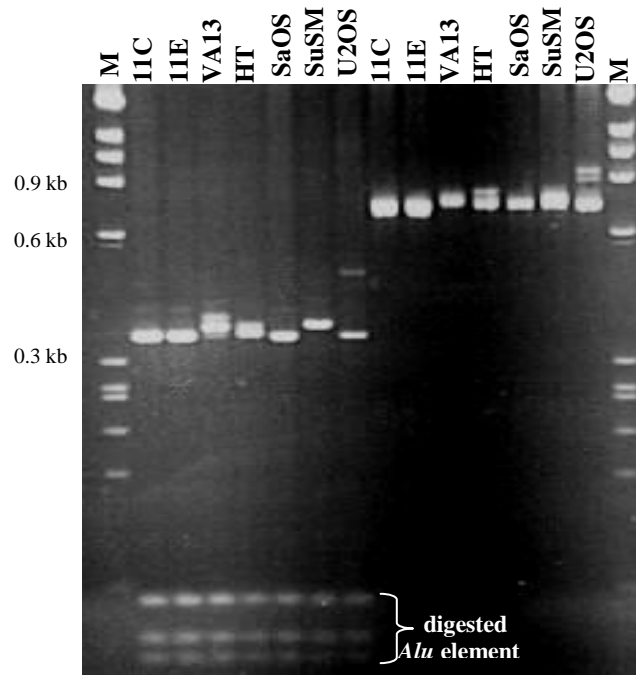


Figure 3.5: PCR amplification of STR.

The first seven lanes on the left show the digested amplicons and resulting *Alu* fragments and the other seven lanes show the undigested PCR products (STR + *Alu*). The *Alu*+STR region was amplified with the 32+0.6R and 32+1.4F primers in the Tel+ JFCF6T.11C (11C) and HT1080 (HT) and the ALT+ JFCF6T.11E (11E), WI38VA13/2RA (VA13), SaOS, SuSM-1 and U2OS cell-lines. The DNA marker λ + Φ 174 was used (M).

After double-digestion of the PCR products, it is clear that most cell-lines analysed are homozygous for this particular STR (350 bp alleles and 380 bp for SUSM-1), with exception of WI38VA13/2RA (350, 380 and 410 bp) and U2OS (350 and 500 bp). The

band corresponding to the 380 bp detected in WI38VA13/2RA results from a heteroduplex formed by the two alleles. Due to the small STR size and the *Alu*-element digestion necessary to improve the detection of mutant length alleles, an extensive study of the STR stability is technically very difficult. However, small aliquots of genomic DNA (20 amplifiable DNA molecules per reaction) were used to amplify the STR in U2-OS cell line to enhance the detection of potential STR length mutants. SP-PCR amplified products of the STR were *HinfI* and *HaeIII* digested before electrophoresis resolution by agarose gel electrophoresis to remove the amplified *Alu* sequence and increase the detection of putative STR-mutants. Both U2OS STR alleles could be detected (350 and 500 bp) but, on a total of 200 amplified molecules, no length mutation was detected (Fig. 3.6). The preliminary data indicates that the instability at this STR does not appear to be extraordinary high in ALT+ cells, although a thorough assessment was not conducted due to technical limitations. Nonetheless, together with the MSNID study, the instability observed at MS32 minisatellite in ALT+ cells seems to be confined to the minisatellite itself.

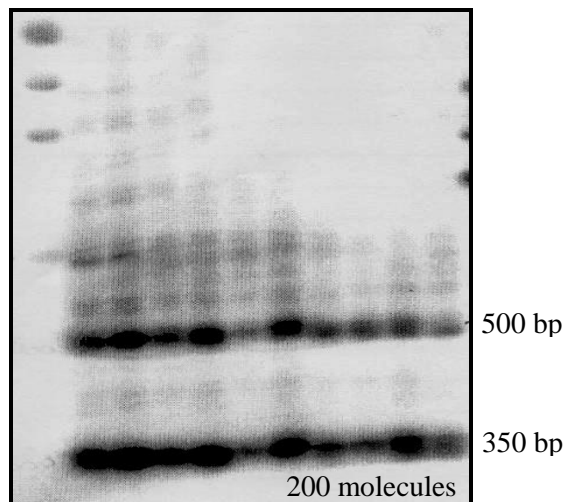


Figure 3.6: Amplification of STR by SP-PCR.

Southern-blot hybridized with a STR-specific probe that detects digested STR products amplified by SP-PCR and resolved by agarose gel electrophoresis. U2-OS (ALT+) cell line is heterozygous for the STR with length alleles of 350 bp and 500 bp. A total of 20 molecules per PCR reaction were amplified.

3.3.2 SCREEN FOR OTHER PUTATIVE INSTABLE LOCI

MS32 minisatellite seems to be the only minisatellite unstable in ALT+ cells, since six other minisatellites (MS1, MS31, CEB1, MS205, B6.7 and DXY14) remain stable in these cells (Jeyapalan et al. 2005). Additionally, during this project (section 3.3.1.1) the stability of one more minisatellite, MSNID close to MS32 was also analysed and the data showed that the MS32 instability does not extend to this minisatellite. The link between MS32 instability and ALT activation becomes even more intriguing considering that the panel of the seven minisatellites analysed share MS32 features that could underlie link between MS32 instability and ALT activation. For example, MS32 minisatellite is very similar to CEB1 in the GC content, length and germ-line instability (Jeffreys, A. J. et al, 2004). Also, MS1 and MS32 are located on chromosome 1 in interstitial positions, which differs from most other minisatellites that cluster at subtelomeric regions (Royle et al, 1988), although MS1 has very short repeat units (9 bp) and might behave more like a microsatellite than a minisatellite. However, there are many other minisatellites in the human genome and, even though MS32 is the only minisatellite of a total of 8 already analysed, other minisatellites might also be affected by ALT activation. Since SP-PCR analysis is an extremely time-consuming technique, a wider study is essential to fully elucidate the extent of minisatellite instability in the genome of ALT+ cells.

The DNA fingerprinting technique relies on the sequence similarity of a multi-locus probe with the minisatellites facilitating their simultaneous detection (Jeffreys et al 1985). Thus, the hybridization of such a probe to Southern-blot of restriction-digested genomic DNA produces a multi-banding profile known as DNA fingerprint. Originally, two probes that detect different sets of minisatellites, 33.15 and 33.6, were used for individual

identification, since the match probability between unrelated individuals was estimated at $<5 \times 10^{-19}$ (Jeffreys et al 1985). Additionally, the two probes are estimated to detect a total of 55 loci in the human genome, even though only one of the two alleles is likely to be scorable in the set of larger (23 to 4 kb) resolved DNA fingerprint fragments (Jeffreys et al 1985). Thus, the original DNA fingerprinting method was used as a powerful technique to quickly test the stability of multiple minisatellites in ALT+ cells. However, some of the minisatellites detected by 33.15 and 33.6 are hypervariable and consequently polymorphic within cell-populations, which could potentially interfere with instability detection. Therefore, to overcome the naturally occurring minisatellite variation present in cell populations, genomic DNA derived from single-cell expansion clones that had undergone 20 population-doublings was used. Any differences seen in the banding-pattern between clones should arise from an increased mitotic instability at a particular locus. If the only minisatellite unstable in ALT+ cells is MS32, re-hybridizing the DNA fingerprints with a MS32-specific probe should match the changes on the banding-pattern observed with the multiple-locus probe. If the differences in the banding do not match MS32 instability tested with the single-locus probe, at least one more minisatellite is likely to also be unstable in ALT+ cells and further studies (to find its identity, localization, etc) should be carried out.

The 33.15 and 33.6 probes, contained in pBluescript vectors, were kindly given by Dr. Esther Signer and were amplified with T3 and T7 primers. Probe 33.6 derives from D1S111 minisatellite, with 37 bp repeat unit, located on 1q24. The 750 bp long product obtained from PCR amplification of the insert is composed of 640 bp of tandem repeat and 110 bp of its flanking sequences. Probe 33.15 originates from the 7q31.3-qter D7S437 minisatellite, composed of repeat units 16 bp long. The 570 bp long amplified product consists of 450 bp of tandem repeat and 120 bp of its flanking DNA. In low stringency

conditions (1xSSC and 0.1% SDS washes) and without the presence of a competitor DNA, probe 33.15 can detect 20 loci and probe 33.6 detects 35 loci in *HinfI* and *HaeIII*- digested genomic DNA (Jeffreys, A. et al 1990). However, the only restriction-enzymes that could be used in this DNA Fingerprints study were *AluI* or *MboI*, since neither recognizes sites within the MS32 variant repeats or the sequence of both probes. Therefore, the minisatellites detected by both DNA fingerprints probes in this study will most likely differ from the ones identified with the original conditions.

The study was performed with the SUSM-1 cell-line, since the MS32 allele sizes had already been characterized for other work (see Chapter 5, section 5.3.1.1). Genomic DNA from each clone was digested with *AluI* and 2 µg were loaded in each lane and resolved by agarose gel electrophoresis. The previously PCR-determined MS32 progenitor alleles for each one of the 8 SUSM-1 clones analysed in this study (Fig. 3.7-a) were confirmed by a Southern-hybridization of the blotted gel with the MS32 single-locus probe (Fig. 3.7-b).

To detect minisatellites (including MS32) that are unstable in ALT+ cell-lines, a low stringent hybridization of the DNA-fingerprint blot to the 33.15 probe was performed on cloned DNAs from the SUSM1 cell-line (Fig. 3.8). Only bands above 2 kb were considered for scoring, since loci smaller than that were very difficult to distinguish as individual bands, either due to resolution conditions used or simply because most of the *AluI*-digested fragments produced were smaller than this, which could have caused the smear observed. Overall, 23 separate bands with sizes above the 2 kb could be scored (marked as red stars, Fig. 3.8) with the 33.15 probe. Other bands could be detected on the selected size range, however, as they were extremely faint or fuzzy, they were not considered for the scoring. Most clones show the same DNA-fingerprinting pattern, which

suggests that most loci detected with the 33.15 probe are stable in ALT+ cell-lines. Some bands are hardly detectable (black stars on clone 1B5, 1H5 and 3H3, Fig. 3.8), which may indicate that that particular locus might have been lost during the clonal expansion. However, as deletion events are common in immortalized cells, whereas new bands are more likely to represent genuine minisatellite mutations, only gain of bands was considered to represent minisatellite instability. No new bands were detected, which indicates that at least at these 23 loci no mutational events are occurring in the SUSM-1 ALT+ cell-line.

The same observations were obtained when the process was repeated and the probe 33.6 was used for hybridization. As expected, the pattern differs greatly from the 33.15 probe, confirming that different loci were detected with each probe. In total, 24 loci could be clearly detected with the 33.6 probe. Once more, some loci seem to have been lost during the clonal expansion (clones 1B5 and 1C4, black stars, Fig. 3.9). However, like the 33.15, also 33.6 hybridization reveals an identical pattern between the analysed clones, which further suggests that most of the loci scored are stable in this ALT+ cell-line.

On the whole, DNA fingerprints of *AluI*-digested genomic DNA derived from clones of the ALT+ SUSM-1 cell-line showed a similar pattern between the clones analysed. Thus, the total of 47 loci analysed with both 33.15 and 33.6 probes do not seem to be highly unstable in the SUSM1 ALT+ cell-line. Nonetheless, at least the MS32 minisatellite instability should have been detected. However, MS32 has almost no sequence homology with the 33.6 probe and shares very few bases with the 33.15 probe (Fig. 3.10), which might explain why the MS32 instability was not detected on these fingerprints. Indeed, when the blots were stripped and re-hybridized with a MS32-specific probe, the superimposition of both 33.15/33.6 and MS32 blots shows that neither of the probes seems to detect MS32, since some MS32 bands do not co-localize with any band

detected by 33.15 (clones 1A4, 1B5, 1C4 and 1H5 on Fig. 3.11-a) or 33.6 (clone 1B5 and 1H5 on Fig. 3.11-b). The MS32 variation amongst SUSM-1 clones emphasizing the high minisatellite instability in these cells is clear therefore, if other minisatellites detected by the DNA fingerprint probes were equally unstable, it should have been detected by the obtained hybridizations.

As a result, 47 loci detected by the 33.15 and 33.6 multilocus probes remain stable in seven SUSM1 clones analysed, suggesting that MS32 is probably the only non-telomeric sequence affected by ALT activation.

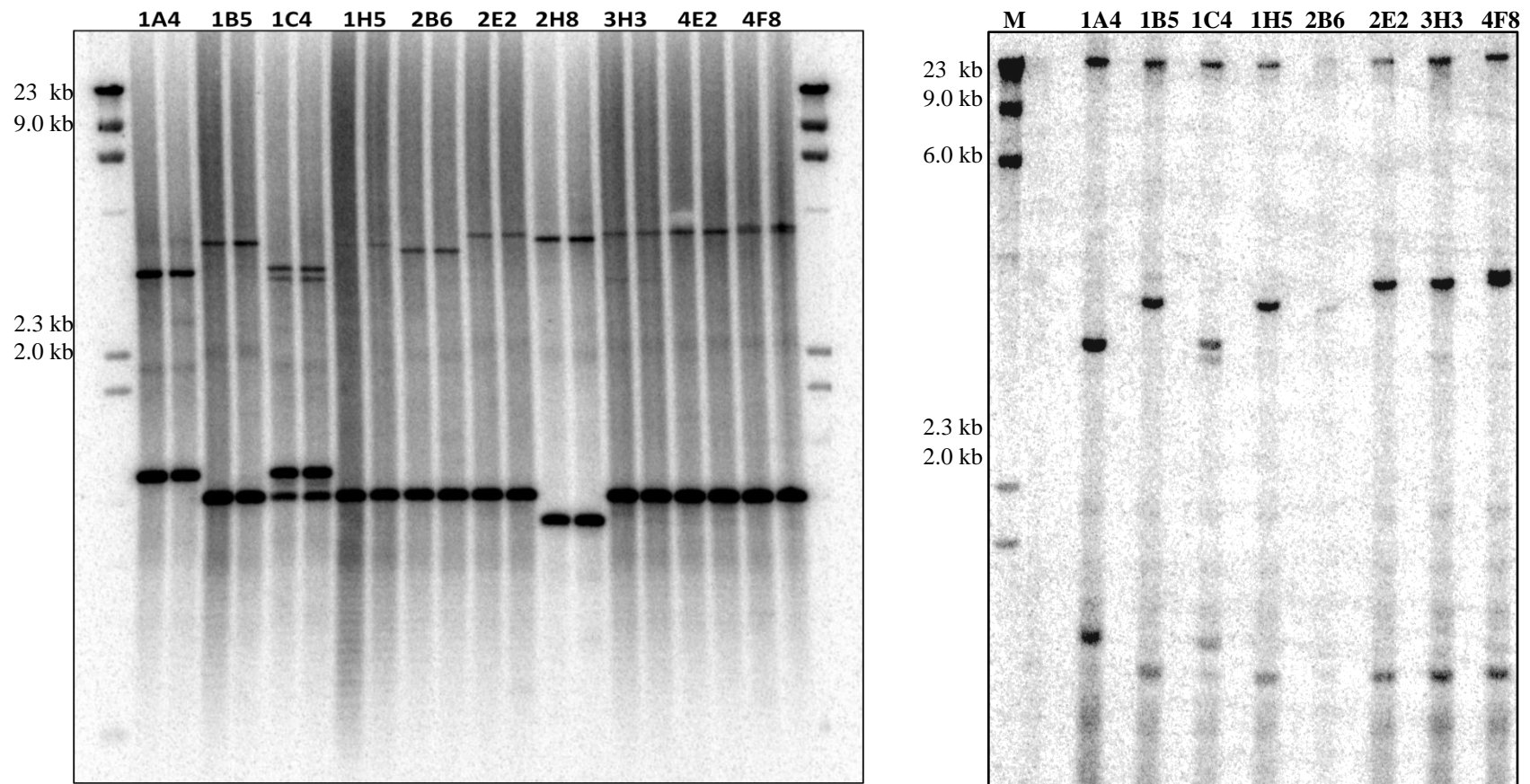


Figure 3.7: Progenitor allele-sizes of MS32 minisatellite in the SUSM-1 clones.

- A Southern-hybridization with the MS32 probe of the products of SP-PCR amplification of MS32 minisatellite in 10 clones derived from clonal expansion of 20PDs of the SUSM-1 cell-line. A duplicate SP-PCR reaction was performed for each clone.
- Southern-hybridization with MS32 probe of 2 µg of *AluI*-digested genomic DNA, from the same samples used for the previous SP-PCR, digested with *AluI* and resolved by agarose gel electrophoresis.

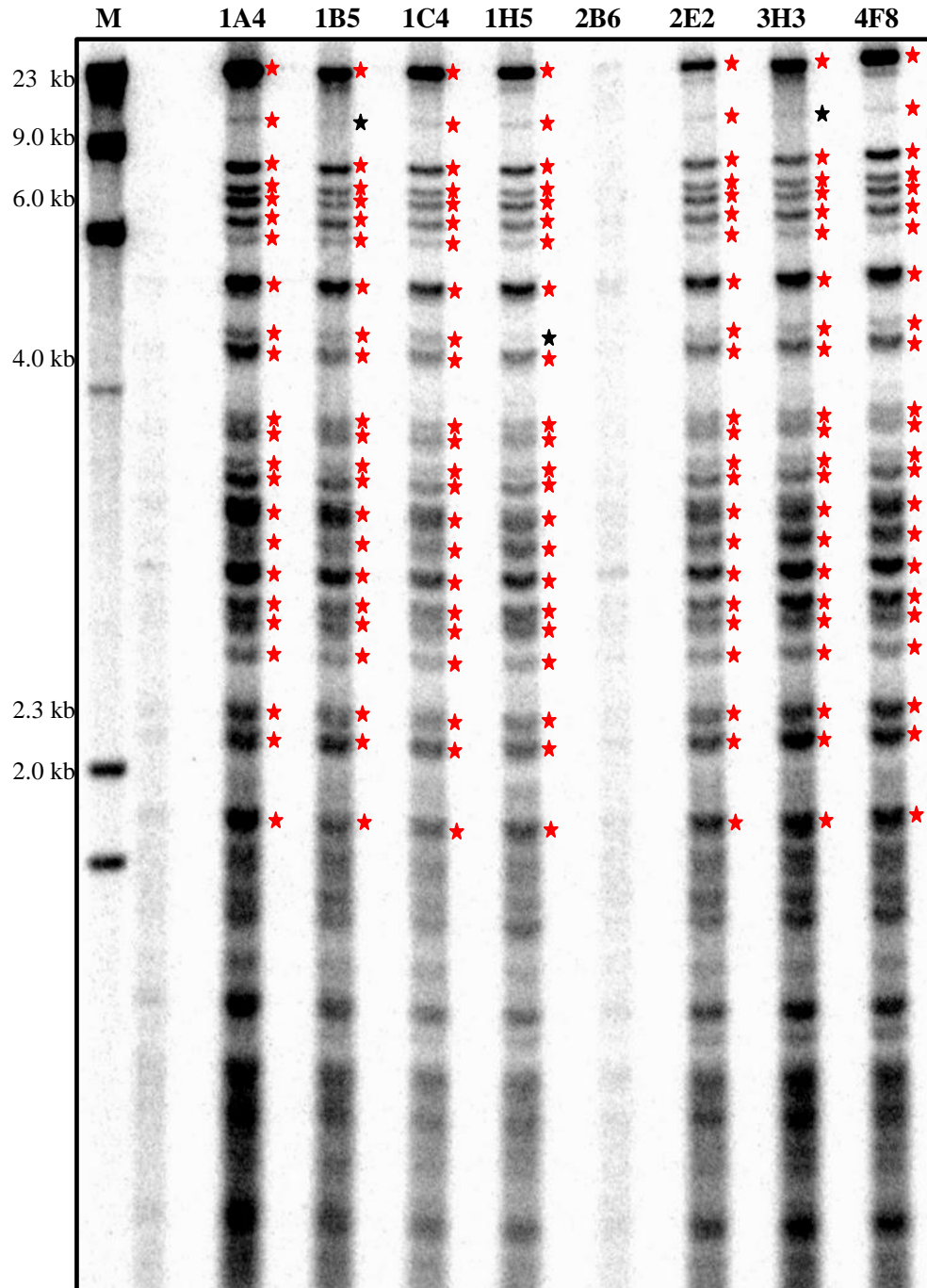


Figure 3.8: DNA fingerprinting with 33.15 probe

SUSM-1 DNA derived from clones digested with *AluI* were resolved by agarose gel electrophoresis, Southern-blotted and hybridized to the 33.15 probe. Red stars identify the bands scored for each clone. Black stars mark either deleted or difficult to detect loci.

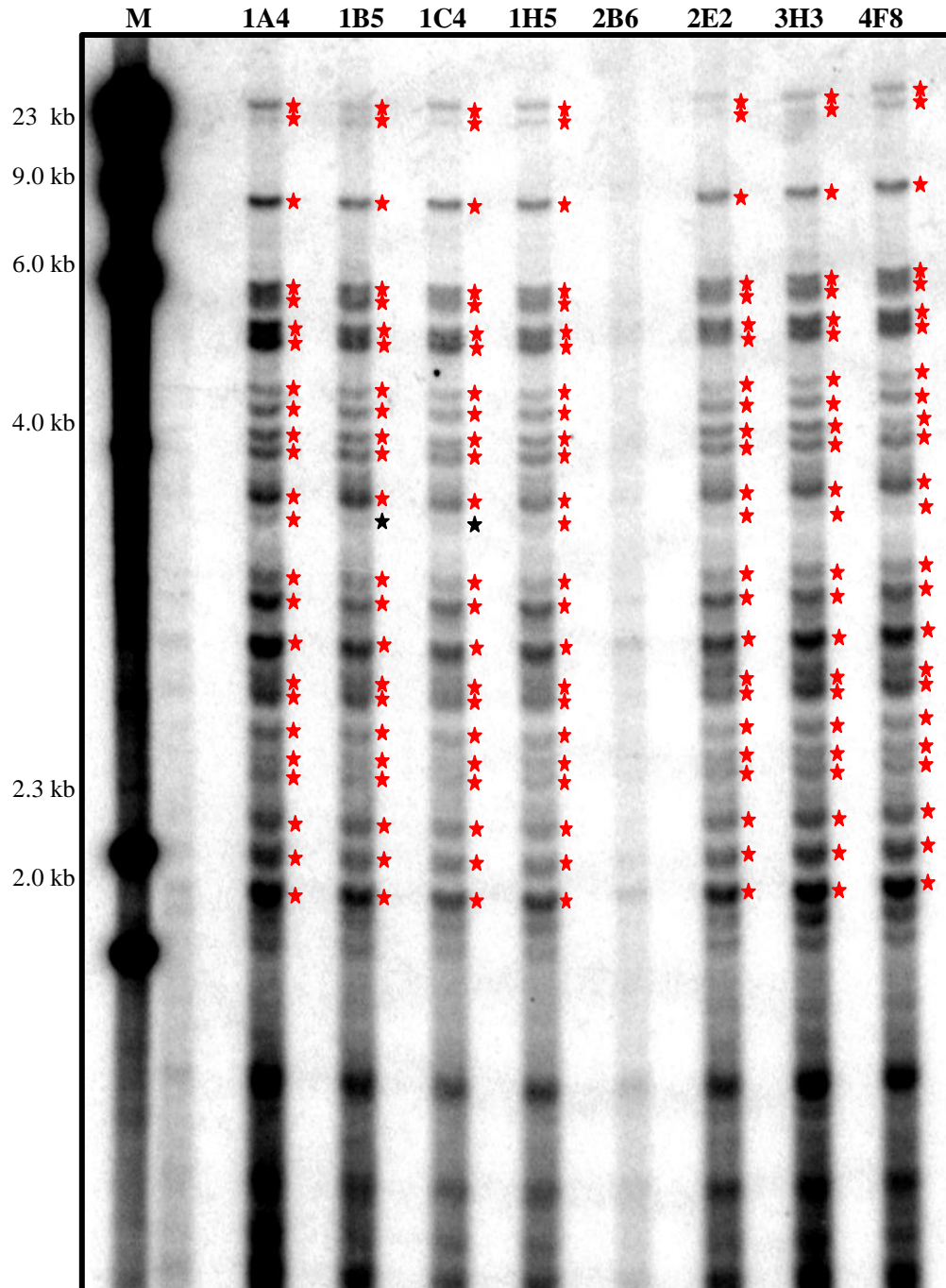


Figure 3.9: DNA fingerprinting with 33.6 probe.

SUSM-1 derived clones, digested with *AluI* were resolved by agarose gel electrophoresis, Southern-blotted and hybridized under low stringency conditions to the 33.6 probe. Red stars point to the scorable bands of each clone. Black stars mark either deleted or difficult to detect loci.

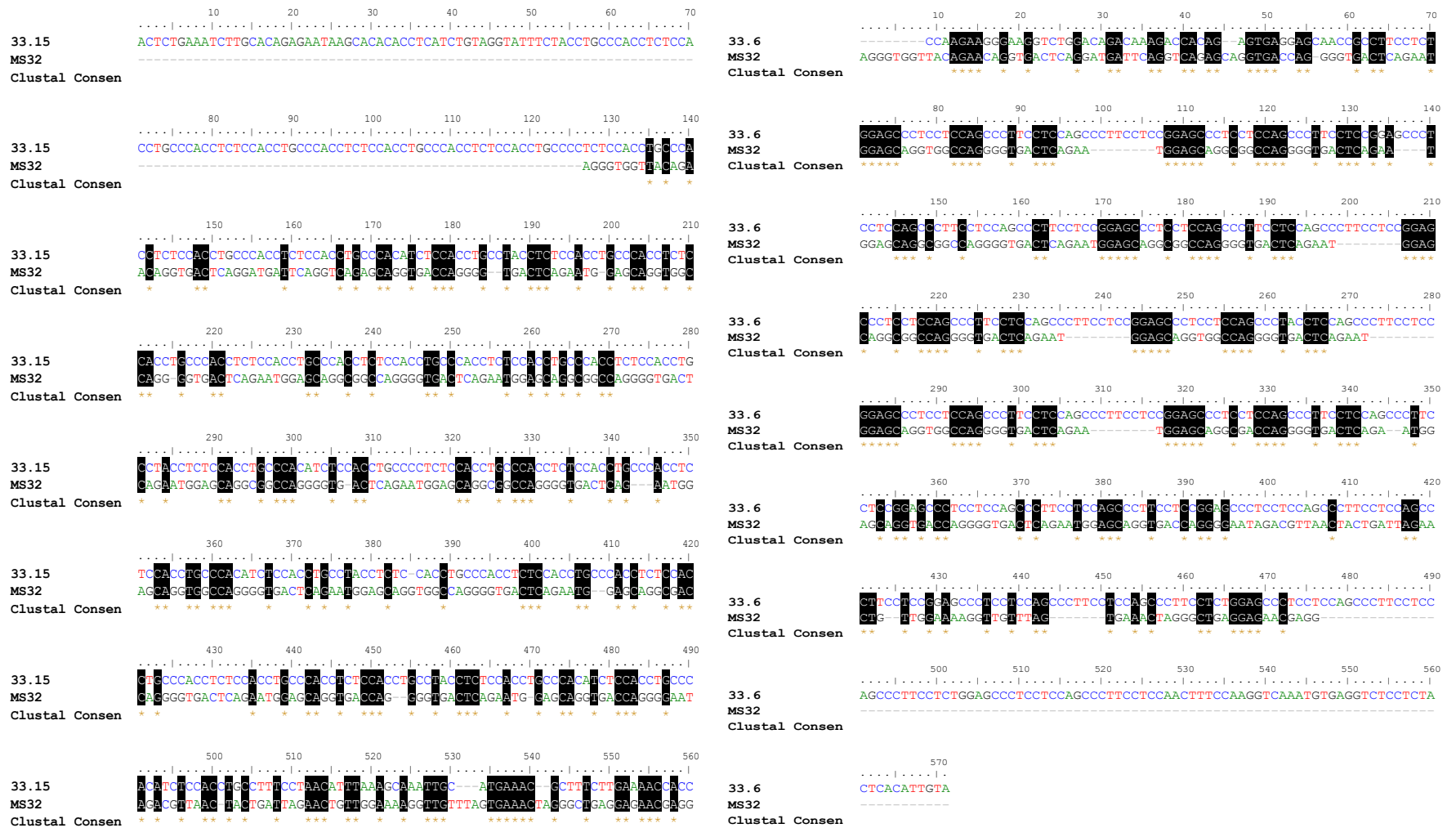


Figure 3.10: Alignment of MS32 sequence with DNA fingerprint probes.

The MS32 sequence, with random interspersions of the four variants, was aligned to the sequence of the probes used for DNA fingerprint 33.15 and 33.6. The homology between the sequences is highlighted in black and by stars.

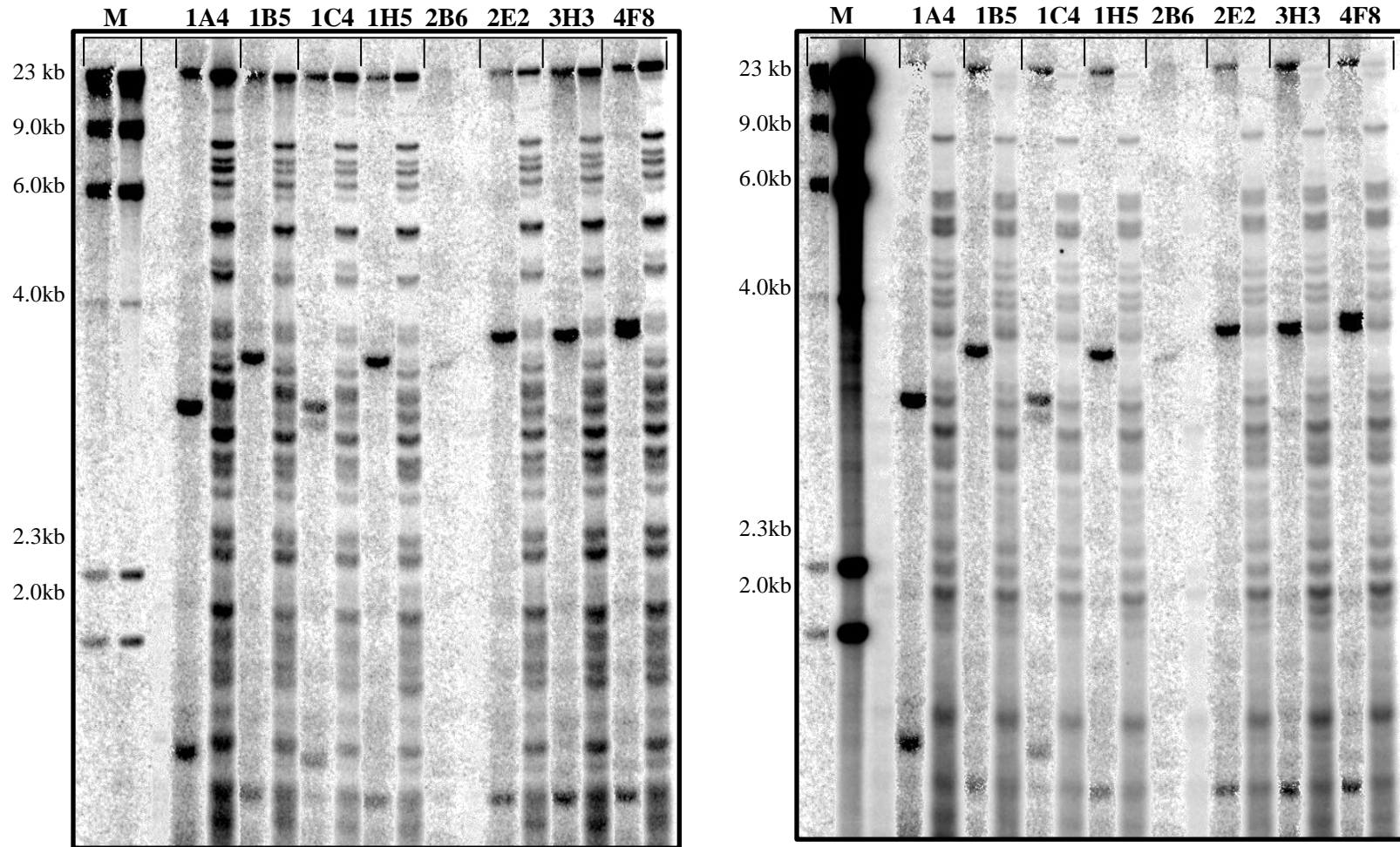


Figure 3.11: Superimposition of 33.15 and 33.6 fingerprints with the MS32 hybridization.

The blots hybridized with 33.15 (a) and 33.6 (b) probes were stripped and re-hybridized with the MS32 probe. The resulting images were superimposed so that, for each clone, the MS32 hybridization lane is on the left of its correspondent 33.15/33.6 one.

3.4 DISCUSSION

The discovery of instability at a non-telomeric genomic locus in ALT+ cells (Jeyapalan, J. et al 2005) raised the possibility that other genomic sequences might be affected by the ALT machinery. Therefore, it was surprising when six other minisatellites (MS1, MS31, CEB1, MS205, B6.7 and DXY14) were shown to remain stable in ALT+ cells (Jeyapalan, J. et al 2005). The possibility that MS32 minisatellite is the only genomic region, apart from telomeres, affected by ALT activation is extremely puzzling, since there is no similarity between MS32 sequence and telomeric DNA. Thus, an analysis of the instability around MS32 minisatellite is essential to determine if the instability is spread throughout the region or exclusively confined to the minisatellite itself.

The MSNID is the closest tandem repeat closest to MS32 and its stability in ALT+ cells was assessed by SP-PCR analysis. The JFCF6T.IJ/11C (Tel+) and 11E (ALT+) cell-lines were chosen for this analysis because they derive from the same parental cell-line, differing in the TMM. A total of 8760 and 4584 molecules were analysed for the Tel+ and for the ALT+ cell-lines, respectively. Only one mutant MSNID molecule was detected in the ALT+ cell-line (Fig. 3.2) and the mutation frequency 2.2×10^{-5} obtained, although similar to the estimated for the germ-line (Jeffreys A. et al. 2005), was not significantly different to the Tel+ cell-line, suggesting that the extreme MS32 instability does not extend to the MSNID minisatellite in ALT+ cells. Additionally, the MS32 instability in the JFCF6T.IJ/11E cell-line is extremely high (Jeyapalan, J. et al., 2005), further supporting that the extraordinary instability observed at MS32 in ALT+ cells does not seem to extend to the MSNID minisatellite, 70 kb from MS32 minisatellite

A thorough investigation of the STR 1kb downstream of MS32 was not possible due to technical problems, although the preliminary PCR and SP-PCR data showed no alterations at this repeated sequence. Consequently, these investigations indicate that the instability observed at MS32 in ALT+ cells is confined to the minisatellite itself.

As mentioned before, six other minisatellites remain stable upon ALT activation. (Jeyapalan, J. et al 2005). Thus, instead of individually screening more minisatellites for instability in ALT+ cells, a DNA fingerprinting approach was used. DNA fingerprints were obtained from seven clones derived from the SUSM-1 ALT+ cell-line, after clonal expansion for 20 PDs. The 33.15 and 33.6 multilocus probes were hybridized under low stringency conditions to *AluI*-digested genomic DNA from the SUSM1 clones. As expected, the probes showed different patterns, indicating that different loci were detected (Fig. 3.8 and 3.9). An estimated 47 loci were analysed in the SUSM1 clones but no instability was observed between them (defined by the gain of new bands). The re-hybridization of both 33.15 and 33.6 blots with a MS32-single locus probe confirmed the high instability at this locus as the MS32 bands varied between clones (5 of the 7 clones analysed showed different MS32 length, Fig. 3.7-b). Thus, it was surprising that neither of the multilocus probes detected the MS32 instability. However, a comparison of the MS32 sequence to the 33.15 and 33.6 probes (Fig. 3.10) revealed very low homology with the former and almost no similarity with the latter, which might indicate that neither of the multilocus probes used detect the MS32 locus, not even with the low stringency conditions used (Fig. 3.11). Therefore, the DNA fingerprint analysis performed suggests that another ~47 loci seem to be stable in the SUSM1 ALT+ cell-line. Further DNA fingerprints on more clones from other ALT+ cell-lines could be performed to confirm these results.

A previous study identified minisatellite instability in DNA fingerprints obtained from Li-Fraumeni Syndrome derived cells, with no telomerase or p53, a background reminiscent of ALT+ cells (Tsutsui et al., 2003). DNA fingerprints were performed on five cell-lines natural and mutagenically-immortalized. When compared to the parental cell-line, most immortalized cell-lines showed minisatellite instability (gain of 1-3 new bands). The DNA fingerprints were performed in *HindI* and *HaeII*-digested DNA, so instability at MS32 minisatellite could not account for the new bands. To investigate the minisatellite alterations observed further, DNA fingerprints were performed in clones derived from each immortalized cell-line and some instability was detected (1 in 6 clones showed 1 new gained band). However, the minisatellite instability was only observed in clones derived from the cell-lines that had been immortalized by either aflatoxin B1 or X-ray radiation, since no change in the DNA fingerprints of clones derived from naturally-immortalized cells were detected. Treatment with both AFB1 and X-ray have been associated with minisatellite instability (Kaplanski, C., et al 1997; Dubrova, Y. et al 1993, respectively) suggesting that the minisatellite instability detected by the DNA fingerprints might be an effect of the mutagenic-treatments rather than a result of activation of an ALT pathway and loss of p53 (Tsutsui et al., 2003). Therefore, the minisatellite instability observed by Tsutsui et al. in LFS mutagenically-immortalized may not be associated with the ALT-like mechanism active in this cell-line.

Thus, MS32 locus is probably the only or one of a very small number of affected minisatellites in ALT+ cells. Nonetheless, even if some unstable minisatellites are being masked by other loci, most of the 47 detected loci will still be stable as the patterns obtained are identical between clones but completely different amongst probes. Furthermore, the conditions used would be able to detect instabilities comparable to the

observed at MS32, further suggesting that this minisatellite is indeed the only non-telomeric locus affected by ALT+.

Therefore, this and previous studies (Tsutsui et al, 2002; Jeyapalan et al, 2005) suggest that most of the minisatellites in ALT+ cells are stable and that the MS32 minisatellite is unique or at least exceptional in sharing high instability following activation of the ALT pathway.

CHAPTER 4: GENE EXPRESSION ACROSS THE MS32 REGION

4.1 BACKGROUND

4.1.1 GENES AROUND MS32

The MS32 minisatellite is located at 1q43, within a 77 kb noncoding region between the Nidogen 1 (*NID1*) gene and the G protein-coupled receptor 137B (*GPR137B*) gene. The gene density in this chromosomal region is average (sixteen genes in the 1 Mb interval around MS32) but the GC content is slightly higher than average (46%). Another particularity of the MS32 region is the presence of a hotspot, with 50 cM Mb⁻¹ of peak activity, centered 200 bp upstream the beginning of the array and responsible for meiotic recombination processes that result in conversion-like (Jeffreys et al 1994) or interallelic crossover events (Jeffreys et al 1998) between MS32 alleles. Even though one of the genes within the 1 Mb region that encompasses MS32 region are known participants in the DNA recombination or DNA repair pathways that have been implicated with the ALT mechanism, most of them are poorly studied (Table 4.1).

TOMM20	233,339,283 233,358,754	translocase of outer mitochondrial membrane 20	part of the preprotein translocase complex of the outer mitochondrial membrane
ARID4B	233,396,833 233,558,155	AT rich interactive domain 4B (RBP1- like)	subunit of the histone deacetylase-dependant SIN3A transcriptional corepressor complex, which functions in diverse cellular processes including proliferation, differentiation, apoptosis, oncogenesis, and cell fate determination.
GGPS1	233,558,376 233,574,467	geranylgeranyl diphosphate synthase 1	catalyzes the trans-addition of the three molecules of IPP onto DMAPP to form geranylgeranyl pyrophosphate, an important precursor of carotenoids and geranylated proteins
TBCE	233,597,351 233,678,903	tubulin-specific chaperone cofactor E	tubulin-folding protein; involved in the second step of the tubulin folding pathway.
B3GALNT2	233,679,868 233,734,404	beta-1,3-N-acetylgalactosaminyltransferase 2	active in synthesizing a unique carbohydrate structure, GalNAc-beta-1-3GlcNAc, on N- and O-glycans
GNG4	233,777,608 233,880,677	guanine nucleotide binding protein (G protein), gamma 4	modulator or transducer in various transmembrane signaling systems
LYST	233,890,969 234,096,843	lysosomal trafficking regulator	regulates intracellular protein trafficking to and from the lysosome
NID1	234,205,755 234,295,104	Basement membrane glycoprotein Nidogen 1	tightly associated with laminin but also binds to collagen IV and perlecan; may play a role in cell interactions with the extracellular matrix
MS32 minisatellite			
LOC343508	1q42.3	similar to aconitase 2 precursor	processed pseudogene
GPR137B	234,372,497 234,438,829	G protein-coupled receptor 137B	transmembrane 7 superfamily member 1
ERO1LB	234,447,083 234,511,908	endoplasmic reticulum oxidoreductin 1-Lbeta	oxidoreductase that oxidizes proteins in the endoplasmic reticulum to produce disulfide bonds. It is required for cell folding, being thus a source of oxidative stress
EDARADD	234,624,303 234,714,631	EDAR-associated death domain	death domain-containing protein, and is found to interact with EDAR, a death domain receptor known to be required for the development of hair, teeth and other ectodermal derivatives
ENO1P	1q43	enolase 1, (alpha)	pseudogene
LGALS8	234,753,362 234,779,619	lectin, galactoside-binding, soluble, 8 (galectin 8)	widely expressed in tumoral tissues and seems to be involved in integrin-like cell interactions
HEATR1	234,780,594 234,834,437	HEAT repeat containing 1	involved in nucleolar processing of pre-18S ribosomal RNA. Involved in ribosome biosynthesis
ACTN2	234,916,393 234,994,181	actinin, alpha 2	actin-binding protein with multiple roles in different cell types
MTR	235,025,204 235,133,904	5-methyltetrahydrofolate-homocysteine methyltransferase	catalyzes the final step in methionine biosynthesis

Table 4-1: Order of genes in the vicinity of MS32 minisatellite and their function.

4.2 AIMS

Changes in the expression levels of genes located near MS32 minisatellite in ALT+ cell-lines could alter the chromatin conformation of the region, exposing MS32 to mechanisms involved in the ALT pathway and affecting its stability. The gene density around MS32 is average but the genes close to MS32 are not fully studied. To investigate whether MS32 instability is linked to a localized chromatin mediated effect caused by altered expression of genes in the vicinity of the minisatellite, expression of genes in the region was examined in ALT+ and non-ALT cell-lines. Moreover, some genes have been found to participate in telomere elongation via the ALT pathway but most of the genes involved in its activation are still largely unknown. In addition, as fundamental participants may not yet have been identified, an expression microarray analysis was performed to find not just differentially expressed genes around MS32 minisatellite but also genes potentially involved in the ALT pathway that could be used for further studies.

4.3 RESULTS

4.3.1 GENE EXPRESSION IN ALT+ VS. TEL+ CELLS

4.3.1.1 MICROARRAY DESIGN

The MS32 instability might be a localized consequence of chromatin remodelling resulting from transcriptional changes in ALT+ cells. Consequently, to screen for differential expressed across the genome but focusing mainly on the genes in the MS32 region, an expression microarray analysis was performed comparing a Tel+ to an ALT+ cell-line. A human cDNA microarray, composed of approximately 6500 genes based on the human gene set from Research Genetics (now Invitrogen, Carlsbad, CA) was used. The array was expanded to include PCR products amplified from cDNA clones of genes in the vicinity of MS32 minisatellite that were not present in the expression microarray (*ARID4B*, *B3GALNT2*, *GNG4*, *NID1*, *ERO1LB* and *EDARADD*). The cDNA clones were obtained from the I.M.A.G.E. collection, held at the MRC Human Gene Mapping Project (<http://www.hgmp.mrc.ac.uk/>) and had been previously verified by sequence analysis (Lesoto, B. et al, unpublished data). Vector-specific primers were used to amplify the cDNA from the IMAGE clones and the resulting PCR products were separated by gel electrophoresis to ensure that a single product was used on the arrays (Fig. 4.1). The array was injected onto prepared poly-L-lysine coated slides using a 32-tip head of a DNA microarrayer, built largely according to the Stanford design

(http://syst.mrctox.le.ac.uk/SystemsToxicology/Microarray_Facilities/Facilities.aspx).

The centre to centre distance of the features was 210 µm and each feature was 90-100 µm in diameter. Before use, the arrays were UV cross-linked.

The expression microarray experiment was performed with RNA from the cell-lines JFCF6T.11C (Tel+) and JFCF6T.11E (ALT+) because they derive from the same

parental cell-line but differ in the activated TMM. The expression levels of each test cell-line were calibrated to a reference cell-line, GM03798, to minimize any variation between biological samples. The lymphoblastoid GM03798 cell-line, derived from a normal donor, was chosen as calibrator since it has a stable karyotype (kindly cytogenetically verified by Jenny Foxon) and grows rapidly in culture so sufficient calibrator RNA was available throughout the experiment. Additionally, dye-swap hybridizations were performed as technical controls to eliminate dye-bias associated with unequal incorporation of the two dyes during the labelling of the cDNA. Thus, a total of 8 arrays (including dye-swaps) were hybridized for the ALT+ and another 8 for the Tel+ cell-line, as schematized in Table 4.3.

Vector + primers	Image clone ID	Gene	Expected insert size	Actual insert size
<i>pCMVSPORT6</i> (T7+M13 rev)	4393885(10088-L14)	<i>B3GALNT2</i>	2049	2000
	5503285(12142-M14)	<i>GNG4</i>	1359	2000
	5555460(12275-K13)	<i>NID1</i>	1272	1000
	4441757(10213-G06)	<i>EDARADD</i>	1219	1762
<i>PBlueScript</i> (T7 + T3)	5261610(11659-G19)	<i>ARID4B</i>	2337	2100
	4826983(AT34-G7)	<i>B3GALNT2</i>	2192	2100
	4799603(AT22-A1)	<i>GNG4</i>	1904	2000
	4829502(AT59-B6)	<i>EROLIB</i>	3052	3000

Table 4-2: I.M.A.G.E. clones used to improve the gene representation of the MS32 region on the expression microarray. A list with all the information from the IMAGE clones obtained, including the vector where the cDNA is inserted, the primers used for PCR amplification, the IMAGE ID, expected size and actual PCR product size obtained with the mentioned primers.

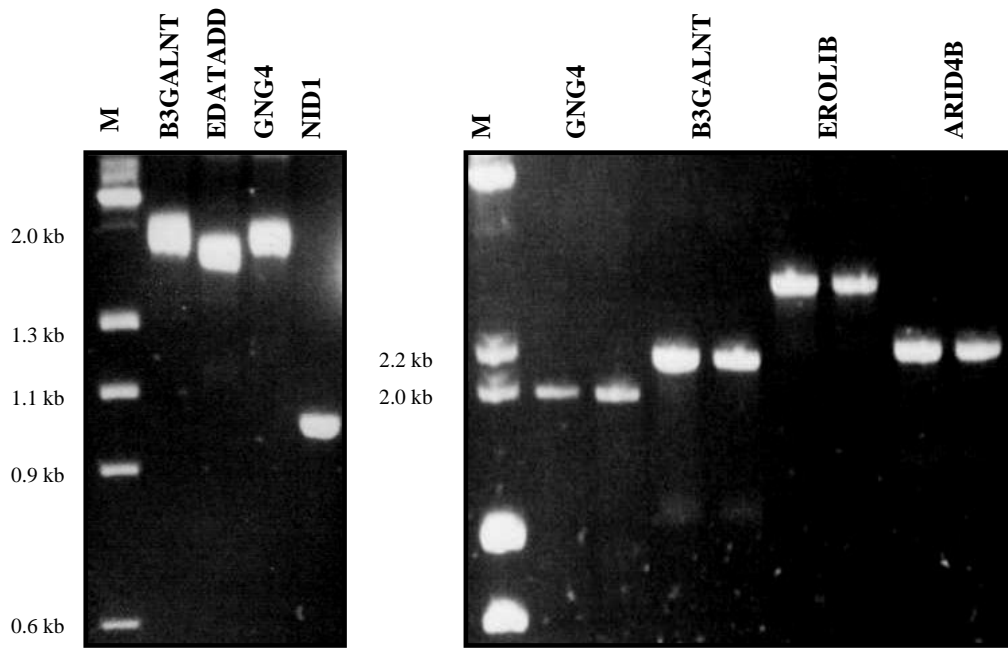


Figure 4.1: Amplification of IMAGE clone containing cDNA of genes from around MS32.

The cDNA of the genes near MS32, not included in the 6500 clone collection used for the array, were PCR amplified from the IMAGE clone vectors and resolved on a 0.8% agarose gel electrophoresis prior to inclusion into the array set for injection on the slides. Markers (M) used were $\lambda + \Phi 174$.

	1 st replicate	2 nd replicate	3 rd replicate	4 rd replicate
Tel+	GMO + 11C	GMO + 11C	GMO + 11C	GMO + 11C
	GMO + 11C	GMO + 11C	GMO + 11C	GMO + 11C
ALT+	GMO + 11E	GMO + 11E	GMO + 11E	GMO + 11E
	GMO + 11E	GMO + 11E	GMO + 11E	GMO + 11E

Table 4-3: Experimental design.

Following RNA extraction and cDNA synthesis, the reference GMO3798 cell-line (GMO) was hybridized against the Tel+ (11C) and the ALT+ (11E) cDNAs. Biological replication was performed by using RNA samples resulting from 4 independent extractions. Dye-swap hybridizations were performed to provide technical replicates to the experiment.

4.3.1.2 EXPRESSION MICROARRAY EXPERIMENT

Total RNA was extracted from the JFCF6T.11C (Tel+), JFCF6T.11E (ALT+) and GMO3798 cells growing in culture and used for first-strand cDNA synthesis. The cDNA synthesis was carried out with an anchor-dT₂₅ and pentadecamer primers, incorporating aadUTP to allow the consequent coupling of the amino-labelled cDNA to specific amino-reactive dyes (Alexa555 and Alexa 647). The dye-coupled aminoallyl cDNA was then hybridized with the previously printed arrays, according to the scheme in table 4.3. A total of 16 hybridizations were performed and used for expression analysis. Fluorescence on the slides was detected by a two-laser scanner Axon4200 and measured with GenePix version 3.0.0.85 software (Axon Instruments, Union City, CA, USA), which converted the image pixels of each array feature into an intensity digital data. The sizes of each feature were firstly determined using the software parameters and then manually adjusted when appropriate. Then, the intensity of each pixel was determined and a median intensity of all the measured pixels within a feature was used as the global intensity value for that particular feature. Before data analysis, a global normalization was performed centering the red/green ratios of each feature to the median intensity of all feature set for each channel (R statistical packages print-tip LOWESS, Fig. 4.2–a and 4.2–b). Normalizing the intensity ratios of both dyes for each feature corrects different dye-intensities caused by factors other than gene expression changes (dye incorporation during labelling, imaging sensitivity) and it eliminates systematic errors. The means of the ratios between the Cy3 and Cy5 channels for each of the 8 pairs of hybridizations obtained were calculated, providing a relative expression level for the genes from the test cell-lines and the calibrator cell-line. Finally, the means of the ratios obtained were used to determine the JFCF6T.11E/JFCF6T.11C ratios for each feature and assess changes in gene expression between the ALT+ and the Tel+ cell-lines.

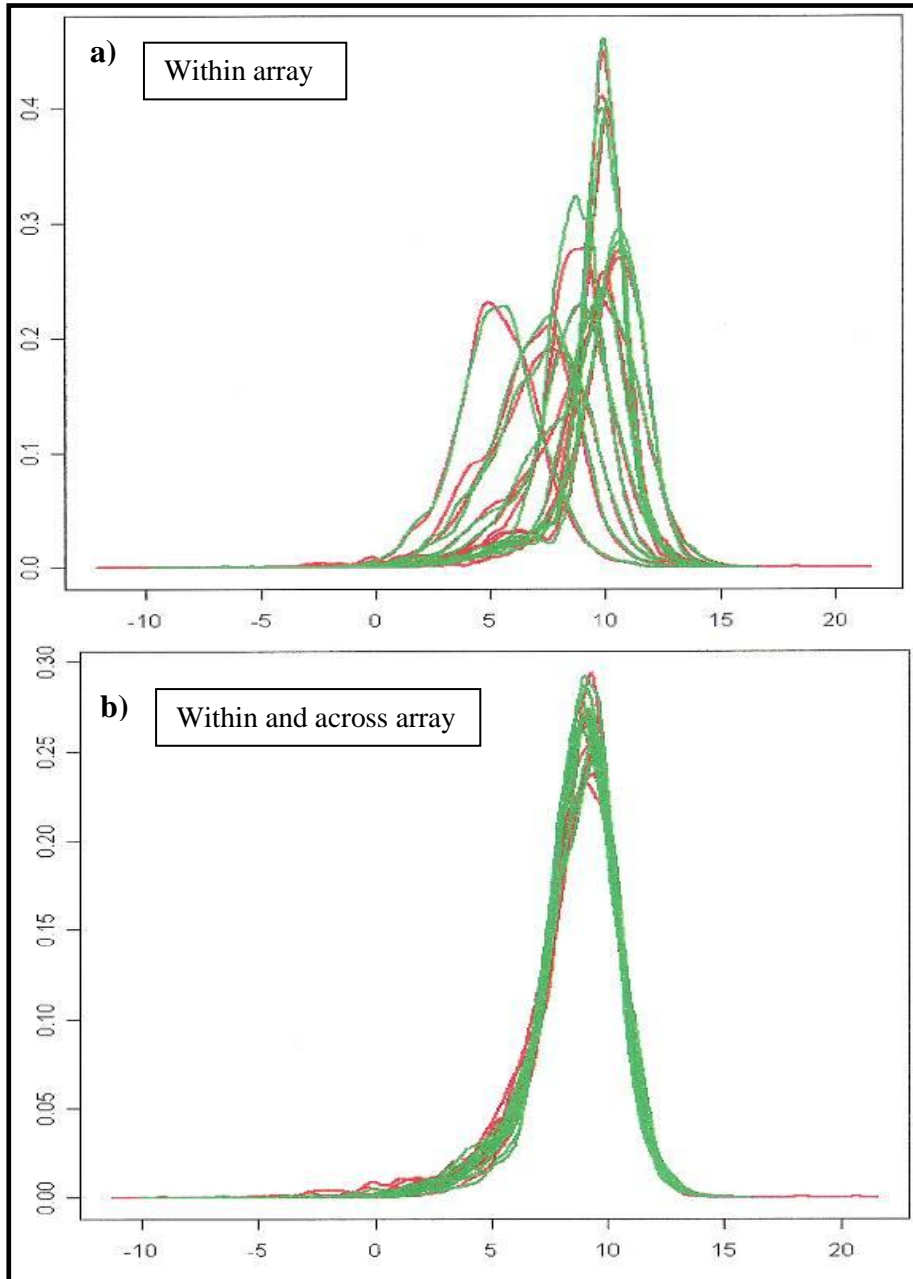


Figure 4.2: Global LOWESS normalization.

Each peak represents the measured green and red intensities in each array. a) A global LOWESS normalization of the green/red ratios was performed for each array. b) After individual array normalization, a global LOWESS between all the arrays was also performed.

4.3.1.3 DATA ANALYSIS

To simplify the gene expression comparison between the two samples the \log_2 of the ratios were used (for a 4 times increase: intensity ratio = 4, so $\log_2 = +2$; for a 4 times decrease: intensity ratio = 0.25, thus $\log_2 = -2$). A statistical analysis of the data was performed using T-test (2 tails, unequal variance) on the \log_2 of the intensity ratio for each gene. The genes in both JFCF6T.11E (ALT+) and JFCF6T.11C (Tel+) that differed from the GMO3798 calibrator cell-line with $p < 0.01$ were then sorted into clusters of genes.

A total of 322 genes were found to be significantly ($p < 0.01$) differentially expressed between JFCF6T.11E (ALT+) and JFCF6T.11C (Tel+) cell-lines. The analysis of the significant differentially expressed genes suggests that transcription in ALT cells appears to be more relaxed than in tel+ cells (61% of the differentially expressed genes are upregulated in ALT+). However, although statistically significant, the differences observed are not considerable as most of the data set differs on 1 or lower fold change (Fig. 4.3). Nonetheless, a group of interesting genes involved in either DNA repair (*ATM*), chromatin reorganization (*ARID4A*), helicase activity (*ATRX*), excision and single-stranded repair (*ERCC1*, *XRCC1*, *XRCC6*), recombination (*RAD51C*) and telomeric repeat binding factor (*TRF1*) can be identified as being upregulated in the ALT+ cell-line whilst others involved in chromatin assembly/disassembly (*CBX5*), cell adhesion (*ENG*) or mitotic sister chromatin segregation (*KIFC1*) seem to be downregulated, when compared to the Tel+ cell-line.

Focusing on the main question of the study, the data set obtained showed no significant changes in the expression levels of the genes around MS32, suggesting no differences in the gene expression levels near the minisatellite between the ALT+ and Tel+ cell-lines.

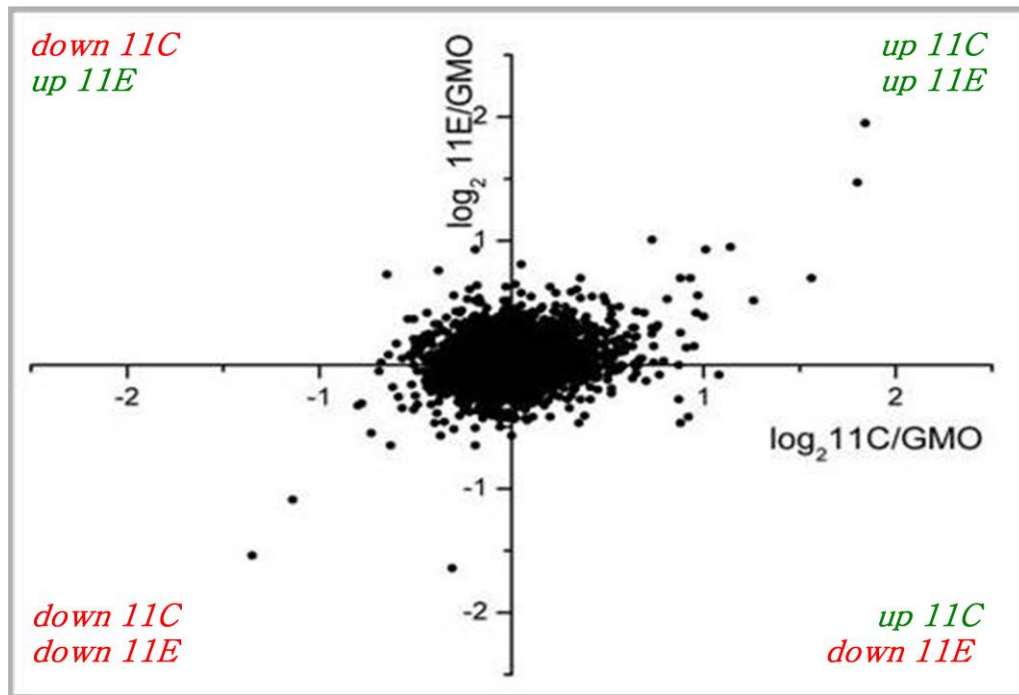


Figure 4.3: Plot of the expression fold-changes of the Tel+ against the ALT+ cell-line

The log₂ ratios of the measured intensities of the JFCF6T/11C (Tel+) vs. calibrator (GMO) were plotted against the log₂ ratios of the JFCF6T.11E (ALT+) vs. calibrator (GMO), showing that most data is contained within the 1 fold change.

Though, using a p-value of 0.01 in such a large data set incorporates a high false positive rate and many of the gene expression changes detected may not be biologically meaningful. Thus, further verifications of this data set should be undertaken before any conclusions are drawn. Additionally, throughout the development of this experiment it came to our attention that, when the purpose of the study is gene identification, it is not necessary to use a calibrator sample in expression microarray experiments (Dobbin et al 2002). Thus, the two test cell-lines JFCF6T.11C (Tel+) and JFCF6T.11E (ALT+) were hybridized against each other. A total of 4 hybridizations were performed to include the dye-swap controls as well as biological replicates with two independently extracted RNA samples for each cell-line (Table 4.4).

1 st replicate	2 nd replicate
11C + 11E	11C + 11E
11C + 11E	11C + 11E

Table 4-4: 2nd experimental design for the expression microarray experiment.

The Tel+ (11C) and the ALT+ (11E) cell-line were tested against each other. To perform biological replicates, RNA samples from two independent extractions were used in different hybridizations. Dye-swap hybridizations were performed to provide technical replicates to the experiment.

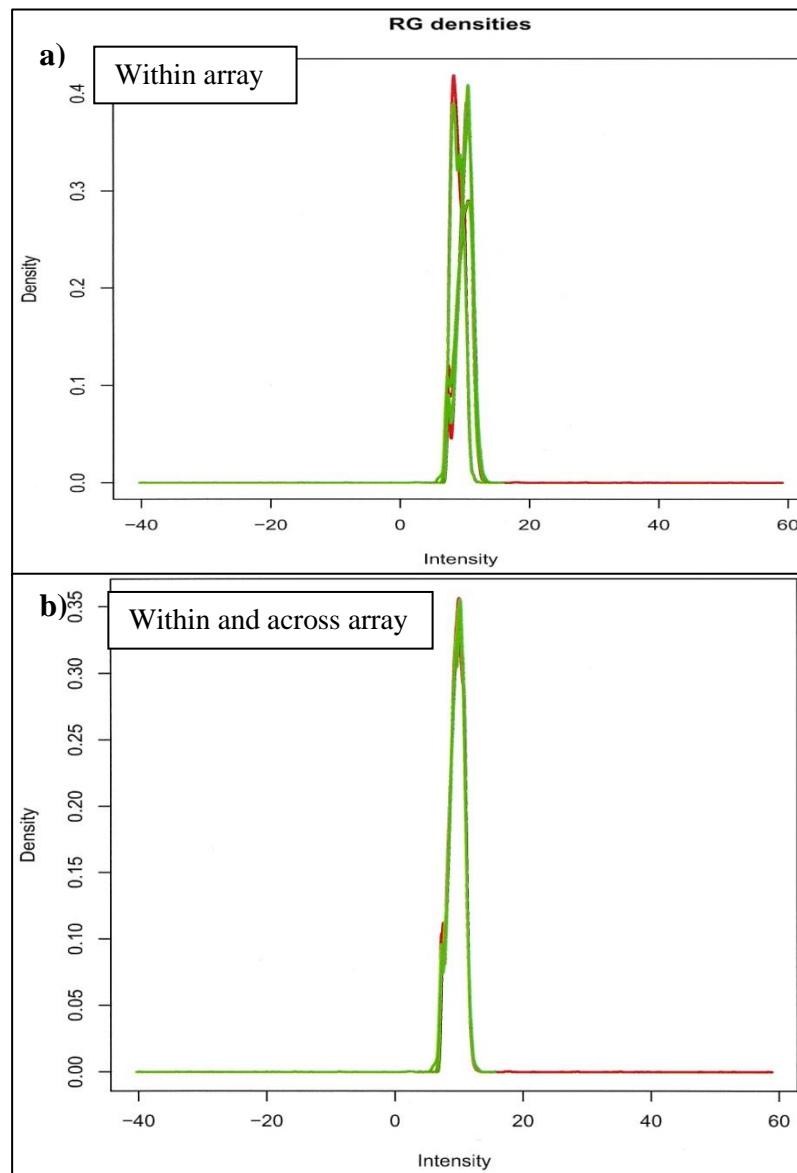


Figure 4.4: Global LOWESS normalization for the 2nd design.

- A global LOWESS normalization of the green/red ratios was performed for each array.
- After individual array normalization, a global LOWESS between the four arrays was also performed.

The second data set was treated and analysed as described for the first data set (Figure 4.4). As seen in the first data set, the general level of transcription in the ALT+ cell-line JFCF6T.11E seems to be higher than in the Tel+ JFCF6T.11C. Most of the significant expression changes observed occur at genes involved in or regulators of transcription (Polymerase RNA II L, General transcription factor IIE, etc), which seem to be upregulated in the ALT+ cell-line. However, selecting genes with significant expression changes of $p < 0.001$ from the first set and comparing to the $p < 0.01$ of the second set, 136 genes were common to both experimental designs (Appendix-4). Furthermore, some of these genes have two different cDNAs included on the array (*ARID4A*, *RAD51C*, *BCL2*, Appendix-4), which strengthens the confidence in the final common set of differentially expressed genes. Thus, several interesting genes seem to be upregulated in the ALT+ compared to the Tel+ cell-line, especially those involved in DNA recombination (*RAD51C*), chromatin remodelling (*ARID4A*), p53 binding protein (*MDM2*), telomere binding (*TRF1*) and apoptosis (*BCL2*-related) all of which could be directly or indirectly involved with the ALT mechanism. Interestingly, one of these genes (*ARID4A*) is closely involved with one gene located in the MS32 minisatellite region (*ARID4B*) and its potential role in ALT+ should be further investigated.

Nonetheless, due to the high data input and consequent statistical analysis, this type of expression array analysis fails to detect minor expression changes that could be significant to the ALT mechanism. Also, the expression microarray study showed no significant changes on the expression levels of genes around MS32 minisatellite.

4.3.2 GENE EXPRESSION AROUND MS32

To address in more detail the hypothesis that genes in the vicinity of MS32 minisatellite show altered expression in ALT+ cell-lines, qPCR was performed on 3 genes and 1 pseudogene that flank MS32. These genes comprise the lysosomal trafficking regulator - *LYST*; the basement membrane protein involved in cell-extracellular matrix interactions - *NID1*; a processed pseudogene similar to aconitase-2-precursor (mitochondria) - *PA* and a transmembrane 7 superfamily member 1 with unknown function – *GPR137B* (Fig. 4.5).

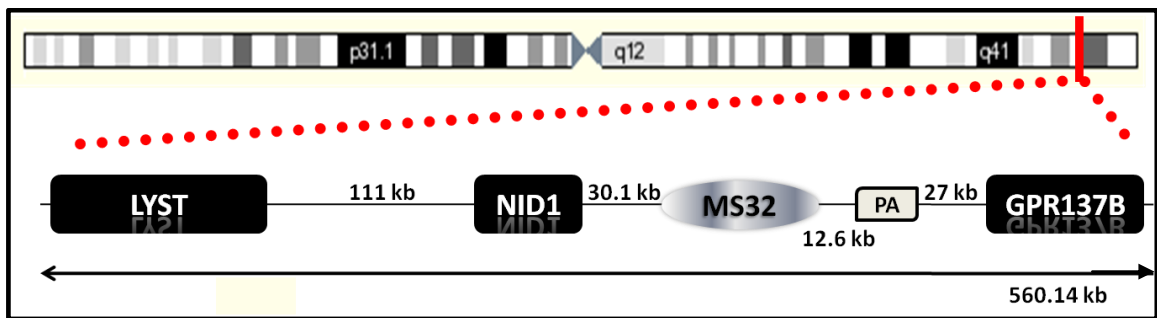


Figure 4.5: Gene distribution around MS32.

The diagram represents a 560.14 kb region of chromosome 1 around the MS32 minisatellite. The 3 closest genes to the tandem repeat (*LYST*, *NID1* and *GPR137B*) are represented as well as distances between them. The processed pseudogene (*PA*) is also represented.

4.3.2.1 PRIMER DESIGN AND QPCR OPTIMIZATION

Total mRNA was extracted from cells and 1µg used for cDNA synthesis with random hexamer primers. The synthesis was performed at 42°C and a DNase I digestion step was included to minimize DNA contamination risk. After cDNA synthesis, each sample was diluted to a final concentration of 100ng/µl (assuming a 100% efficiency of the cDNA synthesis). For each cell-line analyzed, two RNA extracts were obtained and each one was used for two independent cDNA synthesis reactions. Finally, each cDNA was tested in triplicate, according to the diagram in Fig. 4.6.

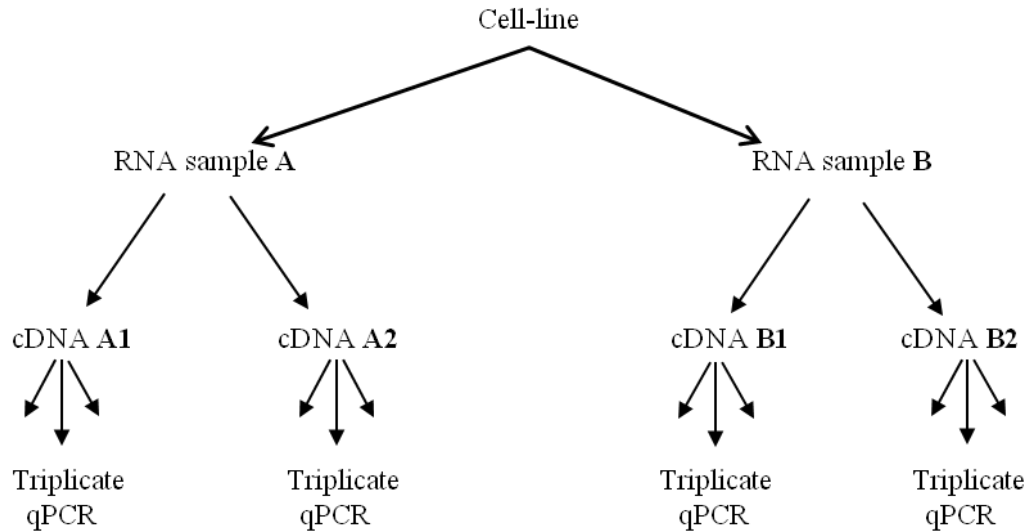


Figure 4.6: Scheme of the qPCR experiment.

A total of 11 cell-lines were analysed throughout this study: the Tel+ GMO3798, T24, HT1080 and JFCF6T.IJ/11C, the normal MRC5 and the ALT+ U2OS, SaOS, WI38VA13/2RA, SUSM1, JFCF6T.IJ/11E and IICF/a2.

One of the most crucial steps in any qPCR analysis is the primer design, as it defines the specificity of the qPCR amplification to the target cDNA. To overcome unwanted genomic DNA contamination in the cDNA samples, sequence-specific primers were designed across exon-exon boundaries so that only cDNA derived from transcripts were amplified. The complete cDNA sequence for each candidate gene was retrieved from NCBI Nucleotide database (<http://www.ncbi.nlm.nih.gov>). The designed primer set was analysed with *Primer 3* software to identify any potential hairpins and primer-dimer interactions and thus minimizing any primer-related effects on the amplification and/or fluorescence detection. Finally, each selected primer was screened against the reference human genome using the *NCBI* Blast function (<http://blast.ncbi.nlm.nih.gov/Blast.cgi>) and with the *UCSC* Blat function (<http://genome.ucsc.edu/cgi-bin>) to ensure its specificity to the target gene. Finally, to ensure that any increase in fluorescence was due to cDNA amplification for the gene of interest and not attributable to non-specific products or primer-dimer artefacts,

dissociation curves were plotted for all PCR products. After optimization of each primer set, dissociation curves for all genes analysed were shown to be specific with only a single peak at the melting temperature of the PCR product (data not shown).

SYBR Green I fluorescence detection was used for quantification of the PCR product since it can be used with unmodified primers and it constitutes a low cost option to quantify the expression of several genes. SYBR green is a fluorescent dye that intercalates to double-stranded DNA emitting green fluorescence. As the fluorescence emitted is directly proportional to the amount of double-stranded DNA, the measurement of the fluorescence can be used to quantify the amount of PCR product in real-time. Gene expression was then quantified based on the threshold cycle (Ct value), the PCR cycle during which the measured fluorescence exceeds a threshold determined by background fluorescence at baseline. Finally, the relative fold change quantification of gene expression was calculated through the $\Delta\Delta C_t$ method ($2^{-\Delta\Delta C_t}$), which requires Ct values and estimated PCR efficiencies of each target gene and a housekeeping gene in both calibrator and test samples (Pfaffl 2001). Consistent with the microarray expression analysis, the GMO3798 cell-line was chosen for calibration of the data (see Chapter 4, section 4.3.1.1 for details) and the relative expression levels of the genes analysed in all cell-lines were calculated as fold change compared to the expression levels detected in GMO3798. The PCR efficiency for each target gene was assessed through a standard curve that expresses a linear relationship between template quantity and target gene expression. Thus, the slope of a \log_{10} plot of a 10-fold dilution series of the reference cDNA (GMO3798) vs. respective Ct values was used for calculating the PCR efficiency with the equation $E = 10(-1/slope) - 1$. If the efficiency was below 90% (minimum required for quantitation by the $\Delta\Delta C_t$ method), further optimizations were performed to determine the best concentration for each primer. Once the estimated efficiency was within the 90-100% range, a validation experiment was performed to

determine if both the target and housekeeping gene (HKG) efficiencies were comparable and suited for analysis by the $\Delta\Delta\text{Ct}$ method. The validation was performed by calculating the ΔCt ($\text{Ct}_{\text{target}} - \text{Ct}_{\text{HKG}}$) on the serial-diluted cDNA reference and plotting it against the \log_{10} cDNA input. If the slope of the graphic approached 0, the experiment was validated and the qPCR conditions for both target and housekeeping gene could be used. Finally, all the reactions were performed in triplicate and only triplicates with standard deviation (SD) value lower than 0.3 were used for further analysis. The expression level of the gene of interest was assessed together with the housekeeping gene (the triplicates of test and HKG were performed in the same plate). Also, to confirm PCR specificity, a melting-curve analysis was performed in the end of each PCR reaction and the products were run on a 1% agarose gel to ensure that a single amplicon of the expected size was present.

4.3.2.2 HOUSEKEEPING GENE SELECTION

Since the efficiency of the cDNA synthesis cannot be assessed, a control for the cDNA input in each reaction is essential for a proper comparison of gene expression levels across samples. Thus, the analyses of the expression level of a gene whose expression is expected to be stable across cell-lines from different tissues and through the cell-cycle is essential as an internal control to be used for data normalization. It is crucial that the expression level of the selected housekeeping gene is constant in all cell-lines examined since an incorrect choice would lead to interpretation errors of experimental results. The glyceraldehyde-3-phosphate dehydrogenase (*G3PDH*) gene is the most widely used housekeeping gene in human qPCR studies and was therefore the choice for data normalization. For each cDNA sample, *G3PDH* triplicates were performed in the same plate as the gene of interest and used to determinate the ΔCt value. Thus, for each cDNA sample, a set of values for the gene of interest and for *G3PDH* were obtained and used for data normalization (Data Analysis I).

However, as the experiment progressed, some studies were published suggesting that *G3PDH* expression levels, as well as of other housekeeping genes, vary across different tissues and conditions. Accordingly, the best qPCR analysis should use an average of the level of expression of two/three housekeeping genes for data normalization (ΔC_t value). Most of the qPCR data had already been obtained at this point so, the expression levels of two other housekeeping genes (Tata-box Binding Protein - *TBP* and Beta-actin - *ACTB*) were determined on the cDNA samples of all cell-lines and a comparison was performed to determine which ones showed the lowest C_t value mean and the lowest standard deviation across all the samples tested during the study (Rabin, R. L. et al.; 2009). The average of the expression levels of the best pair or of the three would then be used for a second data analysis (data Analysis II).

The qPCR conditions for each housekeeping gene tested were optimized (Fig. 4.7, 4.8 and 4.9) and the amplification efficiencies were determined as 92.1% for the *G3PDH* gene, 98.9% for the *ACTB* and 90.5% for the *TBP*. The expression levels of the three housekeeping genes analyzed across the panel of 11 cell-lines tested are quite similar, with the exception of the U2OS cell-line that seems to express lower levels of the three genes (Fig. 4.7, 4.8 and 4.9–c). Nonetheless, as *G3PDH* shows the lowest C_t mean (16.718) and also the lowest SD (1.569) it still was the best housekeeping gene for data normalization, which gives more confidence to the data analysis previously done (Data Analysis I). Though, to ensure the most accurate analysis of the data and consequent interpretation of the results, the mean value of the *G3PDH* and *ACTB* C_t values were used for a second data analysis (Data Analysis II) that was then compared to the first data analysis.

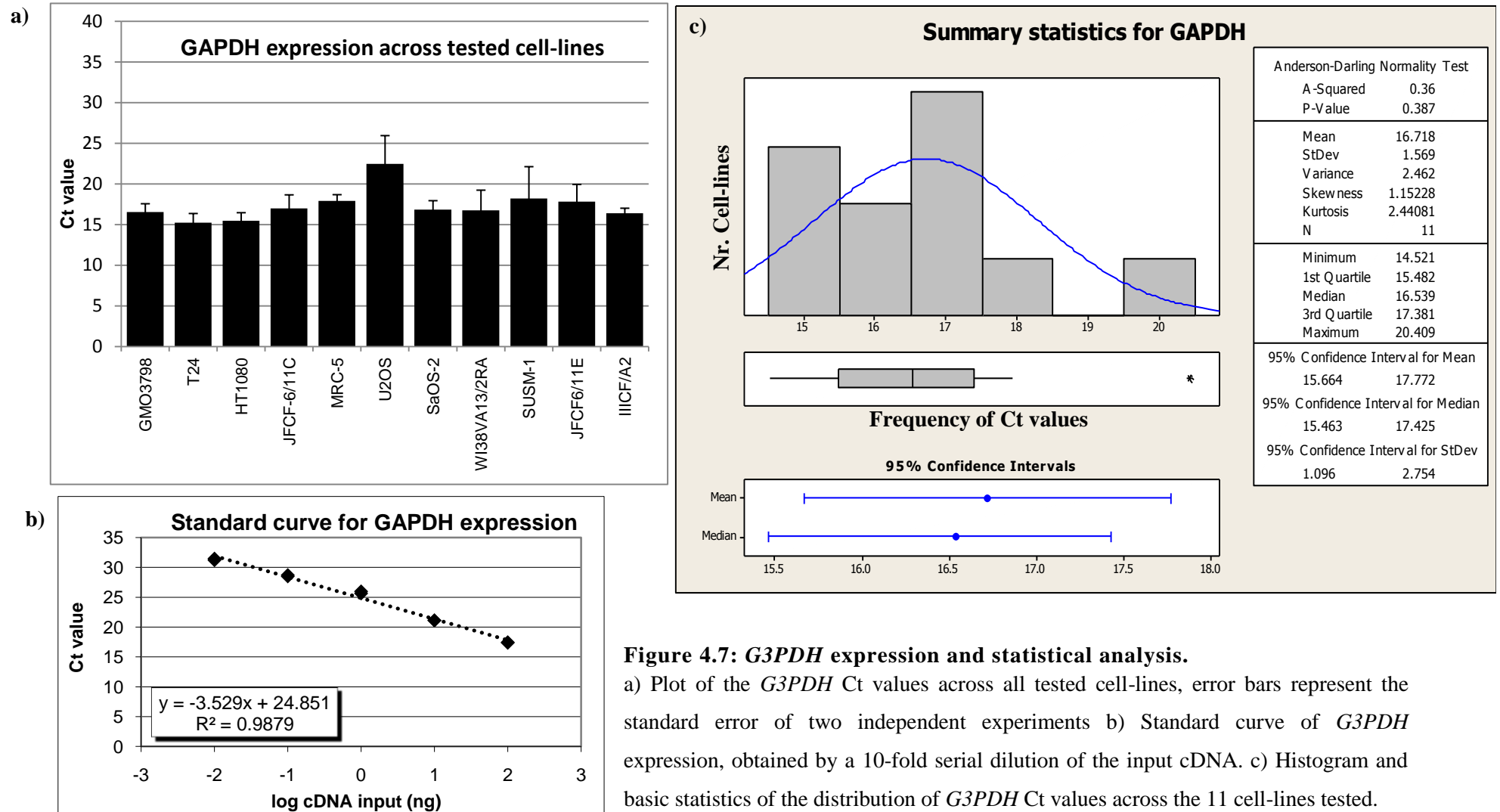


Figure 4.7: *G3PDH* expression and statistical analysis.

a) Plot of the *G3PDH* Ct values across all tested cell-lines, error bars represent the standard error of two independent experiments b) Standard curve of *G3PDH* expression, obtained by a 10-fold serial dilution of the input cDNA. c) Histogram and basic statistics of the distribution of *G3PDH* Ct values across the 11 cell-lines tested.

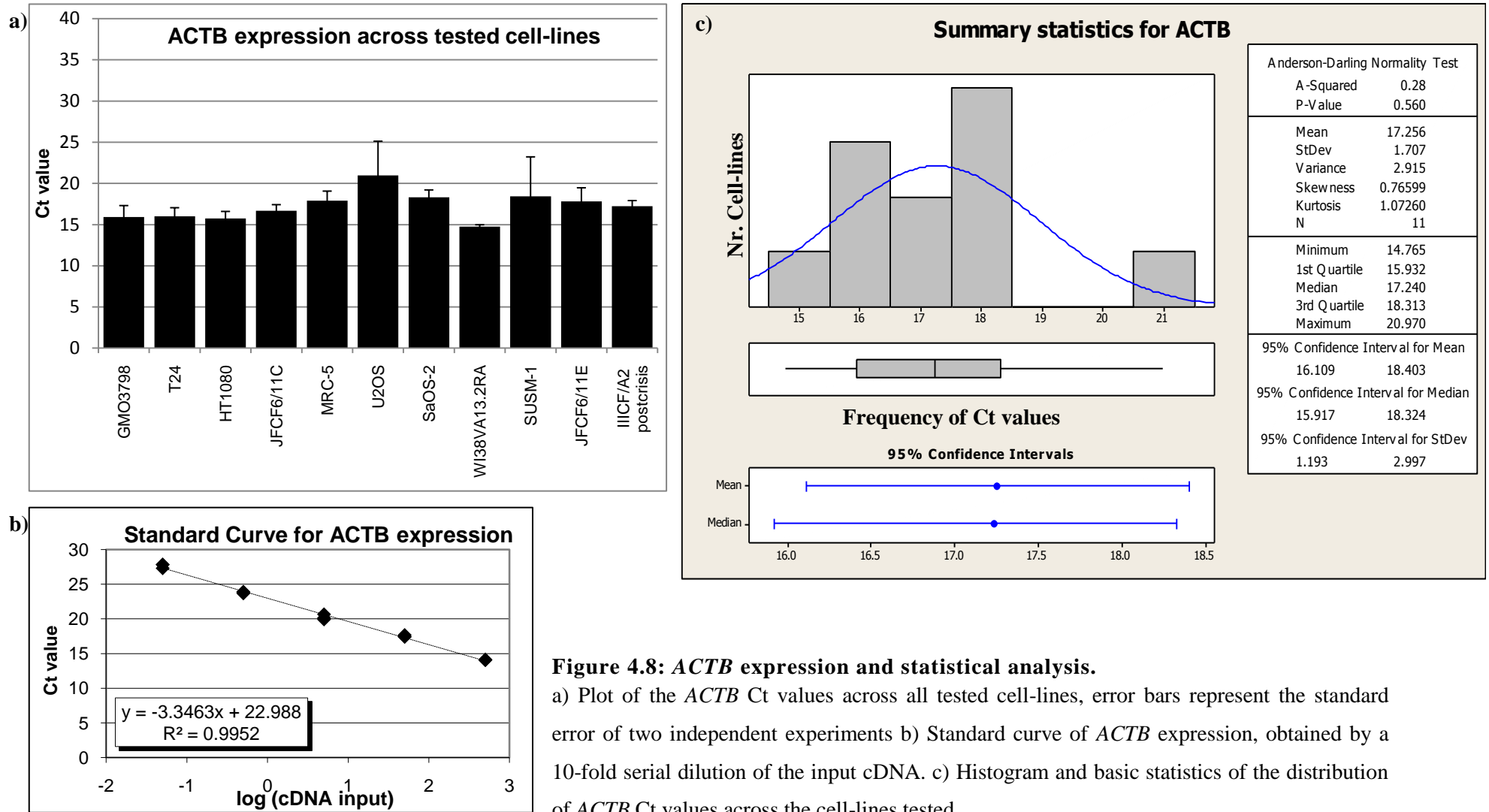


Figure 4.8: ACTB expression and statistical analysis.

a) Plot of the *ACTB* Ct values across all tested cell-lines, error bars represent the standard error of two independent experiments b) Standard curve of *ACTB* expression, obtained by a 10-fold serial dilution of the input cDNA. c) Histogram and basic statistics of the distribution of *ACTB* Ct values across the cell-lines tested.

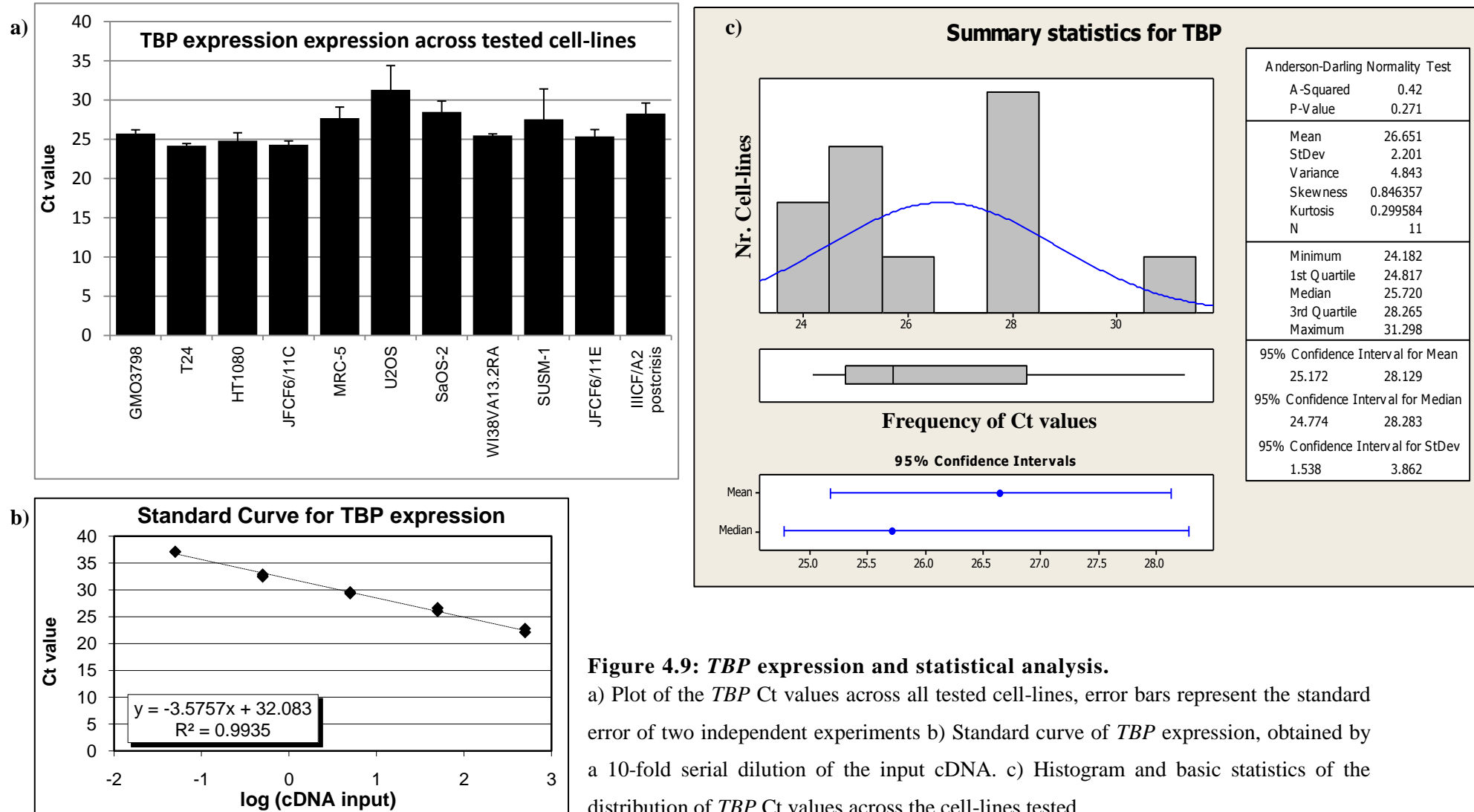


Figure 4.9: TBP expression and statistical analysis.

a) Plot of the *TBP* Ct values across all tested cell-lines, error bars represent the standard error of two independent experiments b) Standard curve of *TBP* expression, obtained by a 10-fold serial dilution of the input cDNA. c) Histogram and basic statistics of the distribution of *TBP* Ct values across the cell-lines tested.

4.3.2.3 NID1 GENE

Nidogene 1 (NID1) is a major component of basement membranes, a highly specialized extracellular matrix found at the epithelial/mesenchymal boundary and around muscle, peripheral nerves, and fat cells. NID1 strongly interacts with laminin (Paulsson et al., 1987; Mayer et al., 1993), collagen IV and perlecan (Aumailley et al., 1993). Thus, NID1 has an important role in establishing and maintaining basement membrane and tissue architecture. Interestingly, as basement membranes compose a physical barrier for cell movement, migration and/or invasion, the role of NID1 becomes extremely important to avoid metastatic formation and progression. Indeed, loss of both nidogen 1 and 2 expressions has been shown to occur in human gastrointestinal tumours, caused by high methylation of both promoters (Ullazi et al. 2007). To determine the expression level of *NID1* in ALT and non-ALT cell-lines, qPCR assay was designed and optimized. Primers that amplified 170 bp across exons 1 and 2 (Fig. 4.10) were used to measure the expression level of *NID1* in 11 cell-lines (Fig. 4.10). To determine the efficiency of the reaction, a standard curve was obtained (Fig. 4.11–a). The calculated efficiency, 92.31%, was comparable to the efficiency of the housekeeping gene, as demonstrated by the validation experiment (Fig. 4.11–b).

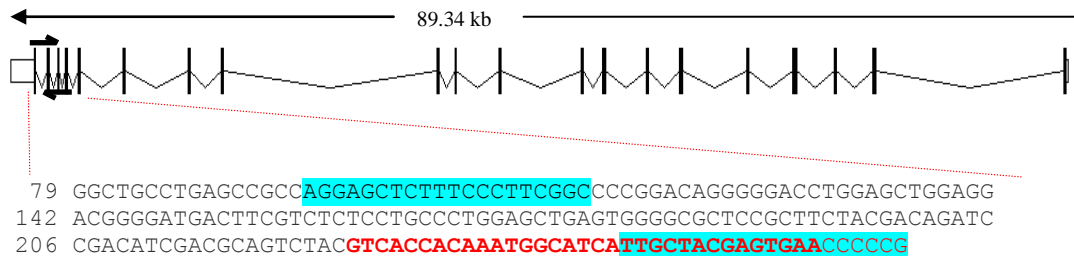


Figure 4.10: Diagram representing NID1 gene.

NID1 gene is composed of 20 exons (vertical black bars; introns are shown in triangular lines) spliced from a 89.34 kb long region. The long arrow represents the coding strand (reverse) and the white box shows the 3' UTR. The half arrows represent the primers used for qPCR amplification across exons 1-2 and the zoomed area shows the cDNA sequence amplified by qPCR. Primer sequences are highlighted in blue and the exon1 sequence is represented in black whilst the exon 2 sequence is red. The numbers represent the cDNA base pairs.

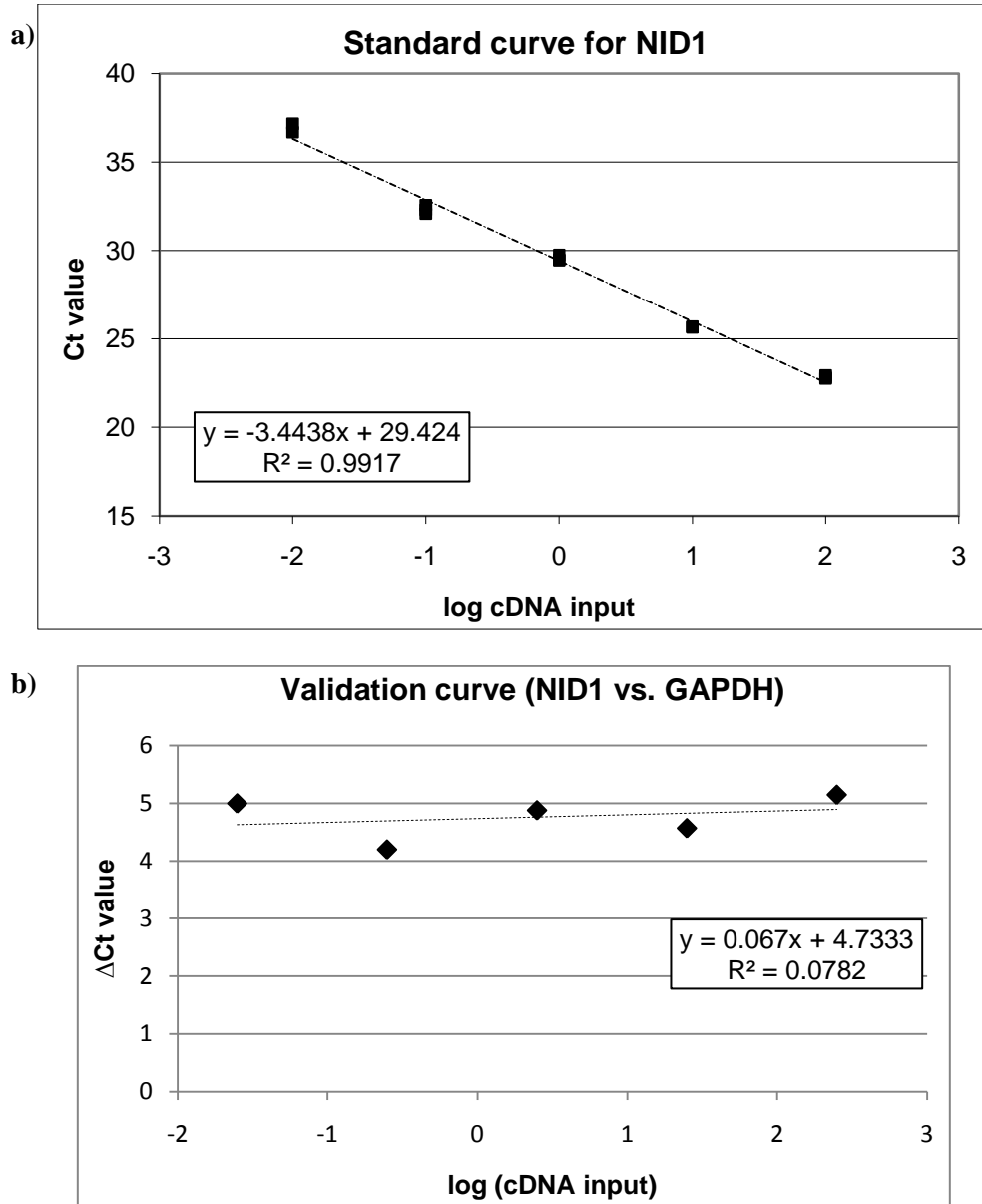


Figure 4.11: Validation of NID1 qPCR amplification.

a) A standard curve was performed with a 10-fold serial dilution of the cDNA input. The logarithm of the cDNA input was plotted against the respective Ct values and the obtained slope was used to determine the PCR efficiency. b) A validation curve was performed by plotting the logarithm of the cDNA input against the Δ Ct (NID1-G3PDH1) values.

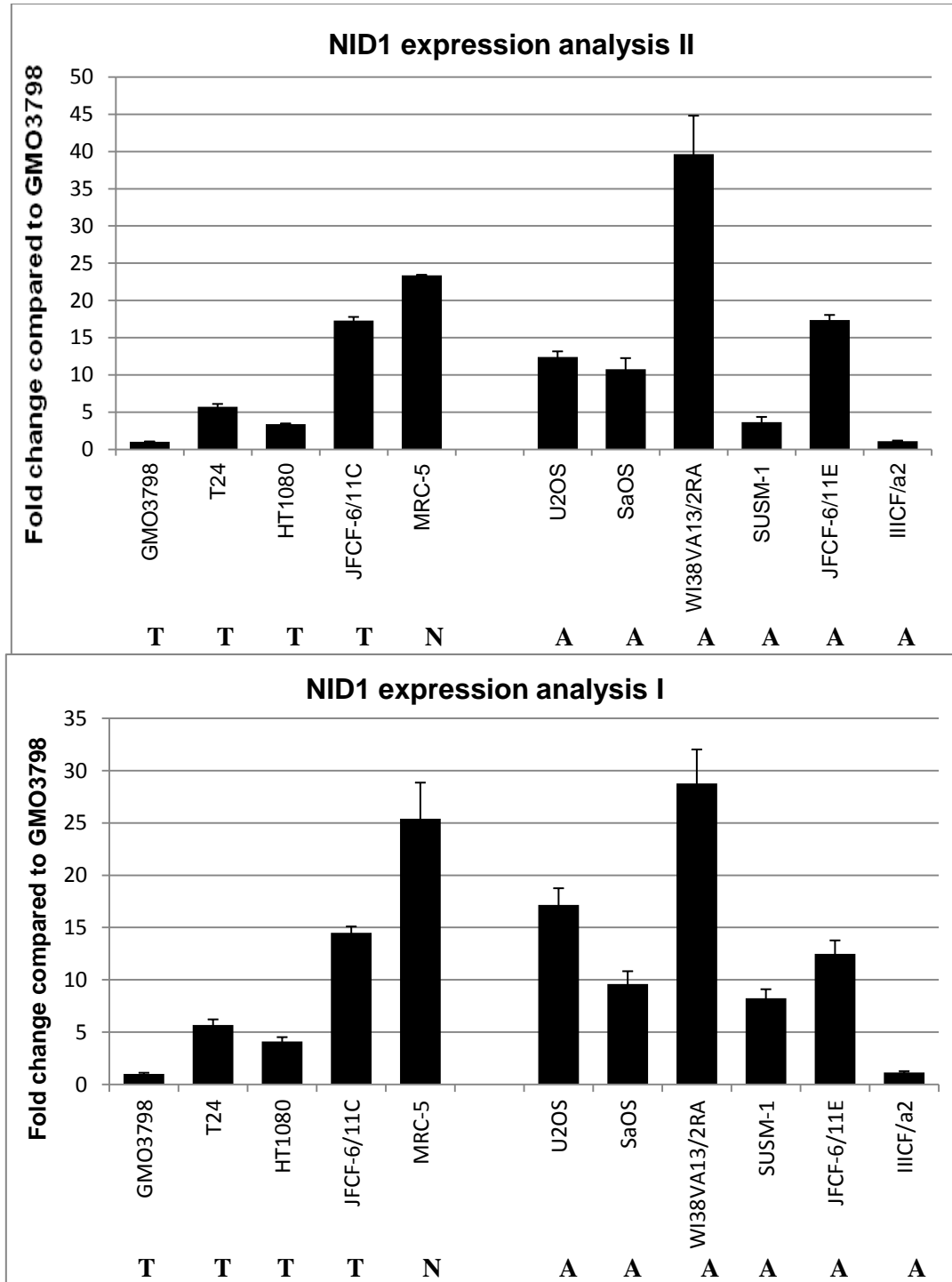


Figure 4.12: NID1 expression levels.

Two-independent RNA extractions were used to obtain the fold changes relative to expression of GMO3798 cell-line. *G3PDH* or *G3PDH* and *ACTB* were used for input normalization and the error-bars reflect the standard deviation. Expression of Telomerase + (T) and normal (N) cell-lines, on the left cluster was compared to the expression of the ALT+ (A) cell-lines, clustered on the right of the graphic.

NID1 transcripts were detected in all cell-lines tested and all show higher expression levels compared to the lymphoblastoid GMO3798 cell-line (tel+) (Fig. 4.12). Each cell-line shows different expression levels, probably reflecting tissue-specific differences (see Appendix-2). However, when the cell-lines are clustered as **ALT+** or **non-ALT** (normal or tel+), according to the Wilcoxon Rank Test, no significant differences in the levels of *NID1* expression were observed between the two clusters (p-value 0.5228/0.6481 data analysis I and II, respectively). Thus, as the preliminary microarray data indicated, *NID1* expression pattern seems not to differ between ALT+ and non-ALT cells, suggesting that transcriptional changes at the gene closest to MS32 are unlikely to be the reason underlying its extraordinary instability in ALT+ cells.

4.3.2.4 LYST GENE

Lysosomal trafficking protein (*LYST*, or also known as Chediak–Higashi Syndrome protein 1 - *CHS1*) is a massive cytosolic protein of 425 kDa (3801 amino acids). The role of *LYST* is not known but the presence of certain domains in the protein indicates that it might be required for intracellular protein trafficking to and from the lysosome. Defects in *LYST* protein are the cause of Chediak-Higashi Syndrome, an autorecessive disorder (Barbosa et al., 1996; Perou et al., 1996).

Though no significant *NID1* expression changes were observed in ALT+ compared to non-ALT cells, *LYST* also locates in MS32 region (225.5 kb upstream the minisatellite) so a qPCR assay was carried out to analyse its expression level in the 11 cell-lines. Primers were designed so that a 136 bp region across exons 3, 4 and 5, could be amplified (Fig. 4.13). The efficiency of the reaction, 92.31%, was calculated from a standard curve (Fig.

4.14–a) and was comparable to the efficiency of the housekeeping gene, as demonstrated by the validation experiment (Fig. 4.14–b).

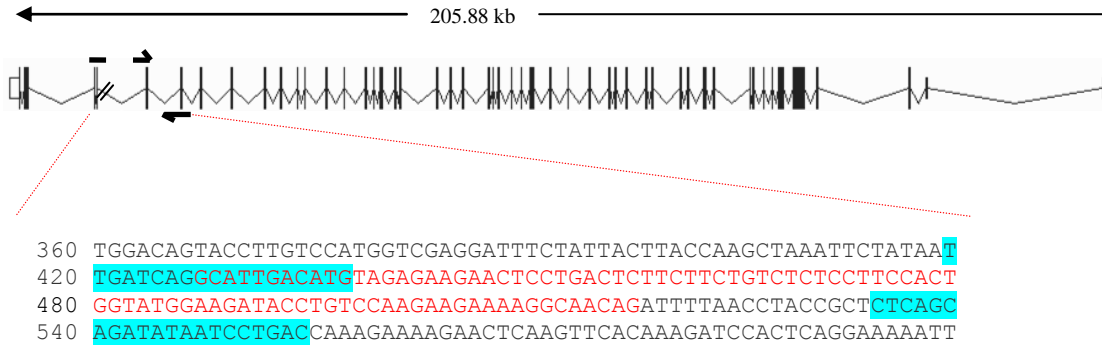


Figure 4.13: LYST diagram.

LYST gene is composed of 53 exons (vertical black bars) spread across a 205.88 kb region (splice sites represented by the triangles). The top arrow represents the coding strand (reverse). The white box on the left represents a UTR. The half arrows represent the primers used for the qPCR experiment amplifying across exons 3-5. The amplified sequence is shown, with the primers highlighted in blue and each exon represented with alternate colours (exon 3 in black, exon 4 in red and exon 5 in black again).

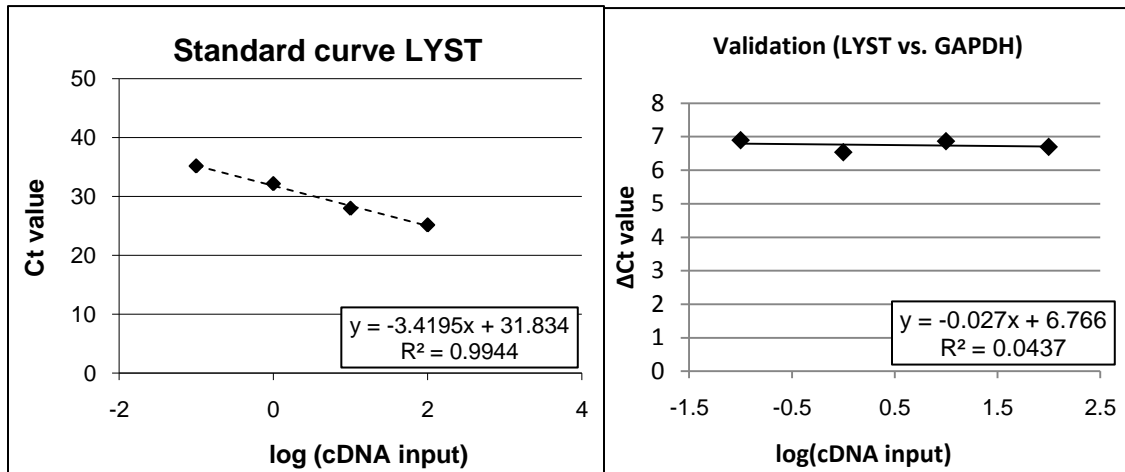


Figure 4.14: Validation of *LYST* qPCR amplification.

a) A 10-fold serial dilution of the cDNA input was performed to test the efficiency of the qPCR reaction. The logarithm of the cDNA input was plotted against the respective Ct values and the obtained slope was used to determine the PCR efficiency. b) To validate the qPCR analysis, the logarithm of the cDNA input was plotted against the Δ Ct (*LYST*-*G3PDH1*) values.

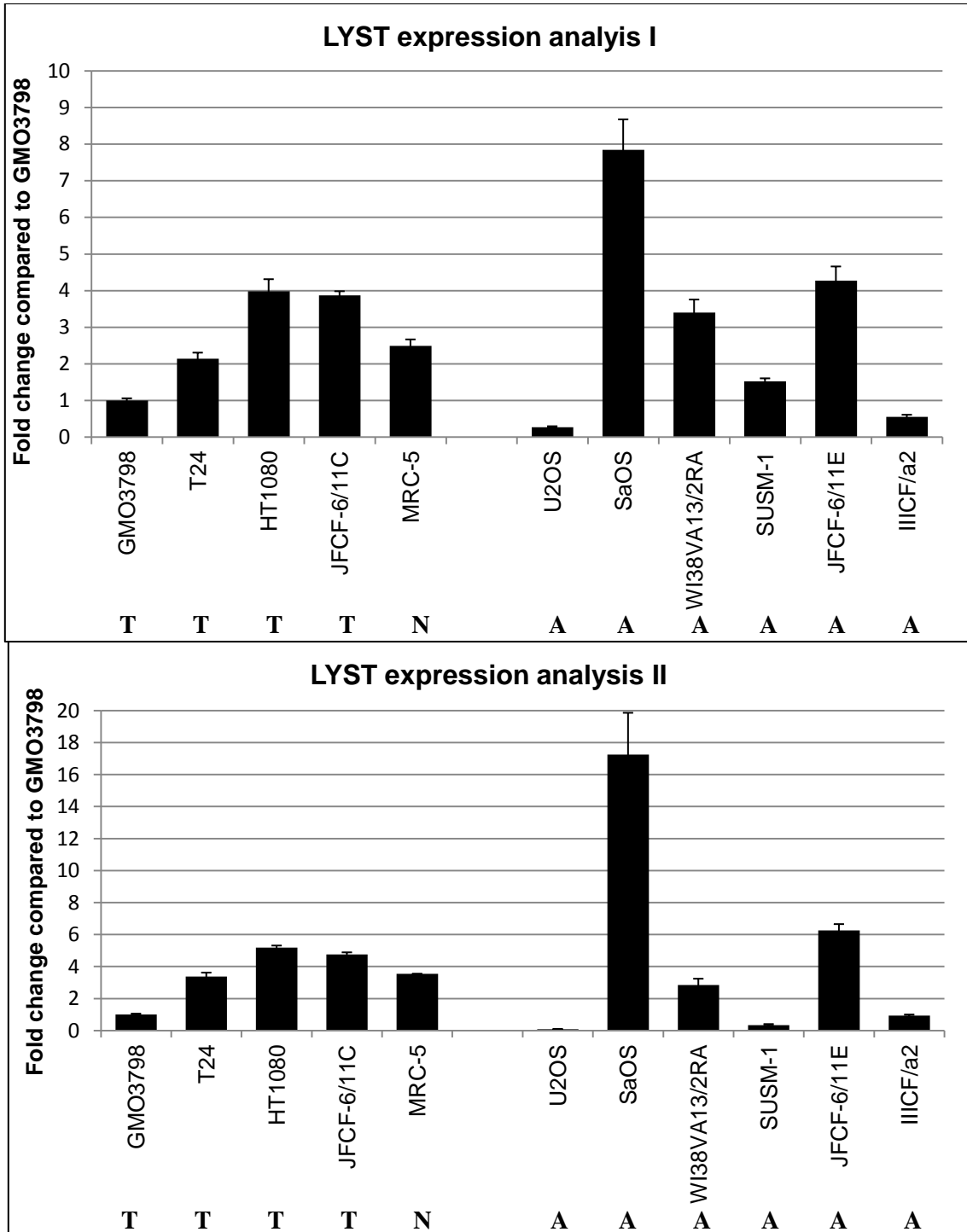


Figure 4.15: *LYST* expression levels.

Bars represent fold changes relative to GMO3798, with template input normalized to G3PDH or to G3PDH and ACTB expression. The error-bars reflect the standard deviation of two independent RNA extractions. Telomerase + (T) and Normal (N) are clustered as **Non-ALT** on the left side of the graphic, whilst the ALT+ (A) cells are represented on the right-side.

As seen in *NIDI* expression analysis, *LYST* expression pattern also greatly differs between the different cell-lines tested (Fig. 4.15). Also, both data analysis show the same fold change levels, with the exception of SaOS cell-line that unexplainably shows a twice fold change on data analysis II (17) than in analysis I (7.5) compared to the calibrator cell-line GMO3798. Contrasting with *NIDI* gene, *LYST* expression levels are lower in U2OS and IICf/a2-postcrisis cell-lines, when compared to the calibrator. Nonetheless, neither data analysis shows significant differences between ALT+ and non-ALT cell-lines (p value 0.9273 for analysis I and 0.5228 for analysis II with the Wilcoxon Rank Test). Therefore, no consistent changes in transcription levels were detected at the *LYST* gene that lies 225 kb upstream the MS32 minisatellite in the ALT+ vs. non-ALT cell-lines tested.

4.3.2.5 GPR137B GENE

G protein-coupled receptor 137B (GPR137B), previously known as TM7SF1, was first described as a membrane protein, which is upregulated during kidney development and an important role in cell-type-specific differentiation-dependent signalling processes was suggested (Spangenberg et al., 1998). GPR137B was also found to be over-expressed in Wilms tumours (Spangenberg et al., 1998) and differentiating osteoclasts (Nomiya et al., 2005). GPR137B is the closest downstream gene to the MS32 minisatellite, locating at 41 kb. Consequently, a qPCR assay to analyse GPR137B transcriptional levels ALT+ and non-ALT cells was performed. Primers amplifying 191 bp across exons 5, 6 and 7 were designed (Fig. 4.16) and the efficiency of the PCR reaction was calculated as 92.31%, through a standard curve (Fig. 4.17–a). A validation experiment (Fig. 4.17–b) showed that

the efficiency was comparable to the obtained for G3PDH amplification, allowing the use of the $\Delta\Delta\text{Ct}$ method for relative quantification of the expression levels.

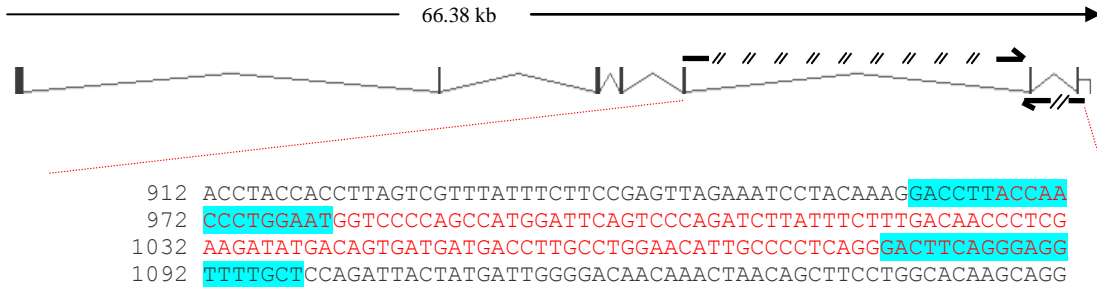


Figure 4.16: GPR173B diagram.

GPR173B gene is distributed along 66.38 kb on 1q34 and is composed of 7 exons (vertical black bars; triangles represent introns). The top arrow represents the coding strand (forward) and the white box the 3' UTR. The primers used for qPCR amplification are shown as half arrows across exons 5-6 (forward) and 6-7 (reverse), which is better shown on the zoomed sequence. The primers' sequence are highlighted in blue and exons are alternatively coloured in black or red.

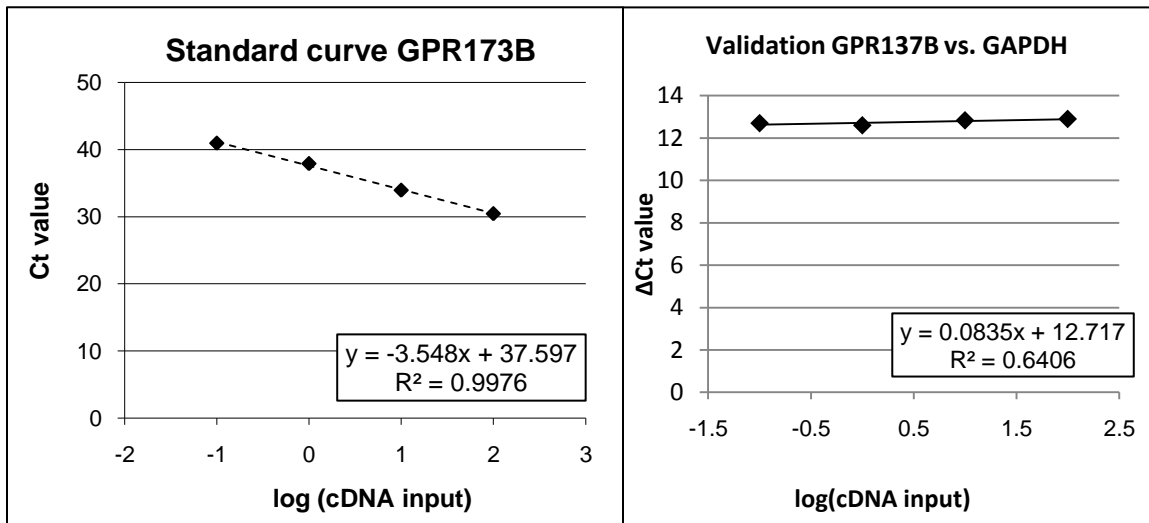


Figure 4.17: Validation of *GPR173B* qPCR.

a) The qPCR reaction efficiency was obtained with a 10-fold serial dilution by plotting the logarithm of the cDNA input with the respective Ct values. b) To validate the analysis, the logarithm of the cDNA input was plotted against the ΔCt (*GPR173B*-*G3PDH1*) values.

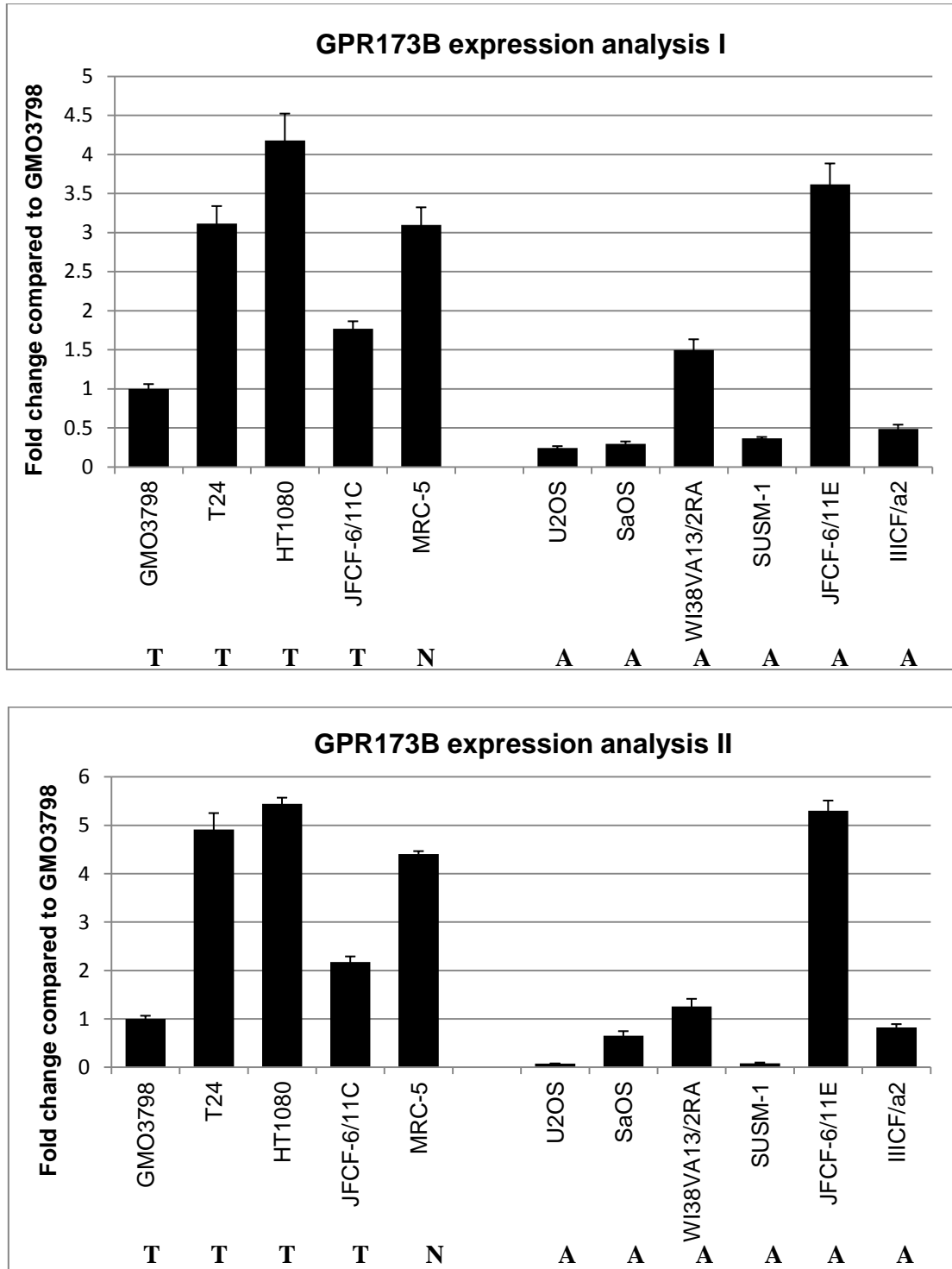


Figure 4.18: GPR173B expression.

The graphics summarize data from two-independent RNA extractions and the error-bars reflect their standard deviation. Telomerase + (T) and normal (N) cell-lines (non-ALT) are clustered on the left-side of the graphic whilst the ALT+ (A) cell-lines are represented on the right-side. The shown fold changes are relative to GMO3798 expression, with internal normalization to G3PDH expression.

GPR173B expression pattern also varies between the different cell-lines tested, although less than observed in *NIDI* and *LYST* (Fig. 4.18). Again, the two different data analysis methodologies applied show very similar fold change patterns compared to the calibrator cell-line. As observed in the both upstream genes analysed, no significant differences could be detected between ALT+ and non-ALT cell-lines (p-value 0.0828 for both analysis according to the Wilcoxon Rank Test). It seems that no common change in the *GPR173B* expression level is associated with the ALT pathway.

4.3.2.6 PUTATIVE NOVEL GENE

Even though MS32 minisatellite is flanked by *NIDI* and *GPR173B* genes, a processed pseudogene has been found at 12.6 kb from its 3' end. Processed pseudogenes are non-functional transcribed pseudogenes that typically lack intronic and promoter sequences, contain poly(A) 3' tails and are flanked by target-site duplications. During evolution, processed pseudogenes tend to accumulate frameshift mutations and premature stop codons (Vanin et al., 1985; Weiner et al., 1986). Processed pseudogenes can either flank genes or lie within intergenic regions. A number of possible mechanisms have been proposed for their expression: use of nearby promoters of protein-coding genes, insertion into a UTR region or cryptic promoter elements in the intergenic DNA (that might have originated from transposable elements, from genomic duplication of promoter regions).

Although no significant differences on the expression levels of the genes around the MS32 minisatellite were found to be associated to the ALT mechanism (see Chapter 4, sections 4.3.1.3 and 4.3.2), differences in the DNA conformation derived from non-genic transcriptional changes in the region could still expose MS32 to molecular mechanisms that

could affect its stability in ALT+ cells. Thus, to clarify if transcriptional changes associated to ALT are occurring in the region, the expression levels of the processed pseudogene were analysed by qPCR.

A BLAST search showed that this particular pseudogene derives from aconitase 2 precursor (*ACO2*), a mitochondrial protein transcribed from a gene located on chromosome 22 (Figure 4.19). The primer design and the qPCR conditions were carefully optimized to guarantee that only the processed pseudogene was amplified. Thus, a primer set that could amplify a 169 bp *ACO2* product (across exons 1 - 2 boundary) and a pseudogene product from chromosome 1 was chosen. However, the 3'-terminal base of the reverse primer is only specific to the pseudogene (cytosine instead of the *ACO2* tyrosine at the same position), which combined with the high annealing temperature (60°C) used, should not amplify the *ACO2* product (Figure 4.19). To confirm that the conditions used were amplifying exclusively a transcript derived from the pseudogene, PCR products derived from three of the tested cell-lines were directly sequenced. The sequencing data confirmed that all products derive from the pseudogene on chromosome 1 since in all sequenced products the 9 diverged nucleotides fully match the pseudogene sequence (Table 4.5).

Reference sequence mRNA NM_001098.2 (spliced from 18 exons on chr. 22)

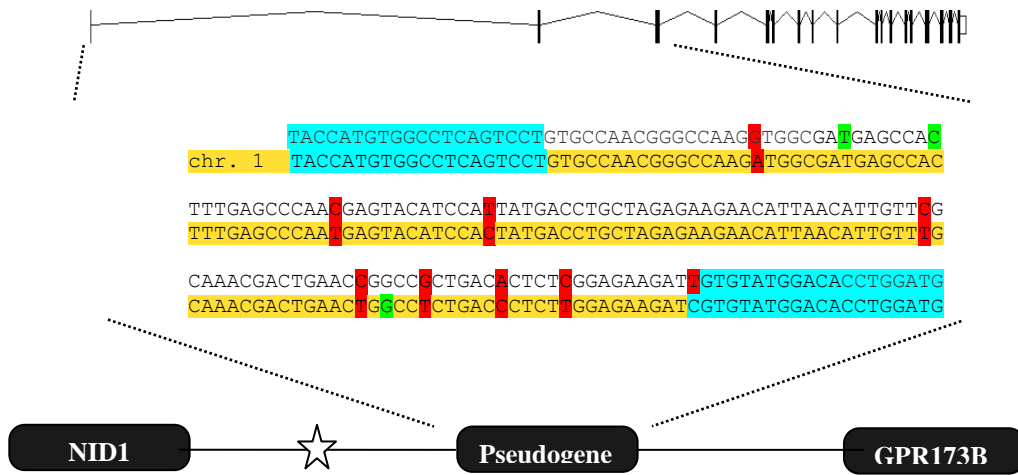


Figure 4.19: Diagram of pseudogene *ACO2*.

The processed pseudogene, on chromosome 1 (highlighted in yellow), derives from the first 3 exons of *ACO2* gene, located on chromosome 22. The PCR amplified regions obtained after optimizations are aligned in the centre. Nucleotide changes (SNPs) between the *ACO2* gene and pseudogene are signalled as red when different or green if identical. Primer positions are highlighted in blue. The star represents MS32 minisatellite location.

Base position (bp)	37	63	75	109	124	129	135	140	150
Cell-lines									
JFCF-6/11C (Tel+)	A	T	C	T	T	T	C	T	C
JFCF-6/11E (ALT+)	A	T	C	T	T	T	C	T	C
WI38VA13/2RA (ALT+)	A	T	C	T	T	T	C	T	C
<i>ACO2 gene sequence</i>	<i>G</i>	<i>C</i>	<i>T</i>	<i>C</i>	<i>C</i>	<i>G</i>	<i>A</i>	<i>C</i>	<i>T</i>

Table 4-5: Sequencing data to confirm pseudogene template for PCR reaction.

The PCR amplicon position of the 9 nucleotide changes between *ACO2* gene and the pseudogene on chr. 1 are represented on the top row. The sequencing data for the three tested cell-lines are represented on the table and for better comparison the bottom row shows the *ACO2* equivalent nucleotide.

Although the sequencing data shows that the products obtained derive from the pseudogene on chromosome 1, it is technically difficult to fully exclude a genomic origin for the analysed PCR products. All RNA samples used in this study had been checked for DNA contamination by spectrophotometry and denaturing gel electrophoresis. Also, all the cDNA samples used were treated with DNase I to eliminate any potentially contaminant genomic DNA. Thus, as the RNA quality had been checked, DNase I used prior to the cDNA synthesis and primers were designed across exon-exon boundaries (for the other genes) and the limiting amount of RNA available, no reverse transcriptase negative (RT-negative) controls were performed on the samples. Thus, the distinction between transcripts and the genomic sequence of the pseudogene on chromosome 1 in the cDNA samples obtained is not possible on the cDNA collection available. Further cDNA synthesis with no reverse-transcriptase should be performed to further investigate whether this pseudogene is being transcribed or not.

4.3.3 CONCLUSION

From the analysis performed, it seems that the use of just one or at least two housekeeping genes for data normalization do not affect the final result since both data analysis I and II showed consistent results. However, a careful analysis of the expression levels of the housekeeping gene across the samples to be tested needs to be performed prior to further analysis, to determine if the HKG expression is constant in the samples to be tested. Considering the expression levels of the three analysed genes, no differences could be observed between ALT+ and non-ALT cells. A clear cell-line specific differential expression was detected, especially on *NIDI* gene that showed the highest cell-line variation on the relative expression compared to GMO3798 (Fig. 4.23) but no association

to a particular type of TMM could be detected. The results suggest that no transcriptional-changes around MS32 minisatellite occur in ALT+ cells compared to non-ALT cells. Nonetheless it is interesting to note that the ALT+ cell-lines seem to show much higher expression variability of *NID1* and *LYST*, when compared to the non-ALT cells analysed.

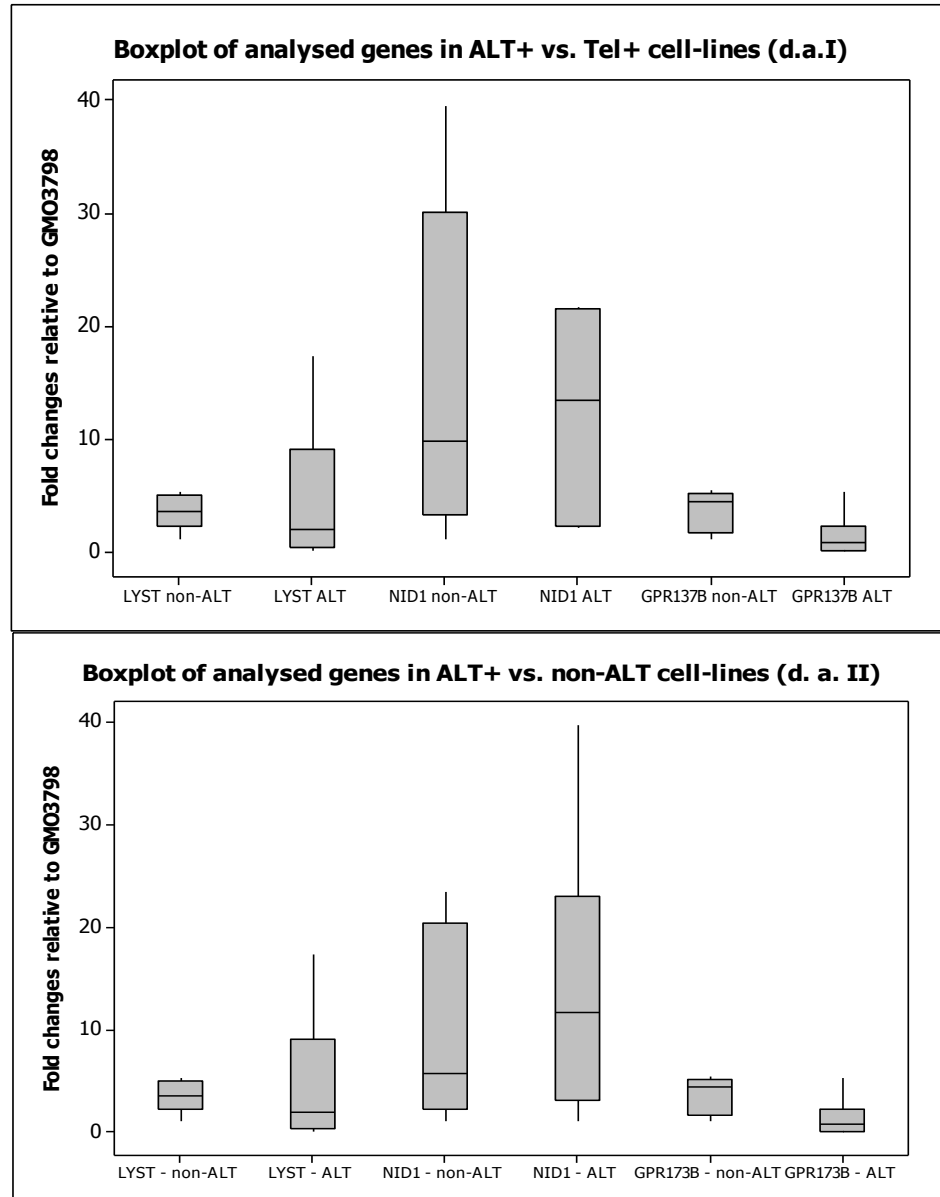


Figure 4.23: Summary of qPCR analysis.

The expression level of the genes analysed, obtained as relative fold changes compared to GMO3798 cells, are summarized in the boxplots shown. For each gene, a boxplot of the fold changes for the Non-ALT and for the ALT cells are represented and shown side by side with the median and standard deviation represented.

4.4 DISCUSSION

The instability of MS32 minisatellite in ALT+ cells is extremely puzzling, since no clear relationship between the minisatellite and the telomere elongation mechanism and/or the telomere itself is evident. Thus, one of the possible reasons for this association would be that transcriptional-changes could alter the conformation of the 1q43 region that includes MS32 minisatellite in ALT+ cells, exposing the minisatellite to cellular machinery that would then result in the observed high instability.

This chapter focuses on experiments performed to test this hypothesis. Many genes have been shown to be involved in the ALT+ mechanism (see Chapter 1, section 1.2) but the exact mechanism still needs to be dissected. Thus, it seemed logical that if expression levels between ALT+ and non-ALT cell-lines were going to be analysed a genome-wide experiment could also be performed to shed some light into yet unknown ALT-players. An experiment was performed to analyse the differential expression between ALT+ and Tel+ cells that originated from the same cell-line. To minimize the effect of sample variation between independent experiments, the expression pattern of the samples were indirectly tested by using a calibrator cell-line to which each one of the test cell-lines was directly compared (see diagram on Fig. 4.2). Additionally, to validate the set of data obtained and to ensure that the calibrator cell-line was not interfering with the results (Dobbin et al 2002), another experiment was conducted in which the ALT+ and the Tel+ cell-line were compared directly. Again, a vast list of genes was found to be significant differently expressed between the two cell-lines. However, when comparing both data sets, a common list of 136 genes was found which increased the confidence in the results and indicated that the calibrator cell-line did not affect the results in an unexpected manner. Several interesting genes were found upregulated in the ALT+ cell-line, including *TRF1*, which

could reflect the presence of longer telomeres in the ALT⁺ cells in comparison to the Tel⁺ ones. Nonetheless, the other telomere binding protein TRF2 and genes known to be involved in the ALT⁺ pathway (for example the components of the MRN complex) or even hTERT, the protein responsible for telomerase activity in Tel⁺ cells were surprisingly not identified as showing transcriptional changes. Although frustrating, it is consistent with ALT being a recombination-like mechanism that “recycles” proteins involved in other(s) DNA repair pathways to elongate telomeres (Dunham et al 2002; Varley et al 2002; Wang, R. et al 2004), which would explain why no significant expression changes were detected as most cells (ALT⁺ and non-ALT) will require the expression of such proteins. Furthermore, no significant changes of hTERT expression between ALT⁺ and Tel⁺ cells is also in accordance with the current model of *hTERT* regulation, where alternative splicing (particularly the α -transcript) negatively regulates telomerase activity and consequently, most cells may express a functional or dysfunctional hTERT transcript (Ulaner et al 1998; Fujiwara, M. et al. 2004; Zaffaroni, N. et al 2005). Thus, the fact that *hTERT* was not detected as upregulated in the Tel⁺ cells might be due to the potential transcription of one of its variants in the ALT⁺ cells. Also, *TRF2* expression was shown not to differ significantly in the ALT⁺ H295R from the Tel⁺ HeLa cells (Fujiwara, M. et al 2006), which is also similar to our findings. One more concern raised about the experimental procedure that might have prevented the detection of important ALT players is the fact that the RNA analysed was extracted from asynchronously growing cells. However, it would be expected that the proportion of cells in a particular cell-cycle stage within the analysed populations would be the same between the ALT⁺ and the Tel⁺ cell-line. Therefore, if a potential key ALT player is more expressed during a specific phase of the cell-cycle, for

example G2 in ALT+ cells, it would be reasonable to expect that an expression difference could still be detected by the expression microarray analysis.

Nonetheless, several potentially interesting genes were upregulated in the ALT+ cells in the list common to both experimental designs. One of these genes codes for RAD51C that forms a complex with XRCC3 protein, it is involved in branch migration and Holliday junction resolution (Lio et al., 2004; Nagaraju, G. et al 2006), probably by ensuring the fidelity of homologous recombination. Also, RAD51C recruitment depends on NBS1 and RPA, which might indicate a role just after DNA end resection (Badie et al 2009). Moreover, XRCC3 seems to be required for t-circle formation in ALT+ cells (Wang et al 2004; Compton et al 2007), suggesting a possible role for the RAD51C-XRCC3 in the ALT+ mechanism that should be further investigated. Another gene upregulated in the ALT+ cell-line is the p53-binding protein MDM2. The combined expression of the adenovirus E1A, Ha-RasV12 and MDM2 were sufficient to transform normal human cells into cells able to form tumours with no telomerase activity (Seger et al 2002). The *P53* tumour-suppressor gene is activated with severe telomere-shortening, which leads to a growth-arrest (Chin et al 1998). Interestingly, the ALT+ cell-line analysed (like most ALT+ cells, with the exception of the U2OS cell-line) is P53-negative. Thus, it would be interesting to investigate whether MDM2, the principal p53-antagonist (Wu et al. 1997) can contribute to cell transformation purely by p53-inhibition or by intervention in other molecular processes, perhaps the ALT mechanism. Finally, another gene upregulated in the ALT+ cell-line is closely involved with one gene located in the MS32 minisatellite region. In fact, ARID4A together with ARID4B (750 kb from MS32 minisatellite) are part of the histone deacetylase-dependant SIN3A transcriptional corepressor complex (Lai et al 2002). Interestingly, both genes have been proposed as mice tumour suppressors, since a

myelodysplastic and myeloproliferative disorder in mice with *Arid4a* and/or *Arid4b* mutations progresses to hematologic malignancies, resembling human CML and AML (Wu et al. 2008). The protein ARID4A interacts with the RB protein (which is inactivated in many tumours and is involved in several cellular processes like cell-cycle control and DNA replication) and the repression of E2F-dependent transcription by ARID4A, ARID4B and RB leads to cell arrest (Binda et al 2006). However, *ARID4B* was not detected as significant differently expressed in the ALT+ cell-line, which indicates that further validations are required to elucidate whether the ARID genes have a specific role in ALT+ cells. Although genes with potential roles on the ALT+ mechanism were identified with the expression analysis, a more exhaustive experiment should be performed with more ALT+ and Tel+ cell-lines as well as normal tissue and tumour-derived samples, perhaps in synchronized populations.

Focusing on the region around MS32 minisatellite, the microarray analysis also showed no significant differences in any of the analysed genes, indicating that no major differences in the expression pattern of the region are occurring in ALT+ cells. However, to determine if more subtle transcriptional changes are occurring in the 1q42-43 region in ALT+ cells, qPCR was used to assess the expression level of individual genes around MS32, in several cell-lines. In total, the relative expression of three genes (*LYST*, *NIDI* and *GPR173B*) was quantified in various ALT+ and non-ALT cell-lines as a fold-change of the expression level of the same calibrator cell-line used for the expression microarray experiment (GMO3798). The results showed great variance in the expression levels of each of the genes analysed between cell-lines, but no significant differences associated with the ALT mechanism were detected, confirming the results obtained by the expression microarray data analysis.

Also, the extensive data analysis performed with one (*G3PDH*) or two (*G3PDH* and *ACTB*) HKG showed no major changes between the two approaches. The HKG expression is used for normalization purposes, it is essential that it remains stable throughout all the experimental conditions (Thellin et al 1999). However, it is unlikely that any gene shows such stable expression, since most genes are likely to be regulated at a particular point (Kubista et al 2006). Thus, the most recent consensus on HKG selection indicates that an expression analysis of different HKG in the samples to be analysed should be performed prior to the qPCR experiment (Andersen et al 2004; Jung et al 2007) and the least variable HKG gene should be used for normalization. Accordingly, our studies showed that the most suited HKG for this study was *G3PDH*, since it showed less expression variation across the 11 cell-lines analysed and the addition of another HKG (*ACTB*) to the normalization step did not significantly alter the results.

Another interesting aspect of the qPCR experiment was the expression variation amongst the cell-lines analysed. Even though no expression changes could be associated to a particular TMM, the expression levels of the 3 genes analysed varied greatly between cell-lines. These changes might reflect cell-line specific expression patterns, since cell-lines with different TMM but derived from the same tissue showed similar gene expression levels (Fig. 4.12, Fig. 4.15 and Fig. 4.18). Particularly, the cell-lines WI38VA13/2RA (ALT+) and the MRC5 (normal), both derived from lung tissue, show the highest expression of *NIDI* gene. Also, the fibroblast HT1080 (Tel+), JFCF6T.IJ/11C (Tel+) and JFCF6T.IJ/11E (ALT+) show similar levels of *LYST* expression. Finally, also the two osteosarcoma-derived ALT+ cell-lines, U2OS and SaOS have comparable expression levels of *NIDI* and *GPR173B*.

In conclusion, no transcriptional-changes specific to ALT+ cells seem to occur around the MS32 minisatellite, which indicates that the observed instability is either specifically triggered by the minisatellite itself or conformational changes unrelated to gene expression.

CHAPTER 5: MS32 INSTABILITY AND THE ALT MECHANISM

5. 1 BACKGROUND

The repetitive nature of DNA repeats confers to these genomic loci a propensity to form unusual DNA structures that can affect their stability. In addition, various other factors may also compromise repeat stability, mainly the number of repeats in the tract or the purity of the repeat array. The direction of replication has also been implicated in the (CTG)_n repeats stability in bacteria (Kang et al. 1995; Samadashwily et al. 1997) and yeast (Freudenreich et al. 1998). Although the precise events leading to repeat instability are not known, the mechanisms affecting the stability of microsatellites and minisatellites seem to differ. Indeed, microsatellites, including trinucleotide repeats, appear to primarily mutate primarily by strand slippage during DNA replication (Schlotterer et al 1992), whilst minisatellites seem to be prone to recombinational processes. Furthermore, the minisatellite sequence is thought to greatly influence the type of mechanisms involved in instability. Instability at GC-rich minisatellites is thought to involve gene conversion-like events in meiosis or unequal sister chromatid exchange and intramolecular recombination during mitosis (Buard. et al 1994; Tamaki, et al 1999; Bois et al, 1999) but the instability at AT-rich minisatellite is even less understood.

In ALT+ cells, telomeres are elongated through rearrangements resulting from both simple intra-allelic events and more complex inter-telomeric recombination events, where the origin of the newly added telomeric repeats is still not known (other telomere or extrachromosomal-telomeric DNA) (Varley et al 2002). However, the activation of the ALT mechanism in cells does not just result in the elongation of telomeres via a recombination-like event but also greatly affects the stability of MS32 minisatellite (Jeyapalan et al 2005).

In the germ-line cells, MS32 minisatellite stability is affected by a meiotic-recombination hotspot located 200 bp of the 5' side of the array. The hotspot is thought to affect MS32 stability in meiotic cells that results in high rates of meiotic mutations (0.8% per molecule in sperm), which are characterized mainly by complex inter-allelic exchanges (crossovers and conversion-like events) polarized to the 5' end of the array. In somatic cells, the MS32 minisatellite is also prone to instability, although at a much lower rate than observed in the germ-line cells (mutation rate in blood cells of 0.004% per haploid genome). The rare mutations observed can be explained by simple intra-allelic events that could arise from replication slippage or sister-chromatid recombination, for example (Jeffreys et al 1994). Curiously, ALT+ cells show a MS32 instability that varies between 0.36% (WI38VA13/2A cell-line) and 0.94% (IIICF/a2 post-crisis cell-line) per somatic cell division, values ~2000-fold higher than the ones observed in normal or Tel+ cells. Also, preliminary studies mapping the interspersed MS32 variant repeats along the repeat array in ALT+ cells have shown that not just simple intra-allelic recombination is responsible for MS32 minisatellite instability in ALT+ cells. Analysis on clonal DNA showed that MS32 mutations in ALT+ cells occur along the array and not polarized to one end, like in germline. Furthermore, a complex interspersed pattern was observed, suggesting that the instability at MS32 minisatellite in ALT+ cells involves complex reshuffling events (Jeyapalan et al 2005).

5.2 AIMS

The relationship between MS32 instability and ALT activation remains unclear. As MS32 minisatellite instability was only observed in somatic ALT+ cells, it is feasible that the underlying mutational mechanisms are similar and that the events observed in ALT telomeres also occur in the minisatellite. Thus, investigation of the MS32 mutational mechanism in ALT+ cells may shed light at the telomere elongation mechanism ALT.

5.3 RESULTS

5.3.1 MUTATION MECHANISM AT MS32 IN ALT+ CELLS

To determine the molecular mechanism responsible for MS32 instability in ALT+ cells, the internal structure of length-mutant alleles of MS32 minisatellite was compared to progenitor alleles (most common allele in a cell population) to understand the nature of MS32 mutations in ALT+ cells.

A library of MS32 mutants was obtained by Single-Molecule PCR amplification (SM-PCR), a technique based on serial dilutions of DNA that allows detection and isolation of single length-mutants (Jeffreys et al 1994). Subsequently, a forward and reverse four-state Minisatellite Variant Repeat PCR (MVR-PCR) was performed to determine the internal structure of MS32 alleles. Essentially, one primer anneals to MS32 flanking DNA and combined with one of four primers specific for each variant of MS32 repeat unit is used to determine the interspersion pattern of the variant repeats. The assembly of the forward and reverse MVR-PCR amplification provides a complete interspersion map of the entire MS32 array (Monckton et al 1993).

To facilitate the understanding of the mechanisms causing mutations in MS32 upon ALT activation, a single-cell clonal expansion was performed in an ALT+ cell line - SUSM1. SUSM1 cell-line was selected for this analysis because the MS32 minisatellite instability in these cells was previously shown to be high (mutation frequency of 0.495 per cell) (Jeyapalan et al 2005), which could enhance the detection of length-mutants. Furthermore, the progenitor MS32 alleles in the SUSM1 cells were short (1.3 and 4 kb, approximately, Fig. 5.1), which allow the assembly of complete MVR-maps of even the longer allele (4 kb is about the maximum limit for a full assembly combining the forward and the reverse MVR-PCR). DNA from clones derived from single-cell expansions was extracted after 20, 30 or 40 population doublings (PDs).

5.3.1.1 DETERMINATION OF MS32 PROGENITOR ALLELES

In order to proceed with the analysis of the mutational mechanism affecting MS32 in ALT+ cells, the lengths of MS32 progenitor alleles of SUSM1 cell-line were determined to allow the identification and subsequent analysis of new length-mutants. MS32 was amplified from *MboI*-digested DNA from selected clones with 32B and 32E primers (380 bp upstream and 75 bp downstream, respectively). Two progenitors were obtained from most clones, except for clone 1C4 that showed four progenitor alleles (Fig. 5.1). Clone 1C4 might have originated from two cells, instead of the intended single-cell or two of the four alleles may have arisen as mutations that occurred very early during the clonal expansion. The size of the small progenitor allele appears stable between clones, ~1.3 kb (30 repeats), whereas the large progenitor varies in length across clones from 3.8 kb - 115 repeats to 4kb – 137 repeats (Fig. 5.1).

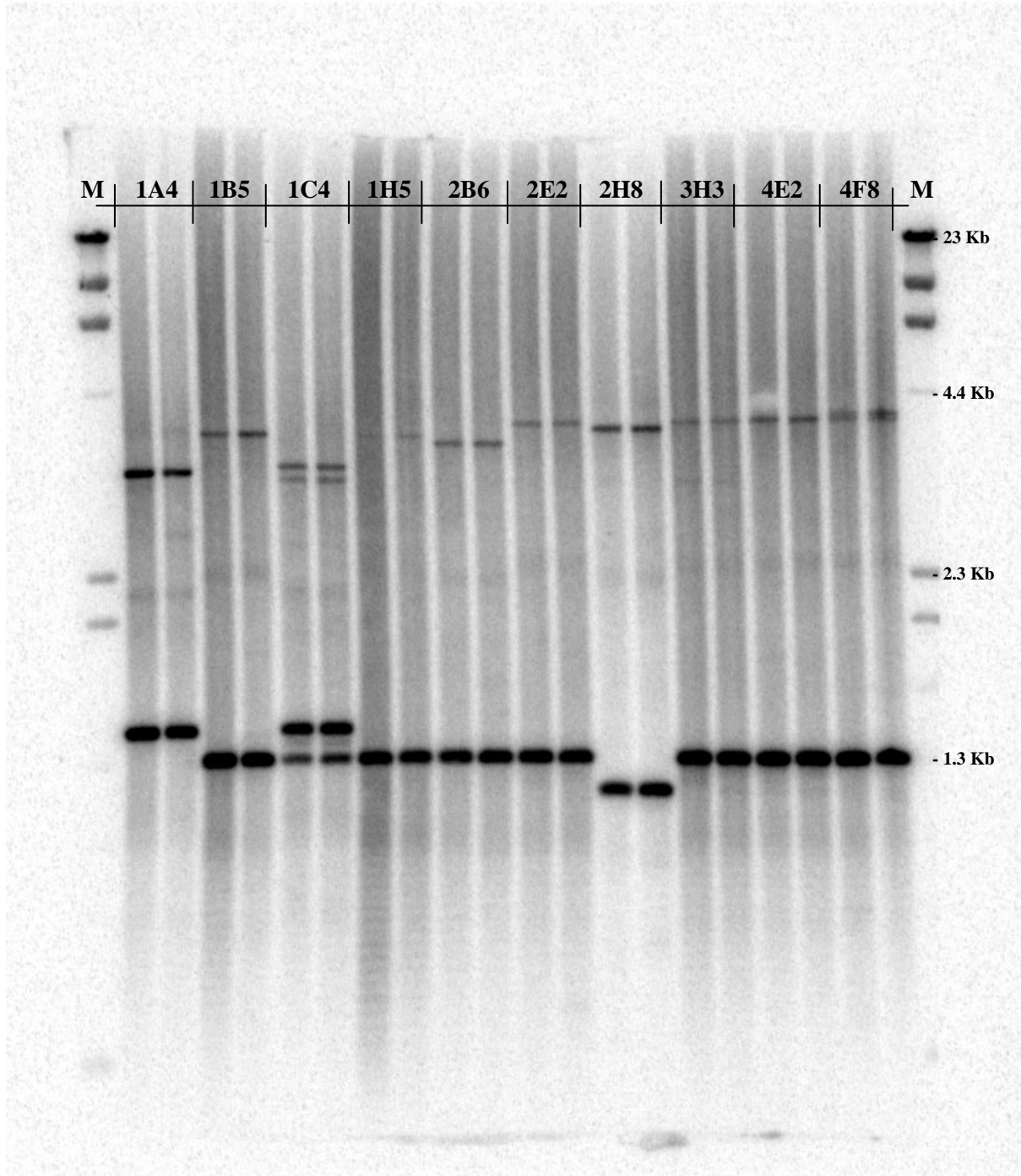


Figure 5.1: Determination of the size of progenitor MS32 alleles in SUSM1 clones. MS32 minisatellite was SP-PCR amplified from 200 pg of genomic DNA to identify predominant alleles in each cell population. A Southern-hybridization with a specific MS32 probe showed that all clones (1A4 to 4F8) have two progenitor alleles, except for clone 1C4 that has four alleles. The size of the small progenitor is 1.3 kb in most clones. The length of large progenitor varies between 3.8 to 4.0 kb among the clones. The DNA marker (M) used is $\lambda + \Phi 174$.

5.3.1.2 MUTATION FREQUENCIES

Previous studies on MS32 instability in ALT+ cells showed that the mutation rate varies between clones derived from the same cell-line, probably resulting from differences in the size of the progenitor MS32 alleles between clones (Jeyapalan et al. 2005). Thus, to identify the clones with higher MS32 mutation rate to be used for mutant screening, a SP-PCR was performed on each clone. Clones 1B5, 1H5 and 3H3 showed a higher number of length mutants, so they were selected for further analysis (Fig. 5.2). The mutation rate for each of the selected clones was calculated by Poisson analysis, which is based on limiting dilutions of DNA to estimate the number of amplifiable MS32 molecules in each SP-PCR reaction with (Jeffreys *et al.*, 1994). The mutation rates obtained vary greatly between clones (Table 5.1). Since clone 3H3 showed the highest mutation rate, similar to the value previously observed by Jeyapalan in another ALT+ cell line (0.36% per cell division in WI38VA13/RA) (Jeyapalan et al 2005), this clone was therefore selected for MVR mapping analysis.

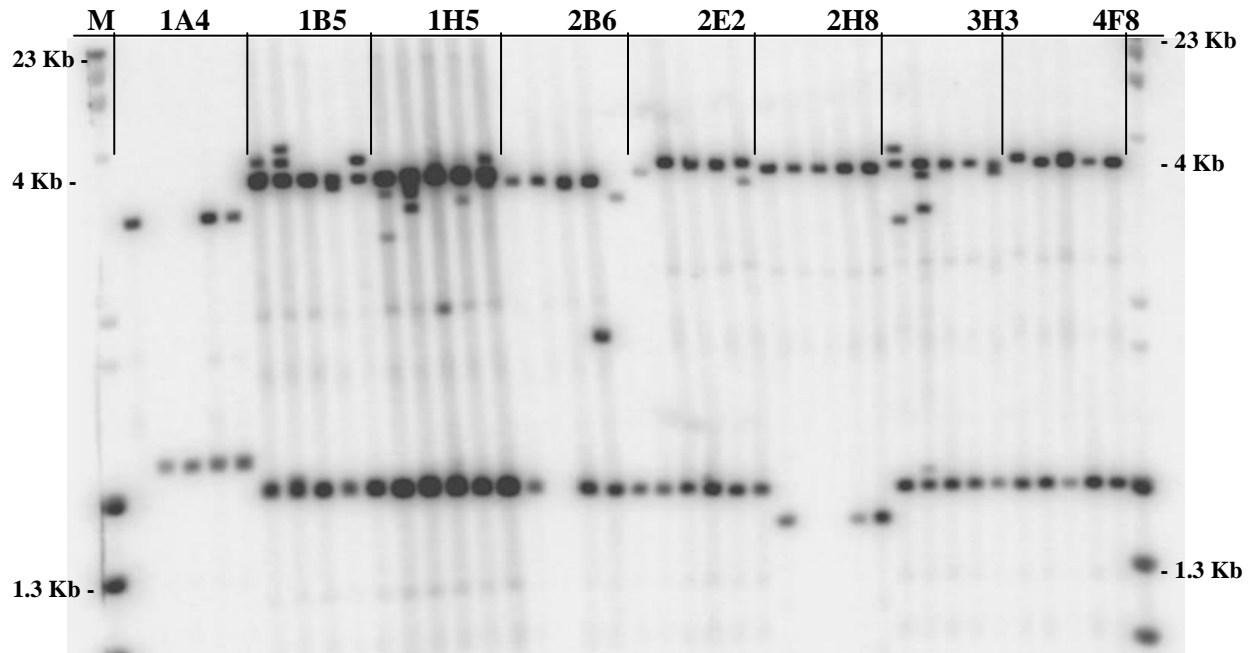


Figure 5.2: Identification of SUMS1 clones with highest MS32 mutation frequency. SP-PCR MS32 products were resolved on an agarose gel electrophoresis and Southern-hybridized to the MS32 probe. Each SP-PCR reaction, with 20 MS32 molecules each, was performed to detect the clones with higher mutation frequencies. The DNA marker (M) used is $\lambda + \Phi$.

Clone	No. of molecules ¹	Mutation Frequency	LCI	UCI	Mutation rate/cell division ²
1B5	(4) 80	0.0500	-0.0028	0.1374	0.0025
1H5	(5) 620	0.0081	0.0021	0.0201	0.0004
3H3	(11) 160	0.0688	0.0199	0.1332	0.0034

¹The number of mutants observed for each clone is shown in brackets. The value for MS32 mutants was obtained from the number of different length (mutant) bands in multiple small-pool PCR reactions. The estimated total number of molecules analysed was determined from Poisson analysis of the DNA sample

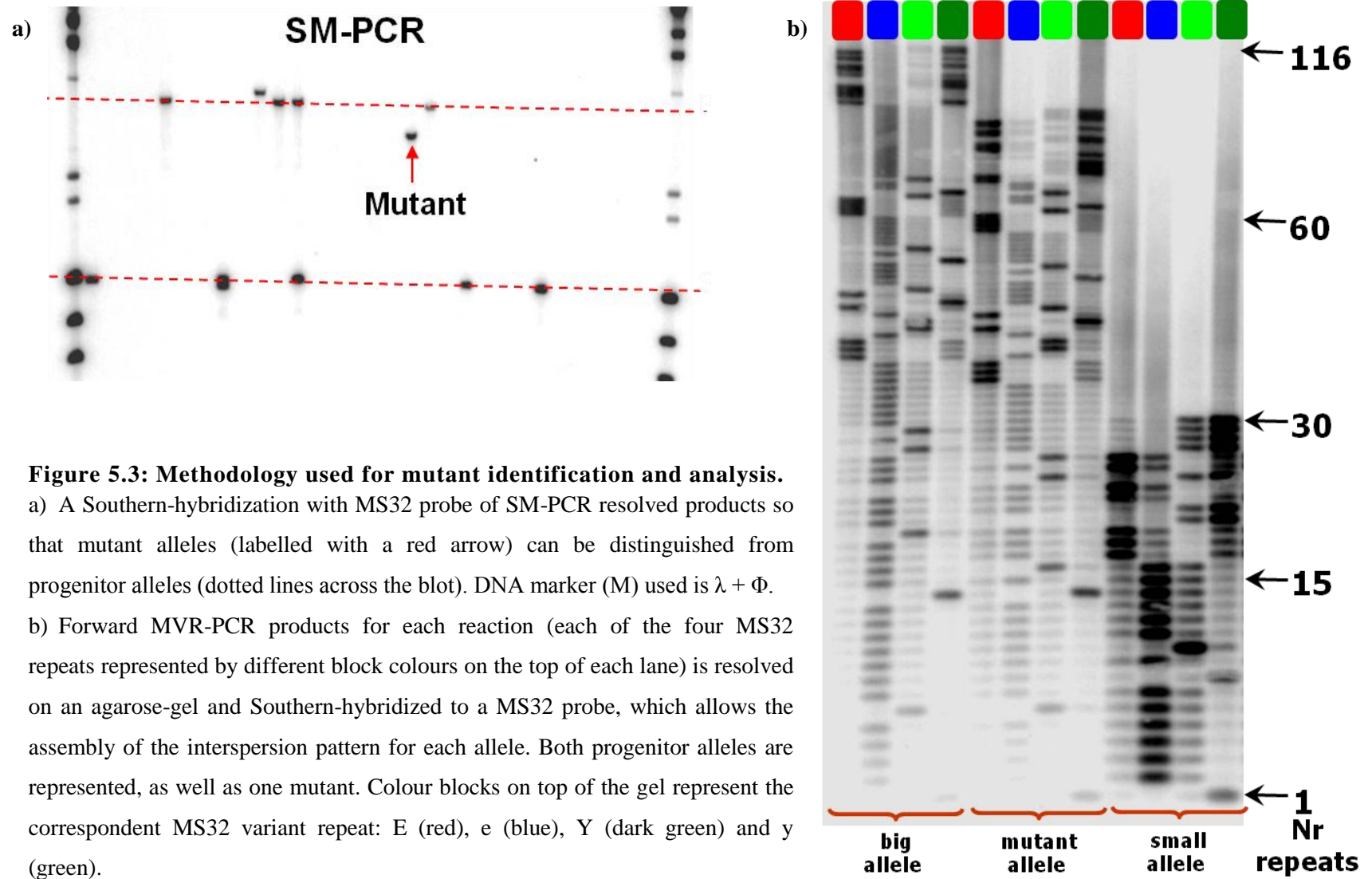
² The mutation rates have been estimated by dividing the mutation frequency by the number of cell divisions (20) determined from the cell count. Assuming that each cell divides to give two daughter cells (2^n =number of cells, where n is number of cell divisions), then 1×10^6 cells results from 20 cell divisions.

Table 5-1: MS32 mutation frequencies obtained by Small-Pool PCR (PD20)

5.3.1.2 MUTATION SPECTRUM

Progenitor and mutant alleles of MS32 minisatellite were separated by gel-electrophoresis resolution of SM-PCR products. The mutants identified by SM-PCR were then used as template for the forward and reverse MVR-PCR reactions, so that full-length maps could be obtained. Thus, the distribution of the four types (E, e, y, Y; see in Chapter 1, section 1.6.1) along the MS32 repeat array of both progenitors and mutant alleles was fully determined and the assembled mutant maps were compared to the progenitors (Fig. 5.3-a). In total, 531 molecules were amplified and 43 length-mutants identified. The length-mutants and 14 progenitor molecules (normal allele size) were isolated for MVR-PCR analysis. Complete MVR-PCR maps (forward and reverse) of 51 molecules were obtained from the 3H3 SUSM1 clone: 7 from the large progenitor, 7 from the small progenitor, 33 mutants derived from the large-allele and 4 mutants derived from the small-allele mutant. After alignment of the MS32 maps, each mutant was assigned to a progenitor allele from, which it was more likely to have derived (according to the similarities of the interspersed maps) (Figure 5.3-b). In total, 72 changes were detected amongst the 37 mutants analysed (Fig. 5.4-b). Predominantly, the MS32 length-mutant arise from deletions events (79.2%), although other events that produced a change in the repeat order (11.1%) or insertions (9.7%) were also detected. The large progenitor allele seems to be much more prone to instability, since 89.2% of the mutants obtained derived from the large progenitor allele (Fig. 5.4-a -b). The MS32 rearrangements identified seem to occur preferentially in the middle of the array, just before a block of 22 type *e* repeats, although the beginning of the array seems also to be prone to changes (5.4-b). A few deletion events were also observed towards the 3' end of the array (mutants A, B, O and c). Interestingly, almost all changes

observed occurred in non-contiguous repeats suggesting that several breakpoints may occur at the same time throughout the array (Fig. 5.4-a).



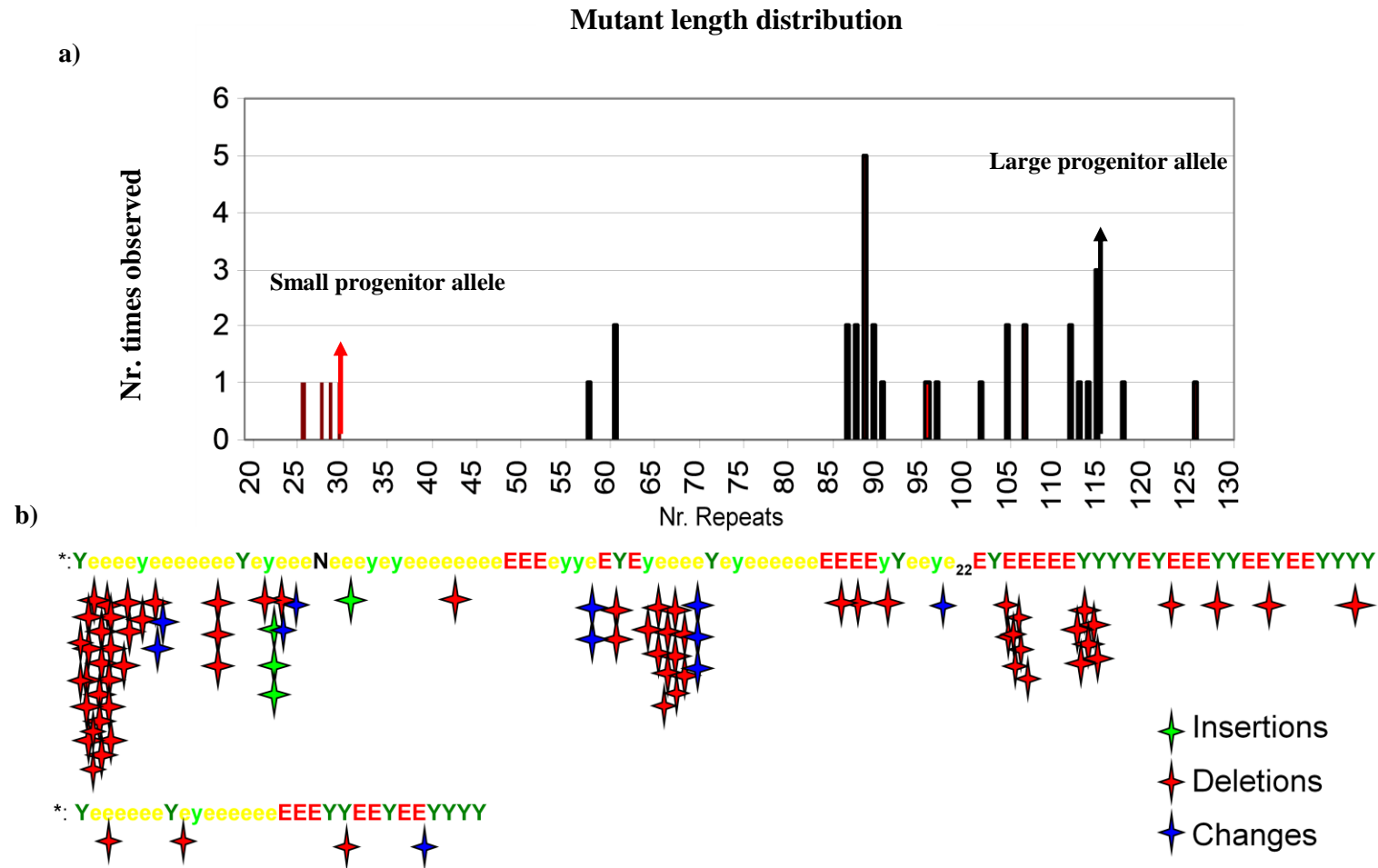


Figure 5.4: Size distribution of mutants and breakpoints for mutational events in each allele.

a) Distribution of mutants according to their sizes. Black lines represent mutants derived from the progenitor allele (black arrow) and red lines represent mutants derived from the small progenitor allele (red arrow). The frequency of each observed size is plotted on the y-axis.

b) Each star represents the site of observed mutational events mapped onto the progenitor alleles (large on top, and smaller on the bottom). The colours represent different types of mutational events: green – insertions, red – deletions and blue – changes.

The analysis was performed on DNA derived from 20 PDs, thus the length-mutants identified are most likely rearrangements arisen from single mutation events. Since the calculated mutation rate for the analysed clone (3H3) is 3.4×10^{-3} per cell-division, the probability of two independent mutations occurring in the 20 population doublings would be very low. Indeed, with the exception of mutant d (in brackets, Fig. 5.5), all mutants were observed only once, which is consistent with the presupposition that mutants arising after 20 PDs would result from a single mutational event (Fig. 5.5). Mutant d was observed 5 times, which may indicate that it is a result of an early mutational event, therefore its higher frequency in the population analysed. However, a possible contamination of this mutant during the amplification procedures could also explain its higher frequency, even though the PCR reactions were always prepared separately from the amplified SP-PCR molecules, which were the last reagent added to the MVR-PCR reaction, precisely to avoid contaminations. Some mutants show a very similar interspersed pattern (S, d, M, V, Z and e), with some deletions in the beginning of the array and a common loss of a block of 26 repeats deleted just before the 22-long patch of small e repeats. A possible explanation is that one event occurred very early on the clonal expansion, resulting in the mutant allele being very frequent within the cell population. Then, another later event could have originated mutants with similar internal structures, like the ones observed. However, if that had happen, a simple mutant with just a loss of the 26-block of repeats would have been expected to appear with a higher frequency. Thus, although the mutants are very alike, they most likely derive from independent single events. In this case, the array seems to have certain breakpoints where events are more likely to occur. Particularly curious is the fact that the few insertions observed occurred exclusively at the 5' end of the array, whilst the 3' end seems prone to give rise to deletions only (Fig. 5.4-b).

Interestingly, some of the mutations observed are quite complex. Mutants D, y, e, I, O, W and i arise from multiple deletions/insertions in non-contiguous repeats, reshuffling the variant repeats to an order with no homology with neither of the progenitor alleles (Fig. 5.5). Flanking sequences or mutagenesis

Site I	Site II
E ↔ Y	E ↔ e
e ↔ y	y ↔ Y

does not seem to be involved in the observed complex rearrangements as these blocks of repeats with unknown origin still retain the MS32 repeats' sequence. Multiple intra-allelic deletions, insertions and changes in the polymorphic sites that would swap the class of repeat unit occurring simultaneously along the array could explain some of these complex rearrangements. Predicted repeat changes caused by transition in the polymorphic sites are detailed in Table 2 and can explain the change from Y to y in repeat 52 of mutant D, but not the change in repeat 45 in the same mutant nor the changes in mutants I, e, O and W.

The most complex rearrangement resulted in mutant i, which starts with a block of 13 repeats that differ from but show patchy homology to the large progenitor allele, followed by a contiguous block of 22 e repeats. The next 10 repeats are from the large progenitor, then two repeats with no evident progenitor origin, another block with homology to either the large or small progenitors, then finally the mutant ends with a set of null and E repeats not seen in either progenitor or other mutants. These complex mutations are probably derived from complex intra-allelic events within one progenitor allele, since no evidence was found for inter-allelic events.

Therefore, mutations observed in the MS32 minisatellite under ALT activation can be divided into three categories: 37.8% are mutations at a single site within the progenitor allele (mutants derive from a deletion of a contiguous block of repeats at one site of the array), 43.2% are mutations occurring at two sites (mutations occur at two non-contiguous

positions along the array) and 19% are complex rearrangements (mutants arise from a mixture of intra-allelic events that result from complex reshuffling of the repeat order and/or addition/deletion of repeats across the array) (Fig. 5.5).

5.3.2 FROM YEAST TO HUMANS – FEN1 ANALYSIS

In yeast, similar complex minisatellite rearrangements were identified in homozygous RAD27 Δ diploid yeast, where the human CEB1-0.6 (14 repeats) and CEB1-1.8 (42 repeats) alleles (Buard et al, 1998) were inserted in the 5' intergenic region of the ARG4 locus (Debrauwere et al, 1999). The authors proposed a model where, in the absence of the flap-endonuclease RAD27, the removal of Okazaki fragments accumulates unprocessed 5' flaps that are recognized as double-strand breaks by DNA repair mechanisms, perhaps the DSB-synthesis-dependent strand annealing (SDSA) (Buard et al., 1998, 2000b; Debrauwère et al., 1999), which forms a D-loop with mismatches due to sequence divergence. A secondary DSB can then be formed, permitting an anomalous order of the repeats to the array when repaired. This defect observed in the absence of RAD27 was partially complemented by hFEN1 (human RAD27 homologue) (Lopes et al 2006) showing that RAD27 prevents sequence duplication and repeat expansion. Additionally, RAD27 Δ haploid yeast show highly heterogeneous telomeres and accumulation of single-stranded G-tail, suggesting that RAD27 is essential for proper lagging C-strand synthesis (Parenteau, et al. 1999).

Flap-endonuclease 1 is involved in multiple DNA processes including replication (Li et al 1995), long-patch base excision repair (Prasad et al 2000), homologous recombination (Kikuchi et al 2005), reinitiation of stalled replication forks and DNA

degradation in apoptotic cells (Zheng et al 2005 and 2007). Recently, hFEN1 was also implicated in human telomere biology since its depletion by RNAi led to sister telomere loss on telomeres replicated by lagging strand DNA synthesis (Saharia et al 2008). Furthermore, disruption of hFEN1 function was shown to cause a mutator phenotype in yeast (Tishkoff et al 1997; Parenteau et al 1999; Parenteau et al 2002) and in mice (Kucherlapati et al 2007; Zheng et al 2007) that might predispose to cancer. In the light of these studies and considering the similar range of mutations observed in CEB1 minisatellite in RAD27 Δ yeast with the ones seen in MS32 in ALT+ cells, an investigation of the hFEN1 functionality in ALT+ cells was performed.

5.3.2.1 HFEN1 EXPRESSION IN ALT+ CELLS

To determine if *hFEN1* was differently expressed in ALT+ cells, qPCR analysis was performed in several ALT+ and non-ALT cell-lines. Human Flap-endonuclease 1 is a small gene, composed of two exons only and located on chromosome 11. The transcript length is 2,247 bps, which translates into a 380 aa protein. To determine the expression levels of *hFEN1* in ALT+ and non-ALT cell-lines, a qPCR assay was designed to amplify 133 bp across the exon boundary (Fig. 5.6). The qPCR assay was optimized according to the parameters described on chapter 4, sections 4.3.2.1 and 4.3.2.2 and the levels of hFEN1 transcripts were compared across ALT+ and non-ALT cells lines by normalizing the data with the housekeeping *G3PDH* expression (Fig. 5.7).

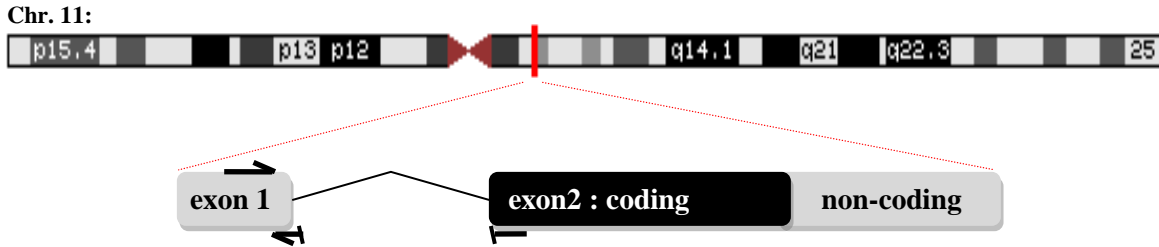


Figure 5.6: Schematic representation of hFEN1 gene.

hFEN1 is located interstitially on chr. 11 and is composed of two exons (grey blocks). Exon 2 comprises the entire coding region (black block). The black arrows represent primers positions for the qPCR assay.

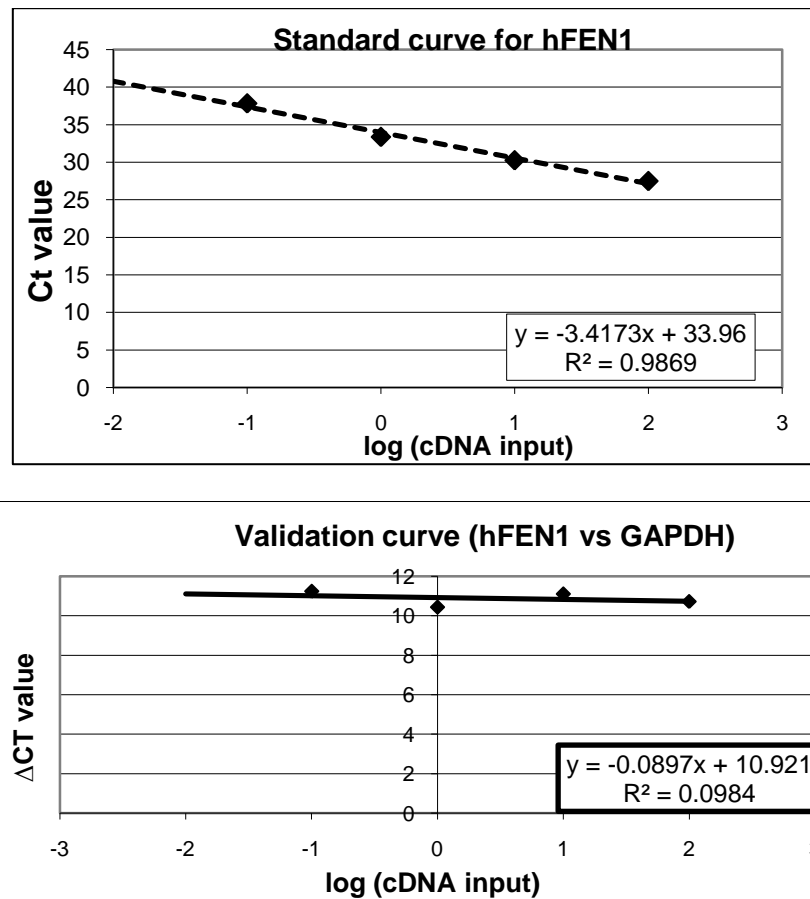


Figure 5.7: *hFEN1* qPCR assay optimization.

A standard curve plotted from a 10-fold serial dilution was used to determine the PCR amplification efficiency for *hFEN1*. Also, a ΔC_t vs. cDNA input were used to validate the assay (for detailed information on the qPCR methods, see chapter 4, section 4.3.2.1 and 4.3.2.2).

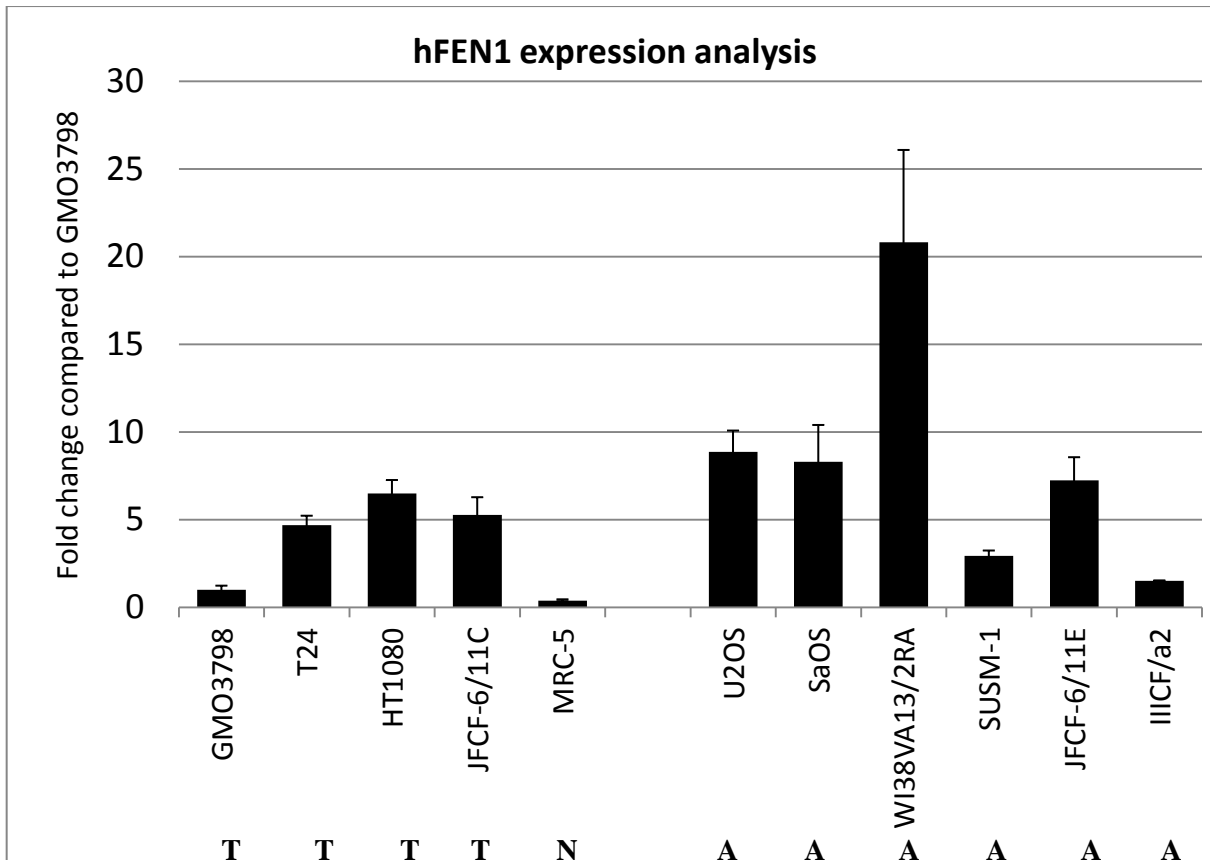


Figure 5.8: *hFEN1* expression analysis in ALT+ and non-ALT cell-lines.

G3PDH was used for the normalization and the bars represent fold changes relative to GMO3798 expression. Error-bars reflect the standard errors of two independent RNA extractions. Non-ALT (Tel+ -T and normal – N) cells are clustered on the left-side of the graphic whilst the ALT+ cells (A) are represented on the right-side (for detailed information on the qPCR methods, see chapter 4, section 4.3.2.1 and 4.3.2.2).

According to the two-sample Wilcoxon rank-sum (Mann-Whitney U) equation, which tested for equality of distributions, no significant difference in *hFEN1* expression was observed between ALT+ and non ALT cell-lines (p-value = 0.4652), suggesting that similar levels of the *hFEN1* transcript occur under different telomere maintenance mechanisms. Cell-type variation is evident, especially in WI38VA13/2RA that shows a 25x higher fold change in comparison to the GMO3798 expression. This cell-line derives from

lung tissue, like the normal MRC5, so the high expression of *hFEN1* in these cells is not evident and should be further confirmed.

5.3.2.2 SCREEN FOR HFEN1 GENOMIC MUTATIONS

Although no significant changes on hFEN1 transcription levels were detected between ALT+ and non-ALT cell-lines, *hFEN1* point mutations could be affecting its full activity and influence MS32 instability in ALT+ cells. In fact, haploinsufficiency of Fen1 in an adenomatous polyposis coli (Apc) mutant genetic background results in microsatellite instability and promotes cancer progression in mice (Kucherlapati et al 2007). Furthermore, several mutations in *hFEN1* associated with different types of human cancers were described and validated as the cause for a strong mutator phenotype through *hFEN1* nuclease activity deficiency without affect DNA replication activity. Most of the *hFEN1* mutations were somatic and heterozygous and two of them - P151L and A159V – that caused reduced nuclease activity, were the most prevalent amongst the human cancers analysed. These findings, together with murine experiments in which 70% of the mice with the equivalent point mutations spontaneously developed tumours, suggested that loss of *hFEN1* function might play a role in cancer initiation and progression (Zheng et al. 2007).

Thus, to screen for point mutations that could affect hFEN1 exonuclease activity and compromise MS32 stability, the *hFEN1* gene was amplified by PCR using genomic DNA isolated from ALT+ and non-ALT+ samples as template. The primers previously used for direct hFEN1 sequencing FEN-1F1 (5'-GTTGAAGGCATGAAGTTGGTGAG-3') and FEN-1R1 (5'-GGTGAAGGAGGTATAATGGG-3') were used as the set amplifies the *hFEN1* gene on chromosome 11 but not the pseudo-*FEN1* gene on chromosome 1

(Zheng et al. 2007). PCR products were purified and sequenced on both strands. A summary of the results for the known non-synonymous SNPs as well as the P151L (rs11541090) and A159V point mutations can be found in Table 5.2. The cell-lines tested showed no mutations in the ORF sequence of *hFEN1*.

Even though no genomic point mutations or significant expression changes were found, indicating that a fully functional hFEN1 in ALT+ cells, some posttranslational modifications on the protein may still be affecting one or more of its functions. However, a recent study that analysed the hFEN1 role in the ALT+ pathway showed that a fully functional hFEN1 is required for proper telomere stability in ALT+ cells. hFEN1 depletion by shRNA in U2OS (ALT+) lead to telomere dysfunction, characterized by an increased number of TIFs and telomeric fusions (Saharia et al 2009). This study supports our findings that a dysfunctional hFEN1 is unlikely to be underlying MS32 instability in ALT+ cells, since a fully functional hFEN1 must be present in ALT+ cells for proper telomere stability. However, the hypothesis that another dysfunctional human homologue of *rad27* could be triggering MS32 instability in ALT+ cells cannot be fully rejected.

SNPs Cell-lines	Intronic	Splice-site	Non-synonymous SNPs						
	rs3218838	rs393487	rs11541090 (P151L)	A159V	rs4989586	rs4989587	rs4989588	rs1803573	rs7931165
IICf/a2 pre-crisis	T	T	C	C	G	C	T	G	T
IICf/post-crisis (ALT+)	T	T	C	C	G	C	T	G	T
NT2D1 (Tel+)	T	T	C	C	G	C	T	G	T
HT1080 (Tel+)	T	T	C	C	G	C	T	G	T
11E (ALT+)	T	T	C	C	G	C	T	G	T
SaOS (ALT+)	T	T	C	C	G	C	T	G	T
U2OS (ALT+)	T	T	C	C	G	C	T	G	T
SUSM1 (ALT+)	T	T	C	C	G	C	T	G	T
WI38 (normal)	T	T	C	C	G	C	T	G	T
WI38V13 (ALT+)	T	T	C	C	G	C	T	G	T
WV (ALT+)	T	T	C	C	G	C	T	G	T

Table 5-2: Screening for *hFEN1* point mutations.

The ORF of *hFEN1* containing the coding region was sequenced in several human cell-lines and the sequence for all the described non-synonymous SNPs and the P151L/A159V is represented on the table.

5.3.2.3 HEXO1 EXPRESSION IN ALT+ CELLS

Other human genes that have similar functions to RAD27 can be hypothesized to play a role in the MS32 instability in ALT+ cells. Exonuclease 1 (hEXO1) has 5' flap-endonuclease activity and if dysfunctional could also originate the accumulation of unprocessed flap-endonucleases that could be recognized as DSBs, similarly to what was proposed in the yeast RAD27 Δ model. hEXO1 also shows 5'-3' exonuclease activity on dsDNA and a weak RNaseH activity, and it is essential for both 5' and 3' nick-directed mismatch repair (Wilson DM. 1998; Shen B., 1999; Modrich P, 2002). hEXO1 seems to overlap at least some functions with hFEN1 in yeast, since hEXO1 overexpression rescued the conditional lethality of RAD27 Δ mutants (Shen B., 1999). Also, *exo1* seems to be involved in an increase in homologous recombination and in chromosomal translocations as response to telomere dysfunction, since its deletion rescued senescence induction in telomere dysfunctional yeast strains (Lydall, et al 2002 and 2004). In fact, yeast strains with mutated *exo1* have linear chromosomes with, instead of telomeric and subtelomeric sequences, large inverted and duplicated repeats (palindromes) at the chromosome ends (Maringele et al 2004). Furthermore, *Exo1*^{-/-} mice showed defects in DNA mismatch repair (increase in microsatellite instability and in cancer susceptibility) (Wei et al., 2003), impaired meiosis and inefficiency of immunoglobulin (Ig) class-switch recombination (Bardwell et al 2004). Also, mice with dysfunctional telomeres and *Exo1*-deficiency showed an extended life span and reduced genomic instability (Schaezlein et al 2007), suggesting a role for *Exo1* in the induction of DNA damage signals, cell-cycle arrest and apoptosis in a telomere dysfunctional background (as has been reported in yeast).

Thus, considering the yeast studies that propose an abnormal accumulation of unprocessed 5' flaps as a trigger for minisatellite instability, the apparent functional overlap

between FEN1 and EXO1 and the lack of detectable hFEN1 dysfunction in ALT+ cells, a possible involvement of hEXO1, instead of hFEN1, in the MS32 instability in ALT+ cells is possible. Thus, a qPCR experiment was initiated to assess *hEXO1* expression levels between ALT+ and non-ALT cells.

hEXO1 is composed of 15 exons (14 coding) that can be translated into three variants that transduce into two isoforms. The isoform *b* (represented in Fig. 5.9) is the most common isoform and has two variants distinguishable through a unique exon present in the 5' UTR of variant two but not in variant one. Isoform *a* is 43 aa shorter than isoform *b*, resulting from a frameshift mutation that results in the use of a upstream stop codon and consequently, an alternate splice-site in the 3' end of the coding region. Primers were designed to specifically amplify 169 bp across the exon 5-6 boundary (Fig. 5.9), which is common to all the three described variants, as there is not much known about the differential function of each variant.

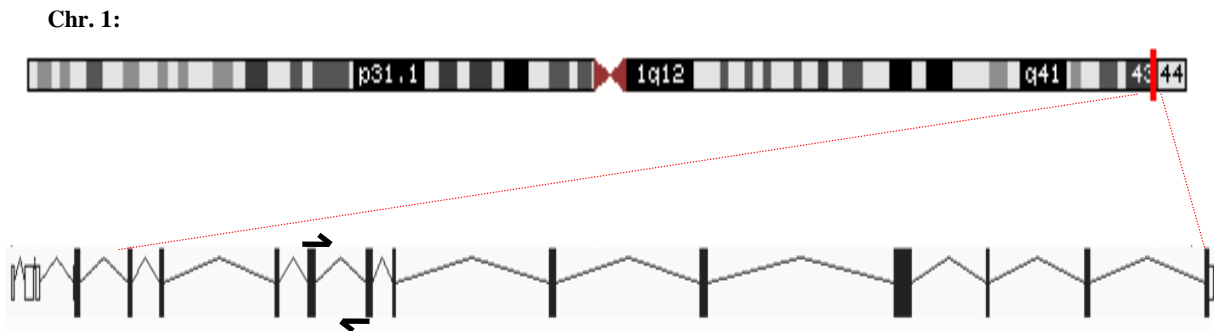


Figure 5.9: Schematic representation of *hEXO1* gene.

hEXO1 is located at 1q42-43 position and consists of 14 exons that yield a ~3 kb transcript. Each bar represents a coding (black) and non-coding (white) exon. The arrows represent the positions of the qPCR assay primers.

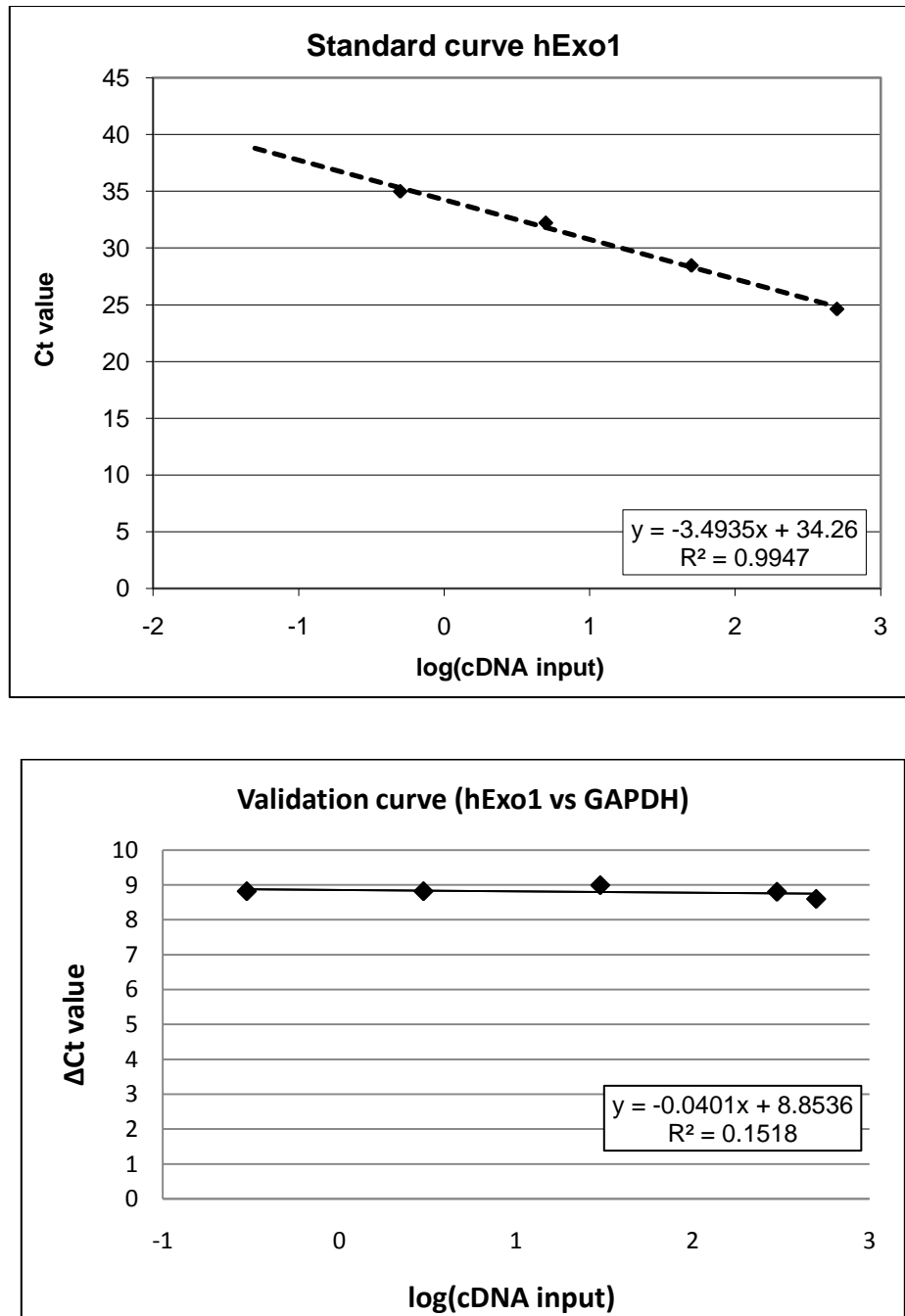


Figure 5.10: *hExo1* qPCR assay optimization.

A standard curve plotted from a 10-fold serial dilution was used to determine the PCR amplification efficiency for *hExo1*. Also, a Δ Ct vs. cDNA input were used to validate the assay (for detailed information on the qPCR methods, see chapter 4, section 4.3.2.1 and 4.3.2.2).

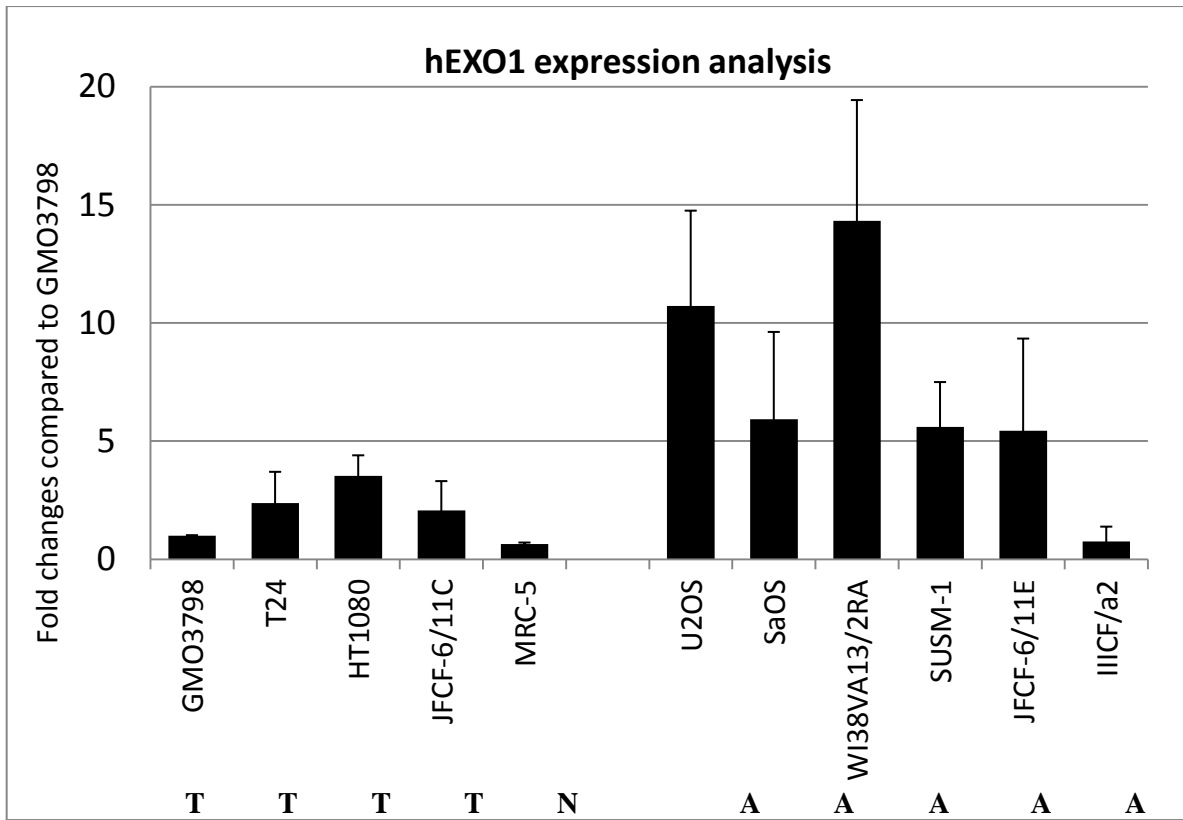


Figure 5.11: *hEXO1* expression analysis.

G3PDH was used for the normalization and the bars represent fold changes relative to GMO3798 expression. Error-bars reflect the standard errors of two independent RNA extractions. Non-ALT cells are clustered on the left-side of the graphic whilst the ALT+ cells are represented on the right-side (for detailed information on the qPCR methods, see chapter 4, section 4.3.2.1 and 4.3.2.2).

A significant higher expression of *hEXO1* was observed in ALT+ cells, compared to non-ALT, as determined by two-sample Wilcoxon rank-sum (Mann-Whitney) equation, used to test for equality of distribution (p-value = 0.0446). The observed higher expression of *hEXO1* in ALT+ cells compared to non-ALT cells needs to be further confirmed by measuring *hEXO1* protein levels. Also, it would be interesting to determine if all variants are equally expressed in ALT+ and non-ALT cells, which might reveal differential function of each one of the *hEXO1* variants.

5.3.3 MS32 EXTRACHROMOSOMAL SEQUENCES

The extrachromosomal DNA in mammalian cells can be divided into two types: small polydispersed circular DNA (spcDNA) found in the nucleus and cytoplasm and large circular DNA (150 to 900 kb), found in the nucleus. SpcDNA, containing mainly repetitive sequences, range from 150 to 2 kb in size and are frequently observed in mammalian cells with genomic instability (Cohen et al 1997). The mechanisms involved in their formation are still not clear, but are thought to result from intrachromosomal recombination, reverse transcription or fragmentation of chromosomal DNA by nucleases (Gaubatz et al 1990; Cohen et al 2006). The size of circular DNA can vary between 1.5 to 900 kb. In cancer cell-lines, the circles are mainly composed of amplified sequences of oncogenes as a result of a deletion of their chromosomal region (Alitalo et al 1985; Bruckert et al 2000; Smith et al 2003; Frater et al 2006).

The presence of extrachromosomal telomeric repeats in telomerase-negative cells was first reported by two independent groups (Ayusawa D. 1998; Tokutake 1998). Since then, telomeric extrachromosomal DNA has been well characterized and its circular form became one of the key markers for ALT. The circular form of extrachromosomal telomeric DNA (t-circles), confirmed by both electronic microscopy (EM) (Griffith et al 2004) and two-dimensional electrophoresis (de Lange et al 2004), show circles with similar size to the loop portion of telomeres. This leads to the hypothesis that t-circles result from homologous recombination events at telomeres (de Lange et al 2004), which is consistent with the recombination-like processes believed to underlie the ALT mechanism. It could also explain the rapid deletion of telomeres observed at low frequency in ALT⁺ cells (Murnane et al., 1994) and the lack of telomeric signals at some chromosome ends in ALT⁺ cells

(Perrem et al., 2001). Furthermore, several studies in Tel⁺ cells seem to support this model: a mutant form of TRF2 causes telomere shortening accompanied by the appearance of t-circles, a process shown to be dependent on key components of HR (XRCC3 and NBS1) since their downregulation causes the disappearance of t-circles (de Lange, 2004). Since t-circles are naturally present in ALT⁺ cells, they have been proposed to participate in the ALT mechanism as a template for telomere elongation via rolling-circle replication (Henson et al. 2002; Natarajan et al 2002). However, loss of t-circles seems to have no significant effect on growth and, in most cases, on telomere length (de Lange, 2004). Additionally, a mechanism to negatively regulate telomere length through telomere-trimming via t-loop resolution and t-circles formation was proposed occur in all human cells and not just ALT⁺ cells. In fact, cells with increased telomerase activity show continuous telomere elongation and, after a plateau stage, cells show heterogeneous telomere length accompanied by the appearance of t-circles. As no intertelomeric recombination was detected, ALT was excluded as responsible for telomere length heterogeneity and t-circle formation (Reddel et al. 2009). Thus, extrachromosomal t-circles might be a by-product of long telomeres rather than being a template for telomere elongation in ALT⁺ cells.

As mentioned above, the study of the molecular mechanism underlying MS32 instability in ALT⁺ cells showed that most mutants arise from deletion events, probably derived from intra-allelic events. Since both the minisatellite and the telomere are tandem repeats, the mechanisms involved in their instability in ALT⁺ cells may be similar. As a high level of MS32 instability is only seen in ALT⁺ cells, it is possible that extrachromosomal circular MS32 sequences are also present. Thus, to better understand the

processes involved in MS32 instability, we investigated whether extrachromosomal MS32 sequences were present in ALT+ cells.

5.3.3.1 DETECTION OF T-CIRCLES BY 2-D ELECTROPHORESIS

Neutral-neutral two-dimensional gel electrophoresis (2D-gel) enables the separation of DNA fragments by size (1st dimension) and then by conformation (2nd dimension). Thus, the various DNA conformations (relaxed circular, supercoiled, single and double-stranded linear) can be separated according to their different migration patterns (Fig. 5.12).

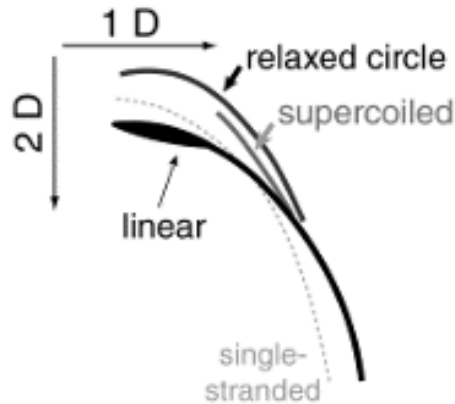


Figure 5.12: Scheme of the migration pattern of DNA structures in 2D-gels.

Preceding extrachromosomal MS32 analysis, the optimization of the 2D-gel electrophoresis was undertaken. The migration patterns of the different DNA structures were firstly tested by 2D-gel of *Hind*III-digested lambda fragments together with open and supercoiled plasmids. Figure 5.13-b shows a clear arc formed by the linear double-stranded (ds) λ -digested fragments and a slower migrating arc formed by the open-circle plasmids. Figure 5.13-c shows the same linear ds-DNA arc almost intersected by the plasmid, which resembles the migration pattern expected for supercoiled DNA.

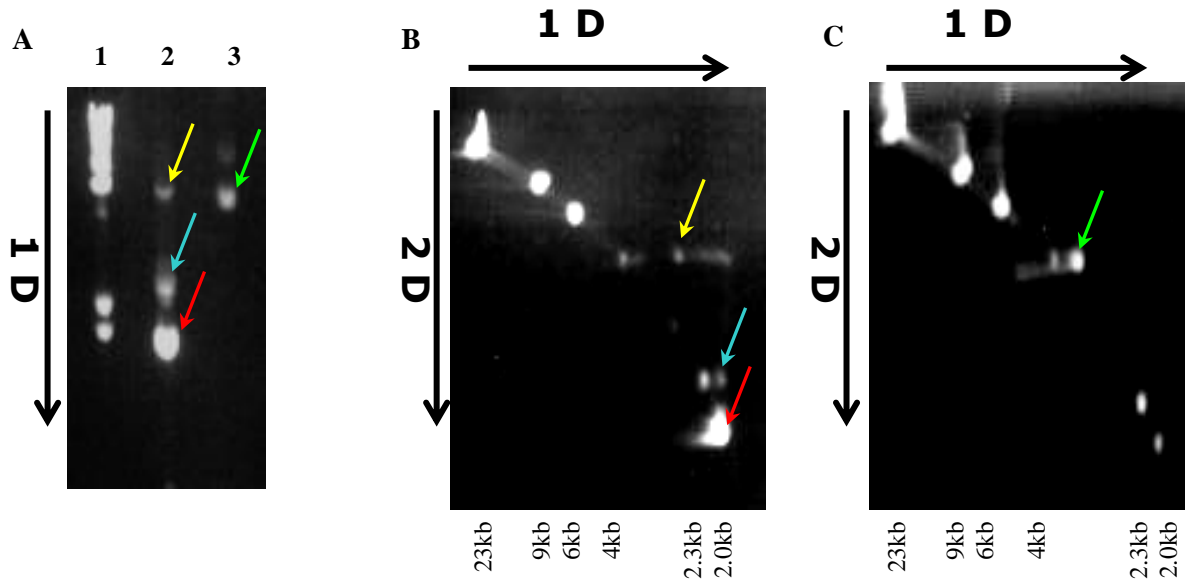


Figure 5.13: Optimization of 2D-gel electrophoresis.

A: 1st dimension gel was performed to check the plasmid sizes. Lane 1: Lambda-digested with *HindIII*; lane 2: pBluescript plasmid (2kb - red arrow), pBluescript plasmid with EROLIB cDNA insert (2.3 kb - blue arrow), pOTB7 with WRN cDNA insert (6Kb – yellow arrow); lane 3: supercoiled pOTB7 with WRN cDNA insert (5.5 kb – green arrow).

B: 2D-gel with lanes 1 + 2 from the gel showed in A. The circular DNA arc can be observed.

C: 2D-gel with lanes 1 + 3 from the gel showed in A. The migration pattern observed for the plasmid resembles the expected supercoiled DNA line.

As ALT+ cells have been shown to have extrachromosomal telomeric circular DNA, the same 2D-gel conditions were applied to *MboI*-digested genomic DNA from SUSM-1 cell-line (ALT+). After Southern-blotting and hybridization to a telomeric probe (TTAGGG), a very clear open-circular and linear ds-DNA arc were detected, as shown in Fig. 5.14. The size of the detected t-circles spans the genomic telomeric signal, which is reminiscent to that previously observed in other ALT+ cells and in the presence of a dysfunctional form of TRF2 (de Lange et al 2004).



Figure 5.14: Telomeric DNA in SUSM1 cell-line.

Genomic SUSM-1 + *MboI* (10 μ g) was resolved in two dimensions, transferred to a nylon membrane and probed against telomeric probe. The arc corresponding to extrachromosomal circular telomeric DNA is evident (arrow).

Although the migration of both linear and open-circular ds-telomeric DNA are well enough resolved to differentiate between them, the resolution of circular DNA smaller than 2 kb can be challenging. If circular DNA from the D1S8 locus (MS32) is present in ALT+ cells, it is likely to be smaller than 2 kb, the sizes of some MS32 alleles detected in various cell-lines. Also, larger amounts of DNA will be necessary since the signal obtained from relaxed-circular telomeric DNA, which most likely derives from several chromosomes, is likely to produce a much fainter signal than the linear telomeric arc and MS32 is only present at one locus. To explore the sensitivity of this methodology, the DNA from several ALT+ cell-lines was resolved by 2D-gel and probed with different variants of telomeric repeats. Interestingly, circular arcs were also detected with all the variant telomeric repeat

probes tested in three different ALT⁺ cell-lines (Fig. 5.15). However, as the signal obtained with the variant probes (TTGGGG; TCAGGG and TGAGGG) was much weaker than the ones observed with the telomeric probe, the linear DNA was digested with exonuclease V (*ExoV*), which rapidly digests linear double-stranded DNA leaving nicked (like the relaxed circles that were detected with telomeric probes) or supercoiled circles unaffected. Thus, the signal obtained from the circular DNA was enhanced and insensitive to the *ExoV* treatment, confirming the presence of variant telomeric repeats as extrachromosomal circles of ALT⁺ cells, (fig. 5.16).

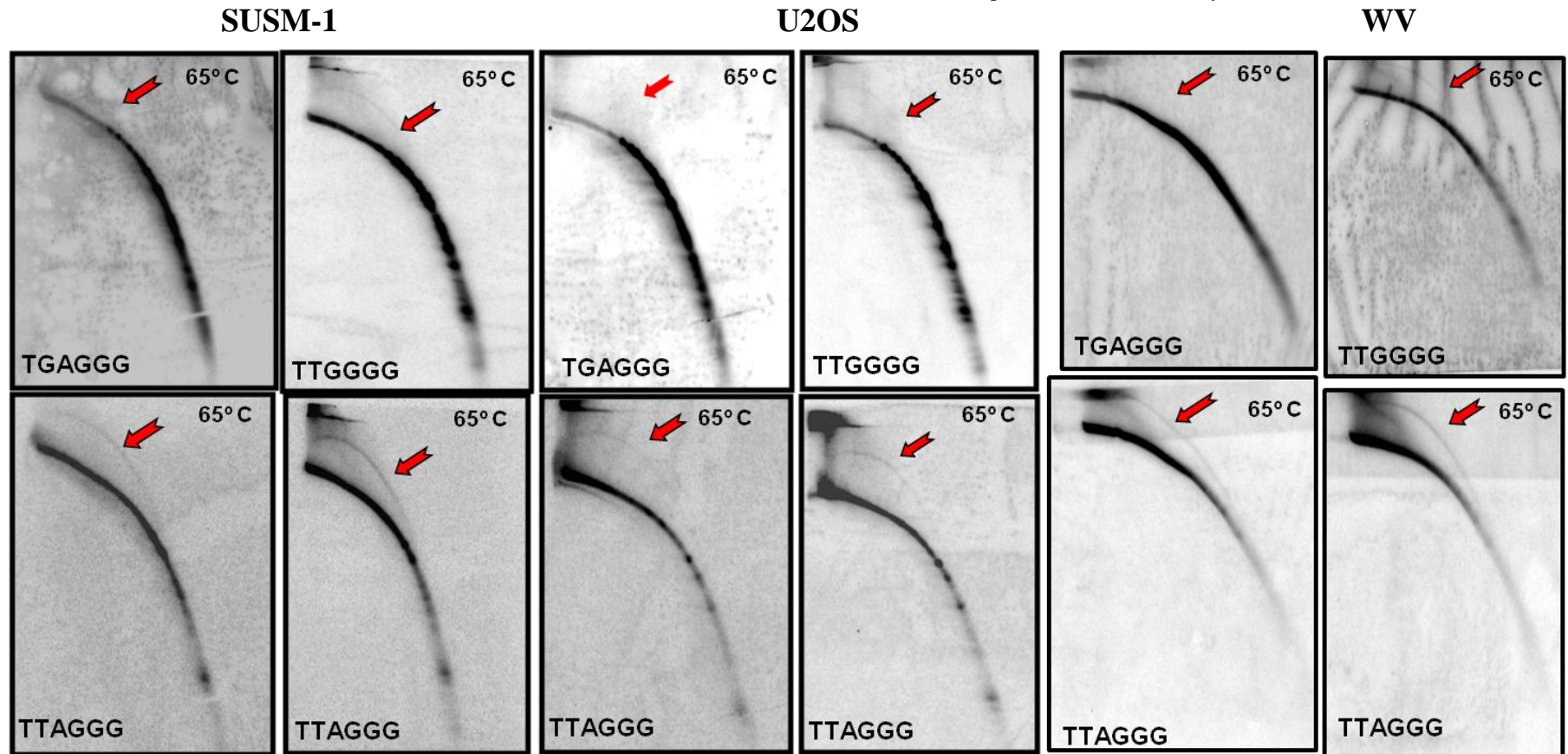


Figure 5.15: Detection of telomeric variants in extrachromosomal circular DNA in ALT+ cells.

Neutral-neutral 2D-gel electrophoresis, followed by Southern-hybridization with a variant telomeric probe at 65C, followed by a re-hybridization of the same blot with a normal telomeric probe show the presence of variants and normal telomeric repeats in extrachromosomal circular DNA (red arrows) in SUSM-1, U2OS and WV ALT+ cell-lines. The top row shows the hybridizations with the variant repeats and, after stripping, the blots were re-hybridized with the TTAGGG probe (bottom row).



Figure 5.16: Variant telomeric repeat detection in circular DNA.

5 μ g of genomic DNA from the SUSM1 cell-line, double digested with *Mbo*I and *Exo*V, was resolved by 2D-gel electrophoresis. A Southern-hybridization to a TCAGGG telomeric variant repeat probe clearly shows a circular arc, after *Exo*V digestion of the linear DNA.

Telomeric extrachromosomal circles have been suggested to derive from homologous-recombination events that occasionally may resolve the t-loop into a t-circle and a shortened telomere. This model for t-circle formation was inferred from observations in cells with a mutant form TRF2 (TRF2^{ΔB}) that lacks the N-terminal domain, where uncapped telomeres shortened and t-circles became detectable. In these cells, formation of t-circles was found to be dependent on the presence of two key players of homologous-recombination, XRCC3 and NBS1 (Compton, S. et al 2007) (fig. 5.17).

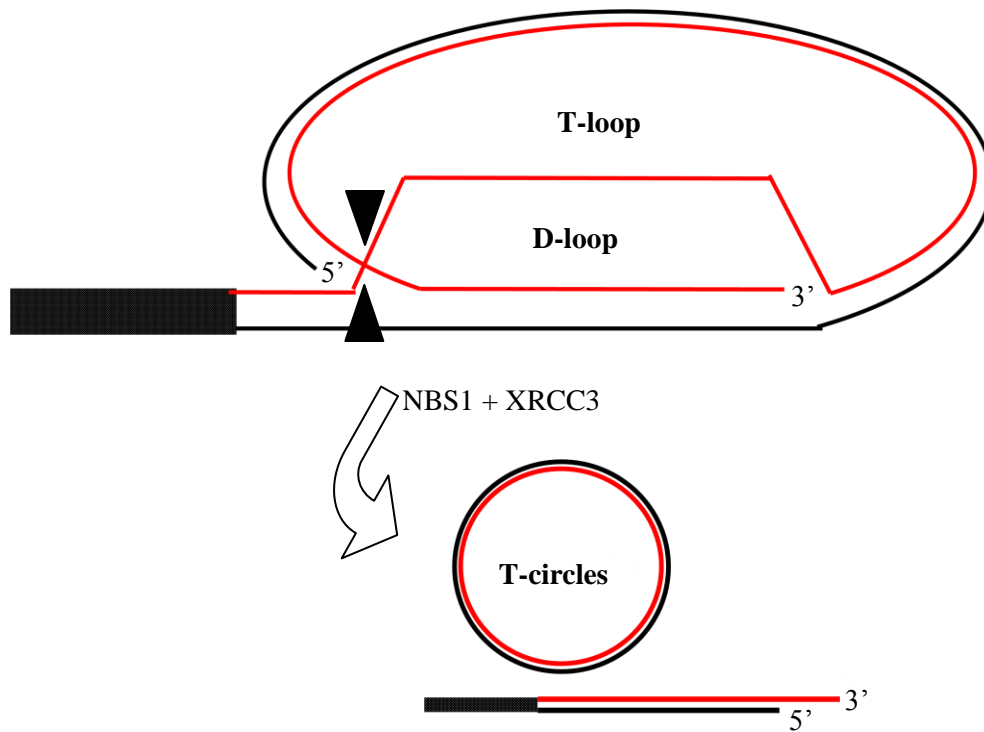


Figure 5.17: T-circle origin model.

The current model for t-circle formation proposes that, in the presence of NBS1 and XRCC3, t-loop resolution at the insertion point on the proximal part of the telomere (black arrows) that results in t-circles and shorter telomeres.

In the ALT+ cell-lines studied, the t-circles seem to be composed of telomeric repeats (TTAGGG) and, in a lower proportion, variant repeats (TCAGGG, TGAGGG and TTTGGG). These findings are very interesting since the distal limit for variant repeats within telomeres is thought to be about 1.9 kb. Thus, if t-circles are formed according to the currently proposed model, the insertion point for the t-loop formation must sometimes be in the region that contains degenerated or sequence variant telomeric repeats.

Although the methodology seem to be robust enough to detect sequences with lower copy number than telomeric repeats (TTAGGG), like telomeric variant repeats, no MS32 extrachromosomal sequences could be detected in any of the cell-lines tested (Fig. 5.18).

However, as mentioned above, some MS32 alleles are smaller than 2 Kb, which seems to be the lower resolution limit of 2D-gel electrophoresis. Also, if there are MS32 sequences in extrachromosomal circles, they most likely result from the events responsible for its instability in ALT+ cells. Thus, as the longest deleted region observed in the MS32 mutants analysed spans 1.6 kb, which falls under the lower limit for resolution, this methodology most likely, does not allow the detection of MS32 extrachromosomal circles if they are smaller than 2 Kb.

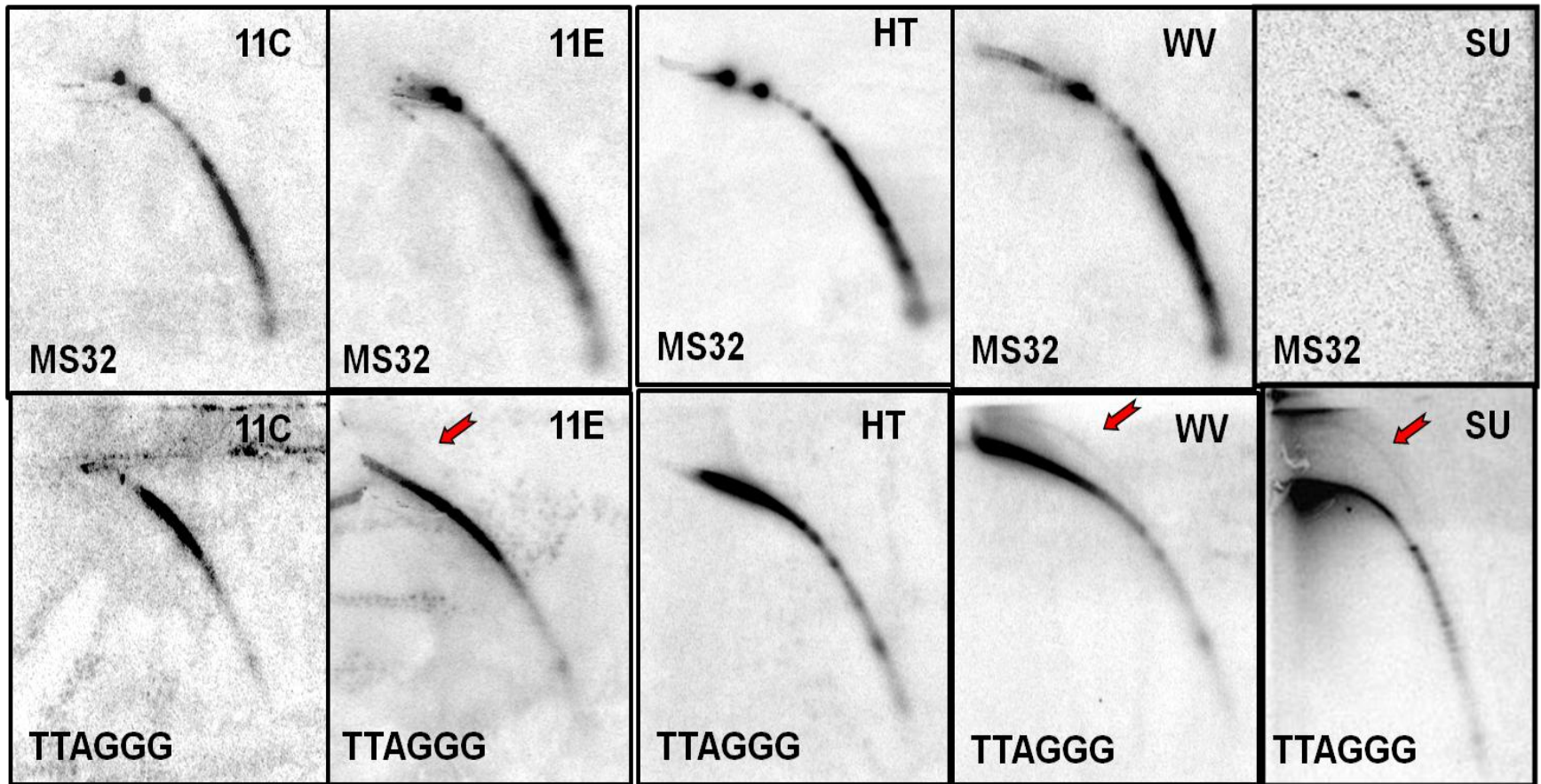


Figure 5.18: MS32 detection by 2D-gel

Neutral-neutral 2D- gel electrophoresis with 10 ug of genomic *Mbo*I-digested DNA from ALT+ (11E, WV and SUSM-1) and Tel+ (11C and HT1080) cell-lines. Southern-hybridization was performed with a MS32 probe (top row), the blots were then stripped and re-hybridized with a telomeric probe (bottom row). Red arrows show observed circular DNA.

5.3.3.2 DETECTION OF CIRCULAR DNA BY TCA

The analysis performed with 2D-gel electrophoresis suggested that ALT+ cells do not have extrachromosomal circular MS32 sequences. However, due to the potential limitation for resolving MS32-circles lower than 2Kb as well as possible sensitivity restrictions, a different methodology was applied in an attempt to detect MS32 circles in ALT+ cells. Telomeric circle amplification (TCA) was adapted by Zellinger et al (Riha 2007) from plasmid and whole-genome amplification techniques based on Φ 29 polymerase strand displacement activity (Blanco and Salas, 1996). This method can generate ssDNA products, ranging up to 100 Kb, via a rolling-circle replication mechanism (Lizardi et al., 1998). Thus, Φ 29 polymerase and a telomere-specific primer, in the presence of t-circles, should produce large ss-telomeric products, that can be resolved from much shorter products resulting from linear DNA molecules.

TCA reactions were prepared with a C-strand (5'-TTAGGGTTAGGGTTAGGG-3') specific primer and *ExoV*-digested genomic DNA from ALT+ and Tel+ cells. A pBlueScript SK-II plasmid containing a cloned chromosome 18 insert was used as a positive control for the TCA conditions. Briefly, genomic *MboI* and *ExoV*-digested DNA was NaOAc and EtOH precipitated and the clean DNA incubated for 5 min at 96°C with the desired primer and the reaction was left to cool down for 1 hour, so that the primer could anneal to all templates around the genome. The Φ 29 polymerase and dNTPs were added to the DNA+primer reaction and the amplification reaction was performed at 30°C for 14 hours. Finally, the reaction was stopped by heat for 20 min at 65°C and the products were resolved. As the final products from the TCA reaction are single-stranded, the electrophoresis was performed under alkaline conditions (0.8% agarose, 50 mM NaOH, and 1 mM EDTA [pH 8]). Southern hybridization with a C-strand specific probe allowed the detection of a high

molecular weight product in ALT+ cells (SaOS) and the telomere-containing plasmid (Plsm) (fig. 5.19).

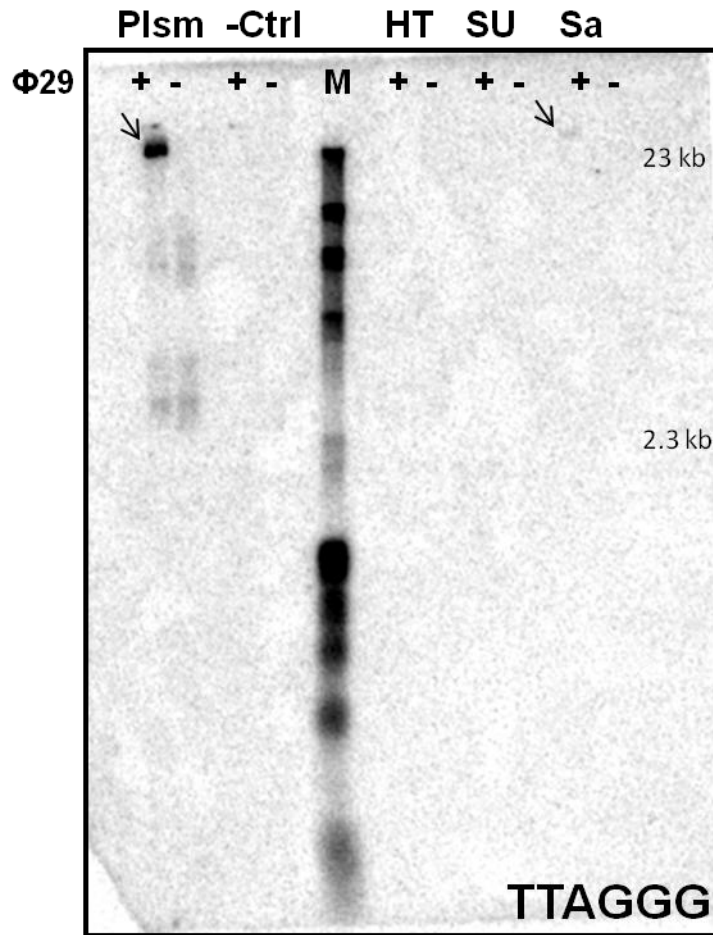


Figure 5.19: Optimixzation of T-circle amplification by TCA.

1 μ g of *Mbo*I and *Exo*V-digested genomic DNA was amplified with a telomeric C-strand specific primer by TCA. The products were resolved by alkaline electrophoresis and the Southern-hybridization of the products with a telomere-specific probe is shown. Plsm: plasmid as positive control; -Ctrl: no DNA control; M: DNA markers $\lambda + \Phi$; HT - HT1080 (Tel+); SU - SUSM-1 (ALT+); Sa - SaOS (ALT+). The signs above each tract represent the addition (+) or not (-) of polymerase 29 to the TCA reactions.

Therefore, TCA appears to provide another methodology for t-circle detection, since it is highly specific for circular DNA, as after *ExoV* digestion only circular DNA could have provided template for rolling-circle amplification. To confirm the specificity of TCA reaction to the targeted circular molecules, primers specific to the telomeric repeat TTAGGG, the variant TCAGGG and the MS32 sequence were tested and Southern-hybridized to the two probes (first, the TCA-blot was hybridized to MS32 probe, stripped and then hybridized to the telomeric probe. As expected, only ALT+ cell-lines (SUSM-1, 11E and WV) and the positive control (plasmid with a telomere insert) TCA reactions primed with the telomeric C-strand specific primer generated a high molecular weight product hybridized to the telomeric probe (Fig. 5.20 and 5.21), confirming the presence of t-circles in these cells. Also, 2D-gel was performed in the same samples (11C, 11E, HT1080 and WV), Southern-hybridized with a MS32-specific probe, followed by re-hybridization with a telomeric probe, to confirm the presence of t-circles in the samples used (Fig. 5.18). The 2D-gel analysis indicated that t-circles are more abundant in the WV cell-line than in the other ALT+ cell-lines (11E and SUSM1), which is confirmed by TCA, as WV cell-line generates more TCA products than the other two (Fig. 5.20 and 5.21). The positive control TCA reaction, primed with a MS32-specific primer or the variant-specific primers also showed a strong high molecular weight product (Fig. 5.20 and more evident in 5.21). The MS32-specific primer has 70% homology with the vector (pBluescript) used as positive control, which might have triggered the TCA reaction to proceed, since the amplification occurs at 30°C. Thus, MS32-primers could easily generate a TCA-product that can hybridize to the telomere probe due to telomeric insert. Furthermore, none of the ALT+ cell-lines showed a TCA-product in the reaction with a MS32-specific primer, confirming that the template for TCA-products detected in the ALT+ cells were t-circles, indeed. Also the

variant-specific primer has 100% homology with the plasmid, as the targeted variant is present in the cloned telomeric insert, which explains the TCA-product detected when this primer was added to the reaction (Fig. 5.21). Nevertheless, none of the cell-lines tested showed a TCA-product that hybridized to the MS32 probe (fig. 5.20 and 5.21). As the copy-number of t-circles is much higher than any potential MS32-circle, DNA-input dilutions were tested to determine the sensitivity of the methodology. Serial dilutions of *MboI*-digested genomic DNA, extracted from the ALT+ WV cell-line, were tested with a telomere-specific primer. As expected, telomeric TCA-product can only be detected with a minimum of 250 ng of input DNA, suggesting that also this methodology may not be sensitive enough to detect the presence of a low copy number of MS32 extrachromosomal circles (Fig. 5.22). Nonetheless, the TCA-products generated with a variant-specific primer were as strong as the ones resulting from telomere-specific primer (fig. 5.21), which may indicate that the number of priming sites has minimal influence on the outcome of the TCA reaction and, consequently, even if there were low number of circular extrachromosomal MS32 sequences, the TCA technique should be sensitive enough to detect them.

Thus, both 2D-gel and TCA analysis confirmed the presence of t-circles in ALT+ cells, composed of not just the common telomeric repeat but also some variants of it (Fig. 5.15), which indicates that, at least in some chromosomes or some cells, the t-loop insertion point is much more proximal than thought. No evidence for the presence of MS32 sequences in the extrachromosomal circular form was found (Fig. 5.18 and 5.21), suggesting that the mechanism responsible for t-circles is not acting at the MS32 minisatellite locus in ALT+ cells.

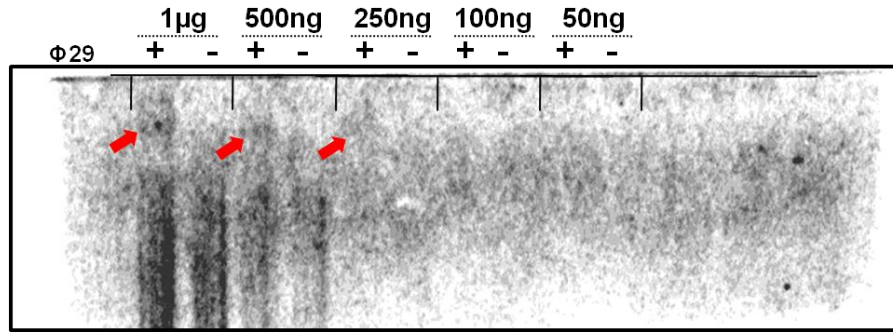


Figure 5.22: TCA-input sensitivity

TCA reactions were set with different inputs (1 µg- 50 ng) of total genomic DNA extracted from WV cells. The TCA products were electrophoresed under alkaline conditions. Southern-hybridization with a telomeric probe detected TCA products in 3 reactions (red arrows)

	Sequence 5' to 3'
Tel1	TTAGGGTTAGGGTTAGGG (3 sites with 2 repeats in plasmid)
Tel-G2	TTAGGGTTAGGGTTAGGGtta
TelG-comp	AGGGTGAGGGTGAGGGTG
TelK-comp	AGGGTCAGGGTCAGGGTC (100% full length identical sites in plasmid)
TelJ-comp	GGGTTGGGGTTGGGGTTG
MS32 (e-FW)	TAG-TTCTGAGTCACCCCTGGCCG

Table 5.3: Sequence of primers used for TCA experiment.

The notes in brackets refer to the homology of the primer sequence to the pBlueScript plasmid with a telomeric insert from chromosome 18, used as positive control for the TCA reactions. The homology of the primer sequence with the plasmid used for positive control reactions is shown in brackets.

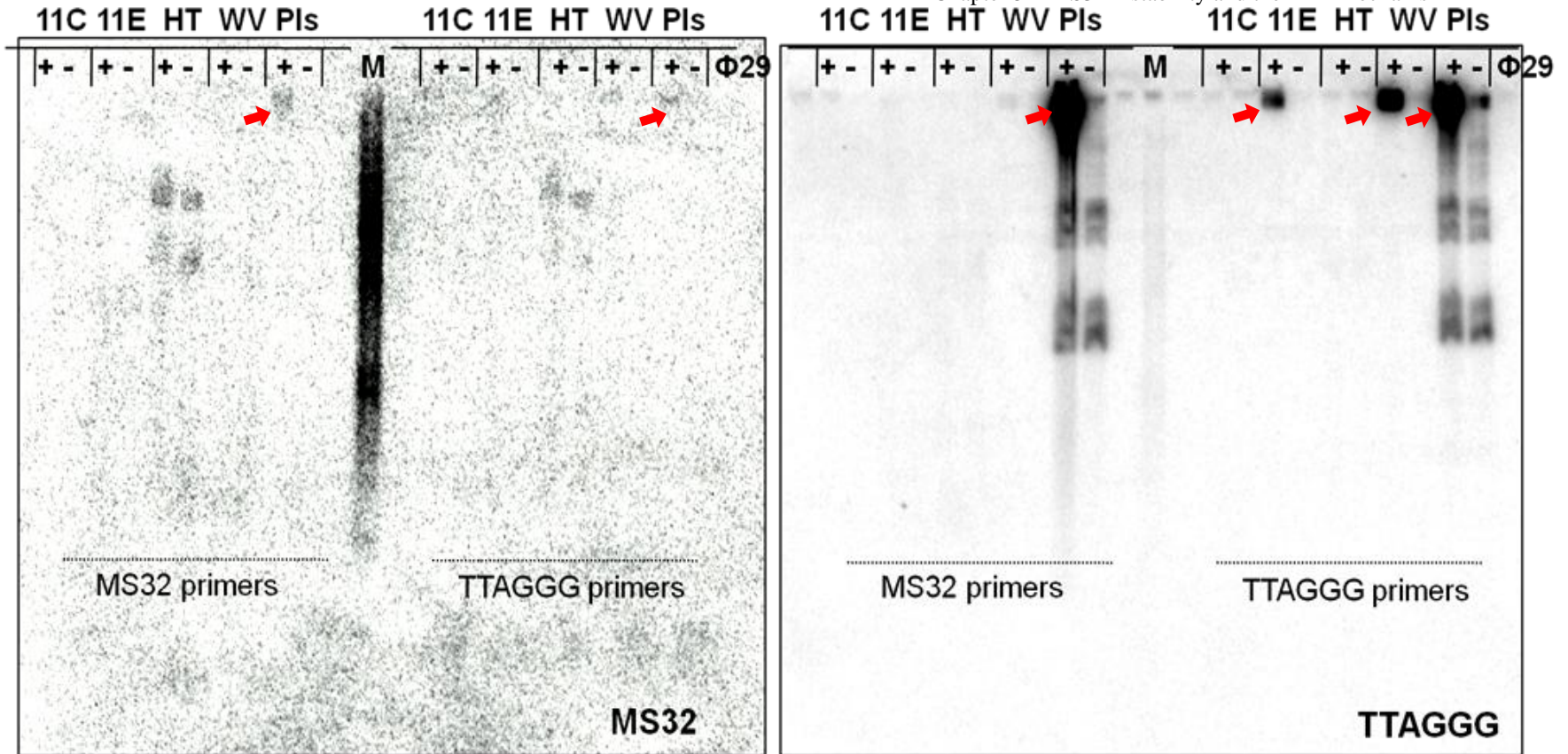


Figure 5.20: Amplification of extrachromosomal circular DNA by TCA.

TCA products were resolved by agarose gel electrophoresis in alkaline conditions, the gel was Southern blotted and hybridized to a MS32-specific probe (left image), stripped and re-hybridized to a telomeric probe (right). The products of TCA reactions primed with MS32-specific primers were loaded on the left the blot, whilst the ones primed with telomere-specific primers are on the right. The signs above each tract represent the addition (+) or not (-) of polymerase 29 to the TCA reactions. Red arrows point to TCA products.

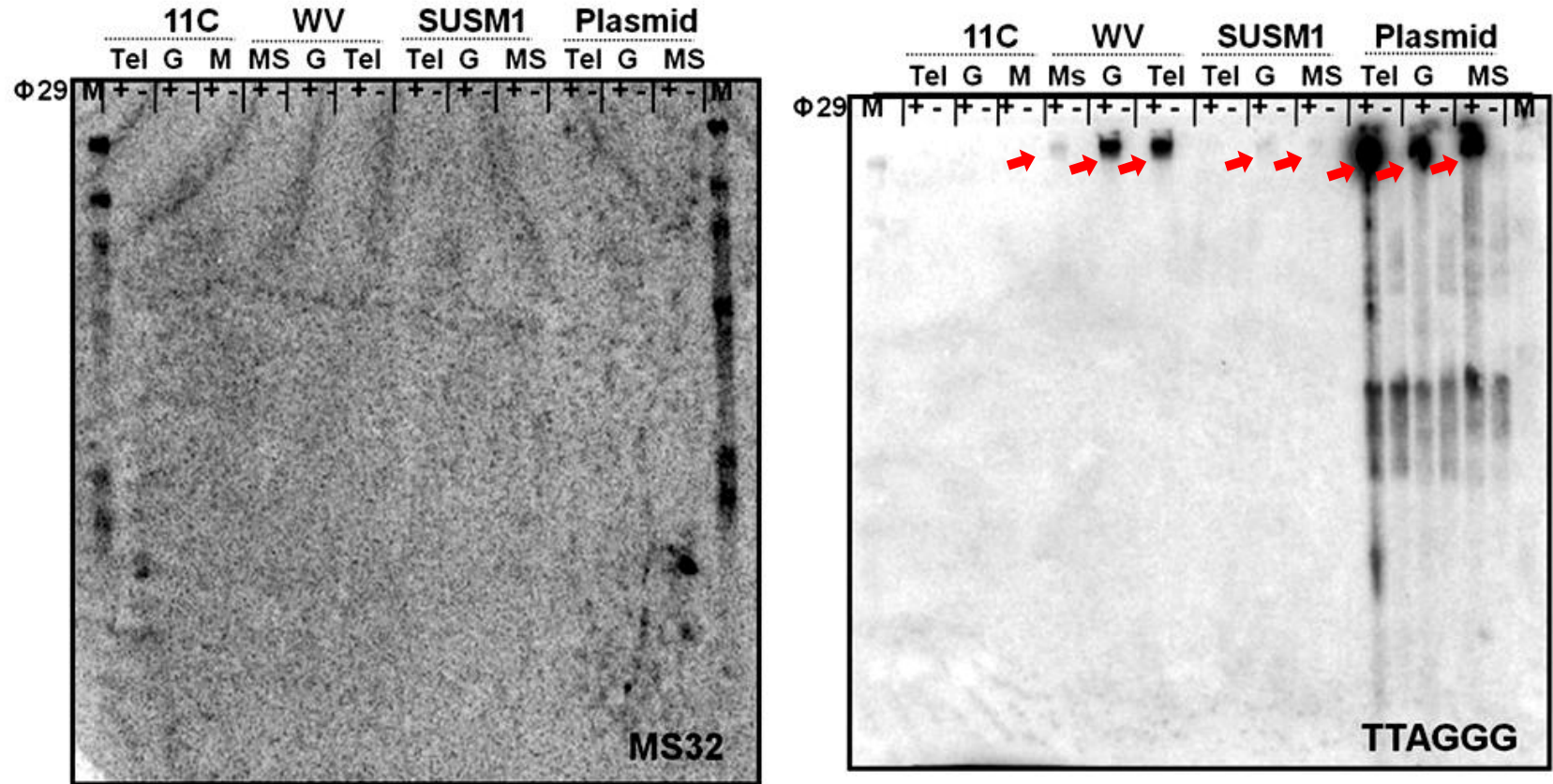


Figure 5.21: TCA efficiency and sensitivity

TCA products were resolved by agarose gel electrophoresis in alkaline conditions, the gel was Southern blotted and hybridized to MS32 probe (left image), stripped and re-hybridized to a telomeric probe (right). The primers used for each TCA reaction are referred to in top of each lane. Tel: telomeric repeat (TTAGGG), G: telomeric variant repeat (TGAGGG) and MS: MS32-specific primer. The samples tested are: 11C (Tel+), WV (ALT+), SUSM-1 (ALT+) and Plasmid (positive control with telomere insert). The signs above each tract represent the addition (+) or not (-) of polymerase 29 to the TCA reactions. Red arrows point to TCA products.

5.4 DISCUSSION

The molecular processes involved in minisatellite instability have been investigated, in order to understand the mechanisms responsible for meiotic and mitotic genomic instability (Jeffreys, A. et al 1988; Jeffreys, A. et al 1990; Monckton, D. et al 1994; Buard, J. 1994; Jeffreys, A. et al 1994; May, C. et al 1996 and Buard, J. 2000). As a consequence of these investigations, powerful PCR based techniques have been developed including the SP-PCR and MVR-PCR analysis (Jeffreys, A. et al 1991). PCR amplification of very small aliquots of DNA allows the identification of mutant molecules amongst a small number of progenitor molecules. Furthermore, length-mutant molecules can be further used to investigate the order of repeats in the array and identify the mutation that underlies the length change.

A better understanding of the mechanisms responsible for MS32 minisatellite instability in ALT+ cells may unveil the relationship between the MS32 instability and the ALT mechanism itself. Previous studies showed that the mutation spectrum of MS32 in ALT+ cells differed from the ones described in human germ-line (Jeyapalan, J. et al 2005). However, complex rearrangements identified could have arisen from an accumulation of sequential mutational events, due to the high instability of MS32 in the ALT+ cells. Thus, to identify mutations arising from single-mutational events, the molecular mechanism underlying MS32 instability in ALT+ cells was determined in SUSM1 cells derived from clonal expansions that had undergone 20 PDs. As previously shown (Jeyapalan, J. et al 2005), the levels of MS32 instability vary between clones (Table 5.1), which might be a consequence of different propensity for mutation according to the allele size. The mutation rates obtained are an underestimation of the instability, as only length-mutants with at least

one repeat deletion or addition in comparison to the progenitor alleles were identified for analysis due to agarose gel resolution limits. The mutation rates obtained are comparable to the values previously observed by Jeyapalan in another ALT+ cell line (0.36% per cell division in WI38VA13/RA) (Jeyapalan, J. et al 2005), The SUSM1 clone with the highest mutation rate, 3.4×10^{-3} per cell-division, was chosen for the analysis (3H3). A total of 51 MS32 molecules were analysed by MVR-PCR: 7 molecules derived from the large progenitor allele, 7 from the small progenitor, 33 mutants derived from the large-allele and 4 mutants derived from the small-allele mutant. Each interspersed map was aligned to the progenitor alleles to determine the type of changes that had occurred. Most of the mutations were deletions (79.2 % of the events), followed by an alteration of the type of variant repeat (11.1%) and insertions of new repeats (9.7%). The results also indicate that a larger repeat array might be more prone to instability (Buard, J. et al 1998; Jauert, P. et al 2005), since 89.2% of the mutants identified derived from the large progenitor allele.

The type and distribution of the changes observed greatly differed from the ones described in germ-line or in normal somatic cells. Amongst the MS32 mutants analysed in sperm DNA, 80% originate from inter-allelic transfers of short (2-10 repeat) segments, in register between donor and recipient alleles. The mutations observed were often relatively complex (repeat reshuffling in the transferred segment, with duplication or deletion in the recipient allele at or near the site of transfer). Moreover, the mutation sites were polarized to the array end adjacent to the meiotic-recombination hotspot and involving unequal crossover (Jeffreys, A. et al, 1998). In fact, the MS32 instability in germline appears to be regulated by the recombination hotspot 200 bp upstream the 5'-end of the array, since a single base transversion in cis is strongly associated with suppression of the homologous recombination at MS32 in the germline (Monckton et al 1994). In contrast, somatic cells

showed apolar process of intra-allelic duplication or deletion of repeat unit blocks, as demonstrated by blood cells analysis (Jeffreys et al 1997). In ALT+ cells, the mutations observed at MS32 minisatellite in SUSM1 cells can be divided into three categories: 37.8% are mutations at a single site within the progenitor allele (mutants derive from a deletion of a contiguous block of repeats at one site of the array), 43.2% are mutations occurring a two sites (mutations occur at two non-contiguous positions along the array) and 19% are complex rearrangements (mutants arise from a mixture of intra-allelic events that result from complex reshuffling of the repeat order and/or addition/deletion of repeats across the array). Contrasting to the non-polarized mutations in somatic cells, in ALT+ cells some sites along the array seem to be particularly prone to the occurrence of rearrangements (Fig. 5.4-b). Interestingly, the 5' end flanked by the meiotic-recombination hotspot is greatly prone to mutations (mainly deletions) in ALT+ cells. Also the middle of the array, just before the block of 22 contiguous *e* repeats shows a high incidence of alterations. This evidence might reflect pauses during replication (perhaps due to a stalled fork), maybe derived from secondary structures formed at these sites. However, complex rearrangements involving extensive reshuffling of the MS32 repeats order suggests that more complex mechanisms are likely to be contributing to MS32 instability in ALT cells. Thus, the different types of rearrangements are most likely derived from different repair events initiated by similar structures/complexes.

Interestingly, the type and proportion of MS32 mutants detected in ALT+ cells was similar to mutants identified in the CEB1 minisatellite inserted into a 5' intergenic region of the ARG4 locus (Debrauwere et al, 1999) of a yeast RAD27 Δ mode I (Lopes et al 2006). This similarity suggests that a similar mechanism might underlie the MS32 instability in ALT+ and the CEB1 in this particular yeast model. It was proposed that in yeast, the

mutations could have arisen from the accumulation of unprocessed 5' flaps after Okazaki fragments removal, due to the absence of the 5' flap-endonuclease Rad27. The 5' flaps might be recognized as double-strand breaks by DNA repair mechanisms and subjected to repair by the DSB-synthesis-dependent strand annealing (SDSA) (Buard et al., 1998, 2000; Debrauwère et al., 1999). The invasion of the sister-chromatid by the DNA repair mechanism will cause the formation of a D-loop with mismatches due to sequence divergence between repeats in the array. A secondary DSB can then occur, permitting an anomalous order of the repeats to the array when repaired. The diagrams on Figure 5.22 represent possible models for the generation of the three types of mutations observed in MS32 in ALT+ cells.

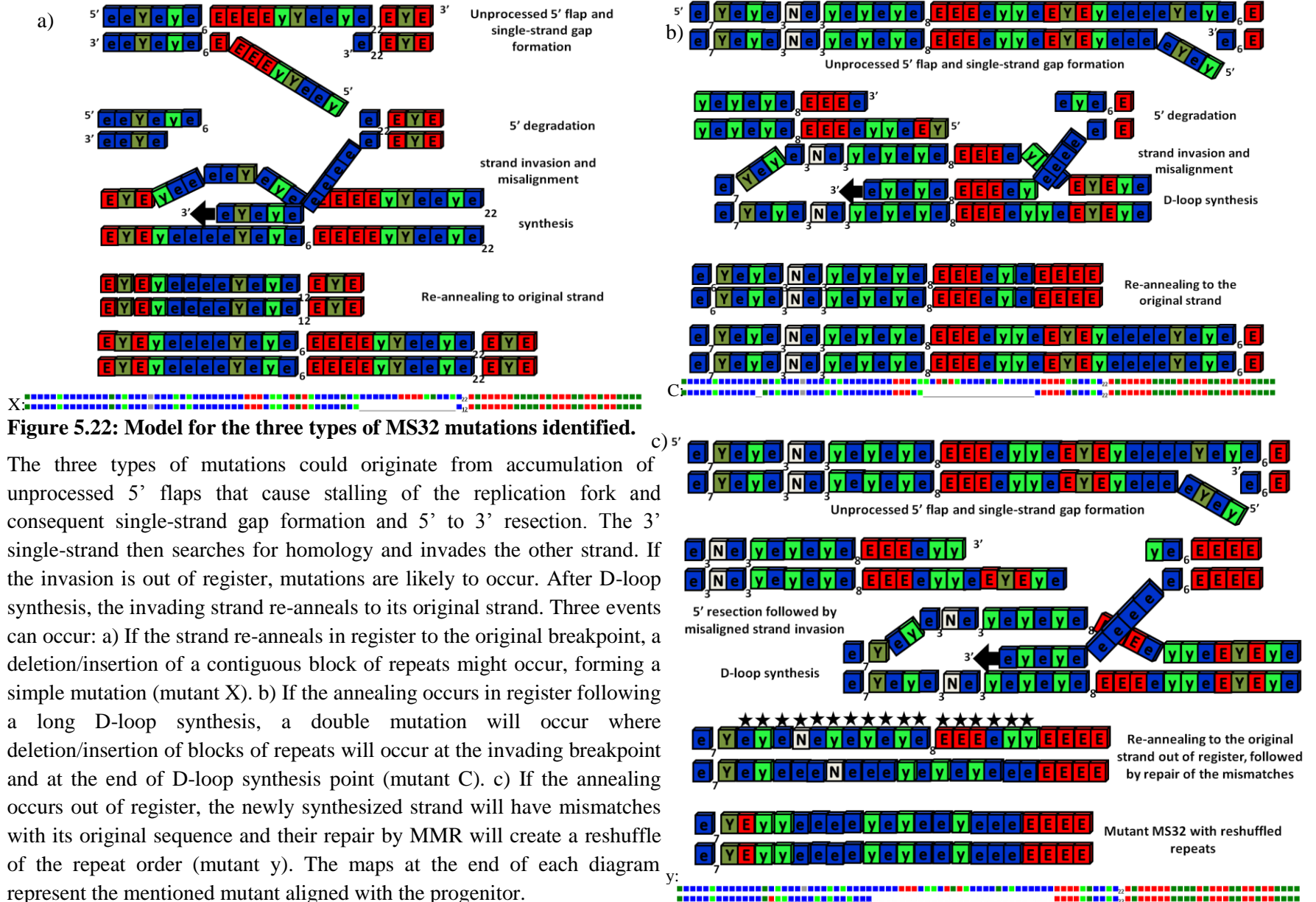


Figure 5.22: Model for the three types of MS32 mutations identified.

The three types of mutations could originate from accumulation of unprocessed 5' flaps that cause stalling of the replication fork and consequent single-strand gap formation and 5' to 3' resection. The 3' single-strand then searches for homology and invades the other strand. If the invasion is out of register, mutations are likely to occur. After D-loop synthesis, the invading strand re-anneals to its original strand. Three events can occur: a) If the strand re-anneals in register to the original breakpoint, a deletion/insertion of a contiguous block of repeats might occur, forming a simple mutation (mutant X). b) If the annealing occurs in register following a long D-loop synthesis, a double mutation will occur where deletion/insertion of blocks of repeats will occur at the invading breakpoint and at the end of D-loop synthesis point (mutant C). c) If the annealing occurs out of register, the newly synthesized strand will have mismatches with its original sequence and their repair by MMR will create a reshuffle of the repeat order (mutant y). The maps at the end of each diagram represent the mentioned mutant aligned with the progenitor.

Therefore, in ALT⁺ cells, the recruitment of a protein involved in the lagging-strand synthesis and DNA repair to the telomeres may cause the accumulation of unprocessed flaps at MS32 and its misrepair result in the instability observed. The events involved in the ALT mechanism are thought to occur during late S-phase, as APBs and several proteins involved in DNA repair and recombination colocalize with telomeres during late S phase/G2, at the same time that incorporation of bromodeoxyuridine at APBs occurs (Chen et al 2000; Grobelny et al 2000). So, late S-phase in ALT⁺ cells differs from Tel⁺ and normal somatic cells in that important key players necessary for proper DNA replication and replication-fork resolution may be recruited to the telomeres to participate in telomere elongation. The resolution of any stalled replication-forks that can often occur at difficult replicating regions, like minisatellites, needs to occur before the end of S-phase. Thus, unresolved structures such as unprocessed 5'-flaps might accumulate at other genome loci, which would then become targets for alternative repair mechanisms that could result in the MS32 instability associated with ALT activation.

In yeast, the CEB1 defects were partially complemented by hFEN1 (human RAD27 homologue) (Lopes et al 2006), which led to the investigation of the levels of *hFEN1* expression in ALT⁺ cells. No significant expression changes associated to ALT⁺ were detected by qPCR analysis across 11 cell-lines tested (Fig. 5.8). However, as *hFEN1* point mutations were associated with a mutator phenotype in mice (Zheng et al 2007), the full coding sequence was screened but no mutations were identified in 11 cell-lines. These results are consistent with the hFEN1 role in the ALT⁺ pathway, especially for proper telomere stability in ALT⁺ cells (Saharia et al 2009).

Nonetheless, hEXO1 another homologue of RAD27 also has flap-endonuclease activity and its overexpression rescued the conditional lethality of RAD27 Δ mutants

(Shen et al 1999). Therefore, the expression levels of *hEXO1* were also analysed by qPCR and a significant increase (p-value 0.0446) in the *hEXO1* levels associated to the ALT+ cell-lines tested was detected (Fig. 5.10).

EXO1 appears to be responsible for the exonucleolytic processing of double strand breaks and has also a role during DNA mismatch repair, replication, recombination, and at the telomeres (Tishkoff et al 1997; Sokolsky et al 2000; Maringele et al 2002; Bertuch et al 2004). Particularly interesting are the observations in yeast, where EXO1 seems to be essential for the appearance of telomerase-negative survivors, probably by promoting telomeric-substrates for recombination (Bertuch et al 2004). Thus, the overexpression of *hEXO1* in the ALT+ cell-lines analysed might reflect a hEXO1 role in ALT+ also in humans. It would be interesting to investigate the effect of a dysfunctional hEXO1 in ALT+ cells. In mice with a telomere dysfunctional background, Exo1 was proposed to have role in the induction of DNA damage signals, cell-cycle arrest and apoptosis (Schaetzlein et al 2007).

The overexpression of *hEXO1* in ALT+ cells seems to contradict the proposed model for MS32 instability due to a higher recruitment of a protein essential for proper lagging-strand synthesis to ALT-telomeres. However, the long length of ALT-telomeres might require a high amount of hEXO1, which alone could explain its higher expression in ALT+ cells. If true, other genomic loci that failed to replicate properly, could form difficult to resolve secondary structures and/or are late replicating regions, would also be prone to the action of DNA repair mechanisms.

EXTRACHROMOSOMAL CIRCULAR DNA

Another ALT+ cell feature is the presence of t-circles. The formation of these structures was shown to require XRCC3 and NBS1 (Compton et al 2007) but the

function of the t-circles is still under debate. Since most MS32 mutations observed derived from large deletions, the presence of MS32 extrachromosomal circular sequences was investigated by 2D-gel electrophoresis and by TCA. Neither methodology detected MS32 circles, although the former has size and copy-number limitations and in the latter sensitivity needs further optimization. Nonetheless, during the optimization of these experiments telomeric variant repeats were found to be present in the t-circles (Fig. 5.15). These findings are very interesting, since the distal limit for variant repeats within telomeres is thought to be about 2-3 kb (Allshire et al 1989; Baird et al 2000). Thus, if t-circles are formed according to the currently proposed model, the insertion point for the t-loop formation must sometimes be in the region that contains degenerated or sequence variant telomeric repeats. Alternatively, as the precise nature of ALT mechanism is still not understood, the recombination-like events acting at these telomeres may insert variant repeats into more distal regions causing them to appear as t-circles. Irrespective of the origins of t-circle formation, the presence of variant repeats in t-circles may mean that they could be the substrate for telomere elongation by the ALT mechanism.

CHAPTER 6:MS32 MINISATELLITE LOCI IN ALT+ VS. NON-ALT CELLS

6.1 AIMS

The extreme instability at the MS32 minisatellite in ALT+ cells is clearly not a consequence of general minisatellite instability or a result of chromatin reorganization initiated by local transcriptional changes (see Chapter 3 and 4, respectively). Thus, the relationship between this particular minisatellite and the ALT mechanism is still unknown. Nevertheless, it seems likely that the D1S8 locus itself must be the trigger for the minisatellite instability in ALT+ cells. Therefore, to investigate further how the D1S8 locus could differ in ALT+ and non-ALT cells, the copy-number and methylation status of the locus were analysed.

6.2 RESULTS

6.2.1 COPY-NUMBER ANALYSIS

Until recently, the most studied form of genetic variation had been single-nucleotide polymorphisms (SNPs) and many common SNPs are now associated to cancer predisposition and other genetic diseases, like for example the TP53 polymorphic variant that confers a reduction in the p53 protein apoptotic potential (Bonafé et al. 2002, 2004; Dumont et al. 2003). However, a new form of genetic variation has emerged that is estimated to cover around 10% of the genome: copy-number variation – CNV (Iafrate et al, 2004; Redon et al., 2006). CNVs represent structural changes in regions where copy number differences were observed between two or more genomes (Iafrate et al, 2004; Feuk et. al, 2006). CNVs can involve gains or losses of genomic DNA regions usually larger than 1kb, conferring a variation to the

diploid copy-number (Sebat et al., 2004; Iafrate et al, 2004). Although common throughout the genomes, a few CNVs have already been implicated with pathologies, like for example the deletion of a region involving 28 genes (7q11-q13) responsible for the Williams-Beuren syndrome (Meyer-Lindenberg et al., 2006), the deletion polymorphism associated to an altered expression of the IRGM gene in Crohn's disease (McCarroll et al 2008) or the increase in beta-defensin's copy-number, associated to psoriasis (Hollox et al 2008). Also, tumour cells have long been characterized by a propensity to acquire copy-number alterations (CNAs), probably resulting from their genomic instability. Interestingly, studies focusing on the association of known common CNVs with tumorigenesis found that around 40% of cancer-associated genes coincided with known CNVs loci, suggesting that some common CNVs may predispose to cancer (Iafrate et al 2004; Shlien et al 2008).

To date, only a single study has been performed to determine the effect of CNVs on a variety of liposarcoma samples, where the Affymetrix Genechip SNP 100K was used as DNA mapping array to find genomic imbalances associated with each TMM (Johnson et al 2006). The study found that ALT+ liposarcomas have, on average, higher levels of genome instability and loss of heterozygosity in comparison to the Tel+ samples. Interestingly, the 1q32.2-44 region, which encompasses the MS32 minisatellite locus has been defined as deleted exclusively in ALT+ liposarcomas, (Johnson et al 2006). Thus, to investigate if the observed deletion in 1q also occurs in other ALT+ cell-types and to contrast with the expression analysis results, the copy-number of the region around MS32 minisatellite was assessed in ALT+ and non-ALT cells.

6.3.1.1 MLPA METHODOLOGY

An extensive number of methodologies can be used for CN analysis. The whole-genome analysis approach, like high-density oligonucleotide single-nucleotide polymorphism (SNP) array platforms, provides a vast set of data on both CNVs and SNPs. However, the DNA template should be of high-quality so whole-genome amplification (WGA) is often necessary prior to the array hybridization. This amplification might compromise a faithful CN analysis, since differential amplification can occur, especially if the DNA is degraded. Recently, new sequencing strategies emerged that allow integrated sequencing and CNV analysis of the DNA samples (Campbell et al 2008).

Another group of methodologies are based on specific targeting and quantification of CN by either PCR or hybridization-based methods. The PCR-based methods include qPCR, multiplex amplifiable probe hybridization (Armour J et al 2000), quantitative multiplex PCR of short fluorescent fragments (Charbonnier et al 2000), paralog ratio testing (Armour et al 2007) and multiplex ligation probe assay (Schouten J et al 2002). Across literature, MLPA has been the most used method for CN analysis probably due to the ability to assess multiple loci in a single experiment. Also, the requirement of quite low DNA quantities and the type of equipment required, common to most laboratories (thermocyclers and capillary electrophoresis) turn MPLA into one of the most affordable techniques. Also, as quite small sequences are targeted (50-70 nt), a more detailed analysis of potential CNV breakpoint sites is possible. The main drawbacks of this technique concerns probe design, which involves some complex procedures and its limitation to 50 loci. However, a vast number of MLPA kits designed mainly for CN analysis as a diagnostic tool are available (MRC Holland, Amsterdam, Netherlands) and custom-kits may also be considered for a particular study.

MLPA consists of a PCR-based method to detect up to 50 specific genomic DNA sequences in one single reaction (Schouten, J.P. et al. 2002). MLPA is an extremely sensitive technique as it can detect small CN changes from very low DNA samples (minimum of 50ng). Briefly, genomic DNA from test cells is mixed with probes for all loci to be analysed (Fig. 6.1-i). Each probe consists of two DNA molecules where the ends match consecutive parts of the target sequence (different coloured lines in the diagram). Probes contain tails with a stuffer sequence (green in Fig. 6.1) with different lengths in each probe and a common sequence at their distal ends (dotted red in Fig. 6.1). The reaction starts by denaturation step that allows the subsequent annealing of the MLPA probes to the targeted genomic loci (Fig. 6.1-ii). A ligation reaction is then carried out to join the annealed ends of each probe (Fig. 6.1-iii). The newly formed double-stranded region in the target loci will be the template for PCR amplification with universal labelled-primers, complementary to the common sequences at the end of each probe (red dotted lines in Fig. 6.1). The labelled-PCR products can then be size-fractionated (for example, by capillary gel electrophoresis). Finally, the intensity of the peak corresponding to each probe are normally compared against a similar profile obtained from a reference genome, which will allow the relative measurement of the relative CN of the target sequence in the genome, in comparison to the reference used. For quality and procedure control purposes, the MLPA kit also contains control fragments. To ensure that the genomic DNA template is enough to provide reliable data analysis, four fragments are included (64, 70, 76 and 82 nt long) whose peaks will only be visible when low or non-DNA is present. Additionally, three DNA and ligation-dependent control probes are included. A 92 nt-long probe that targets a sequence in the 2q14 region, a 88 nt -long probe that recognizes a sequence on 6p21.3, a CpG island in the FANCE gene promoter and a 96 nt-long fragment targeting

the 1p36 CpG island in the TP73 gene. Thus, the peaks correspondent to these three control probes will only be present when sufficient DNA has been added and the ligation step occurred. Also, the 88 and 96-fragments are a further denaturation control, since they target GC-rich regions that are more difficult to denature.

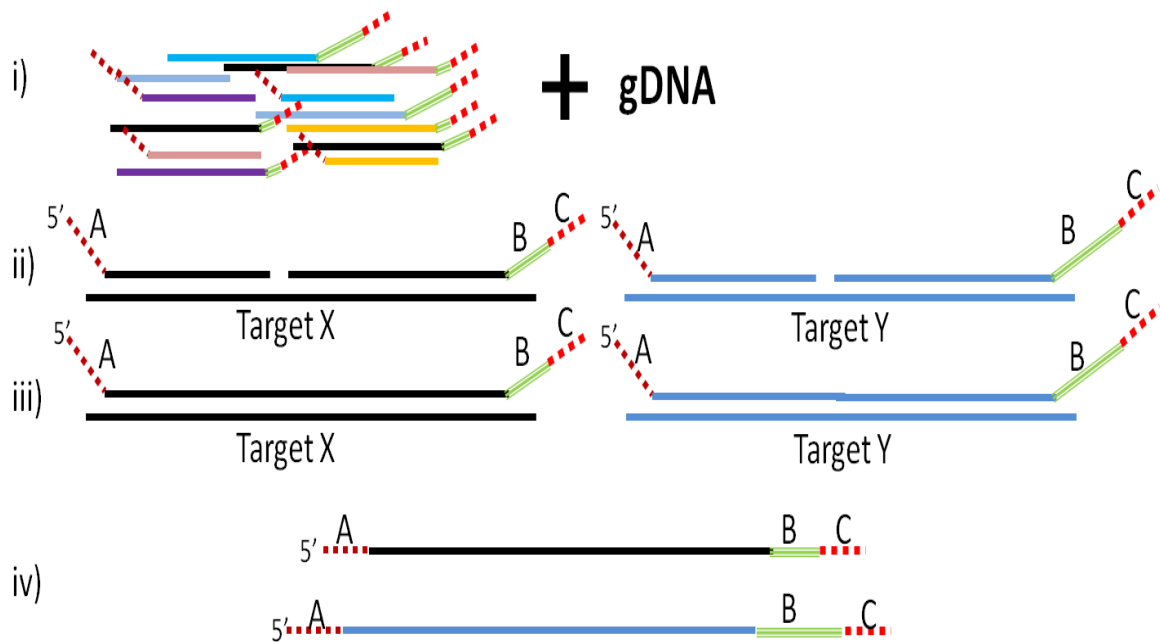


Figure 6.1: Diagram representing the MLPA reaction.

MLPA is a PCR based kit composed of up to 50 sequence-specific probes (i) that hybridize to target genomic regions (ii). A ligation step (iii) ensures that only the correctly hybridized probes will be amplified by the subsequent PCR reaction (iv). Each probe is flanked by the same forward primer (A) and reverse (C) FAM-labelled primers, which allows identical PCR conditions for the amplification of all targets. A stuffer sequence of varied length on each probe (B) provides a unique length for each product, essential for their differentiation by electrophoresis.

A MLPA kit was specifically designed by the company MRC Holland (Amsterdam, Netherlands) to detect copy-number changes in the region 1q21.1-q44. A total of 41 probes were developed targeting 29 loci along the region of interest and 12 control loci, 4 in chromosome 1 and the remaining 8 in other chromosomes (see Fig. 6.2 and Table 6.1 for detailed information on each probe). The PCR products obtained by

the multiplex amplification reactions ranged from 124 to 481 bp. The MLPA protocol was performed as previously described (Schouten, J.P. et al. 2002) using 150 ng of genomic DNA. Briefly, DNA was denatured and hybridized overnight to the probemix. A ligation reaction was performed to join both parts of each probe and the successfully hybridized target-regions PCR amplified with the labelled PCR forward (GGGTTCCCTAAGGGTTGGA) and the unlabelled reverse (GTGCCAGCAAGATCCAATCTAGA) primers. Finally, one microliter of the amplified product was analyzed with the ABI-3130XL Genetic Analyzer (Applied Biosystems, Foster City, CA), using LIZ-500 as internal size standard. The fragment-size calling was performed on GeneMapper version 4.1 (Applied Biosystems, Foster City, CA) and the quality of the electropherograms was evaluated by comparing the peaks of the ligation-independent probes (included in the MLPA kit). The samples with control-peaks bigger than half the size of the peaks of other probes were thus discarded from further analysis due to failure of the ligation reaction.

Data analysis was performed with MRC-Coffalyser software (version 9.4, MRC-Holland, Amsterdam, Netherlands). All probes (test and controls) were used for normalization of the data and then each sample was normalized to the reference diploid cell-line GMO3798. A population analysis was performed by using the signals of all probes (excluding outliers) and a regression was performed with an adapted least of squares regression method. Then, each probe from the reference diploid genome (GMO3798) was used to determine the ratio of the CN in the samples analysed and the median value of all the ratios was estimated as the final ratio (Table 6.2). The limits for normal CN ratios were set at 0.7 and 1.3, values below considered as deletions and above as amplifications. For each cell-line, at least two independently obtained MLPA ratios were used for the final data analysis..

The final averaged ratios can be found in Table 6.2 and Figure 6.3. The top rows on Table 6.2 show the normalization method applied (Population analysis) and the controls performed by the Coffalyser software for the DNA quantity, ligation reaction, slope correction control (Pearson value) and the median absolute value (MAD). All samples included in the final analysis have passed the normalization tests (represented by green, or orange for MAD, boxes in table 6.2). The MAD value is the median absolute deviation of each independent probe to the final median ratio or in other words indicates whether all probes agree on the found ratio, providing a control for the normalization method applied. If each reference probe creates the same result, the MAD value is zero (green) or close to zero (orange, showing some aberrations); when the MAD value is high (red) a different normalization method should be applied. Thus, as all the samples showed either green or orange MAD values, the obtained ratios were used for data interpretation.

Overall, CN changes in the 1q32.2-44 region associated exclusively with the ALT+ (JFCF6T.IJ/11E, IIICF/a2, SUSM1, U2OS, WI38VA13/2RA and WV) or to non-ALT (JFCF6T.IJ/11C, HT1080 and IIICF-precrisis) cell-lines were not found. Indeed, none of the CN changes detected can be associated with a single TMM. Most of the CN alterations identified are on the edge of the defined limits (0.7 - 1.3) and the addition of more replicates may shift the final result to a normal ratio. Thus, the CN changes falling between 0.6 and 1.4 were not considered for this analysis, as further replicates should be performed to determine whether these changes are biologically significant. Nonetheless, some observed CN changes were detected with more than one probe, suggesting that at least some of the identified alterations are likely to be real.

The Tel+ JFCF6T.IJ/11C cell-line shows a significant amplification on both probes of the *MCP* gene (a cofactor for the complement factor I), a potentially real CN

alteration as both ratios are very similar (1.79 and 1.77) and higher than the 1.3 established limit. In this cell-line, high ratios were also obtained towards the end of chromosome 1, although the very last probe has a normal ratio suggesting that, if real, the detected amplification does not extend towards the very end of the chromosome. Deletions were also observed on *EGFR* (chr. 7) and *NF1* (chr. 17) genes. Interestingly, *EGFR*, an epidermal growth factor receptor, was one of the genes whose expression was significantly altered on the 2nd microarray experiment (see chapter 4, section 4.3.1.3). In fact, *EGFR* expression was shown to be significantly lower in JFCFC6T.IJ/11C than in the 11E cell-line (p-value 0.0037), which might be a result of the detected deletion.

The ALT+ JFCFC6T.IJ/11E cell-line shows an amplification of the *ZNF669* zinc-finger gene locus.

Several borderline CN alterations were identified in the Tel+ HT1080 cell-line that should be further confirmed by more MLPA reactions, since only two replicas passed all the control tests for this cell-line and were included in the analysis. However, a major deletion was detected in the *MTAP* gene on chr. 9, which encodes an enzyme involved in the polyamine metabolism. *MTAP* gene is often co-deleted with the tumour suppressor p16 gene in many cancers (Carrera et al 1984). Interestingly, it had already been reported that there is no expression of the *MTAP* gene (both by RNA and protein levels measurements) in the HT1080 cell-line had (Tang et al. 2000), which strongly supports the MLPA results obtained. Thus, this study shows that a genomic deletion might be the underlying reason for the previously described lack of *MTAP* expression in HT1080 cells. Finally a deletion was also observed in calpain 3 gene - *CAPN3* (chr. 15), a major intracellular protease.

A large deletion was detected towards the end of chromosome 1 in the ALT+ IICF/a2 cell-line. Although the ratios obtained are similar to the defined lower limit,

three consecutive probes across *RYR2* (ryanodine receptor) and *FH* (fumarate hydratase) genes and also on the last probe of the same chromosome arm suggest that the identified deletions might be biologically relevant. Also, several control probes show CN changes, which might be an indication that the genome had already undergone high level of instability.

The ALT+ WI38VA13/2RA cell-line was the cell-line analysed with most CN changes detected. Some alterations are on the defined limits, thus further confirmation is required. However, other significant CN alterations were observed. Similarly to the JFCFC6T.IJ/11C cells, the three probed loci on *MCP* gene seem to be amplified. Furthermore, like IICF/a2 cells, also the *RYR2* probes show a deletion. Finally, a major amplification of the zinc finger *ZNF669* gene was also detected, similar to the JFCFC6T.IJ/11E cells.

All the changes detected on the remaining ALT+ SUSM-1 and IICF-precrisis need to be confirmed, since the ratios are very similar to the defined limits. The ALT+ U2OS and WV cell-lines show no CNV in any of the test or control probes.

Despite the copy-number changes detected on individual cell-lines and considering all the changes that need further confirmation, no alterations were commonly detected in ALT+ cell-lines indicating that, in contrast to the 1q32.2-44 deletion previously detected in ALT+ liposarcomas (Johnson et al, 2006), no major copy-number changes occur in the ALT+ cell-lines analysed.

length	gene	mapview	next probe	chr. pos.	LPO	probe
436	PARK7	01-007.953553	14956.3 Kb	01p36.23	CCTGCACAGATGGCGGCTATC	AGGCCCTTCCGGTTTTCTGCTCCTTCAGTATCTCCT
124	EPHB2	01-022.909899	74521.3 Kb	01p36.12	TGCCCGGGCTGGATGGCTATTCT	GCTGGCTGCGCGGTGGCGGCGGCTGTGT
445	DPYD	01-097.431241	10061.1 Kb	01p21.3	CGAAGAACTACAAGACTGGGATGGACAG	AGTCCAGTACTGTGAGTACCAGAAAAGGAAACCAG
256	NTNG1	01-107.492319	36737.1 Kb	01p13.3	CTTGTGAGCTGTGAACATTGAGGATCACT	CAGGGTTATCGGATGTACAACGGGAGAGCCATCGCTTTGCT
454	PEX11B	01-144.229421	5409.3 Kb	01q21.1	CCACAAGTTTCTACGCCTGGGTAACCTCA	GCAGATGCCCTTGAGTCAGCCAAAAGAGCTGTTCACCTAT
328	PSMB4	01-149.638755	3892.1 Kb	01q21.3	CATTCGGTCCACTCCCGATTCTTCATGGA	TCCGGCGTCTGCACTTTACAGAGGTCCAATCACGCGGACC
364	PKLR	01-153.530889	844.6 Kb	01q22	CGGCATCAAGATCATCAGCAA	AATTGAGAACCACGAAGGCGTGAAGAGGTGAGGC
220	LMNA	01-154.375455	5171.0 Kb	01q21.2	CCTGTGCTCACACTCTCTCTCTGTGTTTT	CTCTCTTAGAGCCCCAGAACTGCAGCATGTAATCTG
226	MPZ	01-159.546436	3.9 Kb	01q23.1	CACCACCTCTCAACTGCACATGCCA	GGCTGCAATTGGTTACTGGCTGAGGACAGC
136	SDHC	01-159.550359	10324.0 Kb	01q23.3	TAAAAACGTGGTGGTTGGCCGGTTGA	GACCCCGAAGAGAAAAGATACTTTGGGTTCCCTCCCTTTCTAATACG
148	MYOC	01-169.874380	2271.0 Kb	01q24.3	TGAAGTCCGAGTAACCTGAAGTTCCTGCT	TCCCGAATTTTGAAGGAGAGCCCATCTGGCTATCTCAG
172	SERPINC1	01-172.145336	6362.3 Kb	01q25.1	TCCGCAATTGAGGACGGCTTCAGTT	TGAAGGAGCAGCTGCAAGACATGGGCTTGTGCTGATCTGTT
196	LHX4	01-178.507596	2304.4 Kb	01q25.2	GTTGGTTTTGAGAAGCAAGGGCCAAA	GAGAAACGCCTGAAGAAGGATGCAGAGGCGCCACCGCT
292	RNASEL	01-180.812018	14099.7 Kb	01q25.2	CCAGAACACTGTGGGTGATCTGCTAAAGT	TCATCCGGAATTTGGGAGAACACATTGATGAAGAAAAGCAT
415	CFH	01-194.911745	4686.0 Kb	01q31.3	CCAATTGCTAGGTGAGATTAATTACCGTGA	ATGTGACACAGATGGATGGACCAATGATATTCTATATGTGAAGGTAGA
283	TNNT2	01-199.597714	3128.2 Kb	01q32.1	CAGACAGAGCGGAAAAGTGGGAA	GAGGCAGACTGAGCGGAAAAGAAGAAGAAGATTCTGG
274	PIK3C2B	01-202.725927	3270.2 Kb	01q32.1	CCTGTGGCTGAAGGAAGCCTTAGCAAT	TCATCCTTCTCTCTGAGAAGTCTGTAGGAAGTCTCAC
208	MCP	01-205.996152	1.4 Kb	01q32.2	GAGCAAAGGCACCAAGATGTGACACTA	CTGGACTGCCAAGCTATTGAGTGTGGCAGAGTAGGGC
409	MCP	01-205.997555	4343.1 Kb	01q32.2	CCTGCAATGGGACTTACGAGTTT	GGTTATCAGATGCACTTTATTGTAATGAGGGTAAGTTGCTCCTTAGA
238	RAMP	01-210.340676	2520.0 Kb	01q32.3	GACTGAGCTTGATGGCCAAAGTTGAAAATCT	TCATTTGGATCTGTGCTGCTTGTGTTGTAAC
185	CENPF	01-212.860661	3726.1 Kb	01q32.3	CGACATTGCCCGGCATCAGGCTTCATCATCTGTGT	TCTCATGGCAGCAAGAGAAGACCCCAAGTCATCTTTTCATC
373	TGFB2	01-216.586720	5471.9 Kb	01q41	CTCAGCTGCTTACCTGACGAC	ACTCGATTTGGACCAAGTTCATGGCCAAAGGGA
166	TP53BP2	01-222.058573	2462.0 Kb	01q41	CAACAAGATCAGCGACAACAGCAACAAGTT	GCTGAGCAGGAGAAACTTAAAAGGCTAAAAGAAATAGCTGAGAATC
319	LIN9	01-224.520551	1882.1 Kb	01q42	CCTTTGGACAAAAACAGCGCCTTCTCGAT	TTTTTATGACCCACCACGGTTACATTACTCCTCCTCT
346	GUK1	01-226.402695	9158.1 Kb	01q42	CAAGGAGCCCCGGCTGTTTGTATGT	GGTCATCATTAACGACAGCCTGGACCAGGCC
MS32 minisatellite						
301	RYR2	01-235.560809	467.2 Kb	01q43	CCAGACCTCTCCATCTGCACCTT	TGTGCTGGAGCAGTCCCTCTCTGTCCGGG
355	RYR2	01-236.028010	34.9 Kb	01q43	CTTGCCATGGACAAGGCAGCTCT	GGACTTCAGTGATGCCAGAGAAAAGAAGAAGC
472	RYR2	01-236.062872	3684.2 Kb	01q43	GAGTCTTCTCGAGCTACGAGACCT	TCACAGAGACACGTGGCAGCCACACTCACCCAGC
247	FH	01-239.747094	2128.8 Kb	01q43	CAGACCTGAGACTACGATGAACCTT	AAGATTGGAGGTGTGACAGAACGCATGCCAGTAAGTGGA
382	AKT3	01-241.875896	778.0 Kb	01q44	TCATTTCTCTCTTCTTGCCCTGTCAG	TCTGTCTGCTACAGCCTGGATAGCTTCTGTCCATTCTTC
481	ADSS	01-242.653849	2678.0 Kb	01q44	CAGGATGTGCGACCTTGTCTGACTTTGA	TGGCTTCTCTGAGAGGTAACCTAAGTGTGTTCAAAATGGAAGG
160	ZNF669	01-245.331833	1776.1 Kb	01q44	GGTAAGAAATGACAACACATTTCAAGTAAATTACAGAA	GTCTTTCCCTATCATCAGTGTATTTATGATTTGGAATGTGGCA
130	ZNF672	01-247.107886		01q44	GGTGAACCTGGCCACAGCTCACC	CTGGAACAGCCACAATGTCTGCCCTTAGAGAAGAACC
154	DYSF	02-071.683404		02p13.3	TGTGGGCCAGGTGCAGGAGACA	TCAAGGATCCTGGATGAGGTGAGCTGGGCGTGGTGGTTG
463	GLRA1	05-151.284440		05q33.1	CGCCGCTGTCCGTGGTATCT	ACGACCCCTCGCTCCAATTTCCCTGGGGCTCTC
427	CDKN1A	06-036.761516		06p21.2	TCCAAAACGCCGGCTGATCTTC	TCCAAGAGGAAGCCCTAATCCGCCACAGGA
265	EGFR	07-055.233957		07p11.2	CTGCCAGCGAGATCTCCTCCA	TCCTGGAGAAAGGAGAACGCCTCCCTCAGCCACC
310	MTAP	09-021.844763		09p21	GCATGACCACAGTTCAGAGGTGTTCTT	GCTAAGGAGGCTGGAATTTGTTACGCAAGTATCGCCATGGC
178	ATM	11-107.620734		11q23	GAGCTTTCAGGTCTAAATCATATCTTAGCAG	CTCTTACTATCTTCTCAAGACTTTGGCTGTCAACTTTTCA
391	CAPN3	15-040.481564		15q15.1	CCTCATCTCATTACATCTGAAGCATCT	TCCTTTCTGTTTCTCTCAAGGTTCCCAAAGAGGTATAGCAGCA
335	NF1	17-026.578679		17q11.2	GCACATGCAAAAATGGGAACAAGCAACAAAAG	CTAATCCTTAACTATCCAAAAGCCAAAATGGAAGATGGCCAGG

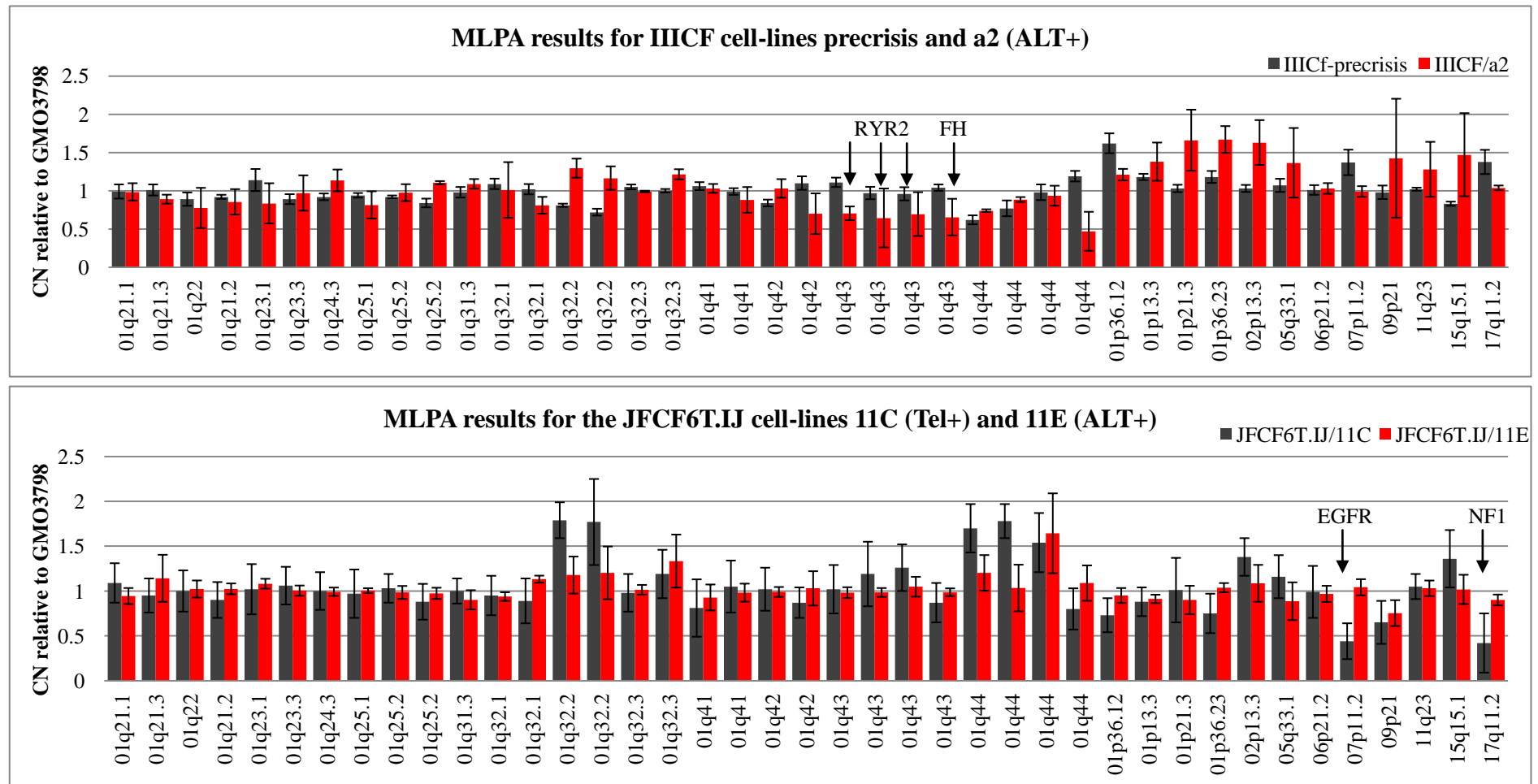
Table 6-1: MLPA kit X-104 probemix.

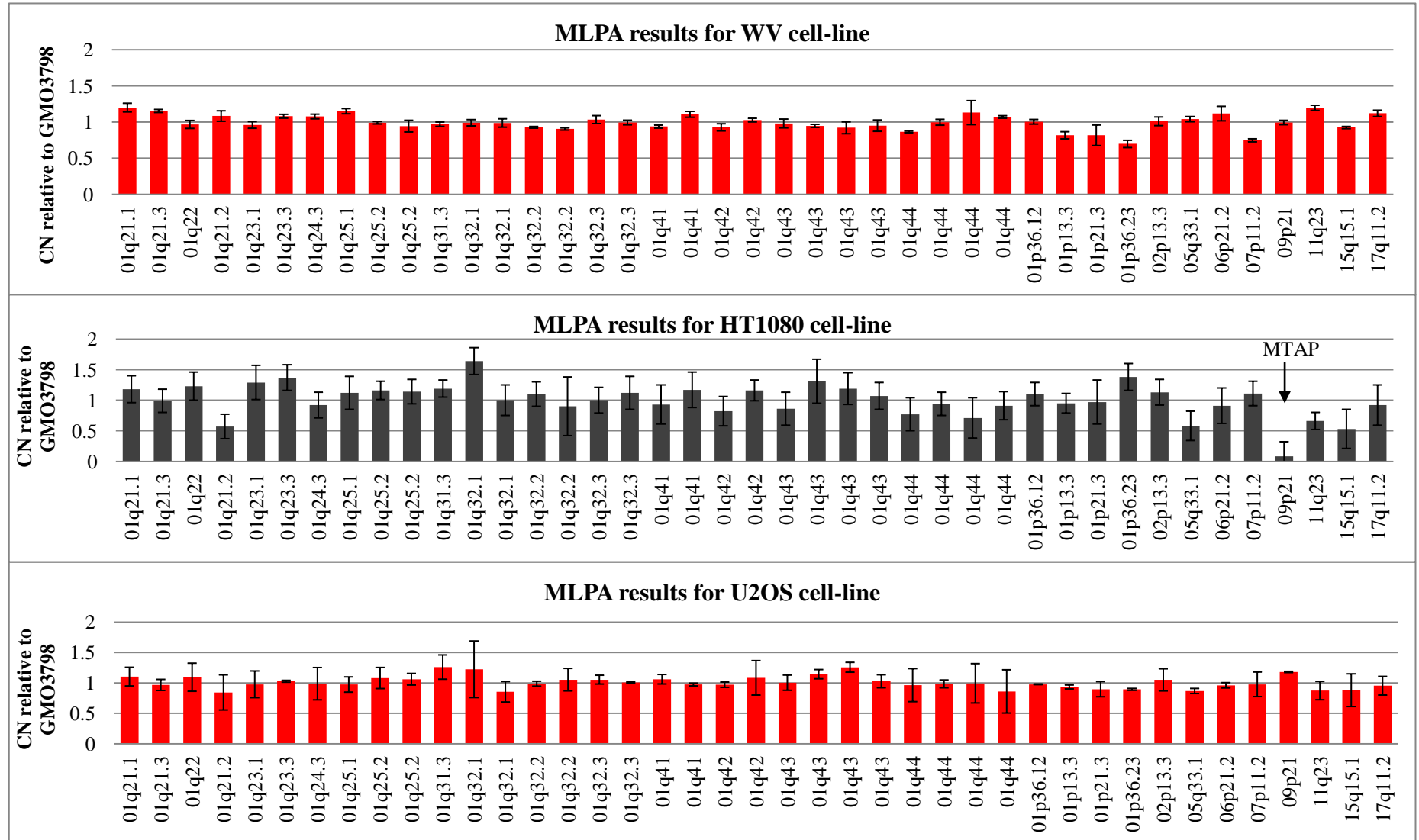
The table indicates the gene name, genomic position of each probe present in the MLPA kit used. Also, the probe sequence (two fragments that will be ligated after the ligation reaction), the distance to the next probe and the final PCR product sizes are shown. MS32 locates 1Mb before the RYR2 gene.

sample name	JFCF6T.IJ/ 11C	JFCF6T.IJ/ 11E	HT1080	IIICF/a2	IIICF- precrisis	SUSM1	U2OS	WI38VA13/ 2RA	WV	
Nr Test Probe	41	41	41	41	41	41	41	41	41	
Nr Control Probe	12	12	12	12	12	12	12	12	12	
Ligation	YES	YES	YES	YES	YES	YES	YES	YES	YES	
PPMC (pearson)	0.91;26	0.93;38	0.93;34	0.9; 4	0.93;31	0.95;31	0.94;30	0.8;25	0.95;33	
MAD all	0.23;40	0.08;40	0.48;40	0.23;40	0.12;40	0.12;40	0.08;40	0.2 ;40	0.09;40	
DNA concentration	OK	OK	OK	OK	OK	OK	OK	OK	OK	
DD OK? (88)	OK	OK	OK	OK	OK	OK	OK	OK	OK	
DD OK? (96)	OK	OK	OK	OK	OK	OK	OK	OK	OK	
Chr pos	Gene	Ratio	Ratio	Ratio	Ratio	Ratio	Ratio	Ratio	Ratio	
01q21.1	PEX11B	1.09	0.96	1.18	0.985	0.99	1.01	1.03	0.89	1.2
01q21.3	PSMB4	0.95	1.09	0.99	0.89	1.01	0.89	0.93	1.05	1.16
01q22	PKLR	1	0.96	1.23	0.775	0.89	1	0.96	0.9	0.94
01q21.2	LMNA	0.9	1.05	0.57	0.855	0.92	1.07	1	0.92	1.12
01q23.1	MPZ	1.02	1.08	1.29	0.835	1.14	1.15	0.85	0.88	0.97
01q23.3	SDHC	1.06	1.01	1.37	0.97	0.89	0.99	1.03	0.88	1.07
01q24.3	MYOC	1	1	0.92	1.135	0.92	1.04	1.14	0.9	1.09
01q25.1	SERPINC1	0.97	1	1.12	0.815	0.94	1.08	1.03	0.9	1.16
01q25.2	LHX4	1.03	1	1.16	0.975	0.92	1.06	0.99	0.77	1
01q25.2	RNASEL	0.88	0.97	1.14	1.105	0.84	1.09	1.01	1.03	0.99
01q31.3	CFH	1	0.9	1.19	1.09	0.98	0.98	1.15	1.02	0.97
01q32.1	TNNT2	0.95	0.94	1.64	1.01	1.09	1.1	0.96	1.21	1.01
01q32.1	PIK3C2B	0.89	1.14	1	0.81	1.02	0.9	0.94	1.34	1.02
01q32.2	MCP	1.79	1.06	1.1	1.295	0.81	0.94	1.01	1.74	0.92
01q32.2	MCP	1.77	1.05	0.9	1.165	0.72	1	1.15	1.47	0.9
01q32.3	RAMP	0.98	1.01	1	0.99	1.05	1	1.09	1.17	1.06
01q32.3	CENPF	1.19	1.2	1.12	1.215	1	0.93	1	1.48	0.98
01q41	TGFB2	0.81	0.98	0.93	1.03	1.06	1	1.1	1.19	0.93
01q41	TP53BP2	1.05	0.97	1.17	0.88	0.99	1.05	0.96	1.15	1.1
01q42	LIN9	1.02	1.01	0.82	1.03	0.84	0.96	0.99	1.35	0.95
01q42	GUK1	0.87	1	1.16	0.7	1.1	0.89	0.92	0.79	1.03
MS32 minisatellite										
01q43	RYR2	1.02	1	0.86	0.705	1.11	0.88	1.06	0.7	1.01
01q43	RYR2	1.19	0.98	1.31	0.645	0.97	1.08	1.11	0.69	0.94
01q43	RYR2	1.26	1.03	1.19	0.695	0.96	0.64	1.21	0.52	0.9
01q43	FH	0.87	0.99	1.07	0.655	1.04	1.03	0.97	0.71	0.99
01q44	AKT3	1.7	1.23	0.77	0.74	0.62	1.08	1.11	1.05	0.87
01q44	ADSS	1.78	0.99	0.94	0.885	0.77	0.56	1.01	0.77	0.99
01q44	ZNF669	1.54	1.6	0.71	0.935	0.98	0.69	1.18	1.83	1.06
01q44	ZNF672	0.8	1.18	0.91	0.47	1.19	0.75	1.05	0.72	1.06
01p36.12	EPHB2	0.73	0.95	1.1	1.21	1.62	1.1	0.98	0.6	0.99
01p13.3	NTNG1	0.88	0.91	0.95	1.38	1.18	1.16	0.92	1.43	0.84
01p21.3	DPYD	1.01	1	0.97	1.66	1.03	1.06	0.83	1.33	0.75
01p36.23	PARK7	0.75	1.05	1.38	1.67	1.18	0.71	0.89	0.79	0.69
02p13.3	DYSF	1.38	0.96	1.13	1.63	1.03	0.89	0.95	1	1.01
05q33.1	GLRA1	1.16	0.83	0.58	1.365	1.07	1.02	0.88	1.12	1.03
06p21.2	CDKN1A	0.99	0.98	0.91	1.03	1.01	0.92	0.94	0.73	1.08
07p11.2	EGFR	0.44	1.03	1.11	0.99	1.37	1.01	0.86	0.79	0.74
09p21	MTAP	0.65	0.68	0.08	1.425	0.98	1.33	1.18	1.12	1
11q23	ATM	1.05	1.01	0.66	1.28	1.02	0.66	0.95	1.38	1.2
15q15.1	CAPN3	1.36	0.95	0.53	1.47	0.83	1	1.03	1.06	0.92
17q11.2	NF1	0.42	0.92	0.995	1.0375	1.376	0.97	0.87	0.82	1.12

Table 6-2: MLPA summary of results.

The average of the ratios obtained from a minimum of two independent MLPA results per cell-line are shown in the table. The chromosome position and the target gene of each probe are shown and data is organized from test probes on 1q to the control probes on other chromosomes, according to their chromosomal position. The first rows show the number of test and control probes considered for each sample; the detection of the internal probes for ligation (92 bp), hybridization, denaturation (DD fragments 88, 96 bp) and if there was enough DNA; the Pearson and MAD values. The ratios following within the set change limit (0.7-1.3) are represented in blue, whilst gains (>1.3) are represented in green and deletion (<0.7) are shown in red.





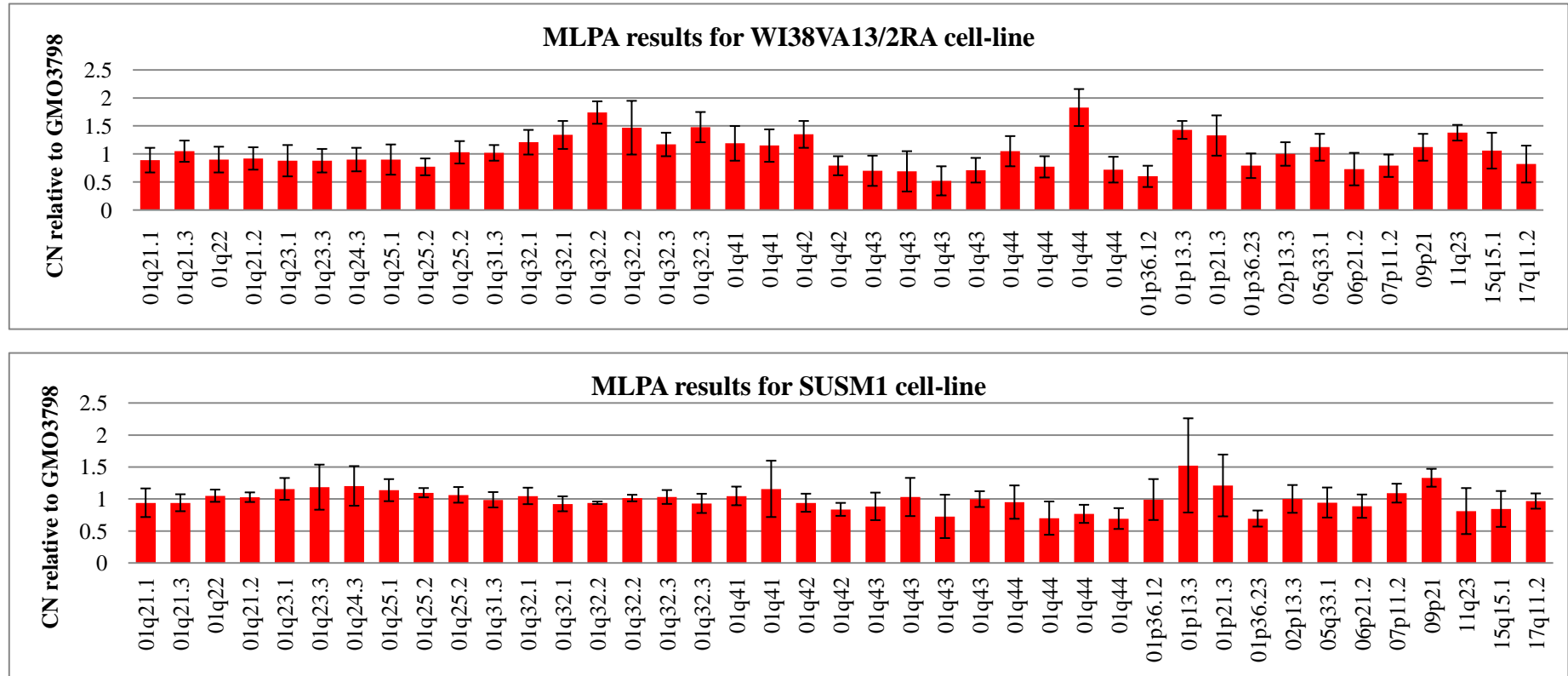


Figure 6.3: MLPA results per cell-line.

The obtained copy-number ratios using GMO3798 as reference were plotted according to their chromosomal position, from the test 1q region to the control regions. Error bars represent standard deviations from a minimum of two independent MLPA experiments for each cell-line tested. Cell-lines with a common progenitor were plotted together (IICF-precrisis vs. IICF/a2 and JFCF6T.IJ/11C vs. JFCF6T.IJ/11E). The ALT+ cell-lines IICF/a2, JFCF6T.IJ/11E, U2OS, WV, WI38VA13/2RA and SUSM1 are represented in red, whilst the IICF-precrisis and the Tel+ JFCF6T.IJ/11C and HT1080 are represented in black.

6.3.1.2 ALU ANALYSIS

Even though the MLPA copy-number analysis performed did not detect copy-number changes in the 1q region between ALT+ and non-ALT cells, another experiment was designed and optimized to validate the results obtained. Also, a better CN determination is achieved by combination of different techniques, since all available methodologies have their limitations.

Human chromosomes contain about 1,000,000 *Alu* copies, which approximately constitutes 11% of the total genome. Most *Alu* insertions have been "fixed" (both of the paired chromosomes have an insertion at the same locus) in the human genome for a long time. The accumulation of mutations within *Alu* elements at different evolutionary time points facilitates their classification into nine subfamilies, each subfamily thought to have arisen from a distinct founder sequence (Britten et al. 1988; Jurka et al 1988). The youngest *Alu* element is thought to be AluY (Batzer et al. 1996). AluSx is thought to be 37 million years old, whilst AluJ (divided into AluJ0 and AluJb) is estimated to be 81 million years (Kapitonov et al. 1996). Due to their sequence similarity, *Alu* elements from the same subfamily constitute genomic loci of highly identical sequences and dispersed throughout the genome, providing a perfect tool for comparison of copy-number in different chromosome regions. An experiment was then designed and developed to relatively quantify the copy-number on 1q in ALT+ vs. non-ALT cells, based on the quantification of *Alu*-elements. Briefly, individual *Alus* dispersed across the MS32 region (test *Alus*) and in other loci (control *Alus*) would be PCR amplified with primers optimized for each specific *Alu*-locus. The amplification would be stopped while still in exponential phase, so that the final PCR products would directly depend on the number of initial copy-number present in each DNA template. The *Alu*-quantification would be achieved by dot-blotting the obtained PCR products and

subsequent hybridization to a radioactive-labelled probe, composed of a sequence common to all amplified *Alus*. The CN of the MS32 minisatellite region could be relatively quantified by comparing the radiation intensities obtained for the sample cell-lines with a reference diploid genome, like GMO3798.

The DNA sequences that flank MS32 minisatellite are rich in *Alu* elements, mainly from the *AluSx* subfamily (Fig. 6.4). This *Alu* subfamily, however, is frequently associated with microsatellites and other tandem repeats (Yandava et al, 1997), like the STR analysed in chapter 3 (see chapter 3, section 3.3.1.2). Thus, the design of specific primers for these *Alus* would be extremely challenging and the neighbour *AluY* subfamily was chosen as the target *Alus* for this experiment.

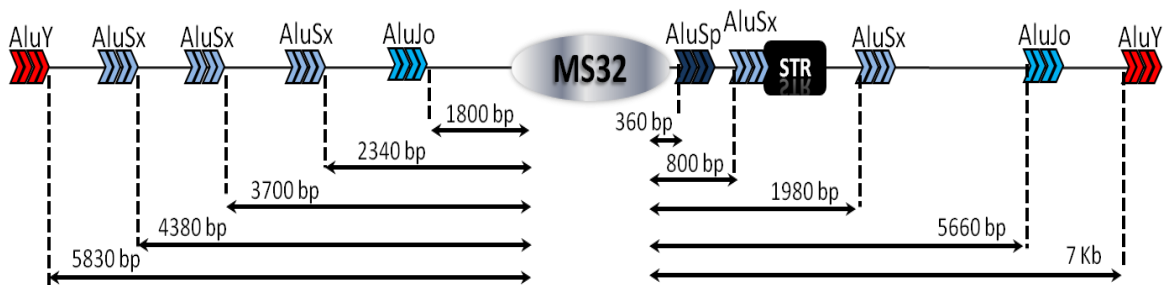


Figure 6.4: *Alu* distribution around MS32 minisatellite.

The diagram represents distances and subfamilies of the *Alus* present in the flanking region of the MS32 minisatellite. The MS32's downstream STR flanked by an *AluSx* element is also shown.

The sequence of the *AluY* element 6 kb downstream MS32 minisatellite was used for a Blastn search (<http://blast.ncbi.nlm.nih.gov>) to identify the most similar *AluY* repeats in the genome (Table 6.3). Five *AluY* were identified in 1q that could be potential targets for determination of the copy-number around MS32 minisatellite. The remaining eleven *AluY* provide control loci dispersed throughout different chromosomes, two of which were on chromosome 1 (6 and 7 on table 6.3)

Alu	Similarity	Chr.	Strand	Start	End	Span
1	92.4%	1	+	239532196	239532461	266
2	100.0%	1	+	234334165	234334432	268
3	94.3%	1	-	202934074	202934296	223
4	93.5%	1	+	193115855	193116116	262
5	93.0%	1	-	153586334	153586591	258
6	93.5%	1	+	58966365	58966637	273
7	92.4%	1	-	9615535	9615800	266
8	95.0%	2	+	144967913	144968187	275
9	94.6%	3	-	137339093	137339367	275
10	95.0%	7	+	97959295	97959569	275
11	95.0%	11	+	44723877	44724151	275
12	94.3%	12	+	52214052	52214326	275
13	95.7%	13	+	85229619	85229887	269
14	94.3%	18	+	1790503	1790777	275
15	96.0%	19	+	19636678	19636943	266
16	93.3%	X	+	87639842	87640122	281

Table 6-3: AluY elements with highest sequence identity to the one near MS32.

The sequence of the AluY 6 kb distal to MS32 (highlighted on row 2 of the table) was blasted against the human genome and 15 other AluY were identified. For each, the similarity, chromosome location (start and end), strand and the query region span are listed on the table above.

A thorough design and optimization of the PCR conditions for each reaction was performed to guarantee the specificity of the reactions to a unique *Alu* locus. Each primer was blasted (www.ncbi.com) against the human genome to identify all potential annealing sites within the genome and only the primers with at least the last three bases on the 3'-end unique to the target *Alu* were selected. Furthermore, the specificity of each selected set of primers was further confirmed by *in-silico* PCR (<http://genome.ucsc.edu/>) (Table 6.4). To determine potential copy-number changes around MS32 minisatellite, eight *Alus* were selected: four test AluY around MS32 (A1-A4) and four controls (A5, A6 on chr. 1, A8 on chr. 2 and A16 on chr. X) (Fig. 6.5).

Even though the primer-sets were carefully designed, the conditions for the PCR reaction were assessed to determine whether they were specific for the intended locus. The main factor ensuring the specificity of a PCR reaction is the temperature to which the primers selectively bind to the target. If too low, misaligns may occur especially at the 3'-end. Therefore, despite the exclusivity of the 3'-end to the target *Alu* being one of the criteria used for primer selection, different annealing temperatures were tested for each primer-set to determine the optimum temperature for obtaining a single-band product. Finally, the single amplicons generated were directly sequenced, with both forward and reverse primers, to confirm that they arise from the specific targeted *Alu* locus and no other products were present with the conditions used. When the resulting sequences had some concerning background, the annealing temperatures were raised to increase the specificity, until a clean product was obtained. All the products were successfully sequenced from the forward primer, confirming the specificity of each reaction to the targeted *Alu*. The reverse sequencing reactions only worked for A1, A2 and A16 since the other *Alus* have a poly-A either at the 3' end (A3, A5, A6 and A8) or in the middle of the sequence (A4), which caused the reverse-reaction to either not work at all or stall, respectively.

	Chr.	Primer Forward (5'- 3')	Primer Reverse (5'- 3')	Final Ta	Length
A1	1	ctagcacattgcaggaacag 1 match 20/20 1 match 13/13 (no 3')	caagtgctccctatctgag 1 match 20/20 1 match 13/13	63 °C	430 bp
A2	1	caggacaggaagaagactc 1 match 19/19 1 match 15/15	tctagagacaaggcctcgc 1 match 19/19 1 match 12/12 (no 3')	63 °C	398 bp
A3	1	agagtgcagcctctcctg 1 match 19/19 1 match 16/16(chr.4 no 3')	tgtgcattaccatctaggc 1 match 19/19 1 match 16/16 (chr.8 no 3')	65 °C	412 bp
A4	1	attaatagtatataacggaat 1 match 22/22 1 match 16/16(chr.7 no 3')	atagcatagattgtctgg 1 match 19/19 1 match 15/15 (chr.7 no 3')	52 °C	668 bp
A5	1	attgtgctaccttcaagcag 1 match 21/21 1 match 16/16(chr.8,no 3')	taccaccagccaagctac 1 match 19/19 1 match 15/15 (no 3')	57 °C	593 bp
A6	1	tgagcattagactccaggaag 1 match 21/21 1 match 17/17(chr6, no 3')	tgtgcatcgtagttagg 1 match 21/21 1 match 14/14(chr 6, no 3')	61 °C	415 bp
A7	1	taagccaaagtaccagcac	taccttagcaacctgattc		
A8	2	acctcttatggctgctg 1 match 19/19 1 match 14/14	gcattgtgaaatattcctgt 1 match 18/18 1 match 14/14	61 °C	335 bp
A9	3	atgtagatctctgacagag 1 match 19/19 1 match 15/15	agtgcagtagcggatctc many perfect match	n/a	----
A10	7	tagaactccagctccag 1 match 19/19 2 match 14/14	ctagtggtgcttcgacctg 1 match 18/18 1 match 12/12	n/a	----
A11	11	tcattgagcagtaacttc 1 match 19/19 1 match 17/18(no match 3')	caactgattagaatcagc 1 match 18/18 1 match 16/16	n/a	----
A12	12	ctgtaatgaacttctaag 1 match 19/19 1 match 12/12	aacagaatcttcttacc 1 match 18/18 1 match 12/12	n/a	----
A13	13	agagtgtactaagcc 1 match 17/17 1 match 14/14	tcttcggagattaagaac 1 match 19/19 1 match 12/12	n/a	----
A14	18	tccttagactaaccaatg 1 match 19/19 1 match 13/13	agactaattcttgatgc 1 match 18/18 1 match 14/14	n/a	----
A15	19	attatatactttaggccg 1 match 19/19 1 match 13/13	acagttaataatagaac 1 match 19/19 1 match 13/13	n/a	----
A16	X	ttcagtcagaagaactggag 1 match 21/21 1 match 17/17 (no 3')	ttcatgtgatccagttctag 1 match 21/21 1 match 16/16	59 °C	417 bp

Table 6-4: Specificity of the primers designed for the *Alu* copy-number study.

The sequence and the matches found with the Blast search for each primer are shown, as well as the similarity between the match and the primer. The optimized annealing temperature (Ta) and the final product length (Length) of the selected 8 *Alus* are also shown.

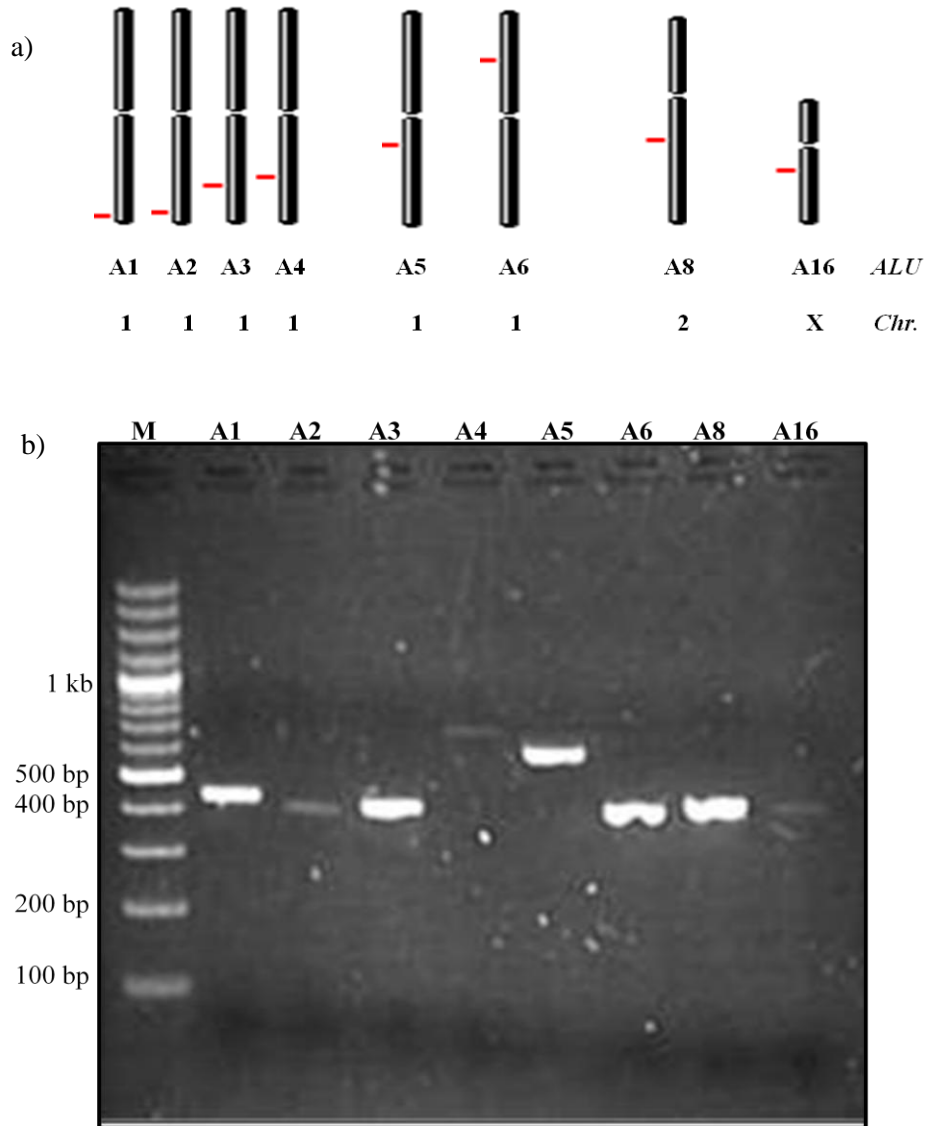


Figure 6.5: Selected AluY for copy-number analysis around MS32 minisatellite.

a) Chromosomal location of the eight selected AluY elements for the copy-number analysis. b) Agarose gel electrophoresis (1% agarose) resolution of PCR products from the selected *Alus* amplified from the GMO3798 cell-line.

The comparison between PCR-products derived from different loci *per se* does not inform about the initial copy-number of a locus. Thus, one essential factor for the success of the experiment was to ensure that the eight analysed *Alus* derive from PCR reactions in the exponential-phase, so that the number of PCR molecules generated is proportional to the copy-number of that specific *Alu* locus in the DNA sample. To

screen for positive reactions, each PCR reaction was set in quintuplicate: four amplified for 27 cycles (a visible band starts appearing between the 32-34 cycles, depending on the *Alu*) for further analysis and the other amplified for 37 cycles to ensure that the reaction had worked.

Prior to the final comparison of the copy-number, another essential factor that had to be considered was the initial DNA input in each reaction. In addition to the quantification of the DNA in the sample aliquots to be analysed by spectrometry and agarose gel electrophoresis, control experiments are crucial for a better comparison of the copy-number. Ideally, several amplifications for each *Alu* from a diploid genome (GMO3798 cell-line) should be blotted into a nylon membrane (0.5, 1, 1.5, 2 and 3 reactions per dot) to determine if copy-number differences can be detected with the methodology used. Then, to detect potential copy-number changes, each ALT+ cell-line would be compared to the diploid genome. Finally, as internal controls to account for potential variations on the DNA quantification for each sample, each *Alu* could be compared to the other *Alus* (region of interest and control regions) within each cell-line (Fig. 6.6).

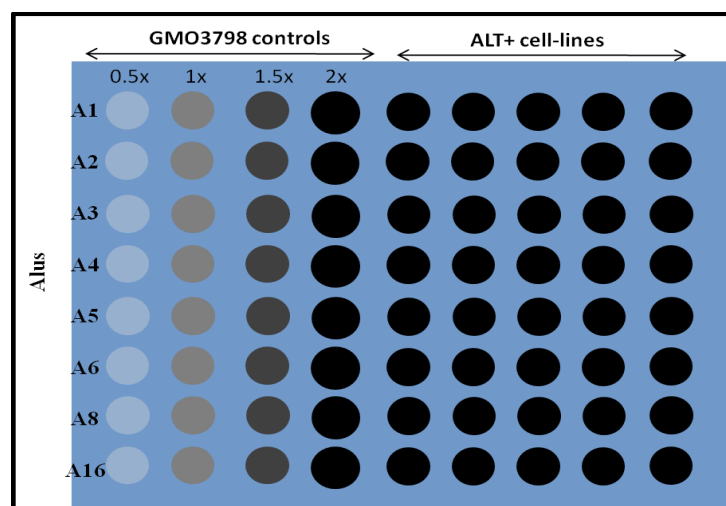


Figure 6.6: Representation of a dot-blot for the *Alu* copy-number analysis. A schematic dot-blot representing the minimum necessary input controls (GMO3798) and the test ALT+ cell-lines. Each dot represents pools of PCR reactions for each *Alu* per cell-line.

However, to test the blotting and hybridization conditions, a preliminary experiment was performed without the control reactions. After optimization of the PCR reaction for each of the eight chosen *Alus* and to test the blotting and hybridization conditions, five PCR reactions were performed per *Alu* on the control diploid cell-line GM03798 and four ALT+ cell-lines (U2OS, SuSM-1, JFCF6T.11E and IICF/a2). The products generated were dot-blotted onto a nylon-membrane, with the reactions amplified 37 cycles as positive controls and the four remaining reactions per *Alu* pooled together and blotted on the same dot. The dot-blot was then hybridized in Church buffer (48 °C, for 4 hours) to a probe common to all amplified *Alus* (ctaaaaatacaaaaaatt), so that no different hybridization efficiencies could interfere with the determination of the initial copy-number of the different loci.

The preliminary results obtained show that both blotting and hybridization conditions tested worked (Fig. 6.7). More PCR reactions should be pooled for each dot, as the signals obtained for four pooled reactions are very weak (Fig. 6.7 - 27 cycles). Also, to determine if the methodology applied has the potential to be CN informative, the intensity of each dot was measured using the IMAGEQuant TL software (GE Healthcare Life Sciences). To normalize the data for each *Alu*, the intensity of each test-dot (27 cycles) was divided by the sum of the intensities of all test-dots per cell-line and plotted by cell-line. The normalized data was then normalized to the diploid control cell-line GM03798, to obtain a relative *Alu* copy-number for the ALT+ cell-lines (Fig. 6.8). From the analysis of the preliminary data, it seems that the methodology applied may indeed inform about copy-number changes through specific *Alu*-amplification and detection. However, template input and loading controls should be included to determine better the copy-number of different loci. This requirement is clearly evident by the preliminary data obtained for A16, a chromosome X *Alu*. U2OS and IICf-

postcrisis cell-lines derive from females, whilst GMO3798 derives from a male (no sex information is available for SUSM1 and JFCF.6T/11E cell-lines). Thus, if the same DNA input had been used for all the reactions, the female cell-lines should have double the A16 copy-number relative to the GMO3798. However, the data obtained from the preliminary dot-blot performed suggests that IIIcF/a2 only has half of the GMO3798 copies of A16 and U2OS has identical number, indicating that further controls are extremely important to avoid any DNA input variation. Thus, input controls are extremely required for proper copy-number determination applying this methodology.

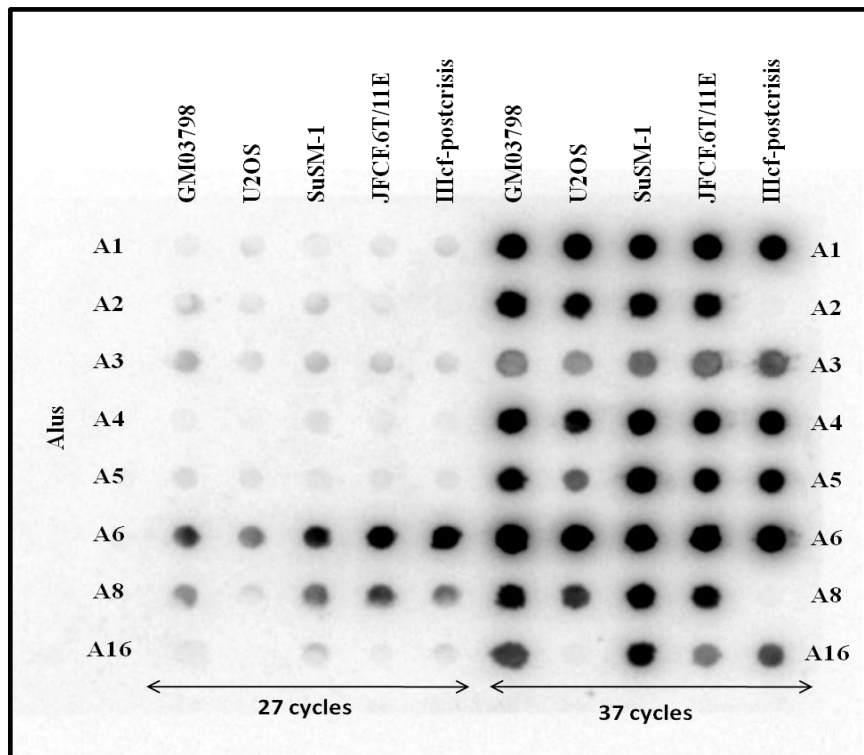


Figure 6.7: Dot-blot for *Alu* copy-number analysis.

The products from four PCR reactions for each Alu per cell-line were pooled into the same dot (27 cycles). The positive control reactions were also dotted to determine if the hybridization conditions were optimum (37 cycles). The GMO3798 (lymphoblastoid) cell-line was used as reference for the ALT+ U2OS, SUSM-1, JFCF6T.IJ/11E and IIIcF/a2 cell-lines.

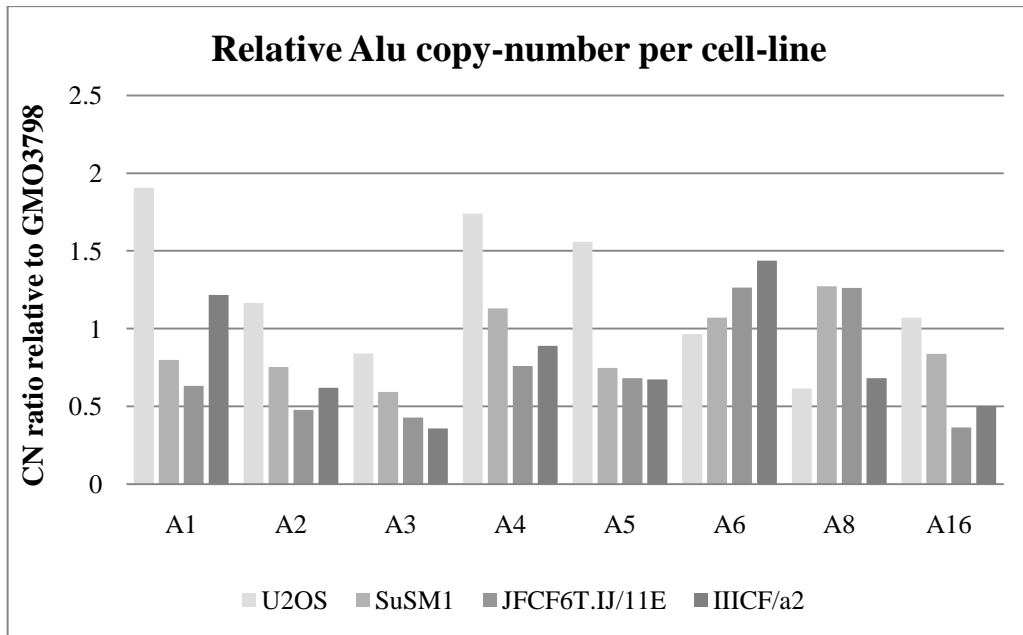


FIGURE 6.8: Alu dot-blotting analysis.

The radiation-intensity obtained on each dot was measured and normalized to the total sum of intensities obtained per cell-line. The normalized intensities of each ALT+ cell-line tested were divided by the GMO3798 reference and the obtained ratio plotted per *Alu* element.

6.3.2 METHYLATION AROUND MS32

Recently, it has emerged that there are differential epigenetic-patterns between cancer and normal somatic cells. Indeed, most tumours show hypermethylation of tumour suppressor genes' promoters and consequent repression of genes that are usually not methylated and thus expressed in normal somatic cells (Jones, 1986; Jones, P. et al 1999; Momparler et al. 2000). Paradoxically, the observed hypermethylation on CpG islands contrasts with the genome-wide hypomethylation of tumour cells. The observed tumour-associated general genomic hypomethylation is thought to result from the particularly high hypomethylation at repeated sequences, since these regions account for 55% of the human genome (Rodriguez, J. et al. 2006). Therefore, the genomic hypomethylation, characterized by a net decrease in the genomic 5-methylcytosine content, of repeated sequences may result in chromosome instability and provide a selective advantage through activation of genes that are usually silenced (Chen et al. 1998; Sutter et al. 2003; Ehrlich et al. 2006). Additionally, as the hypomethylation has been observed in different types of repeats, such as long interspersed nuclear element 1 (LINE-1), *Alus* and alpha satellite (SAT-a) sequences, it has been suggested that a genome-wide hypomethylation mechanism might occur in tumour cells, rather than an individual hypomethylation of repetitive sequences and subsequent selection of the hypomethylated-states by the tumour cells (Bollati et al 2009).

One of the best characterized markers for heterochromatin is the methylation of cytosines in CpG dinucleotides, which can be investigated by bisulfite sequencing (Frommer et al, 1992). Sodium bisulfite preferentially deaminates cytosines to uracils when compared to a very slow deamination of 5-methylcytosine to thymine, in single-stranded DNA (Shapiro et al 1973). Thus, fully denatured genomic DNA treated with the chemical under certain conditions allows the exclusive conversion of cytosines to

uracils, leaving the 5-methylcytosines unconverted. The resulting modified DNA can be used as template for PCR reactions where only the 5-methylcytosines will be amplified as cytosines, whereas both the cytosines converted to uracils and the original thymines will be amplified as thymines. Thus, sequencing of these PCR products can inform about the original methylation status of each strand since after the bisulfite treatment the DNA strands are no longer complimentary.

The analysis of the methylation status in the MS32 minisatellite region might therefore reveal potential changes that might underlie the MS32 instability in ALT+ cells. As a direct analysis of the methylation status of the MS32 repeat array by bisulfite sequencing is technically challenging, an experiment to determine the methylation-status in the regions flanking the minisatellite was performed first.

Before the bisulfite treatment and subsequent sequencing, the genomic DNA of the cell-lines to be tested was screened to determine the genotype of the cell-lines to be analysed. Thus, a PCR product of 3.5 kb upstream the minisatellite was obtained with the 32-3.5F and 32PR primers for each cell-line and subsequently sequenced with 32-1.6F and 32-0.9F primers, whilst a 1.2 kb downstream product was obtained with 32ER2 and 32+1.4F primers and sequenced with the former. The sequence revealed that the cell-lines MRC-5 (normal) heterozygous and the SUSM-1 (ALT+) homozygous at the H2C/T SNP (Table 6.5). Thus, in MRC5 cells, depending which base is present in the samples analysed, a CpG dinucleotide may or may not be present, which may exclude this particular site from the methylation analysis. The SUSM-1 cell-line is not informative at this site. No SNPs were identified in the 300 bp downstream region to be analysed.

The genomic DNA of the top strand was converted so that the CpG dinucleotides were highlighted and all the cytosines (C) were transformed into thymines (T). The

bisulfite-primers for the upstream region flanking MS32 had been designed previously (R. Neumann and A. J. Jeffreys). For the downstream region, primers were designed with a minimum of 21 bp length, ~ 30% GC content and without overlapping any CpG dinucleotide (Fig. 6.6.).

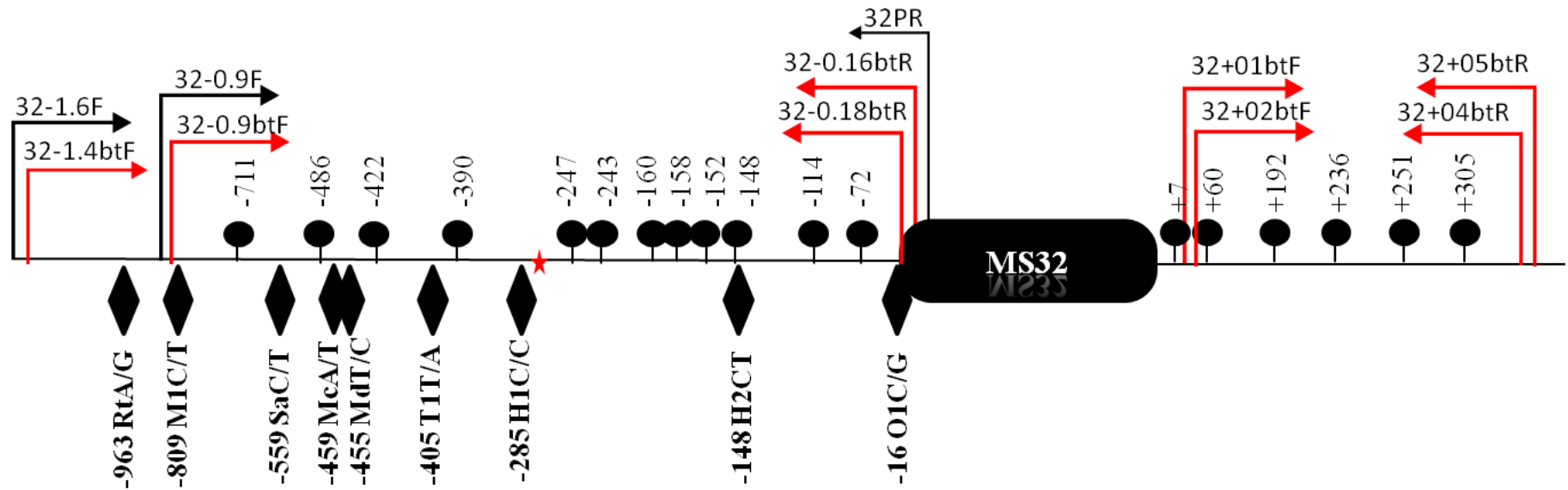


Figure 6.6: MS32 minisatellite flanking region.

The diagram represents the SNPs (diamond), CpG dinucleotides (lollipop-shape) and the primers (arrows) used for the methylation study. The distance of each CpG to the MS32 array is represented in bp. The primers used for genotyping are represented as black arrows, whilst the red arrows show the primers used for the bisulfite-analysis. The red star represents the centre of the meiotic hotspot.

	RtA/G	M1C/T	SaC/T	McA/T	MdT/C	T1T/A	H1G/C	H2C/T	O1C/G
	-963	-809	-559	-459	-455	-405	-285	-148	-16
NT2D1	A	T	C	A	T	T	G	C	G
HT1080	A	T/C	C	A	T	T	G	C	G
MRC5	A	T/C	C	A	T	T	G/C	T/C	G
IIIcF-postcrisis	A	T	C	A	T	T	G	C	G
JFCF6T.IJ/11C	A	T	C	A	T	T	G	C	G
JFCF6T.IJ/11E	A	T	C	A	T	T	G	C	G
WI38	A	C	C	A	T	T	G/C	C	G
WI38-13VA/2RA	A	C	C	A	T	T	G/C	C	G
SUSM-1	G	C	C	A	T	T	C	T	G

Table 6-5: Genotyping of the upstream region of MS32 minisatellite.

The 5'-flanking region of MS32 minisatellite was sequenced and the genotype of each cell-line analysed is summarized in the table. The distance of each SNP from the MS32 minisatellite is shown.

Traditionally, after bisulfite sequencing methylation state of the DNA sample is inferred by PCR amplification, cloning and sequencing. However, the PCR amplification could introduce a bias due to the different efficiencies between templates. Alternatively, single-molecule PCR approaches overcome the PCR and the cloning bias, since the products can be sequenced directly. Due to time-constrictions, genomic DNA from single-cell clonal populations was bisulfite treated to overcome the vector-cloning process or single-molecule amplification required for the sequencing process. Populations arising from single-cell cloning would be expected to show identical patterns if the methylation state remains stable but, to confirm this assumption, 6-10 DNA samples from clones of each cell-line were bisulfite-treated and analysed. Briefly, 1 µg of *BamHI*-digested genomic DNA was bisulfite treated with the EpiTect Bisulfite Kit (QIAGEN), according to the manufacturer's protocol. The bisulfite-treated DNA was bound to the membrane of an EpiTect spin column and washed, the membrane-bound DNA was desulfonated and the desulfonation agent removed. The pure converted DNA was eluted and used for the PCR amplification. 1 µl of the elute was the template for a primary PCR reaction, performed with the 32-1.4btF + 32-0.16btR primers for the upstream flanking region and the 32+01btF + 32+05btR primers for the downstream region, both amplified for 38 cycles. Secondary nested-PCRs were then set up with the 32-0.9btF + 32-0.18btR primers (upstream) and the 32+02btF + 32+04btR (downstream) for another 38 cycles. The reactions showed expected products of 900 bp for the upstream and 360 bp for the downstream regions, on 1% agarose gel electrophoresis. The products were Exo1 + shrimp alkaline phosphatase (SAP) to remove the primers and sequenced with the 32-0.18btR primer (upstream) and the 32+04btR primer (downstream). The efficiency of the bisulfite-treatment was confirmed by the full conversion of non-CpG cytosines in all the sequences analysed. The results of the

bisulfite sequencing are shown on the diagrams of Figure 6.7. Eight cell-lines were analysed: the normal WI38 (eight clones) and its derived ALT+ WI3813VA/2RA (eight clones); the Tel+ JFCF6T.IJ/11C (seven clones) and its ALT+ equivalent JFCF6T.IJ/11E (eight clones); the ALT+ IICF/a2 (six clones), the ALT+ SUSM-1 (seven clones); the Tel+ HT1080 (seven clones) and the Tel+ NT2D1 (six clones). A total of 12 CpG dinucleotides were analysed on the upstream flanking region of MS32 minisatellite and 5 (6 in the IICF/a2 cell-line) on the downstream region.

As expected, the clones derived from the same cell-lines show very similar methylation-status between each other, which validates the initial assumption and overcomes the necessity for either cloning the products or perform time-consuming single-molecule amplifications. Also, in contrast with the mentioned techniques to obtain single molecule methylation maps, more CpG dinucleotides show hemimethylation (mix of methylation and unmethylation) since the sequences were obtained directly from secondary-PCR and thus are the result of two alleles.

To determine methylation differences around MS32, the methylation-status for individual CpG dinucleotides of each clone analysed was scored according to the sequencing result: 1 for 100% of methylated molecules (just a C peak on the chromatogram), 0.5 when a mixture of methylated and unmethylated molecules was detected (both C and T peaks visible on the chromatogram) and 0 for 100% of unmethylated molecules (T peak). For each cell-line, the obtained scores for each CpG site of all clones were summed up and divided by the number of analysed clones. The resulting value was used to determine the percentage of methylation at each CpG dinucleotide and compared across cell-lines by plotting the percentages obtained on each CpG according to their distance from the minisatellite (Fig. 6.8 and Table 6.6).

Overall, the MS32 downstream region seems to be heavily methylated across all analysed cell-lines, whilst the upstream region shows a mixed pattern between methylated, hemi-methylated and unmethylated CpGs (with the exception of NT2D1 that seems to be heavily methylated across both regions) (Fig. 6.7). Interestingly, the two pairs of cell-lines show very similar methylation patterns except for the area covered by the 3 CpG sites immediately upstream of MS32 on WI38 vs. WI3813VA/2RA and the area around the 5 CpG just upstream MS32 on the JFCF6T.IJ pair. In fact, the 150 bp region upstream MS32 minisatellite appears to be unmethylated mainly in the ALT+ cell-lines (Fig. 6.7 and 6.8). A statistical analysis per CpG dinucleotide between ALT+ and non-ALT cell-lines confirmed a significant difference on the CpG closest to the minisatellite 5'-end (p-value of 0.00503, two-tailed t-test, Table 6.7). Furthermore, the JFCF6T.IJ/11E cell-line shows a random methylation pattern in the 5' flanking region. Thus, if excluded from the analysis the previous CpG at position -114 is also significantly differently methylated between ALT+ and non-ALT (p-value of 0.02286, compared to a p-value of 0.06033 considering JFCF6T.IJ/11E, two-tailed t-test) (Fig. 6.9 and Table 6.7).

Therefore, the analysis performed on eight cell-lines suggests a methylation alteration between ALT+ and non-ALT cells, in the 5' region immediately flanking MS32 minisatellite. Although the affected area is small, a maximum of 150 bp, the loosening of the methylation level might extend through the minisatellite exposing it to the cellular processes responsible for instability observed in ALT+ cells.

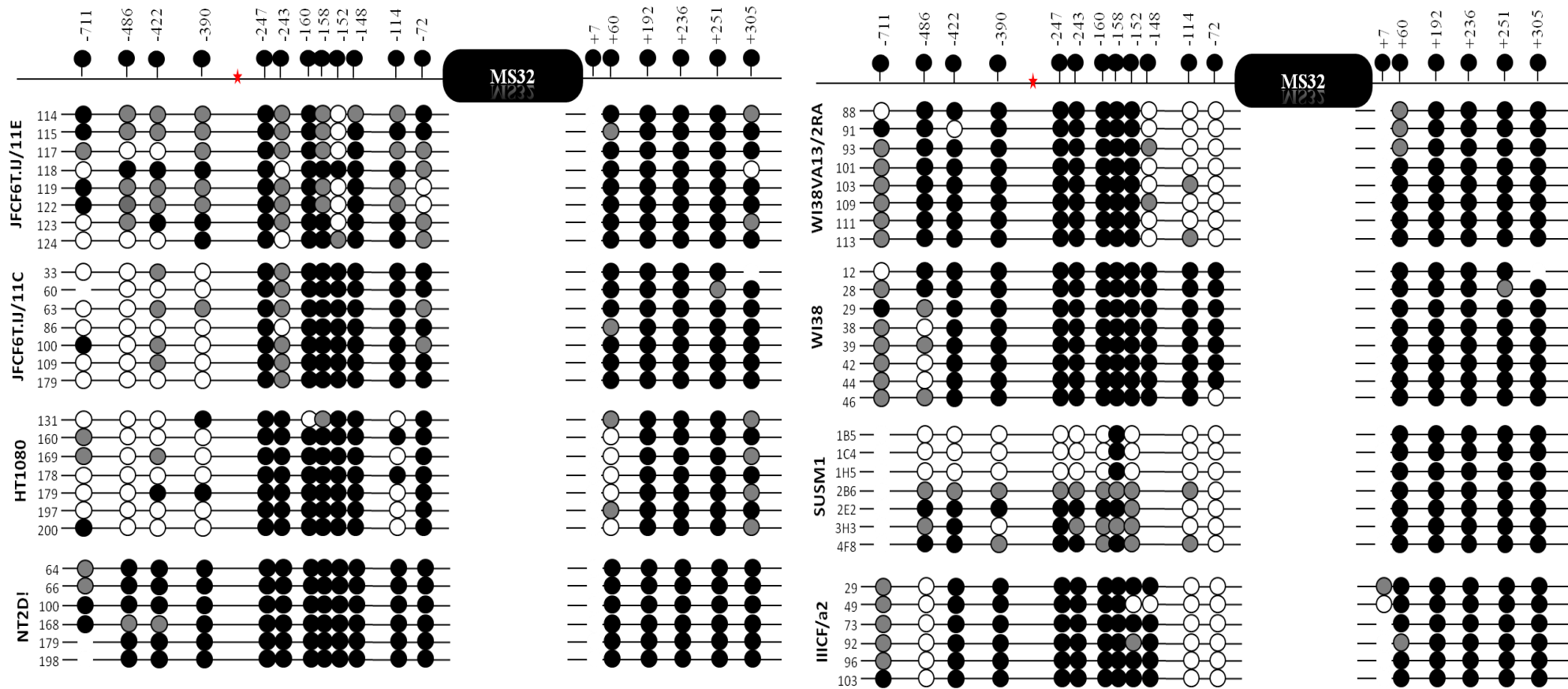


Figure 6.7: Methylation levels at each CpG site of each analysed clone per cell-lines.

Full dot represents 100% methylation, grey dots 20-80% methylation (according to the peak sizes in the chromatogram) and white dots represent 0% methylation. When no sequencing information could be obtained, the CpG dinucleotides are marked as a gap. The numbers represent the clone ID for each cell-line.

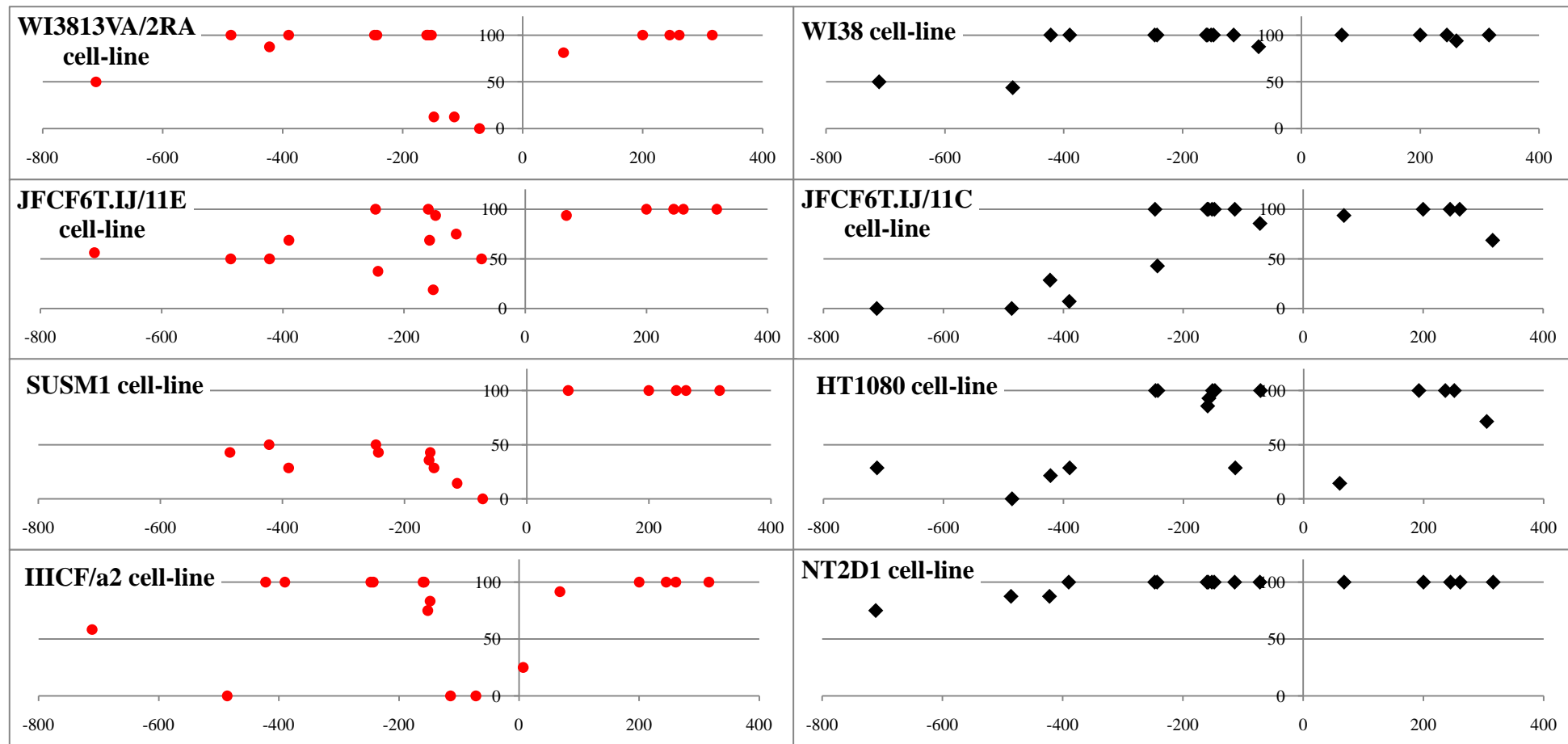


Figure 6.8: Methylation-status of the regions flanking MS32 minisatellite.

The methylation state (%) per CpG site for each cell-line were plotted against their physical location relative to the MS32 minisatellite (negative and positive coordinates refer to the upstream and downstream regions, respectively). For comparison, the results for the normal (WI38) and Tel+ (JFCF6T.IJ/11C, HT1080 and NT2D1) cell-lines were plotted in black, whilst the ALT+ (WI38-13VA/2RA, JFCF6T.IJ/11E, IICF/a2 and SUSM-1) cells were represented in red.

	-711	-486	-422	-390	-247	-243	-160	-158	-152	-148	-114	-72	7	60	192	236	251	305
WI38	50	43.8	100	100	100	100	100	100	100	100	100	87.5	n/a	100	100	100	93.8	100
WI38-13VA/2RA	50	100	87.5	100	100	100	100	100	100	12.5	12.5	0	n/a	81.3	100	100	100	100
JFCF6T.IJ/11C	0	0	28.6	7.1	100	42.9	100	100	100	100	100	85.7	n/a	92.9	100	100	92.9	100
JFCF6T.IJ/11E	56.2	50	50	68.8	100	37.5	100	68.8	18.8	93.8	75	50	n/a	93.8	100	100	100	68.8
IIICf/a2	41.7	0	100	100	100	100	100	100	75	83.3	0	0	25	91.7	100	100	100	100
SUSM1	n/a	42.9	50	28.6	50	42.9	35.7	42.9	28.6	no CpG	14.3	0	n/a	100	100	100	100	100
HT1080	28.6	0	21.4	28.6	100	100	85.7	92.86	100	100	28.6	100	n/a	14.3	100	100	100	71.4
NT2D1	75	87.5	87.5	100	100	100	100	100	100	100	100	100	n/a	100	100	100	100	100

Table 6-6: Percentage of methylation per CpG dinucleotide on each cell-line.

The methylation-status at each CpG dinucleotide was determined by scoring the level of methylation observed on the sequencing-chromatograms. A CpG site showing 100% of methylated molecules would be scored *I*, a mixture of methylated and unmethylated molecules would be 0.5 and 100% of unmethylated molecules would have a score of 0. Then, the summed scores of all the clones analysed per CpG were divided by the number of clones analysed in each cell-lines and the resulting percentages are summarized on the table, according to their distance (in bp) to the MS32 minisatellite (first row, negative and positive coordinates refer to the upstream or downstream regions, respectively). The CpG dinucleotides that failed to be sequenced in all clones of the same cell-line are represented by **n/a**. Due to a SNP at the position -148 in SuSM1 cell-line no informative site is present at this site (**no CpG**).

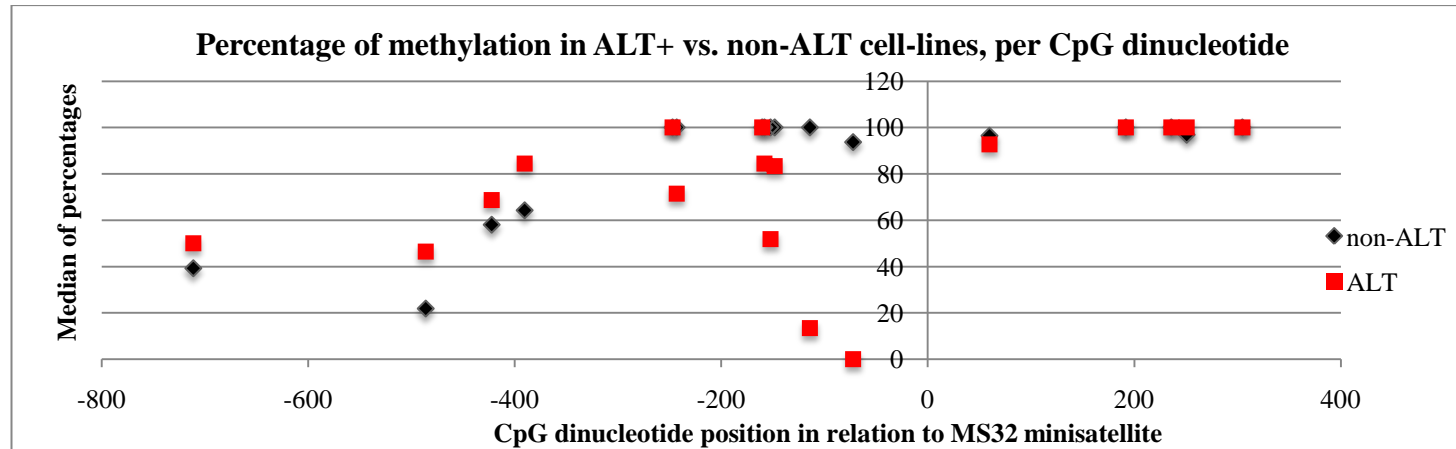


Figure 6.9: Methylation per CpG site between ALT+ and non-ALT cell-lines.

The analysed cell-lines were grouped according as ALT+ (red) and non-ALT (black). The median of the percentages obtained for the methylation at each CpG dinucleotide were calculated and plotted against their physical location in reference to the MS32 minisatellite.

	-711	-486	-422	-390	-247	-243	-160	-158	-152	-148	-114	-72	60	192	236	251	305
non-ALT	39.2	21.9	58	64.3	100	100	100	100	100	100	100	93.75	96.4	100	100	96.9	100
ALT+	50	46.4	68.75	84.4	100	71.4	100	84.4	51.8	83.3	<i>13.4/12.5</i>	0	92.7	100	100	100	100
P-value	0.55	0.62	0.62	0.62	0.39	0.51	0.49	0.24	0.10	0.29	0.06/0.023	0.005	0.53	n/a	n/a	0.18	0.95

Table 6-7: Statistical analysis of the methylation-status between ALT+ and non-ALT cells.

The cell-lines were grouped as ALT+ (WI3813VA/2RA, JFCF5T.IJ/11E, SUSM-1 and IIICF/a2) and non-ALT (WI38, JFCF6T.IJ/11C, HT1080 and NT2D1) and the median percentage of methylation per CpG site calculated. A two-tailed t-test was performed to determine the significance of the differences observed and the respective p-values are shown on the table. In italic, at position -114, it is shown the median and p-value obtained if JFCF6T.IJ/11E cell-line is excluded from the analysis.

An investigation to determine whether the hypomethylation observed on the CpG dinucleotides upstream the MS32 minisatellite in ALT+ cells extends towards the repeated sequence was performed. A direct analysis of the methylation-status of MS32 minisatellite by bisulfite sequencing would be technically challenging. Furthermore, as only one CpG dinucleotide is present in two of the four variant repeats, the bisulfite-sequencing would only be informative if the full variant-repeat interspersions maps were known for each clone analysed, as an unmethylated CpG dinucleotide would be masked as the respective no-CpG repeat variant (T/C SNP polymorphism). Nonetheless, the variation of the MS32 repeats allowed the design of a methylation-sensitive digestion that could partially indicate the methylation-status of MS32 minisatellite.

The methylation-sensitive restriction enzyme *TauI* (5'-GCSG^AC-3') recognizes the MS32 variant repeat *e*, which is one of the two variants with a CpG dinucleotide. Thus, the digestion of genomic DNA with the flanking enzyme *AluI* (control) and a second-digestion with *TauI* (test only) may indicate the methylation status of the minisatellite. If the MS32 alleles show the same length as the non-digested control, all the CpGs on the *e* repeats have to be methylated. If, however, the digested-pattern shifts in comparison to the control, at least some CpG dinucleotides present in *e* variants are unmethylated.

An *AluI*-digestion of 4 µg of genomic DNA from seven different cell-lines was performed and the DNA was precipitated and washed on 70% ethanol. Then, DNA was divided into two groups: a control group (+ -) to which only *TauI* buffer and water were added and a test group (+ +) where *TauI* enzyme was added to the buffer and water. *TauI* digestion was performed for 16 hours, to guarantee that all unmethylated sites could be digested, the products run on a 1.2% agarose gel electrophoresis and MS32 detected by Southern-blotting (Fig. 6.10)

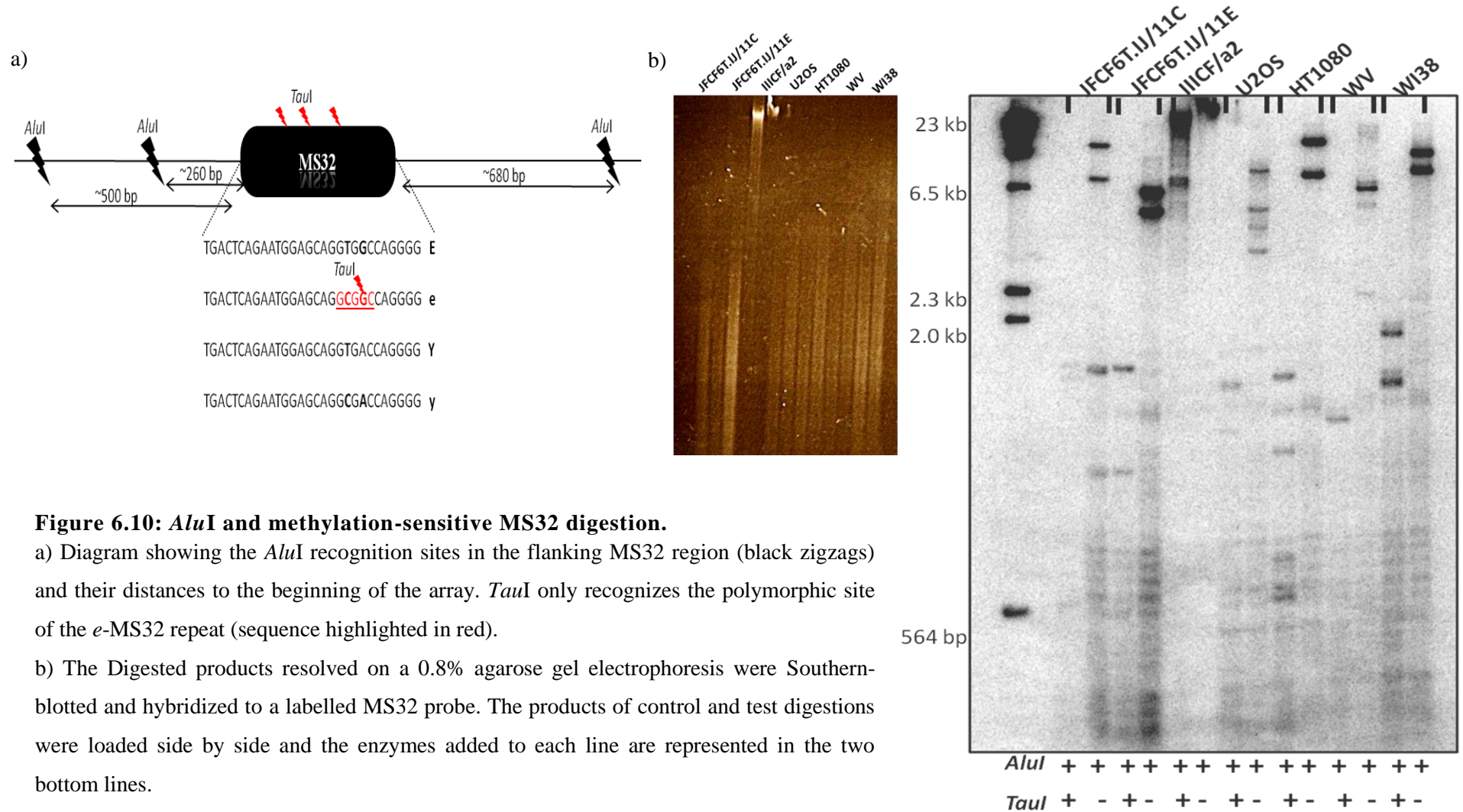


Figure 6.10: *AluI* and methylation-sensitive MS32 digestion.

a) Diagram showing the *AluI* recognition sites in the flanking MS32 region (black zigzags) and their distances to the beginning of the array. *TauI* only recognizes the polymorphic site of the *e*-MS32 repeat (sequence highlighted in red).

b) The Digested products resolved on a 0.8% agarose gel electrophoresis were Southern-blotted and hybridized to a labelled MS32 probe. The products of control and test digestions were loaded side by side and the enzymes added to each line are represented in the two bottom lines.

The *AluI*-digested MS32 alleles (+ -, Fig. 6.10) were further digested in all cell-lines with the methylation-sensitive *TauI* (+ +, Fig. 6.10). A loading-error on the test JFCF6T.IJ/11C (some of the double-digested JFCF6T.IJ/11E was accidentally loaded in the same well) and a failure on the *AluI* digestion of IICF/a2 prevented the comparison of the degree of digestion on both cell-lines (Fig. 6.10-a). However, it seems that the ALT+ cell-lines U2OS and WV show a higher *TauI* digestion when compared to the Tel+ HT1080 or the normal WI38 cell-line. The differences observed on the intensity of the double-digested products might be a consequence of a higher incidence of *e* repeats on these cells and thus, more available sites prone to digestion or it may result from an elevated and perhaps biased towards one end unmethylation of MS32 minisatellite in ALT+ cells.

The results of the methylation-sensitive double-digestion show that all cell-lines have at least some unmethylated *e*-MS32 repeats, which indicates that the observed hypomethylation adjacent to the MS32 minisatellite 5'-end in ALT+ cells does not extend throughout the minisatellite.

6.4 DISCUSSION

The instability at the D1S8 locus associated with the activation of the ALT mechanism is limited to the MS32 locus itself. Also, no expression changes were found in the genes flanking the minisatellite. Another possibility concerns some genomic or structural local alteration between ALT+ and non-ALT cells that could be the underlying factor exposing the minisatellite, promoting its instability. A better understanding of this potential change, despite not explaining the link between MS32 instability and the ALT mechanism, will certainly elucidate the pathway(s) involved.

The copy-number of the region around MS32 minisatellite was assessed in ALT+ and non-ALT cell-lines, by MLPA analysis. An MLPA kit was specifically designed to cover 29 loci across the 1q32.2-44 region, comprising the MS32 minisatellite and previously shown to be exclusively deleted in ALT+ liposarcomas (Johnson et al 2006). The MLPA results obtained did not identify this particular deletion in any of the nine cell-line analysed, independently of the TMM. Furthermore, none of the identified CN changes could be associated to a particular TMM, suggesting that the alterations observed are most likely derived from the genomic instability typical of cancer-cells.

Most CN alterations identified are on the border of the defined limits (0.7-1.3) and further MLPA replicates should be performed to confirm if these changes are biological. Also, the detection of CN changes in the analysed cell-lines is not surprising since they are either tumour derived or immortalized by p53 inactivation. Thus, the alterations identified are probably biological and result from ongoing genomic instability. Additionally, some of the identified CN changes can be confirmed by more than one probe, like the 3 probe amplification in the WI38VA13/2RA cells across *MCP* and *RAMP*

genes or the deletion of a region comprising part of the *RYR2* and *FH* genes in the IICF/a2 cells, which indicates that this particular CN alterations might be real. Interestingly, some MLPA data correlates with the expression microarray analysis performed on the JFCF6T.IJ cell-lines. Indeed, the deletion of copy of the *EGFR* gene identified by MLPA analysis in the JFCF6T.IJ/11C cells might be the underlying cause for the significantly lower expression of this gene detected by the microarray experiment (p-value 0.0037). Additionally, the deletion of both copies of the *MTAP* gene in the HT1080 cell-line might explain the previously described lack of RNA or protein levels of the *MTAP* gene in these cells (Tang et al 2000). Furthermore, the MLPA data seems to be in accordance with previous analysis of the MS32 minisatellite. MS32 SP-PCR amplification in the IICF/a2 revealed one single MS32 allele (Jeyapalan et al 2005). Accordingly, the MLPA data in the region comprising the minisatellite shows one copy deletion across the 1q43 in these cells (although the ratios obtained are near the defined limits). The same deletion is also observed in the WI38VA13/2RA cells, which also show amplification of a neighbouring region (1q32.20-1q42). This amplification observed is in accordance with the same MS32 minisatellite study, where three alleles seem to be amplified in these cells (Jeyapalan et al 2005). Therefore, this evidence strongly indicates that some of the identified changes are real and the changes with values close to the defined limits should be confirmed with more replicates. Nonetheless, even though the MLPA technique and the data analysis performed seem robust enough to determine CN, no changes could be associated to either TMM around MS32 minisatellite or across any of the loci analysed.

To confirm that indeed no CN alterations occur around MS32 minisatellite, an *Alu*-amplification experiment was designed. *Alu* elements constitute identical-sequence loci dispersed throughout the genome, providing a good target for copy-number analysis. Eight *AluY* elements were chosen for the analysis: four to test the MS32 minisatellite region and other four controls. PCR optimizations were performed to ensure that each reaction was exclusively amplifying the targeted *Alu* and direct sequencing of each amplicon confirmed the specificity. The eight amplified *Alus* were dot-blotted into nylon-membranes and hybridized with a probe composed of a sequence common to all targets. Preliminary results confirmed that the blotting and hybridization conditions were optimized. Moreover, the analysis of preliminary experiment suggests that copy-number changes can potentially be detected by this methodology, providing that enough products are pooled and all controls are included, especially the DNA input controls (Fig. 6.5).

No copy-number changes around MS32 specific to TMM appear to occur, suggesting that other particularity of this region must be the trigger for its instability in ALT+ cells. Although previous analysis showed that no local transcriptional-related chromatin alterations were found associated to the ALT+ cells (see chapter 4, section 4.3.2), an opening of the chromatin resulting from changes on the methylation levels around MS32 minisatellite could expose the repeats to the cellular processes responsible for its instability.

Therefore, the DNA methylation statuses of the regions immediately adjacent to the MS32 minisatellite were determined in ALT+ and non-ALT cells. Genomic DNA of 6 to 8 clones from each cell-line was bisulfite treated and was sequence-analysed. The methylation patterns observed between clones was consistent, confirming that during the

clonal expansion no major methylation changes occurred, at least in both analysed regions (Fig. 6.6).

The region flanking the 3' MS32 end appears to be heavily methylated in all cell-lines tested, contrasting with the 5' flanking region that shows a much higher variation of the methylation levels. Nonetheless, a maximum of 150 bp of the flanking sequence immediately adjacent to the 5' end of the array seems to be unmethylated exclusively in the ALT+ cell-lines (Fig. 6.8). Curiously, the level of unmethylation at these sites directly correlates with the previously described mutation frequencies of MS32 minisatellite on these ALT+ cell-lines (Jeyapalan et al 2005, Table 6.8). In fact, IICF/a2 was shown to have the highest MS32 mutation frequency (0.93) and it is also the cell-line with 100% of unmethylation in the 150 bp region immediately flanking the 5' end of the array. The lower MS32 instability observed in ALT+ cell-lines was in JFCF6T.IJ/11E (0.118), the cell-line also showing the most random methylation-pattern on the mentioned area.

Mutation Frequency	
IICF/a2	0.93
SUSM1	0.495
WI38VA13/2RA	0.285
JFCF6T.IJ/11E	0.118
HT1080	0.005
NT2D1	0
JFCF6T.IJ/11C	n/a

Table 6-8: MS32 mutation frequencies.

The mutation frequency were estimated by maximum likelihood analysis of the numbers of mutants observed in each small-pool-PCR reaction, together with the number of small-pool-PCR reactions containing non-mutant MS32 progenitor allele(s) and the number of Poisson reactions containing MS32 molecules. Figure reproduced from Jeyapalan et al. 2005.

Hence, it is tempting to speculate that lower methylation levels in the region flanking the 5' end of the minisatellite stimulate an open-chromatin conformation in the region, exposing the MS32 minisatellite to molecular mechanisms that will trigger its instability. Therefore, in ALT+ cells showing lower methylation in the MS32 flanking 5' region, the chromatin around MS32 might be more relaxed in comparison to non-ALT cells, which might facilitate the high instability observed in these cells. The investigation of whether chromatin-boundary elements (like CTCF) have different binding capacity to this region in ALT+ compared to non-ALT cells would elucidate this hypothesis.

To further investigate the extent of unmethylation in ALT+ cells, a methylation-sensitive digestion was performed with the *TauI* enzyme. The methylation-sensitive *TauI* recognizes the *e* MS32 repeat, one of the two with one CpG site. All cell-lines tested, ALT+ and non-ALT, showed *TauI* digestion, indicating that at least some of the MS32 *e* repeats are unmethylated in all cell-lines.

Another curious aspect of the methylation experiment is the fact that hypomethylation was detected in the MS32 minisatellite in all cell-lines, since methylation-sensitive digested products were obtained in all samples and suggesting that at least part of the array is unmethylated in all cell-lines tested. However, recent studies demonstrate that tandem repeats might differ from other repetitive elements regarding the previously described tumour-associated hypomethylation of repetitive DNA (Ehrlich et al 2002). Indeed, hypo and hypermethylation of NBL2, a tandem array of 1.4 kb repeat units, was found in different cancer cells (Nishiyama et al 2005). Also the tandem repeat D4Z4 was shown to have variable methylation status between different tumour cells. Some groups showed D4Z4 hypomethylation in cancers, cancer-derived cell lines, and

cells treated with demethylating agents or deficient in DNA methyltransferase (Cheng et al 2004; Cadieux et al. 2006). In contrast, hypo and hypermethylated in cancers of the same type, with the first D4Z4 repeat unit behaving very differently from the rest of the D4Z4 array with respect to changes in DNA methylation have also been described (Choi et al 2009). Therefore, these studies and the methylation analysis around MS32 minisatellite suggest that, in contrast to interspersed repeats, tandem repeats may show an epigenetic plasticity in cancer cells.

Interestingly, the D4Z4 study also demonstrated that the chromatin immediately proximal to the array had a very different accessibility to DNaseI than the array itself, suggesting a different chromatin structure at the proximal border than in the body of the array (Tsumagari et al 2008), which can possibly be occurring at the MS32 minisatellite.

Further experiments to determine if there are changes on the DNase I, CTCF or other chromatin-related proteins accessibility to the region flanking the 5' end of MS32 minisatellite should be performed to confirm if indeed ALT+ cells show an open-chromatin conformation around MS32 minisatellite, in comparison to the non-ALT cells.

CHAPTER 7: CONCLUSION AND FUTURE WORK

Telomeres are extremely important for genome stability as they protect the end of the chromosomes, preventing degradation and end-to-end fusion. Moreover, telomere integrity is essential for cell viability as the shortening of telomeres resulting from the successive cell divisions ultimately leads to a growth arrest. However, inactivation of mechanisms responsible for senescence induction may force cells in crisis to activate a telomere maintenance mechanism, to preserve the length of the telomeres and continue on dividing. The most common TMM is telomerase activation, a reverse transcriptase that elongates shortened telomeres by addition of *de novo* telomeric repeats. However, the Alternative Lengthening of Telomeres (ALT) mechanism may also be activated, and is especially frequent in cancers of mesenchymal origin, like liposarcomas and sarcomas. Despite of both telomerase and ALT have been extensively studied, especially due to their potential as anti-cancer therapies targets, the molecular processes involved in the ALT pathway are not fully understood.

ALT+ cells have particular characteristics that have been used as markers for this type of cancer cells but also as tools to dissect the molecular processes involved. For example the interference with the ALT-associated PML bodies (APB) integrity has been used to study indirectly the proteins that might be essential for the ALT pathway and therefore, prove to be essential for its proper function at telomeres. One of the most curious phenotypes of ALT+ cells is an extreme instability at the MS32 minisatellite (D1S8) (Jeyapalan et al 2005). The MS32 minisatellite has no obvious characteristics that explain the instability associated with the activation of the ALT mechanism, hence this study aimed to investigate this relationship.

Previous studies had found that MS32 minisatellite was the only minisatellite amongst seven (MS1, MS31, CEB1, MS205, B6.7 and DXY14) whose stability was affected in ALT+ cells (Jeyapalan et al 2005). Thus, an analysis of other tandem repeats near MS32 was performed to determine whether their stability is also affected by ALT activation. The analysis of MSNID minisatellite and preliminary STR, the closest tandem repeats to the MS32 locus showed that the MS32 instability does not extend to the nearby tandem repeats, suggesting that the extreme MS32 instability is confined to the minisatellite itself.

To determine whether MS32 is likely to be the only minisatellite affected by the ALT mechanism, a further investigation was performed to screen for other potentially unstable minisatellites. DNA fingerprints from seven clones (20 PDs) derived from the ALT+ SUSM-1 cell-line were obtained and hybridized to two multilocus probes. The DNA fingerprints of seven SUSM1 clones identified further 47 loci that seem to remain stable in the SUSM1 ALT+ cell-line. Thus, MS32 locus could potentially be the only or one of a small number of loci that are affected by ALT activation. Clones derived from at least one more ALT+ cell-line should be analysed, to verify these results. Some other loci might be unstable in ALT+ cells but the conditions used to resolve the fragments resulting from the *AluI* digestion do not permit their detection.

In summary, this and previous studies (Tsutsui et al, 2002; Jeyapalan et al, 2005) suggest that most minisatellites remain stable in ALT+ cells. Therefore, the causes of the MS32 instability seem to be dependent on the minisatellite itself, which is also supported by the findings that the instability does not extend to the nearby tandem repeats. A possible explanation for the particular instability at MS32 minisatellite would be

transcriptional-changes altering the conformation of the region comprising the minisatellite in ALT+ cells, exposing the minisatellite to cellular machinery that would then result in the observed high instability.

No expression changes common to the ALT+ cells analysed were detected by expression microarray in the region around MS32 minisatellite. To validate this result and to determine if subtle transcriptional changes are occurring on the 1q42-43 locus in ALT+ cells, qPCR was performed on the three genes flanking MS32. Even though great variance in the expression levels of the genes analysed between cell-lines was detected, no significant differences associated to the ALT mechanism were observed, confirming the results obtained by the expression microarray data analysis (Fig. 4.23).

Together, both studies indicate that no transcriptional-changes associated to the ALT+ mechanism seem to occur in the region comprising the MS32 minisatellite. Thus, the MS32 instability in ALT+ cells is either specifically triggered by the minisatellite itself or by chromatin changes not related to transcription.

In fact, the analysis of the methylation levels of the region comprising MS32 minisatellite in ALT+ and non-ALT cells appear to indicate that methylation changes occur exclusively at ALT+ cells. Determination of the methylation status of the region flanking the minisatellite by bisulfite sequencing revealed that 2 of the 3 CpGs in the 150 bp region immediately adjacent to the 5' end of the MS32 array are unmethylated in ALT+ cell-lines (Fig. 6.8). In contrast, the region adjacent to the 3' MS32 end appears to be heavily methylated in all cell-lines tested. Furthermore, the level of unmethylation at the flanking 5' end seems to directly correlate with the described mutation frequencies of MS32 minisatellite for each ALT+ cell-lines (Jeyapalan et al, 2005, see Table 6.8).

Therefore, the lower methylation levels in the region flanking the minisatellite might confer an open-chromatin conformation to the MS32 minisatellite, which could expose the tandem repeats to the molecular mechanism responsible for its instability. In conclusion, it appears that the unmethylation of the region flanking the 5' MS32 end in ALT+ cells might confer a more relaxed chromatin conformation in the region, facilitating the high instability observed in these cells.

To investigate the extent of unmethylation in ALT+ cells further, a methylation-sensitive digestion was performed. All cell-lines tested have some degree of unmethylated MS32 (Fig. 6.9). This result indicates that the observed ALT-associated unmethylation is restricted to the flanking the 5' end, since unmethylation within MS32 occurs independently of the TMM. It would be interesting to investigate whether this unmethylation confers a different accessibility of chromatin-related protein, like CTCF, to this region in ALT+ cells. Additionally, a DNaseI assay could confirm if this region has indeed a different chromatin conformation between ALT+ and non-ALT cells. Also, this data confirms the findings that tandem repeats might not be affected by the same mechanisms involved in the tumour-associated hypomethylation of repetitive DNA (Ehrlich et al 2002; Nishiyama et al 2005; Cheng et al, 2004; Cadieux et al. 2006), since both ALT+ and Tel+ cells showed some degree of unmethylation at the MS32 minisatellite.

A study in liposarcomas had previously identified a 1q32.2-44 deletion exclusive of ALT+ liposarcomas (Johnson et al, 2006). To investigate whether this ALT-associated deletion, comprising the MS32 region, was also present in other ALT+ cell-lines, the copy-number around MS32 minisatellite was assessed by MLPA and *Alu* analysis in

ALT+ and non-ALT cell-lines. The MLPA technique was applied using a specifically-designed kit for this experiment (see chapter 6, section 6.3.1.1), covering 29 loci across the mentioned region. The MLPA results obtained did not identify such a large deletion in the nine cell-lines analysed (Table 6.2 and Figure 6.3), although the IICF/a2 cell-line shows a partial deletion of this region. Additionally, none of the identified CN changes by the MLPA analysis could be associated to a particular TMM, since they only occurred at a particular cell-line. However, since most of the identified CN changes are on the border of the limits defined for this analysis (0.7-1.3), more MLPA replicates should be included in the study to confirm if the changes are real or a reflection of technical fluctuations. Nonetheless, some of the identified CN alterations were confirmed by more than one probe, like the amplification in WI38VA13/2RA across *MCP* and *RAMP* genes or the deletion of a region comprising part of the *RXR2* and *FH* genes in IICF/a2. Furthermore, some CN changes identified correlate with the expression microarray data. For example, the *EGFR* allele deletion identified by MLPA in the JFCF6T.IJ/11C cell-line might explain the significantly lower expression of this gene detected by the microarray experiment (p-value 0.0037). Also, the full deletion of the *MTAP* gene on the HT1080 cell-line is possibly the reason for the described lack of RNA or protein levels of this gene in these cells (Tang et al 2000). Consequently, the identical results obtained by different methodologies strongly indicate that at least some of the identified CN changes and expression alterations are biologically significant.

The understanding of the mechanism underlying the MS32 instability in ALT+ cells might indirectly identify key players in the ALT-mechanism. Thus, the mechanisms involved in the MS32 instability were investigated by the identification of the mutation spectrum of the minisatellite in these cells. As most MS32 mutations observed derived from large deletions and since t-circles are one of the particularities of ALT+ cells, the presence of extrachromosomal circular MS32 sequences was investigated but no MS32 circles were detected. Interestingly, however, was the finding of variant repeats in the t-circles. These findings are very remarkable, since the distal limit for variant repeats within telomeres is thought to be about 2-3 kb (Allshire et al 1989; Baird et al 2000). Thus, this data suggests very proximal point of invasion of the 3' overhang during t-loop formation.

Finally, considering again the spectrum of MS32 mutants and their frequencies observed in ALT+ cells, it was interesting to find that they were similar to mutants identified in the CEB1 minisatellite inserted in yeast RAD27 Δ model (Lopes et al 2006). The proposed model for CEB1 instability in yeast considered the accumulation of unprocessed 5' flaps after removal of the Okazaki fragments due to the absence of the 5' flap-endonuclease RAD7 as the trigger structures for the instability observed. DSB-synthesis-dependent strand annealing (SDSA) (Buard et al., 1998, 2000; Debrauwère et al., 1999) might recognize the 5' flaps as DSB. The invasion of a template molecule by the DNA repair mechanism would form a D-loop with mismatches due to sequence divergence. The repair of these mismatches could create a reshuffling in the repeat order. To investigate whether this model is likely to be the one occurring at MS32 in ALT+ cells, the expression levels of two RAD27 human homologues (hFEN1 and hEXO1) were

assessed in these cells. No *hFEN1* significant expression changes associated to ALT activation were detected by qPCR analysis across 11 cell-lines tested (Fig. 5.8). Furthermore, sequence analysis of the coding *hFEN1* genomic region revealed no point mutations, suggesting that hFEN1 is fully functional in ALT+ cells. These findings are in agreement with an hFEN1 role in telomere stability in ALT+ cells (Saharia et al 2009). However, a significant *hEXO1* overexpression associated to ALT+ cells was detected (Fig. 5.10). Since EXO1 seems to be essential for the appearance of telomerase-negative yeast survivors (Bertuch et al 2004), the overexpression of *hEXO1* in the ALT+ cell-lines analysed might reflect a role in telomere maintenance also in humans. Thus, it would be interesting to investigate the effect of a dysfunctional hEXO1 in ALT+ cells.

Considering the model for 5'-flap accumulation as the trigger for MS32 instability in ALT+ cells, the overexpression of *hEXO1* in ALT+ cells seems to contradict this hypothesis. Nonetheless, a higher recruitment of hEXO1 for proper lagging-strand synthesis to ALT-telomeres could explain the overexpression in ALT+ cells. Thus, genomic loci that have failed to properly replicate, could form difficult to resolve secondary structures and/or are late replicating regions, would still be prone to an accumulation of 5'-flaps and trigger DNA repair mechanisms, like the SDSA. One possible experiment to verify this hypothesis would be to investigate whether the MS32 minisatellite locus behaves as a fragile site in ALT+ cell-lines. Fragile-sites are late-replicating genomic loci (Glover et al 1984), thus in the presence of a DNA replication partial inhibitor, like aphidicolin, this sites appear as chromosome breaks. Thus, it would be extremely interesting to determine whether in ALT+ cells MS32 locus appears as a chromosomal break after aphidicolin treatment. If so, that could explain why MS32 is

unstable in these cells, whilst other minisatellites remain stable. Furthermore, that could also confirm the proposed model for a defect in the lagging-strand synthesis as the trigger for MS32 instability. Even though as seen in this study ALT+ cells have functional flap-endonucleases, a higher recruitment in late S-phase for proper telomere elongation would result on late replicating regions, like fragile sites, to be prone to DNA repair mechanisms.

It became clear from this project that the MS32 minisatellite instability observed in ALT+ cells is constrained within itself and that MS32 is maybe the only minisatellite affected by ALT activation. A screen for potential reasons for the instability at this specific locus revealed a potential for chromatin conformation alterations, triggered by an unmethylated short region flanking the 5' end of the minisatellite that seems to exclusively occur in ALT+ cells. Furthermore, the characterization of the mutational spectrum of MS32 in ALT+ cells uncovered a mutational mechanism different from the ones acting in the germ or soma cells. The mutations observed could have arisen from a DNA repair mechanism, for example SDSA, triggered by a defect on the lagging-strand synthesis, like the accumulation of unprocessed 5'-flaps. The precise nature of such putative defect is not known but a higher recruitment of proteins involved in DNA replication to telomeres by the ALT mechanism could leave regions that are more difficult and/or replicate later, like potentially the MS32 minisatellite, exposed to the action of DNA repair mechanisms.

APPENDICES

Solution	Preparation
10xKinase Mix	700mM Tris-HCl [pH 7.5], 100mM MgCl ₂ , 50mM spermidine trichloride, 20mM dithiothreitol. Stored at -20oC.
10xTAE	0.4M Tris-Ac, 0.05M NaAc, 0.001M EDTA. Adjusted to pH 7.8 with acetic acid.
10xTE	100mM Tris-HCl [pH 8.0], 10mM EDTA.
10xTBE	44.5mM Tris-borate [pH 8.3], 1mM EDTA.
11.1x Buffer	Tris-HCl [pH 8.8], ammonium sulphate, magnesium chloride, 2-mercaptoethanol, EDTA [pH 8.8], 4 dNTPs, and BSA
20xSSC	3M NaCl, 0.3M Tri-Sodium Citrate.
Church Buffer	250ml 14% SDS, 250ml Na ₂ HPO ₄ pH 7.2, 2ml 0.5M EDTA pH 8.0
Column Wash	1xTE, 0.1% SDS.
Denaturing mix	0.5M NaOH, 2M NaCl, 25mM EDTA, 0.1g bromophenol blue.
DEPC water	0.1% diethyl-pyrocabonate in 200ml sterile water. Autoclaved.
DNA loading Dye	10ml 50xTAE, 12.48g Ficoll, 0.1g bromophenol blue. Final volume 100ml with sterile water.
Ethidium bromide	10mg/ml (dissolved in distilled water)
Kinase stop sol.	25mM disodium EDTA, 0.1%SDS, 10mM ATP. Stored at -20oC.
Lysis buffer	100 mM Tris-HCl pH 7.5, 100 mM NaCl, 10 mM EDTA, 1% sarkosyl
5x Oligo labelling buffer (OLB)	10 µl Solution A (1250µl 2M Tris HCl pH 8.0; 50µl 5M Mg ₂ Cl ₂ ; 36µl 2-mercaptoethanol; 10µl 100 mM dATP, dGTP, dTTP in 700 µl water) 25 µl solution B (2M Hepes pH 6.6) 15 µl solution C (random hexamer sodium salt [GE Healthcare]) Stored at -20oC.
Oligo stopping solution (OSS)	20mM NaCl 20mM Tris-HCl pH 7.5, 2mM EDTA, 0.25% SDS
PBS/BSA Buffer	0.2% (w/v) fraction PBS in BSA, 65oC overnight, filtered (0.2µm). Stored at 4oC.
PBS (pH 7.4)	4.3 mM Na ₂ HPO ₄ , 137 mM NaCl, 2.7 mM KCl, 1.4 mM KH ₂ PO ₄
Proteinase K	10mg/ml (dissolved in distilled water). Stored at -20oC.
Rnase	10mg/ml Rnase, 10 mM Tris-HCl pH 7.5, 15 mM NaCl Stored at -20oC.
RNase-away solution	0.4M NaOH, 0.1% SDS
SSC	15 mM Na citrate, 150 mM Na chloride

0.5M Sodium phosphate pH 7.2	342ml of 1M Na ₂ HPO ₄ and 158ml of 1M NaH ₂ PO ₄ in 1l dH ₂ O.
Southern Denaturing sol.	0.5M NaOH, 1M NaCl.
Southern Depurinating sol.	0.25M HCl.
Southern Neutralising sol.	0.5M Tris-HCl [pH 7.5], 3M NaCl.
5x TAE loading mix	1 ml 50x TAE (0.2M Tris Acetate, 0.1M sodium acetate, 1M EDTA pH 8.3), 1.25 g Ficoll, 10 mg Bromophenol blue in 10 ml water
tRNA buffer	1 ng/ μ l tRNA and 5 mM Tris

Appendix-1

Cell-line	Origin	TMM	APB	MS32 and telomeres	Particularities
GMO3798	Lymphoblastoid, 10-year caucasian male, SV40	Tel+	-	n/a	46,XY; 2% of cells show random chromosome loss
T24	Bladder carcinoma, caucasian female	Tel+	-	n/a	p53 mutation
NT2D1	Fibroblast (testis carcinoma), caucasian,	Tel+	-	2 alleles (5.8 and 5.2kb) HV mapped 12qA+B	aneuploidy
HT1080	Fibroblast (fibrosarcoma), Caucasian male, EBV	Tel+	-	2 alleles (8.2 and 5.5kb) HV mapped 12qB	hTERT expression; p53 mutated; pseudo diploidy mode=46
HeLA	Fibroblast (cervical carcinoma), Negro male	Tel+	-	n/a	n/a
JFCF-6/T.1J/11C	Fibroblast, SV40	Tel+	-	2 alleles (4.4 and 4kb)	n/a
IIICF/a2 - precrisis	Fibroblast (breast), female, Li Frauman patient	-	-	1 allele (~10kb)	p53 mutated (null)
MRC-5	fibroblast (lung), male, normal	-	-	n/a	-----
WI38	lung fibroblast, female, normal	-	-	2 alleles (5.5 and 6.5kb) HV mapped 12qAdel+B	wt p53
WI38VA13/2RA	lung fibroblast, caucasian female, SV40	ALT+	+	3 alleles (4.5, 5, 6.6kb) HV mapped 12qAdel+B	no TERC expression, wt p53
Saos-2	Fibroblast (osteosarcoma), Caucasian female,	ALT+	+	2 alleles (5 and 5.5kb)	p53-null
U2-OS	Fibroblast (osteosarcoma), caucasian female,	ALT+	+	1 allele (4kb) (only 1 MS1 allele)	wt p53; p16 not expressed due to methylation on exon1; no expression estrogen receptors
SUSM-1	Fibroblast (liver), chemical ¹	ALT+	+	2 alleles (4 and 1.3 kb)	p53 mutated Introduction of chr7 suppressors division and causes senescence
W-V	Fibroblast (Werner-syndrome), male, SV40	ALT+	+	2 alleles (2.1 and 4.4kb)	WRN-/-
IIICF/a2 - postcrisis	Fibroblast (breast), female Li-Frauman patient, spontaneous	ALT+	+	No definite progenitor alleles. HV mapped 12qA+B, 16p/q	p53 mutated (null)
JFCF-6/T.1J/11E	Fibroblast, SV40	ALT+	+	2 alleles (5 and 7kb)	n/a

Appendix-2

Primer name	Sequence	Template	Reference
G3PDH-FW	GAAGGTCGGAGTCAACGGATTT	qPCR	Specifically designed
G3PDH-Rv	ATGGGTGGAATCATATTGGAAC	qPCR	Specifically designed
ACTB-Fw	TCCTTCCTGGGCATGGAG	qPCR	Specifically designed
ACTB-Rv	AGGAGGAGCAATGATCTTGATCTT	qPCR	Specifically designed
TBP-Fw	CCTAAAGACCATTGCACTTCG	qPCR	Specifically designed
TBP-Rv	CTTCACTCTTGGCTCCTGTG	qPCR	Specifically designed
hEXO1-Fw	GCTCCCTATGAAGCTGATGC	qPCR	Specifically designed
hEXO1-Rv	ACATTCCCTAGCCGAGCTTGA	qPCR	Specifically designed
GPR137B-Fw	GACCTTACCAACCCTGGAAT	qPCR	Specifically designed
GPR137B-Rv	CATCAGACCTCCCTGAAGTC	qPCR	Specifically designed
LYST-Fw	TTGATCAGGCATTGACATG	qPCR	Specifically designed
LYST-Rv	GTCAGGATTATATCTGCTGAG	qPCR	Specifically designed
PSEUDO-ACO2-Fw	TACCATGTGGCCTCAGTCCT	qPCR	Specifically designed
PSEUDO-ACO2-Rv	CATCCAGGTGTCCATACACG	qPCR	Specifically designed
NID1-Fw	AGGAGCTCTTCCCTTCGGC	qPCR	Specifically designed
NID1-Rv	GGTTCCCGGAGATCTCTTTC	qPCR	Specifically designed
FEN1qPCR-FW	aggcggctgaacgtcag	qPCR	Specifically designed
FEN1qPCR-Rv	acagaggagggatgactggc	qPCR	Specifically designed
ALU-ASO	CTAAAAATACAAAAAATT	ASO used as Alu-specific probe	
MS32B	AAGCTCTCCATTTCCAGTTTCTGG	MS32 analysis	Jeffreys et al 1997
MS32E	CTTCCTCGTTCTCCTCAGCCCTAG	MS32 analysis	Jeffreys et al 1997
MS32D2	CGACTCGCAGATGGAGCAATG	MS32 analysis	Neumann & Jeffreys
MS32PR	GAAGGGTGGTTACAGAACAGG	MS32 analysis	Jeffreys et al 1998
MS32+1.4F	GGTAGCCACATCTCTGCATGATCTC	MS32 analysis	Neumann & Jeffreys
MS32+1.4Nf	GCTAATCAAGTCACATGAGATCATG	MS32 analysis	Neumann & Jeffreys
MS32+0.6R	GTCAAGGCAGATTTGAAGGGAG	MS32 analysis	Neumann & Jeffreys
MS32+0.6F2NR	GCAAGTGCAGGAGATAGAGAGAG	MS32 analysis	Neumann & Jeffreys
MVR-PCR E-F	TAG-TTCTGAGTCACCCCTGGCCA	MVR-PCR	Tamaki et al 1993
MVR-PCR E-R	TAG-ACTCAGAATGGAGCAGGTGG	MVR-PCR	Tamaki et al 1993
MVR-PCR e-F	TAG-TTCTGAGTCACCCCTGGCCG	MVR-PCR	Tamaki et al 1993
MVR-PCR e-R	TAG-ACTCAGAATGGAGCAGGCCG	MVR-PCR	Tamaki et al 1993
MVR-PCR Y-F	TAG-TTCTGAGTCACCCCTGGTCA	MVR-PCR	Tamaki et al 1993
MVR-PCR Y-R	TAG-ACTCAGAATGGAGCAGGTGA	MVR-PCR	Tamaki et al 1993
MVR-PCR y-F	TAG-TTCTGAGTCACCCCTGGTCG	MVR-PCR	Tamaki et al 1993
MVR-PCR y-R	TAG-ACTCAGAATGGAGCAGGCCA	MVR-PCR	Tamaki et al 1993
T7	AATACGACTCACTATAG	33.15+33.6	
T3	ATTAACCCTCACTAAAG	33.15+33.6	

32+01btF	TGATTTAGAATGGAGTAGGTG	3' methylation	Specifically designed
32+02btF	AATTATTGATTAGAATTGTTGG	3' methylation	Specifically designed
32+03btF	AAAGGTTGTTTGTAGTAAATTAG	3' methylation	Specifically designed
32+04btR	AAACCATACTTCTTAAATCC	3' methylation	Specifically designed
32+05btR	TTCTACAAATAACTTCTCACTC	3' methylation	Specifically designed
32-018btF	TATAGAATAGGTGATTTAGGATG	5' methylation	Neumann & Jeffreys
32-016btF	GATGATTTAGGTTAGAGTAG	5' methylation	Neumann & Jeffreys
32+ENbtR	AATTTCACTAAACAACCTTTTCC	5' methylation	Neumann & Jeffreys
32-1.4btF	GGTATTAGATAATTAGGGATAGT	5' methylation	Neumann & Jeffreys
32-0.9btF	GTGTTATGATAGAGTTAAGTAG	5' methylation	Neumann & Jeffreys
32-0.5btF	GTTTTTGGAAAAATTTGTGTAGA	5' methylation	Neumann & Jeffreys
32-0.19btR	CTATTCTATAACCACCTTC	5' methylation	Neumann & Jeffreys
A1-Fw	CTAGCACATTGCAGGAACAG	Alu analysis	Specifically designed
A1-Rv	CAAGGTGCTCCCTATCTGAG	Alu analysis	Specifically designed
A2-Fw	CAGGACAGGAAGAAGACTC	Alu analysis	Specifically designed
A2-Rv	TCTAGAGACAAGGCCTCGC	Alu analysis	Specifically designed
A3-Fw	AGAGTGAGACGCTCTCCTG	Alu analysis	Specifically designed
A3-Rv	TGTGCATTACCATCTAGGC	Alu analysis	Specifically designed
A4-Fw	ATTAATAGTGATATAACGGAAT	Alu analysis	Specifically designed
A4-Rv	ATAGCATAGATTTGTCTGG	Alu analysis	Specifically designed
A16-Fw	TTCAGTGCAGAAGAAGACTGGAG	Alu analysis	Specifically designed
A16-Rv	TTCATGTGATCCAGTTCTAG	Alu analysis	Specifically designed
A5-Fw	ATTGTGCTACCTTTCAAGCAG	Alu analysis	Specifically designed
A5-Rv	TACCACCACGCCAAGCTAC	Alu analysis	Specifically designed
A6-Fw	TGAGCATTAGACTCCAGGAAG	Alu analysis	Specifically designed
A6-Rv	TGTGCATCGTAGTGTAGG	Alu analysis	Specifically designed
A8-Fw	ACCTCTCTTATGGCTGCTG	Alu analysis	Specifically designed
A8-Rv	GCATGTGTGAAATATTCCTGT	Alu analysis	Specifically designed
Tel1	TTAGGGTTAGGGTTAGGG	T-circle TCA	N. J. Royle
Tel-G2	TTAGGGTTAGGGTTAGGGtta	T-circle TCA	Specifically designed
TelG-comp	AGGGTGAGGGTGAGGGTG	T-circle TCA	N. J. Royle
TelK-comp	AGGGTCAGGGTCAGGGTC	T-circle TCA	N. J. Royle
TelJ-comp	GGGTTGGGGTTGGGGTTG	T-circle TCA	N. J. Royle

Appendix-3

Clone ID	11C/11E	Name of gene
SNRPN-AA683321-NA	0.516323453	Small nuclear ribonucleoprotein polypeptide N
LTA-AA910185-Correct	0.506160055	Lymphotoxin alpha (TNF superfamily, member 1)
HLA-DPB1-AA486627-NA	0.485685847	Major histocompatibility complex, class II, DP beta 1
PRG1-AA278921-NA	0.461378325	Proteoglycan 1, secretory granule
HLA-DRA-R48091-NA	0.450579851	Major histocompatibility complex, class II, DR alpha
BCL2L1-NM_001191-Correct	0.433206001	BCL2-like 1
CASP10-AI336849-Correct	0.420766269	Caspase 10, apoptosis-related cysteine peptidase
CFLAR-AA115792-NA	0.371547196	CASP8 and FADD-like apoptosis regulator
ASAH1-AA664155-NA	0.363650829	N-acylsphingosine amidohydrolase (acid ceramidase) 1
LTA-W74395-NA	0.35713766	Lymphotoxin alpha (TNF superfamily, member 1)
CCND2-AI142479-NA	0.355343629	Cyclin D2
CCR7-AI672677-Correct	0.335926397	Chemokine (C-C motif) receptor 7
KRT5-AA160595-NA	0.335186597	Keratin 5 (epidermolysis bullosa simplex,)
IL1RN-T72877-NA	0.325194416	Interleukin 1 receptor antagonist
LCPI-W73144-NA	0.321751513	Lymphocyte cytosolic protein 1 (L-plastin)
CD83-AA083671-NA	0.321599176	CD83 molecule
AARS-AA156571-NA	0.314716706	Alanyl-tRNA synthetase
CCNG1-AA083032-NA	0.310780993	Cyclin G1
SSR4-AA486261-NA	0.307427302	Signal sequence receptor, delta (translocon-associated protein delta)
HCLS1-AA424681-NA	0.260398015	Hematopoietic cell-specific Lyn substrate 1
TNF-AI242177-Correct	0.257751476	Tumor necrosis factor (TNF superfamily, member 2)
ACVR1-AA136882-NA	0.254185308	Activin A receptor, type I
TRAF1-AI400707-Correct	0.252257736	TNF receptor-associated factor 1
TNFAIP3-AA476272-Correct	0.213423453	Tumor necrosis factor, alpha-induced protein 3
GABRB1-R24969-NA	0.176398481	Gamma-aminobutyric acid (GABA) A receptor, beta 1
PDK3-N94823-NA	0.174838434	Pyruvate dehydrogenase kinase, isozyme 3
CSNK2A2-AA054996-NA	0.157859132	Casein kinase 2, alpha prime polypeptide
PSCDBP-AA490903-NA	0.153074099	Pleckstrin homology, Sec7 and coiled-coil domains, binding protein
BCL2A1-AA459491-NA	0.147524461	BCL2-related protein A1
RPS8-AA683050-NA	0.141527899	Ribosomal protein S8
FDFT1-AA679352-NA	0.130892462	Farnesyl-diphosphate farnesyltransferase 1
BRAF-NM_004333-Correct	0.128302606	V-raf murine sarcoma viral oncogene homolog B1
CDC16-AA223933-Correct	0.118105596	Cell division cycle 16 homolog (S. cerevisiae)
HBEGF-R14663-NA	0.104845784	Heparin-binding EGF-like growth factor
AMPD2-AA485376-NA	0.076493189	Adenosine monophosphate deaminase 2 (isoform L)
SLC7A5-AA419177-NA	0.072341094	Solute carrier family 7 (cationic amino acid transporter, y+ system), member 5
MKRN2-NM_014160-Correct	0.043158998	Makorin, ring finger protein, 2
YES1-AU133140-Correct	0.032784639	V-yes-1 Yamaguchi sarcoma viral oncogene homolog 1
COL8A1-AA872420-NA	0.027492282	Collagen, type VIII, alpha 1
TAGLN2-H08564-NA	0.01111442	Transgelin 2
VPS41-AA143559-NA	-0.008056382	Vacuolar protein sorting 41 (yeast)
GPC5-AA878391-NA	-0.031280141	Glypican 5
CNN1-AA398400-NA	-0.033496161	Calponin 1, basic, smooth muscle
ACTN3-AA196115-NA	-0.03747742	Actinin, alpha 3
NAPA-AA425754-NA	-0.050835765	N-ethylmaleimide-sensitive factor attachment protein, alpha

FLNB-AA486239-NA	-0.05456511	Filamin B, beta (actin binding protein 278)
FGF5-W46575-NA	-0.060378538	Fibroblast growth factor 5
KRT18-AA664179-Correct	-0.064074713	Keratin 18
GSTM2-AI761469-Correct	-0.071711925	Glutathione S-transferase M2 (muscle)
MDM2-AA687987-Correct	-0.083519302	Mdm2, transformed 3T3 cell double minute 2, p53 binding protein
RPL19-T81168-Correct	-0.093070306	Ribosomal protein L19
TOP1-AA232856-NA	-0.101802239	CS0DD001YF18 of Neuroblastoma Cot 50-normalized (human)
TNNI2-AA182927-NA	-0.103943392	Troponin I type 2 (skeletal, fast)
HSPA1B-AI452579-Correct	-0.112368837	Heat shock 70kDa protein 1B
SPP1-AA775616-NA	-0.119604186	Secreted phosphoprotein 1 (osteopontin, bone sialoprotein I, early T-lymphocyte activation1)
SPARC-H95960-NA	-0.120731656	Secreted protein, acidic, cysteine-rich (osteonectin)
SLC2A1-H58873-NA	-0.122332977	Solute carrier family 2 (facilitated glucose transporter), member 1
DKK3-AA425947-NA	-0.125518889	Dickkopf homolog 3 (Xenopus laevis)
NPTX1-H22481-NA	-0.126246684	Neuronal pentraxin I
CCT5-AA629692-NA	-0.13083686	Chaperonin containing TCP1, subunit 5 (epsilon)
HPRT1-N47312-NA	-0.135569792	Hypoxanthine phosphoribosyltransferase 1 (Lesch-Nyhan syndrome)
UNG-H15112-NA	-0.136294387	Uracil-DNA glycosylase
ELF3-AA433851-NA	-0.143933824	E74-like factor 3 (ets domain transcription factor, epithelial-specific)
KDEL2-AA486516-NA	-0.145089926	KDEL (Lys-Asp-Glu-Leu) endoplasmic reticulum protein retention receptor 2
FGB-T73858-NA	-0.148899688	Fibrinogen beta chain
MYH11-AA126989-NA	-0.153211225	Myosin, heavy chain 11, smooth muscle
AGRN-AA458878-Correct	-0.163154894	Agrin
CASP5-W60764-NA	-0.166763181	Caspase 5, apoptosis-related cysteine peptidase
EXT1-AA487582-NA	-0.171016381	Exostoses (multiple) 1
SFTPC-AA487571-NA	-0.172723876	Surfactant, pulmonary-associated protein C
AKR7A2-T62865-NA	-0.17501847	Aldo-keto reductase family 7, member A2 (aflatoxin aldehyde reductase)
PSMB1-T68824-NA	-0.177676421	Proteasome (prosome, macropain) subunit, beta type, 1
TM4SF8-AA287196-NA	-0.17968432	Tetraspanin 3
PROCR-T47442-NA	-0.185527391	Protein C receptor, endothelial (EPCR)
PTGS2-AA644211-Correct	-0.187718254	Prostaglandin-endoperoxide synthase 2 (prostaglandin G/H synthase and cyclooxygenase)
AHCY-AA485626-NA	-0.189514433	S-adenosylhomocysteine hydrolase
LY6E-AA865464-NA	-0.192244083	Lymphocyte antigen 6 complex, locus E
HIF1A-AA598526-NA	-0.192921318	Hypoxia-inducible factor 1, alpha subunit (basic helix-loop-helix transcription
GLIPR1-AA251930-NA	-0.195278836	GLI pathogenesis-related 1 (glioma)
DPH2L1-AA670380-NA	-0.196801196	DPH1 homolog (S. cerevisiae)
ADRBK1-R88247-NA	-0.205643597	Adrenergic, beta, receptor kinase 1
RAD51C-T64278-NA	-0.207389598	RAD51 homolog C (S. cerevisiae)
VIM-AA486321-NA	-0.209968024	Vimentin
MYL9-AA877166-NA	-0.215822586	Myosin, light chain 9, regulatory
GLS-AI383124-NA	-0.232242477	Glutaminase
MFGE8-AA449667-NA	-0.247700125	Milk fat globule-EGF factor 8 protein
ANXA1-H63161-NA	-0.248737714	Annexin A1
S100A11-AA464731-NA	-0.253362984	S100 calcium binding protein A11
ABP1-T46924-NA	-0.259683498	Amiloride binding protein 1 (amine oxidase (copper-containing))
CD99L2-AA490911-NA	-0.266786496	CD99 molecule-like 2
TEGT-AA629591-NA	-0.268291063	Testis enhanced gene transcript (BAX inhibitor 1)

CD151-AA443118-NA	-0.270874995	Tetraspanin 4
MYO1B-AA047778-NA	-0.271649219	Myosin IB
HNRPUL1-AA464198-NA	-0.276781552	Heterogeneous nuclear ribonucleoprotein U-like 1
MT1B-H72723-NA	-0.282911248	Metallothionein 1A (functional)
APP-W42849-NA	-0.303458533	Amyloid beta (A4) precursor protein (peptidase nexin-II, Alzheimer disease)
H1F0-W69399-NA	-0.305346965	H1 histone family, member 0
MT1G-H53340-NA	-0.313214954	Metallothionein 1G
TERF1-BF592946-Correct	-0.313986959	Telomeric repeat binding factor (NIMA-interacting) 1
TACSTD2-AA454810-NA	-0.314317586	Tumor-associated calcium signal transducer 2
MTCH2-BM666932-Correct	-0.319913341	Mitochondrial carrier homolog 2 (C. elegans)
FOS-BF855049-Correct	-0.329226428	V-fos FBJ murine osteosarcoma viral oncogene homolog
EMR3-W67173-NA	-0.349596152	Integrin, beta 1 (fibronectin receptor)
TFPI-T50282-NA	-0.353702584	Tissue factor pathway inhibitor (lipoprotein-associated coagulation inhibitor)
MT1F-T56281-NA	-0.358718803	Metallothionein 1A (functional)
APP-W42849-NA	-0.368451508	Amyloid beta (A4) precursor protein (peptidase nexin-II, Alzheimer disease)
PRODH-W76467-NA	-0.370196566	Proline dehydrogenase (oxidase) 1
ADH1B-W21470-NA	-0.372218693	Alcohol dehydrogenase 1C (class I), gamma polypeptide
TGFBI-R80636-NA	-0.384798991	Transforming growth factor, beta-induced, 68kDa
ANXA5-AA451895-NA	-0.391749279	Annexin A5
COL6A1-N28431-NA	-0.392221371	Collagen, type VI, alpha 1
EPHA2-H84480-NA	-0.393501765	EPH receptor A2
IFITM2-AA862371-NA	-0.39925843	Interferon induced transmembrane protein 2 (1-8D)
CYR61-AA777187-Correct	-0.402687332	Cysteine-rich, angiogenic inducer, 61
SPINT2-AA459039-NA	-0.403489896	Serine peptidase inhibitor, Kunitz type, 2
COL6A1-N28431-NA	-0.412790032	Collagen, type VI, alpha 1
TIMP2-AA486280-NA	-0.41579264	TIMP metalloproteinase inhibitor 2
AGXT-N57872-NA	-0.420107678	Alanine-glyoxylate aminotransferase
GTF2E1-AA455964-NA	-0.428164697	General transcription factor IIE, polypeptide 1, alpha 56kDa
MYL6-AA488346-NA	-0.446688618	Myosin, light chain 6, alkali, smooth muscle and non-muscle
NR4A1-W23937-NA	-0.449919916	Nuclear receptor subfamily 4, group A, member 1
TRIP-AA186427-NA	-0.452845555	TRAF interacting protein
PON3-T57140-NA	-0.453504617	Paraoxonase 3
AKR7A2-T62865-NA	-0.468043169	Aldo-keto reductase family 7, member A2 (aflatoxin aldehyde reductase)
RAD51C-T64278-NA	-0.468896042	RAD51 homolog C (S. cerevisiae)
EIF3S6-AA669674-NA	-0.469678828	Eukaryotic translation initiation factor 3, subunit 6 48kDa
S100A10-AA444051-NA	-0.474424648	S100 calcium binding protein A10
MT1B-H72723-NA	-0.512183189	Metallothionein 1A (functional)
ARID4A-AI206923-NA	-0.513011015	AT rich interactive domain 4A (RBP1-like)
NR4A1-W23937-NA	-0.547723819	Nuclear receptor subfamily 4, group A, member 1
POLR2L-AA873691-NA	-0.607278516	Polymerase (RNA) II (DNA directed) polypeptide L, 7.6kDa
FN1-AA742408-NA	-0.62559907	Fibronectin 1
TGFBI-AA633901-Correct	-0.653978191	Transforming growth factor, beta-induced, 68kDa
MYH11-AI357713-NA	-0.943433403	Interferon, alpha-inducible protein 6

Appendix-4: List of the 136 genes common to both microarray experiments. The clone ID shows the gene accession number and the sequencing result (correct/bad). The ratio between 11C/11E is shown (positive numbers show higher expression in the Tel+ than in the ALT+ and vice-versa). The most relevant genes for this study are highlighted in bold

BIBLIOGRAPHY

- Aaltonen, L.A., Peltomaki, P., Leach, F.S., Sistonen, P., Pylkkanen, L., Mecklin, J.P., Jarvinen, H., Powell, S.M., Jen, J. & Hamilton, S.R. 1993, "Clues to the pathogenesis of familial colorectal cancer", *Science (New York, N.Y.)*, vol. 260, no. 5109, pp. 812-816.
- Agrawal, D., Chen, T., Irby, R., Quackenbush, J., Chambers, A.F., Szabo, M., Cantor, A., Coppola, D. & Yeatman, T.J. 2002, "Osteopontin identified as lead marker of colon cancer progression, using pooled sample expression profiling", *J Natl Cancer Inst*, vol. 94, pp. 513-521.
- Ahn, B., Lee, J.W., Jung, H., Beck, G. & Bohr, V.A. 2009, "Mechanism of Werner DNA helicase: POT1 and RPA stimulates WRN to unwind beyond gaps in the translocating strand", *PLoS one*, vol. 4, no. 3, pp. e4673.
- Aisner, D.L., Wright, W.E. & Shay, J.W. 2002, "Telomerase regulation: not just flipping the switch", *Current opinion in genetics & development*, vol. 12, no. 1, pp. 80-85.
- Al-Wahiby S, Slijepcevic P. 2005 "Chromosomal aberrations involving telomeres in BRCA1 deficient human and mouse cell lines" *Cytogenet Genome Res.* vol. 109, no 4, pp 491-6.
- Alec J. Jeffreys, A. J., Tamaki, K., MacLeod, A., Monckton, D.G., Neil, D.L. & Armour, J.A.L. 1994, "Complex gene conversion events in germline mutation at human minisatellites", *Nature Genetics*, vol. 6, pp. 136-- 145.
- Alexander, M.K. & Zakian, V.A. 2003, "Rap1p telomere association is not required for mitotic stability of a C(3)TA(2) telomere in yeast", *The EMBO journal*, vol. 22, no. 7, pp. 1688-1696.
- Ali Hazratia, Marc Ramis-Castellortb, Sovan Sarkarc, Louise J. Barbera, Christopher J. Schofieldb, John A. Hartleya & Peter J. McHugh 2008, "Human SNM1A suppresses the DNA repair defects of yeast pso2 mutants.", *DNA Repair*, vol. 7, no. 2, pp. 230-238.
- Alitalo, K., Winqvist, R., Keski-Oja, J., Ilvonen, M., Saksela, K., Alitalo, R., Laiho, M., Knuutila, S. & De La Chapelle, A. 1985, "ACUTE MYELOGENOUS LEUKAEMIA WITH C-MYC AMPLIFICATION AND DOUBLE MINUTE CHROMOSOMES", *The Lancet*, vol. 326, no. 8463, pp. 1035-1039.
- Allshire RC., Dempster M. & Hastie ND. 1989, "Human telomeres contain at least three types of G-rich repeat distributed non-randomly", *Nucleic Acids Research*, vol. 17, no. 12, pp. 4611--27.
- Almeida, A., Paul, T.J., Magdelenat, H. & Radvanyi, F. 2004, "Gene expression analysis by real-time reverse transcription polymerase chain reaction: influence of tissue handling", *Anal Biochem*, vol. 328, pp. 101-108.
- Amiard, S., Doudeau, M., Pinte, S., Poulet, A., Lenain, C., Faivre-Moskalenko, C., Angelov, D., Hug, N., Vindigni, A., Bouvet, P., Paoletti, J., Gilson, E. & Giraud-Panis, M. 2007, "A topological mechanism for TRF2-enhanced strand invasion", vol. 14, no. 2, pp. 154.
- Andersen, C.L., Jensen, J.L. & Orntoft, T.F. 2004, "Normalization of Real-Time Quantitative Reverse Transcription-PCR Data: A Model-Based Variance Estimation Approach to Identify Genes Suited for Normalization, Applied to Bladder and Colon Cancer Data Sets", *Cancer research*, vol. 64, no. 15, pp. 5245-5250.
- Andreyeva, E.N., Belyaeva, E.S., Sameshin, V.F., Pokholkova, G.V. & Zhimulev, I.F. 2005, "Three distinct chromatin domains in telomere ends of polytene chromosomes in

- Drosophila melanogaster* Tel mutants", *Journal of cell science*, vol. 118, no. 23, pp. 5465-5477.
- Appelgren, H., Cederberg, H. & Rannug, U. 1997, " Mutations at the human minisatellite MS32 integrated in yeast occur with high frequency in meiosis and involve complex recombination events.
", *Molecular Genetics and Genomics*, vol. 256, pp. 7--17.
- Armour, J.A., Crosier, M. & Jeffreys, A.J. 1996, "Distribution of tandem repeat polymorphism within minisatellite MS621 (D5S110)", *Annals of Human Genetics*, vol. 60, no. Pt 1, pp. 11-20.
- Armour, J.A., Palla, R., Zeeuwen, P.L., den Heijer, M., Schalkwijk, J. & Hollox, E.J. 2007, "Accurate, high-throughput typing of copy number variation using paralogue ratios from dispersed repeats", *Nucleic acids research*, vol. 35, no. 3, pp. e19.
- Armour, J.A., Wong, Z., Wilson, V., Royle, N.J. & Jeffreys, A.J. 1989, "Sequences flanking the repeat arrays of human minisatellites: association with tandem and dispersed repeat elements", *Nucleic acids research*, vol. 17, no. 13, pp. 4925-4935.
- Atkinson, S.P., Hoare, S.F., Glasspool, R.M. & Keith, W.N. 2005, "Lack of telomerase gene expression in alternative lengthening of telomere cells is associated with chromatin remodeling of the hTR and hTERT gene promoters", *Cancer research*, vol. 65, no. 17, pp. 7585-7590.
- Auer, H., Lyianarachchi, S., Newsom, D., Klisovic, M.I., Marcucci, G. & Kornacker, K. 2003, "Chipping away at the chip bias: RNA degradation in microarray analysis", *Nat Genet*, vol. 35, pp. 292-293.
- Aumailley, M., Battaglia, C., Mayer, U., Reinhardt, D., Nischt, R., Timpl, R. & Fox, J.W. 1993, "Nidogen mediates the formation of ternary complexes of basement membrane components", *Kidney international*, vol. 43, no. 1, pp. 7-12.
- Azzalin, C.M., Reichenbach, P., Khorianti, L., Giulotto, E. & Lingner, J. 2007, "
Telomeric Repeat-Containing RNA and RNA Surveillance Factors at Mammalian Chromosome Ends
", *Science*, vol. 318, pp. 798.
- Badie, S., Liao, C., Thanasoula, M., Barber, P., Hill, M.A. & Tarsounas, M. 2009, "RAD51C facilitates checkpoint signaling by promoting CHK2 phosphorylation", *The Journal of cell biology*, vol. 185, no. 4, pp. 587-600.
- Bae, N.S. & Baumann, P. 2007, "A RAP1/TRF2 Complex Inhibits Nonhomologous End-Joining at Human Telomeric DNA Ends", *Molecular cell*, vol. 26, no. 3, pp. 323-334.
- Bai, Y. & Murnane, J.P. 2003, "Telomere instability in a human tumor cell line expressing a dominant-negative WRN protein", *Human genetics*, vol. 113, no. 4, pp. 337-347.
- Bailey, S.M., Brenneman, M.A. & Goodwin, E.H. 2004, "Frequent recombination in telomeric DNA may extend the proliferative life of telomerase-negative cells", *Nucleic acids research*, vol. 32, no. 12, pp. 3743-3751.
- Baird, D.M., Jeffreys, A.J. & Royle, N.J. 1995, "Mechanisms underlying telomere repeat turnover, revealed by hypervariable variant repeat distribution patterns in the human Xp/Yp telomere", *The EMBO journal*, vol. 14, no. 21, pp. 5433-5443.
- Barbosa, M.D., Nguyen, Q.A., Tchernev, V.T., Ashley, J.A., Detter, J.C., Blaydes, S.M., Brandt, S.J., Chotai, D., Hodgman, C., Solari, R.C., Lovett, M. & Kingsmore, S.F. 1996,

- "Identification of the homologous beige and Chediak-Higashi syndrome genes", *Nature*, vol. 382, no. 6588, pp. 262-265.
- Bardwell, P.D., Woo, C.J., Wei, K., Li, Z., Martin, A., Sack, S.Z., Parris, T., Edelman, W. & Scharff, M.D. 2004, "Altered somatic hypermutation and reduced class-switch recombination in exonuclease 1-mutant mice", *Nature immunology*, vol. 5, no. 2, pp. 224-229.
- Bassi, D.E., Cicco, L.D., Cenna, J., Litwin, S., Cukierman, E. & Klein-Szanto, A. 2005, "PACE4 expression in mouse basal keratinocytes results in basement membrane disruption and acceleration of tumor progression", *Cancer Res*, vol. 65, pp. 7310-7319.
- Batzer, M.A., Deininger, P.L., Hellmann-Blumberg, U., Jurka, J., Labuda, D., Rubin, C.M., Schmid, C.W., Zietkiewicz, E. & Zuckerkandl, E. 1996, "Standardized nomenclature for Alu repeats", *Journal of Molecular Evolution*, vol. 42, no. 1, pp. 3-6.
- Baumann, P. & Cech, T.R. 2001, "Pot1, the Putative Telomere End-Binding Protein in Fission Yeast and Humans", *Science*, vol. 292, no. 5519, pp. 1171-1175.
- Baumgartner, B.L. & Lundblad, V. 2005, "Telomere identity crisis. [Review] [31 refs]", *Genes & development*, vol. 19, no. 21, pp. 2522-2525.
- Baur, J.A., Zou, Y., Shay, J.W. & Wright, W.E. 2001, "Telomere Position Effect in Human Cells", *Science*, vol. 292, no. 5524, pp. 2075-2077.
- Bechard, L.H., Butuner, B.D., Masologites, G., McRae, W., Topcu, Z. & McEachern, M.J. 2008, "Mutant telomeric repeats in yeast can disrupt the negative regulation of recombination-mediated telomere maintenance and create an ALT-like phenotype", *Mol.Cell.Biol.*, .
- Bechter, O.E., Zou, Y., Shay, J.W. & Wright, W.E. 2003, "Homologous recombination in human telomerase-positive and ALT cells occurs with the same frequency", *EMBO reports*, vol. 4, no. 12, pp. 1138-1143.
- Bechter, O.E., Zou, Y., Walker, W., Wright, W.E. & Shay, J.W. 2004, "Telomeric recombination in mismatch repair deficient human colon cancer cells after telomerase inhibition", *Cancer research*, vol. 64, no. 10, pp. 3444-3451.
- Benetti, R., García-Cao, M. & Blasco, M.A. 2007, "Telomere length regulates the epigenetic status of mammalian telomeres and subtelomeres", *Nature Genetics*, vol. 39, pp. 243--250.
- Benetti, R., Gonzalo, S., Jaco, I., Schotta, G., Klatt, P., Jenuwein, T. & Blasco, M.A. 2007, "Suv4-20h deficiency results in telomere elongation and derepression of telomere recombination", *The Journal of Cell Biology*, .
- Berg, I., Neumann, R., Cederberg, H., Rannug, U. & Jeffreys, A.J. 2003, "Two modes of germline instability at human minisatellite MS1 (locus D1S7): complex rearrangements and paradoxical hyperdeletion", *American Journal of Human Genetics*, vol. 72, no. 6, pp. 1436-1447.
- Bertuch, A.A., Buckley, K. & Lundblad, V. 2003, "The way to the end matters--the role of telomerase in tumor progression.[comment]. [Review] [29 refs]", *Cell Cycle*, vol. 2, no. 1, pp. 36-38.
- Bertuch, A.A. & Lundblad, V. 2004, "EXO1 contributes to telomere maintenance in both telomerase-proficient and telomerase-deficient *Saccharomyces cerevisiae*", *Genetics*, vol. 166, no. 4, pp. 1651-1659.

- Bertuch, A.A. & Lundblad, V. 2003, "The Ku heterodimer performs separable activities at double-strand breaks and chromosome termini", *Molecular and cellular biology*, vol. 23, no. 22, pp. 8202-8215.
- Bhattacharyya, S., Keirse, J., Russell, B., Kavecansky, J., Lillard-Wetherell, K., Tahmaseb, K., Turchi, J.J. & Groden, J. 2009, "Telomerase-associated protein 1, HSP90, and topoisomerase IIalpha associate directly with the BLM helicase in immortalized cells using ALT and modulate its helicase activity using telomeric DNA substrates", *The Journal of biological chemistry*, vol. 284, no. 22, pp. 14966-14977.
- Bichara, M., Wagner, J. & Lambert, I.B. 2006, "Mechanisms of tandem repeat instability in bacteria", *Mutation Research/Fundamental and Molecular Mechanisms of Mutagenesis*, vol. 598, no. 1-2, pp. 144-163.
- Biederman, J., Yee, J. & Cortes, P. 2004, "Validation of internal control genes for gene expression analysis in diabetic glomerulosclerosis", *Kidney Int*, vol. 66, pp. 2308-2314.
- Binda, O., Roy, J. & Branton, P.E. 2006, "RBP1 Family Proteins Exhibit SUMOylation-Dependent Transcriptional Repression and Induce Cell Growth Inhibition Reminiscent of Senescence", *Molecular and cellular biology*, vol. 26, no. 5, pp. 1917-1931.
- Blackburn, E.H. 2001, "Switching and Signaling at the Telomere", *Cell*, vol. 106, no. 6, pp. 661-673.
- Blagoev, K.B. & Goodwin, E.H. 2008, "Telomere exchange and asymmetric segregation of chromosomes can account for the unlimited proliferative potential of ALT cell populations", *DNA Repair*, vol. 7, no. 2, pp. 199-204.
- Blanco, L. & Salas, M. 1996, "Relating structure to function in phi29 DNA polymerase", *The Journal of biological chemistry*, vol. 271, no. 15, pp. 8509-8512.
- Blanquicett, C., Johnson, M.R., Heslin, M. & Diasio, R.B. 2002, "Housekeeping gene variability in normal and carcinomatous colorectal and liver tissues: applications in pharmacogenomic gene expression studies", *Anal Biochem*, vol. 303, pp. 209-214.
- Blasco MA., Lee HW., Hande MP., Samper E., Lansdorp PM., DePinho RA. & Greider CW. 1997, "Telomere shortening and tumor formation by mouse cells lacking telomerase RNA", *Cell*, vol. 91(1), pp. 25--34.
- Blasco MA, FAU - Rizen, M., Rizen M, FAU - Greider, C.W., Greider CW, FAU - Hanahan, D. & Hanahan D "Differential regulation of telomerase activity and telomerase RNA during multi-stage tumorigenesis.", - *Nat Genet.*1996 Feb;12(2):200-4., , no. 1061-4036 (Print).
- Blasco, M.A. 2002, "Telomerase beyond telomeres", *Nature Reviews.Cancer*, vol. 2, no. 8, pp. 627-633.
- Blessing, W.D., Stolier, A.J., Teng, S.C., Bolton, J.S. & Fuhrman, G.M. 2002, "A comparison of methylene blue and lymphazurin in breast cancer sentinel node mapping", *American Journal of Surgery*, vol. 184, no. 4, pp. 341-345.
- Bode-Boger, S.M., Scalera, F. & Martens-Lobenhoffer, J. 2005, "Asymmetric dimethylarginine (ADMA) accelerates cell senescence", *Vascular Medicine*, vol. 10, no. SUPPL. 1, pp. S65-S71.
- Bodnar, A.G., Ouellette, M., Frolkis, M., Holt, S.E., Chiu, C., Morin, G.B., Harley, C.B., Shay, J.W., Lichtsteiner, S. & Wright, W.E. 1998, "Extension of Life-Span by Introduction of Telomerase into Normal Human Cells", *Science*, vol. 279, no. 5349, pp. 349-352.

- Bois, P., Collick, A., Brown, J. & Jeffreys, A.J. 1997, "Human minisatellite MS32 (D1S8) displays somatic but not germline instability in transgenic mice", *Human molecular genetics*, vol. 6, no. 9, pp. 1565-1571.
- Bois, P. & Jeffreys, A.J. 1999, "Minisatellite instability and germline mutation", *Cellular and molecular life sciences : CMLS*, vol. 55, no. 12, pp. 1636-1648.
- Bollati, V., Fabris, S., Pegoraro, V., Ronchetti, D., Mosca, L., Deliliers, G.L., Motta, V., Bertazzi, P.A., Baccarelli, A. & Neri, A. 2009, "Differential repetitive DNA methylation in multiple myeloma molecular subgroups", *Carcinogenesis*, vol. 30, no. 8, pp. 1330-1335.
- Bonafe, M., Salvioli, S., Barbi, C., Mishto, M., Trapassi, C., Gemelli, C., Storci, G., Olivieri, F., Monti, D. & Franceschi, C. 2002, "P53 Codon 72 Genotype Affects Apoptosis by Cytosine Arabinoside in Blood Leukocytes", *Biochemical and biophysical research communications*, vol. 299, no. 4, pp. 539-541.
- Bonafe, M., Salvioli, S., Barbi, C., Trapassi, C., Tocco, F., Storci, G., Invidia, L., Vannini, I., Rossi, M., Marzi, E., Mishto, M., Capri, M., Olivieri, F., Antonicelli, R., Memo, M., Uberti, D., Nacmias, B., Sorbi, S., Monti, D. & Franceschi, C. 2004, "The different apoptotic potential of the p53 codon 72 alleles increases with age and modulates in vivo ischaemia-induced cell death", *Cell death and differentiation*, vol. 11, no. 9, pp. 962-973.
- Bradshaw, P.S., Stavropoulos, D.J. & Meyn, M.S. 2005, "Human telomeric protein TRF2 associates with genomic double-strand breaks as an early response to DNA damage", *Nature genetics*, vol. 37, no. 2, pp. 193-197.
- Brinkhof, B., Spee, B., Rothuizen, J. & Penning, L.C. 2006, "Development and evaluation of canine reference genes for accurate quantification of gene expression", *Anal Biochem*, vol. 356, pp. 36-43.
- Britten, R.J. & Kohne, D.E. 1968, "Repeated sequences in DNA. Hundreds of thousands of copies of DNA sequences have been incorporated into the genomes of higher organisms", *Science (New York, N.Y.)*, vol. 161, no. 841, pp. 529-540.
- Bruckert, P., Kappler, R., Scherthan, H., Link, H., Hagmann, F. & Zankl, H. 2000, "Double Minutes and c-MYC Amplification in Acute Myelogenous Leukemia: Are They Prognostic Factors?", *Cancer genetics and cytogenetics*, vol. 120, no. 1, pp. 73-79.
- Bryan, T.M., Englezou, A., Dalla-Pozza, L., Dunham, M.A. & Reddel, R.R. 1997, "Evidence for an alternative mechanism for maintaining telomere length in human tumors and tumor-derived cell lines.[see comment]", *Nature medicine*, vol. 3, no. 11, pp. 1271-1274.
- Bryan, T.M., Englezou, A., Dunham, M.A. & Reddel, R.R. 1998, "Telomere length dynamics in telomerase-positive immortal human cell populations", *Experimental cell research*, vol. 239, no. 2, pp. 370-378.
- Bryan, T.M., Englezou, A., Gupta, J., Bacchetti, S. & Reddel, R.R. 1995, "Telomere elongation in immortal human cells without detectable telomerase activity", *EMBO Journal*, vol. 14, no. 17, pp. 4240-4248.
- Bryan, T.M. & Reddel, R.R. 1997, "Telomere dynamics and telomerase activity in in vitro immortalised human cells", *European Journal of Cancer Part A*, vol. 33, no. 5, pp. 767-773.
- Buard, J., Barthes, P., Grey, C. & de Massy, B. 2009, "Distinct histone modifications define initiation and repair of meiotic recombination in the mouse", *The EMBO journal*, vol. 28, no. 17, pp. 2616-2624.

- Buard, J., Bourdet, A., Yardley, J., Dubrova, Y. & Jeffreys, A.J. 1998, "Influences of array size and homogeneity on minisatellite mutation", *The EMBO journal*, vol. 17, no. 12, pp. 3495-3502.
- Buard, J., Collick, A., Brown, J. & Jeffreys, A.J. 2000, "Somatic versus germline mutation processes at minisatellite CEB1 (D2S90) in humans and transgenic mice", *Genomics*, vol. 65, no. 2, pp. 95-103.
- Buard, J., Shone, A.C. & Jeffreys, A.J. 2000, "Meiotic recombination and flanking marker exchange at the highly unstable human minisatellite CEB1 (D2S90)", *American Journal of Human Genetics*, vol. 67, no. 2, pp. 333-344.
- Buard, J. & Vergnaud, G. 1994, "Complex recombination events at the hypermutable minisatellite CEB1 (D2S90)", *The EMBO journal*, vol. 13, no. 13, pp. 3203-3210.
- Bukowy, Z., Harrigan, J.A., Ramsden, D.A., Tudek, B., Bohr, V.A. & Stevnsner, T. 2008, "WRN Exonuclease activity is blocked by specific oxidatively induced base lesions positioned in either DNA strand", *Nucleic acids research*, vol. 36, no. 15, pp. 4975-4987.
- Bustin, S.A. 2002, "Quantification of mRNA using real-time reverse transcription PCR (RT-PCR): trends and problems", *J Mol Endocrinol*, vol. 29, pp. 23-39.
- Bustin, S.A. 2000, "Absolute quantification of mRNA using real-time reverse transcription polymerase chain reaction assays", *J Mol Endocrinol*, vol. 25, pp. 169-193.
- Bustin, S.A., Benes, V., Nolan, T. & Pfaffl, M.W. 2005, "Quantitative real-time RT-PCR--a perspective", *J Mol Endocrinol*, vol. 34, pp. 597-601.
- Bustin, S.A. & Nolan, T. 2004, "Pitfalls of quantitative real-time reverse-transcription polymerase chain reaction", *J Biomol Tech*, vol. 15, pp. 155-166.
- Cabuy E, Newton C, Slijepcevic P. 2008 "BRCA1 knock-down causes telomere dysfunction in mammary epithelial cells." *Cytogenet Genome Res. Col.* 122, pp 336-42
- Cadioux, B., Ching, T., VandenBerg, S.R. & Costello, J.F. 2006, "Genome-wide Hypomethylation in Human Glioblastomas Associated with Specific Copy Number Alteration, Methylenetetrahydrofolate Reductase Allele Status, and Increased Proliferation", *Cancer research*, vol. 66, no. 17, pp. 8469-8476.
- Capper, R., Britt-Compton, B., Tankimanova, M., Rowson, J., Letsolo, B., Man, S., Haughton, M. & Baird, D.M. 2007, "The nature of telomere fusion and a definition of the critical telomere length in human cells", *Genes and Development*, vol. 21, no. 19, pp. 2495-2508.
- Carrera, C.J., Eddy, R.L., Shows, T.B. & Carson, D.A. 1984, "Assignment of the gene for methylthioadenosine phosphorylase to human chromosome 9 by mouse-human somatic cell hybridization", *Proceedings of the National Academy of Sciences of the United States of America*, vol. 81, no. 9, pp. 2665-2668.
- Cavazos, D., Deming, B., Montellano, R. & Marciniak, R.A. 2003, ""Type I" ALT telomere maintenance in a human cell line", *Cancer Epidemiology Biomarkers & Prevention*, vol. 12, no. 11, pp. 1306S-1307S.
- Celli, G.B., Denchi, E.L. & de Lange, T. 2006, "Ku70 stimulates fusion of dysfunctional telomeres yet protects chromosome ends from homologous recombination", vol. 8, no. 8, pp. 890.

- Cerone MA, Londono-Vallejo JA, Bacchetti S 2001, "Telomere maintenance by telomerase and by recombination can coexist in human cells", *Human molecular genetics*, vol. 10, no. 18, pp. 1945-1952.
- Cerone, M.A., Autexier, C., Londono-Vallejo, J.A. & Bacchetti, S. 2005, "A human cell line that maintains telomeres in the absence of telomerase and of key markers of ALT", *Oncogene*, vol. 24, no. 53, pp. 7893-7901.
- Cesare, A.J. & Griffith, J.D. 2004, "Telomeric DNA in ALT cells is characterized by free telomeric circles and heterogeneous t-loops", *Molecular & Cellular Biology*, vol. 24, no. 22, pp. 9948-9957.
- Chai, W., Du, Q., Shay, J.W. & Wright, W.E. 2006, "Human Telomeres Have Different Overhang Sizes at Leading versus Lagging Strands", *Molecular cell*, vol. 21, no. 3, pp. 427-435.
- Chaillet, J.R. 1994, "Genomic imprinting: lessons from mouse transgenes", *Mutation research*, vol. 307, no. 2, pp. 441-449.
- Chang, S., Khoo, C.M., Naylor, M.L., Maser, R.S. & DePinho, R.A. 2003, "Telomere-based crisis: Functional differences between telomerase activation and ALT in tumor progression", *Genes & development*, vol. 17, no. 1, pp. 88-100.
- Charbonnier, F., Raux, G., Wang, Q., Drouot, N., Cordier, F., Limacher, J., Saurin, J., Puisieux, A., Olschwang, S. & Frebourg, T. 2000, "Detection of Exon Deletions and Duplications of the Mismatch Repair Genes in Hereditary Nonpolyposis Colorectal Cancer Families Using Multiplex Polymerase Chain Reaction of Short Fluorescent Fragments", *Cancer research*, vol. 60, no. 11, pp. 2760-2763.
- Chen, Q., Ijzerman, A. & Greider, C.W. 2001, "Two survivor pathways that allow growth in the absence of telomerase are generated by distinct telomere recombination events", *Molecular & Cellular Biology*, vol. 21, no. 5, pp. 1819-1827.
- Chen, Y.C., Su, Y.N., Chou, P.C., Chiang, W.C., Chang, M.C., Wang, L.S., Teng, S.C. & Wu, K.J. 2005, "Overexpression of NBS1 contributes to transformation through the activation of phosphatidylinositol 3-kinase/Akt", *Journal of Biological Chemistry*, vol. 280, no. 37, pp. 32505-32511.
- Chen, Y., Hakin-Smith, V., Teo, M., Xinarianos, G.E., Jellinek, D.A., Carroll, T., McDowell, D., MacFarlane, M.R., Boet, R., Baguley, B.C., Braithwaite, A.W., Reddel, R.R. & Royds, J.A. 2006, "Association of Mutant TP53 with Alternative Lengthening of Telomeres and Favorable Prognosis in Glioma", *Cancer Research*, vol. 66, no. 13, pp. 6473-6476.
- Cheng, W.H., Muftic, D., Muftuoglu, M., Dawut, L., Morris, C., Helleday, T., Shiloh, Y. & Bohr, V.A. 2008, "WRN is required for ATM activation and the S-phase checkpoint in response to interstrand cross-link-induced DNA double-strand breaks", *Molecular biology of the cell*, vol. 19, no. 9, pp. 3923-3933.
- Cheng, W.H., Muftuoglu, M. & Bohr, V.A. 2007, "Werner syndrome protein: functions in the response to DNA damage and replication stress in S-phase", *Experimental gerontology*, vol. 42, no. 9, pp. 871-878.
- Chiang, Y.C., Teng, S.C., Su, Y.N., Hsieh, F.J. & Wu, K.J. 2003, "c-Myc directly regulates the transcription of the NBS1 gene involved in DNA double-strand break repair.[erratum appears in J Biol Chem. 2004 Apr 16;279(16):16894]", *Journal of Biological Chemistry*, vol. 278, no. 21, pp. 19286-19291.
- Chin, L., Pomerantz, J. & DePinho, R.A. 1998, "The INK4a/ARF tumor suppressor: one gene—two products—two pathways", *Trends in biochemical sciences*, vol. 23, no. 8, pp. 291-296.

- Choi, S.H., Worswick, S., Byun, H.M., Shear, T., Soussa, J.C., Wolff, E.M., Douer, D., Garcia-Manero, G., Liang, G. & Yang, A.S. 2009, "Changes in DNA methylation of tandem DNA repeats are different from interspersed repeats in cancer", *International journal of cancer. Journal internationale du cancer*, vol. 125, no. 3, pp. 723-729.
- Cleton-Jansen, A.-., Buerger, H. & Hogendoorn, P.C.W. 2005, "Central high-grade osteosarcoma of bone: Diagnostic and genetic considerations", *Current Diagnostic Pathology*, vol. 11, no. 6, pp. 390-399.
- Cohen, S., Regev, A. & Lavi, S. 1997, "Small polydispersed circular DNA (spcDNA) in human cells: association with genomic instability", *Oncogene*, vol. 14, no. 8, pp. 977-985.
- Cohen, Z., Bacharach, E. & Lavi, S. 2006, "Mouse major satellite DNA is prone to eccDNA formation via DNA Ligase IV-dependent pathway", *Oncogene*, vol. 25, no. 33, pp. 4515-4524.
- Collick, A., Dunn, M.G. & Jeffreys, A.J. 1991, "Minisatellite binding protein Msbp-1 is a sequence-specific single-stranded DNA-binding protein", *Nucleic acids research*, vol. 19, no. 23, pp. 6399-6404.
- Collick, A., Norris, M.L., Allen, M.J., Bois, P., Barton, S.C., Surani, M.A. & Jeffreys, A.J. 1994, "Variable germline and embryonic instability of the human minisatellite MS32 (D1S8) in transgenic mice", *The EMBO journal*, vol. 13, no. 23, pp. 5745-5753.
- Collins, K. 2000, "Mammalian telomeres and telomerase. [Review] [47 refs]", *Current opinion in cell biology*, vol. 12, no. 3, pp. 378-383.
- Collins, K. & Mitchell, J.R. 2002, "Telomerase in the human organism. [Review] [150 refs]", *Oncogene*, vol. 21, no. 4, pp. 564-579.
- Compton, S.A., Tolun, G., Kamath-Loeb, A.S., Loeb, L.A. & Griffith, J.D. 2008, "The Werner syndrome protein binds replication fork and holliday junction DNAs as an oligomer", *The Journal of biological chemistry*, vol. 283, no. 36, pp. 24478-24483.
- Compton, S.A., Choi, J., Cesare, A.J., Ozgur, S. & Griffith, J.D. 2007, "Xrcc3 and Nbs1 Are Required for the Production of Extrachromosomal Telomeric Circles in Human Alternative Lengthening of Telomere Cells", *Cancer Research*, vol. 67, no. 4, pp. 1513-1519.
- Cooper, J.P., Nimmo, E.R., Allshire, R.C. & Cech, T.R. 1997, "Regulation of telomere length and function by a Myb-domain protein in fission yeast", *Nature*, vol. 385, no. 6618, pp. 744-747.
- Costa, A., Daidone, M.G., Daprai, L., Villa, R., Cantu, S., Pilotti, S., Mariani, L., Gronchi, A., Henson, J.D., Reddel, R.R. & Zaffaroni, N. 2006, "Telomere Maintenance Mechanisms in Liposarcomas: Association with Histologic Subtypes and Disease Progression", *Cancer Research*, vol. 66, no. 17, pp. 8918-8924.
- Crabbe, L., Jauch, A., Naeger, C.M., Holtgreve-Grez, H. & Karlseder, J. 2007, "Telomere dysfunction as a cause of genomic instability in Werner syndrome", *Proceedings of the National Academy of Sciences of the United States of America*, vol. 104, no. 7, pp. 2205-2210.
- Crabbe, L., Verdun, R.E., Haggblom, C.I. & Karlseder, J. 2004, "Defective telomere lagging strand synthesis in cells lacking WRN helicase activity", *Science (New York, N.Y.)*, vol. 306, no. 5703, pp. 1951-1953.
- d'Adda di Fagagna F, FAU - Reaper, P.M., Reaper PM, FAU - Clay-Farrace, L., Clay-Farrace L, FAU - Fiegler, H., Fiegler H, FAU - Carr, P., Carr P, FAU - Von Zglinicki, T., Von Zglinicki T, FAU - Saretzki, G., Saretzki G, FAU - Carter, N.P., Carter NP, FAU - Jackson, S.P. &

- Jackson SP "A DNA damage checkpoint response in telomere-initiated senescence.", - *Nature*.2003 Nov 13;426(6963):194-8.Epub 2003 Nov 5., , no. 1476-4687 (Electronic).
- De Cian, A., Lacroix, L., Douarre, C., Temime-Smaali, N., Trentesaux, C., Riou, J. & Mergny, J. 2008, "Targeting telomeres and telomerase", *Biochimie*, vol. 90, no. 1, pp. 131-155.
- de Kok, J., Roelofs, R.W., Giesendorf, B.A., Pennings, J.L., Waas, E.T., Feuth, T., Swinkels, D.W. & Span, P.N. 2005, "Normalization of gene expression measurements in tumor tissues: comparison of 13 endogenous control genes", *Lab Invest*, vol. 85, pp. 154-159.
- de Lange, T. 2005, "Shelterin: the protein complex that shapes and safeguards human telomeres. [Review] [84 refs]", *Genes & development*, vol. 19, no. 18, pp. 2100-2110.
- de Lange, T. 2004, "T-loops and the origin of telomeres.[erratum appears in Nat Rev Mol Cell Biol. 2004 Jun;5(6):492]. [Review] [47 refs]", *Nature Reviews Molecular Cell Biology*, vol. 5, no. 4, pp. 323-329.
- de Lange, T. 2002, "Protection of mammalian telomeres. [Review] [80 refs]", *Oncogene*, vol. 21, no. 4, pp. 532-540.
- de Lange, T. 1998, "Length control of human telomeres", *Cancer Journal From Scientific American*, vol. 4, no. Suppl 1, pp. S22-5.
- de Lange, T. & Jacks, T. 1999, "For better or worse? Telomerase inhibition and cancer. [Review] [21 refs]", *Cell*, vol. 98, no. 3, pp. 273-275.
- de Lange, T. & Petrini, J.H. 2000, "A new connection at human telomeres: association of the Mre11 complex with TRF2. [Review] [87 refs]", *Cold Spring Harbor symposia on quantitative biology*, vol. 65, pp. 265-273.
- Debrauwere, H., Gendrel, C.G., Lechat, S. & Dutreix, M. 1997, "Differences and similarities between various tandem repeat sequences: Minisatellites and microsatellites", *Biochimie*, vol. 79, no. 9-10, pp. 577-586.
- Dedhar, S., Jewell, K., Rojiani, M. & Gray, V. 1992, "The receptor for the basement membrane glycoprotein entactin is the integrin alpha 3/beta 1", *J Biol Chem*, vol. 267, pp. 18908-18914.
- Denchi, E.L. & de Lange, T. 2007, "Protection of telomeres through independent control of ATM and ATR by TRF2 and POT1", vol. 448, no. 7157, pp. 1071.
- Deng, Z., Dheekollu, J., Broccoli, D., Dutta, A. & Lieberman, P.M. 2007, "The Origin Recognition Complex Localizes to Telomere Repeats and Prevents Telomere-Circle Formation", *Current Biology*, vol. 17, no. 22, pp. 1989-1995.
- Dheda, K., Huggett, J.F., Chang, J.S., Kim, L.U., Bustin, S.A., Johnson, M.A., Rook, G.A. & Zumla, A. 2005, "The implications of using an inappropriate reference gene for real-time reverse transcription PCR data normalization", *Anal Biochem*, vol. 344, pp. 141-143.
- Ding, S., Larson, G.P., Foldenauer, K., Zhang, G. & Krontiris, T.G. 1999, "Distinct mutation patterns of breast cancer-associated alleles of the HRAS1 minisatellite locus", *Human molecular genetics*, vol. 8, no. 3, pp. 515-521.
- Djojosebroto, M.W., Chin, A.C., Go, N., Schaetzlein, S., Manns, M.P., Gryaznov, S., Harley, C.B. & Rudolph, K.L. 2005, "Telomerase antagonists GRN163 and GRN163L inhibit tumor growth and increase chemosensitivity of human hepatoma", *Hepatology*, vol. 42, no. 5, pp. 1127-1136.

- Dobbin, K. & Simon, R. 2002, "Comparison of microarray designs for class comparison and class discovery", *Bioinformatics*, vol. 18, no. 11, pp. 1438-1445.
- Dong, L.J., Hsieh, J.C. & Chung, A.E. 1995, "Two distinct cell attachment sites in entactin are revealed by amino acid substitutions and deletion of the RGD sequence in the cysteine-rich epidermal growth factor repeat 2", *J Biol Chem*, vol. 270, pp. 15838-15843.
- Dong, Y.P., Seki, M., Yoshimura, A., Inoue, E., Furukawa, S., Tada, S. & Enomoto, T. 2007, "WRN functions in a RAD18-dependent damage avoidance pathway", *Biological & pharmaceutical bulletin*, vol. 30, no. 6, pp. 1080-1083.
- Draskovic I, Arnoult N, Steiner V, Bacchetti S, Lomonte P & Londono-Vallejo A "Probing PML body function in ALT cells reveals spatiotemporal requirements for telomere recombination.", - *Proc Natl Acad Sci U S A*.2009 Aug 26., , no. 1091-6490 (Electronic).
- Du, C.W., Wen, B.G., Li, D.R., Lin, Y.C., Zheng, Y.W., Chen, L., Chen, J.Y., Lin, W. & Wu, M.Y. 2005, "Latent membrane protein-1 of Epstein-Barr virus increases sensitivity to arsenic trioxide-induced apoptosis in nasopharyngeal carcinoma cell", *Experimental Oncology*, vol. 27, no. 4, pp. 267-272.
- Dubrova, Y.E., Jeffreys, A.J. & Malashenko, A.M. 1993, "Mouse minisatellite mutations induced by ionizing radiation", *Nature genetics*, vol. 5, no. 1, pp. 92-94.
- Dubrova, Y.E., Nesterov, V.N., Krouchinsky, N.G., Ostapenko, V.A., Neumann, R., Neil, D.L. & Jeffreys, A.J. 1996, "Human minisatellite mutation rate after the Chernobyl accident", *Nature*, vol. 380, no. 6576, pp. 683-686.
- Dubrova, Y.E., Plumb, M., Brown, J., Boulton, E., Goodhead, D. & Jeffreys, A.J. 2000, "Induction of minisatellite mutations in the mouse germline by low-dose chronic exposure to gamma-radiation and fission neutrons", *Mutation research*, vol. 453, no. 1, pp. 17-24.
- Dumont, P., Leu, J.I., Della Pietra, A.C., 3rd, George, D.L. & Murphy, M. 2003, "The codon 72 polymorphic variants of p53 have markedly different apoptotic potential", *Nature genetics*, vol. 33, no. 3, pp. 357-365.
- Dunham, M.A., Neumann, A.A., Fasching, C.L. & Reddel, R.R. 2000, "Telomere maintenance by recombination in human cells", *Nature Genetics*, vol. 26(4):, pp. 447--50.
- Dziadek, M. 1995, "Role of laminin-nidogen complexes in basement membrane formation during embryonic development", *Experientia*, vol. 51, pp. 901-913.
- Ehrlich, M., Woods, C.B., Yu, M.C., Dubeau, L., Yang, F., Campan, M., Weisenberger, D.J., Long, T., Youn, B., Fiala, E.S. & Laird, P.W. 2006, "Quantitative analysis of associations between DNA hypermethylation, hypomethylation, and DNMT RNA levels in ovarian tumors", *Oncogene*, vol. 25, no. 18, pp. 2636-2645.
- Eklom, P., Eklom, M., Fecker, L., Klein, G., Zhang, H.Y., Kadoya, Y., Chu, M.L., Mayer, U. & Timpl, R. 1994, "Role of mesenchymal nidogen for epithelial morphogenesis in vitro", *Development*, vol. 120, pp. 2003-2014.
- Ellsworth, D.L., Shriver, M.D. & Boerwinkle, E. 1995, "Nucleotide sequence analysis of the apolipoprotein B 3' VNTR", *Human molecular genetics*, vol. 4, no. 5, pp. 937-944.
- Enomoto T. 2001, " Functions of RecQ family helicases: possible involvement of Bloom's and Werner's syndrome gene products in guarding genome integrity during DNA replication.", *J Biochem (Tokyo)*, vol. 129, pp. 501-507.

- Fajkus, J., Sykorova, E. & Leitch, A.R. 2005, "Telomeres in evolution and evolution of telomeres", *Chromosome Research*, vol. 13, no. 5, pp. 469-479.
- Fan, Q., Zhang, F., Barrett, B., Ren, K. & Andreassen, P.R. 2009, "A role for monoubiquitinated FANCD2 at telomeres in ALT cells", *Nucl.Acids Res.*, .
- Farkas, E.A., Stolier, A.J., Teng, S.C., Bolton, J.S. & Fuhrman, G.M. 2004, "An argument against routine sentinel node mapping for DCIS", *American Surgeon*, vol. 70, no. 1, pp. 13-17.
- Fasching, C.L., Bower, K. & Reddel, R.R. 2005, "Telomerase-independent telomere length maintenance in the absence of alternative lengthening of telomeres-associated promyelocytic leukemia bodies", *Cancer research*, vol. 65, no. 7, pp. 2722-2729.
- Fasching, C.L., Neumann, A.A., Muntoni, A., Yeager, T.R. & Reddel, R.R. 2007, "DNA Damage Induces Alternative Lengthening of Telomeres (ALT) Associated Promyelocytic Leukemia Bodies that Preferentially Associate with Linear Telomeric DNA", *Cancer Research*, vol. 67, no. 15, pp. 7072-7077.
- Ferguson, B.M. & Fangman, W.L. 1992, "A position effect on the time of replication origin activation in yeast", *Cell*, vol. 68, no. 2, pp. 333-339.
- Feuk, L., Marshall, C.R., Wintle, R.F. & Scherer, S.W. 2006, "Structural variants: changing the landscape of chromosomes and design of disease studies", *Human molecular genetics*, vol. 15 Spec No 1, pp. R57-66.
- Ford, L.P., Zou, Y., Pongracz, K., Gryaznov, S.M., Shay, J.W. & Wright, W.E. 2001, "Telomerase can inhibit the recombination-based pathway of telomere maintenance in human cells", *Journal of Biological Chemistry*, vol. 276, no. 34, pp. 32198-32203.
- Fox, J.W., Mayer, U., Nischt, R., Aumailley, M., Reinhardt, D., Wiedemann, H., Mann, K., Timpl, R., Krieg, T. & Engel, J. 1991, "Recombinant nidogen consists of three globular domains and mediates binding of laminin to collagen type IV", *Embo J*, vol. 10, pp. 3137-3146.
- Frater, J.L., Hoover, R.G., Bernreuter, K. & Batanian, J.R. 2006, "Deletion of MYC and presence of double minutes with MYC amplification in a morphologic acute promyelocytic leukemia-like case lacking RARA rearrangement: could early exclusion of double-minute chromosomes be a prognostic factor?", *Cancer genetics and cytogenetics*, vol. 166, no. 2, pp. 139-145.
- Freudenreich, C.H., Kantrow, S.M. & Zakian, V.A. 1998, "Expansion and Length-Dependent Fragility of CTG Repeats in Yeast", *Science*, vol. 279, no. 5352, pp. 853-856.
- Frommer, M., McDonald, L.E., Millar, D.S., Collis, C.M., Watt, F., Grigg, G.W., Molloy, P.L. & Paul, C.L. 1992, "A genomic sequencing protocol that yields a positive display of 5-methylcytosine residues in individual DNA strands", *Proceedings of the National Academy of Sciences of the United States of America*, vol. 89, no. 5, pp. 1827-1831.
- Fry M, FAU - Loeb, L.A. & Loeb LA "Human werner syndrome DNA helicase unwinds tetrahelical structures of the fragile X syndrome repeat sequence d(CGG)n.", - *J Biol Chem*.1999 Apr 30;274(18):12797-802., , no. 0021-9258 (Print).
- Fujiwara, M., Kamma, H., Wu, W., Hamasaki, M., Kaneko, S., Horiguchi, H., Matsui-Horiguchi, M. & Satoh, H. 2004, "Expression and alternative splicing pattern of human telomerase reverse transcriptase in human lung cancer cells", *International journal of oncology*, vol. 24, no. 4, pp. 925-930.
- Gagos, S., Chiourea, M., Christodoulidou, A., Apostolou, E., Raftopoulou, C., Deustch, S., Jefford, C., Irminger-Finger, I., Shay, J.W. & Antonarakis, S.E. 2008, "Pericentromeric

- Instability and Spontaneous Emergence of Human Neoacrocentric and Minute Chromosomes in the Alternative Pathway of Telomere Lengthening", *Cancer Res*, vol. 68, no. 19, pp. 8146-8155.
- Galkina, S., Lukina, N., Zakharova, K. & Rodionov, A.V. 2005, "Interstitial (TTAGGG)(n) sequences are not hot spots of recombination in the chicken lampbrush macrochromosomes 1-3", *Chromosome Research*, vol. 13, no. 6, pp. 551-557.
- Garcia-Cao, M., O'Sullivan, R., Peters, A.H., Jenuwein, T. & Blasco, M.A. 2004, "Epigenetic regulation of telomere length in mammalian cells by the Suv39h1 and Suv39h2 histone methyltransferases", *Nature genetics*, vol. 36, no. 1, pp. 94-99.
- Gasser, S.M., Hediger, F., Taddei, A., Neumann, F.R. & Gartenberg, M.R. 2004, "The function of telomere clustering in yeast: The circe effect", *Cold Spring Harbor symposia on quantitative biology*, vol. 69, pp. 327-337.
- Gaubatz, J.W. 1990, "Extrachromosomal circular DNAs and genomic sequence plasticity in eukaryotic cells", *Mutation research*, vol. 237, no. 5-6, pp. 271-292.
- Giannini, G., Rinaldi, C., Ristori, E., Ambrosini, M.I., Cerignoli, F., Viel, A., Bidoli, E., Berni, S., D'Amati, G., Scambia, G., Frati, L., Screpanti, I. & Gulino, A. 2004, "Mutations of an intronic repeat induce impaired MRE11 expression in primary human cancer with microsatellite instability", *Oncogene*, vol. 23, no. 15, pp. 2640-2647.
- Gicquel, C., Rossignol, S., Cabrol, S., Houang, M., Steunou, V., Barbu, V., Danton, F., Thibaud, N., Le Merrer, M., Burglen, L., Bertrand, A.-., Netchine, I. & Le Bouc, Y. 2005, "Epimutation of the telomeric imprinting center region on chromosome 11p15 in Silver-Russell syndrome", *Nature genetics*, vol. 37, no. 9, pp. 1003-1007.
- Gilson, E. & Géli, V. 2007, "How telomeres are replicated", *Nature Reviews Molecular Cell Biology*, vol. 8.
- Glare, E.M., Divjak, M., Bailey, M.J. & Walters, E.H. 2002, "beta-Actin and G3PDH housekeeping gene expression in asthmatic airways is variable and not suitable for normalising mRNA levels", *Thorax*, vol. 57, pp. 765-770.
- Gonzalo, S., Jaco, I., Fraga, M.F., Chen, T., Li, E., Esteller, M. & Blasco, M.A. 2006, "DNA methyltransferases control telomere length and telomere recombination in mammalian cells", *Nature Cell Biology*, vol. 8, pp. 416-- 424.
- Gottschling, D.E., Aparicio, O.M., Billington, B.L. & Zakian, V.A. 1990, "Position effect at *S. cerevisiae* telomeres: Reversible repression of Pol II transcription", *Cell*, vol. 63, no. 4, pp. 751-762.
- Greenberg RA, FAU - O'Hagan, R.C., O'Hagan RC, FAU - Deng, H., Deng H, FAU - Xiao, Q., Xiao Q, FAU - Hann, S.R., Hann SR, FAU - Adams, R.R., Adams RR, FAU - Lichtsteiner, S., Lichtsteiner S, FAU - Chin, L., Chin L, FAU - Morin, G.B., Morin GB, FAU - DePinho, R.A. & DePinho RA "Telomerase reverse transcriptase gene is a direct target of c-Myc but is not functionally equivalent in cellular transformation." - *Oncogene*.1999 Feb 4;18(5):1219-26., , no. 0950-9232 (Print).
- Greider, C.W. & Blackburn, E.H. 1987, "The telomere terminal transferase of tetrahymena is a ribonucleoprotein enzyme with two kinds of primer specificity", *Cell*, vol. 51, no. 6, pp. 887-898.
- Griffith, J.D., Comeau, L., Rosenfield, S., Stansel, R.M., Bianchi, A., Moss, H. & de Lange, T. 1999, "Mammalian telomeres end in a large duplex loop.[see comment]", *Cell*, vol. 97, no. 4, pp. 503-514.

- Grobelny, J.V., Godwin, A.K. & Broccoli, D. 2000, "ALT-associated PML bodies are present in viable cells and are enriched in cells in the G(2)/M phase of the cell cycle", *Journal of cell science*, vol. 113, no. Pt 24, pp. 4577-4585.
- Grobelny, J.V., Kulp-McEliece, M. & Broccoli, D. 2001, "Effects of reconstitution of telomerase activity on telomere maintenance by the alternative lengthening of telomeres (ALT) pathway", *Human molecular genetics*, vol. 10, no. 18, pp. 1953-1961.
- Hakin-Smith, V., Jellinek, D.A., Levy, D., Carroll, T., Teo, M., Timperley, W.R., McKay, M.J., Reddel, R.R. & Royds, J.A. 2003, "Alternative lengthening of telomeres and survival in patients with glioblastoma multiforme", *Lancet*, vol. 361, no. 9360, pp. 836-838.
- Haller, F., Kulle, B., Schwager, S., Gunawan, B., von, H.A., Sultmann, H. & Fuzesi, L. 2004, "Equivalence test in quantitative reverse transcription polymerase chain reaction: confirmation of reference genes suitable for normalization", *Anal Biochem*, vol. 335, pp. 1-9.
- Hardy, C.F., Sussel, L. & Shore, D. 1992, "A RAP1-interacting protein involved in transcriptional silencing and telomere length regulation", *Genes & development*, vol. 6, no. 5, pp. 801-814.
- Harley CB, FAU - Futcher, A.B., Futcher AB, FAU - Greider, C.W. & Greider CW "Telomeres shorten during ageing of human fibroblasts.", - *Nature*.1990 May 31;345(6274):458-60., , no. 0028-0836 (Print).
- Hazelrigg, T., Levis, R. & Rubin, G.M. 1984, "Transformation of white locus DNA in *Drosophila*: Dosage compensation, zeste interaction, and position effects", *Cell*, vol. 36, no. 2, pp. 469-481.
- Hediger, F. & Gasser, S.M. 2006, "Heterochromatin protein 1: Don't judge the book by its cover!", *Current opinion in genetics & development*, vol. 16, no. 2, pp. 143-150.
- Henson, J.D., Hannay, J.A., McCarthy, S.W., Royds, J.A., Yeager, T.R., Robinson, R.A., Wharton, S.B., Jellinek, D.A., Arbuckle, S.M., Yoo, J., Robinson, B.G., Learoyd, D.L., Stalley, P.D., Bonar, S.F., Yu, D., Pollock, R.E. & Reddel, R.R. 2005, "A robust assay for alternative lengthening of telomeres in tumors shows the significance of alternative lengthening of telomeres in sarcomas and astrocytomas", *Clinical Cancer Research*, vol. 11, no. 1, pp. 217-225.
- Henson, J.D., Neumann, A.A., Yeager, T.R. & Reddel, R.R. 2002, "Alternative lengthening of telomeres in mammalian cells", *Oncogene*, vol. 21, no. 4 REV. ISS. 1, pp. 598-610.
- Herman, J.G., Graff, J.R., Myohanen, S., Nelkin, B.D. & Baylin, S.B. 1996, "Methylation-specific PCR: a novel PCR assay for methylation status of CpG islands", *Proc Natl Acad Sci U S A*, vol. 93, pp. 9821-9826.
- Higaki, T., Watanabe, T., Tamatomi, I., Tahara, H., Sugimoto, M., Furuichi, Y. & Ide, T. 2004, "Terminal telomere repeats are actually short in telomerase-negative immortal human cells", *Biological & pharmaceutical bulletin*, vol. 27, no. 12, pp. 1932-1938.
- Hills, M., Jeyapalan, J.N., Foxon, J.L. & Royle, N.J. 2007, "Mutation mechanisms that underlie turnover of a human telomere-adjacent segmental duplication containing an unstable minisatellite", *Genomics*, vol. 89, no. 4, pp. 480-489.
- Hiyama, E. & Hiyama, K. 2002, "Clinical utility of telomerase in cancer. [Review] [75 refs]", *Oncogene*, vol. 21, no. 4, pp. 643-649.
- Hockemeyer, D., Sfeir, A.J., Shay, J.W., Wright, W.E. & de Lange, T. 2005, "POT1 protects telomeres from a transient DNA damage response and determines how human chromosomes end", *EMBO Journal*, vol. 24, no. 14, pp. 2667-2678.

- Hoff-Olsen, P., Meling, G.I. & Olaisen, B. 1995, "Somatic mutations in VNTR-locus D1S7 in human colorectal carcinomas are associated with microsatellite instability", *Human mutation*, vol. 5, no. 4, pp. 329-332.
- Hollox, E.J. 2008, "Copy number variation of beta-defensins and relevance to disease", *Cytogenetic and genome research*, vol. 123, no. 1-4, pp. 148-155.
- Hollox, E.J., Atia, T., Cross, G., Parkin, T. & Armour, J.A. 2002, "High throughput screening of human subtelomeric DNA for copy number changes using multiplex amplifiable probe hybridisation (MAPH)", *Journal of medical genetics*, vol. 39, no. 11, pp. 790-795.
- Hollox, E.J., Barber, J.C., Brookes, A.J. & Armour, J.A. 2008, "Defensins and the dynamic genome: what we can learn from structural variation at human chromosome band 8p23.1", *Genome research*, vol. 18, no. 11, pp. 1686-1697.
- Hollox, E.J., Huffmeier, U., Zeeuwen, P.L., Palla, R., Lascorz, J., Rodijk-Olthuis, D., van de Kerkhof, P.C., Traupe, H., de Jongh, G., den Heijer, M., Reis, A., Armour, J.A. & Schalkwijk, J. 2008, "Psoriasis is associated with increased beta-defensin genomic copy number", *Nature genetics*, vol. 40, no. 1, pp. 23-25.
- Hopfner, K.P., Craig, L., Moncalian, G., Zinkel, R.A., Usui, T., Owen, B.A., Karcher, A., Henderson, B., Bodmer, J.L., McMurray, C.T., Carney, J.P., Petrini, J.H. & Tainer, J.A. 2002, "The Rad50 zinc-hook is a structure joining Mre11 complexes in DNA recombination and repair", *Nature*, vol. 418, no. 6897, pp. 562-566.
- Horowitz, H. & Haber, J.E. 1984, "Subtelomeric regions of yeast chromosomes contain a 36 base-pair tandemly repeated sequence", *Nucleic Acids Research*, vol. 12, pp. 7105-7121.
- Hug, N. & Lingner, J. 2006, "Telomere length homeostasis", *Chromosoma*, vol. 115, no. 6, pp. 413-425.
- Huggett, J., Dheda, K., Bustin, S. & Zumla, A. 2005, "Real-time RT-PCR normalisation; strategies and considerations", *Genes Immun*, vol. 6, pp. 279-284.
- Iafrate, A.J., Feuk, L., Rivera, M.N., Listewnik, M.L., Donahoe, P.K., Qi, Y., Scherer, S.W. & Lee, C. 2004, "Detection of large-scale variation in the human genome", *Nature genetics*, vol. 36, no. 9, pp. 949-951.
- Ibanez de Caceres, I., Frolova, N., Varkonyi, R.J., Dulaimi, E., Meropol, N.J., Broccoli, D. & Cairns, P. 2004, "Telomerase is frequently activated in tumors with microsatellite instability.[see comment]", *Cancer Biology & Therapy*, vol. 3, no. 3, pp. 289-292.
- Imbeaud, S., Graudens, E., Boulanger, V., Barlet, X., Zaborski, P., Eveno, E., Mueller, O., Schroeder, A. & Auffray, C. 2005, "Towards standardization of RNA quality assessment using user-independent classifiers of microcapillary electrophoresis traces", *Nucleic Acids Res*, vol. 33, pp. e56.
- Inglis, P.W., Rigden, D.J., Mello, L.V., Louis, E.J. & Valadares-Inglis, M.C. 2005, "Monomorphic subtelomeric DNA in the filamentous fungus, *Metarhizium anisopliae*, contains a RecQ helicase-like gene", *Molecular Genetics and Genomics*, vol. 274, no. 1, pp. 79-90.
- Iyer, S., Chadha, A.D. & McEachern, M.J. 2005, "A mutation in the STN1 gene triggers an alternative lengthening of telomere-like runaway recombinational telomere elongation and rapid deletion in yeast", *Molecular & Cellular Biology*, vol. 25, no. 18, pp. 8064-8073.
- Janssens, N., Janicot, M., Perera, T. & Bakker, A. 2004, "Housekeeping genes as internal standards in cancer research", *Mol Diagn*, vol. 8, pp. 107-113.

- Jauert, P.A., Edmiston, S.N., Conway, K. & Kirkpatrick, D.T. 2002, "RAD1 Controls the Meiotic Expansion of the Human HRAS1 Minisatellite in *Saccharomyces cerevisiae*", *Molecular and cellular biology*, vol. 22, no. 3, pp. 953-964.
- Jeffreys, A.J. 1997, "Spontaneous and induced minisatellite instability in the human genome", *Clinical science (London, England : 1979)*, vol. 93, no. 5, pp. 383-390.
- Jeffreys, A.J., Allen, M.J., Armour, J.A., Collick, A., Dubrova, Y., Fretwell, N., Guram, T., Jobling, M., May, C.A. & Neil, D.L. 1995, "Mutation processes at human minisatellites", *Electrophoresis*, vol. 16, no. 9, pp. 1577-1585.
- Jeffreys, A.J., Barber, R., Bois, P., Buard, J., Dubrova, Y.E., Grant, G., Hollies, C.R., May, C.A., Neumann, R., Panayi, M., Ritchie, A.E., Shone, A.C., Signer, E., Stead, J.D. & Tamaki, K. 1999, "Human minisatellites, repeat DNA instability and meiotic recombination", *Electrophoresis*, vol. 20, no. 8, pp. 1665-1675.
- Jeffreys, A.J., MacLeod, A., Neumann, R., Povey, S. & Royle, N.J. 1990, "'Major minisatellite loci' detected by minisatellite clones 33.6 and 33.15 correspond to the cognate loci D1S111 and D7S437", *Genomics*, vol. 7, no. 3, pp. 449-452.
- Jeffreys, A.J., MacLeod, A., Tamaki, K., Neil, D.L. & Monckton, D.G. 1991, "Minisatellite repeat coding as a digital approach to DNA typing", *Nature*, vol. 354, no. 6350, pp. 204-209.
- Jeffreys, A.J., Monckton, D.G., Tamaki, K., Neil, D.L., Armour, J.A., MacLeod, A., Collick, A., Allen, M. & Jobling, M. 1993, "Minisatellite variant repeat mapping: application to DNA typing and mutation analysis", *EXS*, vol. 67, pp. 125-139.
- Jeffreys, A.J., Neil, D.L. & Neumann, R. 1998, "Repeat instability at human minisatellites arising from meiotic recombination", *The EMBO journal*, vol. 17, no. 14, pp. 4147-4157.
- Jeffreys, A.J. & Neumann, R. 2009, "The rise and fall of a human recombination hot spot", *Nature genetics*, vol. 41, no. 5, pp. 625-629.
- Jeffreys, A.J. & Neumann, R. 2005, "Factors influencing recombination frequency and distribution in a human meiotic crossover hotspot", *Human molecular genetics*, vol. 14, no. 15, pp. 2277-2287.
- Jeffreys, A.J. & Neumann, R. 1997, "Somatic mutation processes at a human minisatellite", *Human molecular genetics*, vol. 6, no. 1, pp. 129-32; 134-6.
- Jeffreys, A.J., Neumann, R., Panayi, M., Myers, S. & Donnelly, P. 2005, "Human recombination hot spots hidden in regions of strong marker association", *Nature genetics*, vol. 37, no. 6, pp. 601-606.
- Jeffreys, A.J., Neumann, R. & Wilson, V. 1990, "Repeat unit sequence variation in minisatellites: a novel source of DNA polymorphism for studying variation and mutation by single molecule analysis", *Cell*, vol. 60, no. 3, pp. 473-485.
- Jeffreys, A.J., Tamaki, K., MacLeod, A., Monckton, D.G., Neil, D.L. & Armour, J.A. 1994, "Complex gene conversion events in germline mutation at human minisatellites", *Nature genetics*, vol. 6, no. 2, pp. 136-145.
- Jeffreys, A.J., Wilson, V., Neumann, R. & Keyte, J. 1988, "Amplification of human minisatellites by the polymerase chain reaction: towards DNA fingerprinting of single cells", *Nucleic acids research*, vol. 16, no. 23, pp. 10953-10971.
- Jeffreys, A.J., Wilson, V. & Thein, S.L. 1985, "Hypervariable 'minisatellite' regions in human DNA", *Nature*, vol. 314, no. 6006, pp. 67-73.

- Jeffreys, A.J., Wilson, V. & Thein, S.L. 1985, "Individual-specific 'fingerprints' of human DNA", *Nature*, vol. 316, no. 6023, pp. 76-79.
- Jeffreys, A.J., Wilson, V., Wong, Z., Royle, N., Patel, I., Kelly, R. & Clarkson, R. 1987, "Highly variable minisatellites and DNA fingerprints", *Biochemical Society symposium*, vol. 53, pp. 165-180.
- Jemal, A., Siegel, R., Ward, E., Murray, T., Xu, J. & Thun, M.J. 2007, "Cancer statistics, 2007", *CA Cancer J Clin*, vol. 57, pp. 43-66.
- Jeyapalan, J.N., Mendez-Bermudez, A., Zaffaroni, N., Dubrova, Y.E. & Royle, N.J. 2008, "Evidence for alternative lengthening of telomeres in liposarcomas in the absence of ALT-associated PML bodies", *International journal of cancer. Journal internationale du cancer*, vol. 122, no. 11, pp. 2414-2421.
- Jeyapalan, J.N., Varley, H., Foxon, J.L., Pollock, R.E., Jeffreys, A.J., Henson, J.D., Reddel, R.R. & Royle, N.J. 2005, "Activation of the ALT pathway for telomere maintenance can affect other sequences in the human genome", *Human molecular genetics*, vol. 14, no. 13, pp. 1785-1794.
- Jiang XR, FAU - Jimenez, G., Jimenez G, FAU - Chang, E., Chang E, FAU - Frolkis, M., Frolkis M, FAU - Kusler, B., Kusler B, FAU - Sage, M., Sage M, FAU - Beeche, M., Beeche M, FAU - Bodnar, A.G., Bodnar AG, FAU - Wahl, G.M., Wahl GM, FAU - Tlsty, T.D., Tlsty TD, FAU - Chiu, C.P. & Chiu CP "Telomerase expression in human somatic cells does not induce changes associated with a transformed phenotype.", - *Nat Genet.* 1999 *Jan;21(1):111-4.*, , no. 1061-4036 (Print).
- Jiang, W.-., Zhong, Z.-., Henson, J.D., Neumann, A.A., Chang, A.C.-. & Reddel, R.R. 2005, "Suppression of alternative lengthening of telomeres by Sp100-mediated sequestration of the MRE11/RAD50/NBS1 complex", *Molecular & Cellular Biology*, vol. 25, no. 7, pp. 2708-2721.
- Jiang, W.-., Zhong, Z.-., Henson, J.D. & Reddel, R.R. 2007, "Identification of candidate alternative lengthening of telomeres genes by methionine restriction and RNA interference", vol. 26, no. 32, pp. 4647.
- Jiang, W., Zhong, Z., Nguyen, A., Henson, J.D., Toouli, C.D., Braithwaite, A.W. & Reddel, R.R. 2009, "Induction of alternative lengthening of telomeres-associated PML bodies by p53/p21 requires HP1 proteins", *The Journal of cell biology*, vol. 185, no. 5, pp. 797-810.
- Jobling, M.A., Bouzekri, N. & Taylor, P.G. 1998, "Hypervariable digital DNA codes for human paternal lineages: MVR-PCR at the Y-specific minisatellite, MSY1 (DYF155S1)", *Human molecular genetics*, vol. 7, no. 4, pp. 643-653.
- Joensuu, T., Kuronen, M., Alakurtti, K., Tegelberg, S., Hakala, P., Aalto, A., Huopaniemi, L., Aula, N., Michellucci, R., Eriksson, K. & Lehesjoki, A.E. 2007, "Cystatin B: mutation detection, alternative splicing and expression in progressive myoclonus epilepsy of Unverricht-Lundborg type (EPM1) patients", *European journal of human genetics : EJHG*, vol. 15, no. 2, pp. 185-193.
- Johnson, F.B., Marciniak, R.A., McVey, M., Stewart, S.A., Hahn, W.C. & Guarente, L. 2001, "The *Saccharomyces cerevisiae* WRN homolog Sgs1p participates in telomere maintenance in cells lacking telomerase", *EMBO Journal*, vol. 20, no. 4, pp. 905-913.
- Johnson, J.E., Varkonyi, R.J., Schwalm, J., Cragle, R., Klein-Szanto, A., Patchefsky, A., Cukierman, E., von Mehren, M. & Broccoli, D. 2005, "Multiple mechanisms of telomere maintenance exist in liposarcomas", *Clinical cancer research : an official journal of the American Association for Cancer Research*, vol. 11, no. 15, pp. 5347-5355.

- Jones, P.A. 1999, "The DNA methylation paradox", *Trends in Genetics*, vol. 15, no. 1, pp. 34-37.
- Jones, P.A. 1986, "DNA Methylation and Cancer", *Cancer research*, vol. 46, no. 2, pp. 461-466.
- Jorgensen, S.M., Kleveland, E.J., Grimholt, U. & Gjoen, T. 2006, "Validation of reference genes for real-time polymerase chain reaction studies in atlantic salmon", *Mar Biotechnol (NY)*, vol. 8, pp. 398-408.
- Jung, M., Xu, C., Ohl, F., Mager, A.K. & Jung, K. 2005, "Transcriptor first strand cDNA synthesis kit: efficient and fast - a comparison to other kits", *Biochemica*, vol. 2, pp. 16-18.
- Jung, M., Ramankulov, A., Roigas, J., Johannsen, M., Ringsdorf, M., Kristiansen, G. & Jung, K. 2007, "In search of suitable reference genes for gene expression studies of human renal cell carcinoma by real-time PCR", *BMC Molecular Biology*, vol. 8, no. 1, pp. 47.
- Jurka, J. & Smith, T. 1988, "A fundamental division in the Alu family of repeated sequences", *Proceedings of the National Academy of Sciences of the United States of America*, vol. 85, no. 13, pp. 4775-4778.
- Kang, S., Jaworski, A., Ohshima, K. & Wells, R.D. 1995, "Expansion and deletion of CTG repeats from human disease genes are determined by the direction of replication in E. coli", *Nature genetics*, vol. 10, no. 2, pp. 213-218.
- Kapitonov, V. & Jurka, J. 1996, "The age of Alu subfamilies", *Journal of Molecular Evolution*, vol. 42, no. 1, pp. 59-65.
- Kaplanski, C., Chisari, F.V. & Wild, C.P. 1997, "Minisatellite rearrangements are increased in liver tumours induced by transplacental aflatoxin B1 treatment of hepatitis B virus transgenic mice, but not in spontaneously arising tumours", *Carcinogenesis*, vol. 18, no. 4, pp. 633-639.
- Karlseder, J., Hoke, K., Mirzoeva, O.K., Bakkenist, C., Kastan, M.B., Petrini, J.H. & de Lange, T. 2004, "The telomeric protein TRF2 binds the ATM kinase and can inhibit the ATM-dependent DNA damage response", *Plos Biology*, vol. 2, no. 8, pp. E240.
- Karlseder, J., Smogorzewska, A. & de Lange, T. 2002, "Senescence induced by altered telomere state, not telomere loss", *Science*, vol. 295, no. 5564, pp. 2446-2449.
- Kashyap, M.K., Kumar, A., Emelianenko, N., Kashyap, A., Kaushik, R., Huang, R., Khullar, M., Sharma, S.K., Singh, S.K., Bhargava, A.K. & Upadhyaya, S.K. 2005, "Biochemical and molecular markers in renal cell carcinoma: an update and future prospects", *Biomarkers*, vol. 10, pp. 258-294.
- Kelly, M.K., Jauert, P.A., Jensen, L.E., Chan, C.L., Truong, C.S. & Kirkpatrick, D.T. 2007, "Zinc regulates the stability of repetitive minisatellite DNA tracts during stationary phase", *Genetics*, vol. 177, no. 4, pp. 2469-2479.
- Kennedy, G.C., German, M.S. & Rutter, W.J. 1995, "The minisatellite in the diabetes susceptibility locus IDDM2 regulates insulin transcription", *Nature genetics*, vol. 9, no. 3, pp. 293-298.
- Kiaris, H., Ergazaki, M. & Spandidos, D.A. 1995, "Instability at the H-ras minisatellite is associated with the spontaneous abortion of the embryo", *Biochemical and biophysical research communications*, vol. 214, no. 3, pp. 788-792.

- Kiaris, H., Hatzistamou, J. & Spandidos, D.A. 1996, "Instability at the H-ras minisatellite in human atherosclerotic plaques", *Atherosclerosis*, vol. 125, no. 1, pp. 47-51.
- Kiaris, H., Spandidos, D.A., Jones, A.S., Vaughan, E.D. & Field, J.K. 1995, "Mutations, expression and genomic instability of the H-ras proto-oncogene in squamous cell carcinomas of the head and neck", *British journal of cancer*, vol. 72, no. 1, pp. 123-128.
- Kikuchi, K., Taniguchi, Y., Hatanaka, A., Sonoda, E., Hochegger, H., Adachi, N., Matsuzaki, Y., Koyama, H., van Gent, D.C., Jasin, M. & Takeda, S. 2005, "Fen-1 Facilitates Homologous Recombination by Removing Divergent Sequences at DNA Break Ends", *Mol.Cell.Biol.*, vol. 25, no. 16, pp. 6948-6955.
- Klingelhutz AJ, FAU - Foster, S.A., Foster SA, FAU - McDougall, J.K. & McDougall JK "Telomerase activation by the E6 gene product of human papillomavirus type 16.", - *Nature*.1996 Mar 7;380(6569):79-82., , no. 0028-0836 (Print).
- Koering CE, FAU - Pollice, A., Pollice A, FAU - Zibella, M.P., Zibella MP, FAU - Bauwens, S., Bauwens S, FAU - Puisieux, A., Puisieux A, FAU - Brunori, M., Brunori M, FAU - Brun, C., Brun C, FAU - Martins, L., Martins L, FAU - Sabatier, L., Sabatier L, FAU - Pulitzer, J.F., Pulitzer JF, FAU - Gilson, E. & Gilson E "Human telomeric position effect is determined by chromosomal context and telomeric chromatin integrity.", - *EMBO Rep*.2002 Nov;3(11):1055-61.Epub 2002 Oct 22., , no. 1469-221X (Print).
- Kohfeldt, E., Sasaki, T., Gohring, W. & Timpl, R. 1998, "Nidogen-2: a new basement membrane protein with diverse binding properties", *J Mol Biol*, vol. 282, pp. 99-109.
- Krontiris, T.G., Devlin, B., Karp, D.D., Robert, N.J. & Risch, N. 1993, "An association between the risk of cancer and mutations in the HRAS1 minisatellite locus", *The New England journal of medicine*, vol. 329, no. 8, pp. 517-523.
- Kubista, M., Andrade, J.M., Bengtsson, M., Forootan, A., Jonák, J., Lind, K., Sindelka, R., Sjöback, R., Sjögreen, B., Strömbom, L., Ståhlberg, A. & Zoric, N. 2006, "The real-time polymerase chain reaction", *Molecular aspects of medicine*, vol. 27, no. 2-3, pp. 95-125.
- Kucherlapati, M., Nguyen, A., Kuraguchi, M., Yang, K., Fan, K., Bronson, R., Wei, K., Lipkin, M., Edelman, W. & Kucherlapati, R. 2007, "Tumor progression in *Apc*^{L638N} mice with *Exo1* and *Fen1* deficiencies", *Oncogene*, vol. 26, pp. 6297-6306.
- Kumakura, S.-., Tsutsui, T.W., Yagisawa, J., Barrett, J.C. & Tsutsui, T. 2005, "Reversible conversion of immortal human cells from telomerase-positive to telomerase-negative cells", *Cancer research*, vol. 65, no. 7, pp. 2778-2786.
- Kumata, M., Shimizu, M., Oshimura, M., Uchida, M. & Tsutsui, T. 2002, "Induction of cellular senescence in a telomerase negative human immortal fibroblast cell line, LCS-AF.1-3, by human chromosome 6", *International journal of oncology*, vol. 21, no. 4, pp. 851-856.
- Kurenova, E.V. & Mason, J.M. 1997, "Telomere functions. A review. [Review] [164 refs]", *Biochemistry-Russia*, vol. 62, no. 11, pp. 1242-1253.
- Lai, A., Kennedy, B.K., Barbie, D.A., Bertos, N.R., Yang, X.J., Theberge, M., Tsai, S., Seto, E., Zhang, Y., Kuzmichev, A., Lane, W.S., Reinberg, D., Harlow, E. & Branton, P.E. 2001, "RBP1 Recruits the mSIN3-Histone Deacetylase Complex to the Pocket of Retinoblastoma Tumor Suppressor Family Proteins Found in Limited Discrete Regions of the Nucleus at Growth Arrest", *Molecular and cellular biology*, vol. 21, no. 8, pp. 2918-2932.
- Lai, S.R., Phipps, S.M.O., Liu, L., Andrews, L.G. & Tollefsbol, T.O. 2005, "Epigenetic control of telomerase and modes of telomere maintenance in aging and abnormal systems", *Frontiers in Bioscience*, vol. 10, pp. 1779-1796.

- Lander, E.S., Linton, L.M., Birren, B., Nusbaum, C., Zody, M.C., Baldwin, J., Devon, K., Dewar, K., Doyle, M., FitzHugh, W., Funke, R., Gage, D., Harris, K., Heaford, A., Howland, J., Kann, L., Lehoczky, J., LeVine, R., McEwan, P., McKernan, K., Meldrim, J., Mesirov, J.P., Miranda, C., Morris, W., Naylor, J., Raymond, C., Rosetti, M., Santos, R., Sheridan, A., Sougnez, C., Stange-Thomann, N., Stojanovic, N., Subramanian, A., Wyman, D., Rogers, J., Sulston, J., Ainscough, R., Beck, S., Bentley, D., Burton, J., Clee, C., Carter, N., Coulson, A., Deadman, R., Deloukas, P., Dunham, A., Dunham, I., Durbin, R., French, L., Grafham, D., Gregory, S., Hubbard, T., Humphray, S., Hunt, A., Jones, M., Lloyd, C., McMurray, A., Matthews, L., Mercer, S., Milne, S., Mullikin, J.C., Mungall, A., Plumb, R., Ross, M., Shownkeen, R., Sims, S., Waterston, R.H., Wilson, R.K., Hillier, L.W., McPherson, J.D., Marra, M.A., Mardis, E.R., Fulton, L.A., Chinwalla, A.T., Pepin, K.H., Gish, W.R., Chissoe, S.L., Wendl, M.C., Delehaunty, K.D., Miner, T.L., Delehaunty, A., Kramer, J.B., Cook, L.L., Fulton, R.S., Johnson, D.L., Minx, P.J., Clifton, S.W., Hawkins, T., Branscomb, E., Predki, P., Richardson, P., Wenning, S., Slezak, T., Doggett, N., Cheng, J.F., Olsen, A., Lucas, S., Elkin, C., Uberbacher, E., Frazier, M., Gibbs, R.A., Muzny, D.M., Scherer, S.E., Bouck, J.B., Sodergren, E.J., Worley, K.C., Rives, C.M., Gorrell, J.H., Metzker, M.L., Naylor, S.L., Kucherlapati, R.S., Nelson, D.L., Weinstock, G.M., Sakaki, Y., Fujiyama, A., Hattori, M., Yada, T., Toyoda, A., Itoh, T., Kawagoe, C., Watanabe, H., Totoki, Y., Taylor, T., Weissenbach, J., Heilig, R., Saurin, W., Artiguenave, F., Brottier, P., Bruls, T., Pelletier, E., Robert, C., Wincker, P., Smith, D.R., Doucette-Stamm, L., Rubenfield, M., Weinstock, K., Lee, H.M., Dubois, J., Rosenthal, A., Platzer, M., Nyakatura, G., Taudien, S., Rump, A., Yang, H., Yu, J., Wang, J., Huang, G., Gu, J., Hood, L., Rowen, L., Madan, A., Qin, S., Davis, R.W., Federspiel, N.A., Abola, A.P., Proctor, M.J., Myers, R.M., Schmutz, J., Dickson, M., Grimwood, J., Cox, D.R., Olson, M.V., Kaul, R., Raymond, C., Shimizu, N., Kawasaki, K., Minoshima, S., Evans, G.A., Athanasiou, M., Schultz, R., Roe, B.A., Chen, F., Pan, H., Ramser, J., Lehrach, H., Reinhardt, R., McCombie, W.R., de la Bastide, M., Dedhia, N., Blocker, H., Hornischer, K., Nordsiek, G., Agarwala, R., Aravind, L., Bailey, J.A., Bateman, A., Batzoglou, S., Birney, E., Bork, P., Brown, D.G., Burge, C.B., Cerutti, L., Chen, H.C., Church, D., Clamp, M., Copley, R.R., Doerks, T., Eddy, S.R., Eichler, E.E., Furey, T.S., Galagan, J., Gilbert, J.G., Harmon, C., Hayashizaki, Y., Haussler, D., Hermjakob, H., Hokamp, K., Jang, W., Johnson, L.S., Jones, T.A., Kasif, S., Kasprzyk, A., Kennedy, S., Kent, W.J., Kitts, P., Koonin, E.V., Korf, I., Kulp, D., Lancet, D., Lowe, T.M., McLysaght, A., Mikkelsen, T., Moran, J.V., Mulder, N., Pollara, V.J., Ponting, C.P., Schuler, G., Schultz, J., Slater, G., Smit, A.F., Stupka, E., Szustakowski, J., Thierry-Mieg, D., Thierry-Mieg, J., Wagner, L., Wallis, J., Wheeler, R., Williams, A., Wolf, Y.I., Wolfe, K.H., Yang, S.P., Yeh, R.F., Collins, F., Guyer, M.S., Peterson, J., Felsenfeld, A., Wetterstrand, K.A., Patrinos, A., Morgan, M.J., de Jong, P., Catanese, J.J., Osoegawa, K., Shizuya, H., Choi, S., Chen, Y.J. & International Human Genome Sequencing Consortium 2001, "Initial sequencing and analysis of the human genome", *Nature*, vol. 409, no. 6822, pp. 860-921.
- Laud PR., Multani AS., Bailey SM., Wu L., Ma J. Kingsley C., Lebel M., Pathak S., DePinho RA. & Chang S. 2005, "Elevated telomere-telomere recombination in WRN-deficient, telomere dysfunctional cells promotes escape from senescence and engagement of the ALT pathway", *Genes Dev.*, vol. 19(21), pp. 2560--70.
- Lenain, C., Bauwens, S., Amiard, S., Brunori, M., Giraud-Panis, M. & Gilson, E. 2006, "The Apollo 5' Exonuclease Functions Together with TRF2 to Protect Telomeres from DNA Repair", *Current Biology*, vol. 16, no. 13, pp. 1303-1310.
- Lester, B.R. & McCarthy, J.B. 1992, "Tumor cell adhesion to the extracellular matrix and signal transduction mechanisms implicated in tumor cell motility, invasion and metastasis", *Cancer Metastasis Rev*, vol. 11, pp. 31-44.
- Levis R, FAU - Hazelrigg, T., Hazelrigg T, FAU - Rubin, G.M. & Rubin GM "Effects of genomic position on the expression of transduced copies of the white gene of *Drosophila*." , - *Science*.1985 Aug 9;229(4713):558-61., , no. 0036-8075 (Print).
- Li B, FAU - Lustig, A.J. & Lustig AJ "A novel mechanism for telomere size control in *Saccharomyces cerevisiae*." , - *Genes Dev*.1996 Jun 1;10(11):1310-26., , no. 0890-9369 (Print).

- Li, B. & de Lange, T. 2003, "Rap1 affects the length and heterogeneity of human telomeres", *Molecular biology of the cell*, vol. 14, no. 12, pp. 5060-5068.
- Li, B., Oestreich, S. & de Lange, T. 2000, "Identification of human Rap1: implications for telomere evolution", *Cell*, vol. 101, no. 5, pp. 471-483.
- Li, X., Li, J., Harrington, J., Lieber, M.R. & Burgers, P.M.J. 1995, "Lagging Strand DNA Synthesis at the Eukaryotic Replication Fork Involves Binding and Stimulation of FEN-1 by Proliferating Cell Nuclear Antigen", *J.Biol.Chem.*, vol. 270, no. 38, pp. 22109-22112.
- Lillard-Wetherell, K., Combs, K.A. & Groden, J. 2005, "BLM helicase complements disrupted type II telomere lengthening in telomerase-negative sgs1 yeast", *Cancer research*, vol. 65, no. 13, pp. 5520-5522.
- Lillard-Wetherell, K., Machwe, A., Langland, G.T., Combs, K.A., Behbehani, G.K., Schonberg, S.A., German, J., Turchi, J.J., Orren, D.K. & Groden, J. 2004, "Association and regulation of the BLM helicase by the telomere proteins TRF1 and TRF2", *Human molecular genetics*, vol. 13, no. 17, pp. 1919-1932.
- Lin, C.Y., Chang, H.H., Wu, K.J., Tseng, S.F., Lin, C.C., Lin, C.P. & Teng, S.C. 2005, "Extrachromosomal telomeric circles contribute to Rad52-, Rad50-, and polymerase delta-mediated telomere-telomere recombination in *Saccharomyces cerevisiae*", *Eukaryotic Cell*, vol. 4, no. 2, pp. 327-336.
- Lio, Y.C., Schild, D., Brenneman, M.A., Redpath, J.L. & Chen, D.J. 2004, "Human Rad51C deficiency destabilizes XRCC3, impairs recombination, and radiosensitizes S/G2-phase cells", *The Journal of biological chemistry*, vol. 279, no. 40, pp. 42313-42320.
- Liotta, L.A., Tryggvason, K., Garbisa, S., Hart, I., Foltz, C.M. & Shafie, S. 1980, "Metastatic potential correlates with enzymatic degradation of basement membrane collagen", *Nature*, vol. 284, pp. 67-68.
- Liu, L., Franco, S., Spyropoulos, B., Moens, P., Blasco, M.A. & Keefe, D.L. 2004, "Irregular telomeres impair meiotic synapsis and recombination in mice.", *Proc Natl Acad Sci U S A*, vol. 101(17), pp. 6496--501.
- Liu, Y., Masson, J.Y., Shah, R., O'Regan, P. & West, S.C. 2004, "RAD51C is required for Holliday junction processing in mammalian cells", *Science (New York, N.Y.)*, vol. 303, no. 5655, pp. 243-246.
- Lizardi, P.M., Huang, X., Zhu, Z., Bray-Ward, P., Thomas, D.C. & Ward, D.C. 1998, "Mutation detection and single-molecule counting using isothermal rolling-circle amplification", *Nature genetics*, vol. 19, no. 3, pp. 225-232.
- Loayza, D. & de Lange, T. 2004, "Telomerase regulation at the telomere: a binary switch.[comment]", *Cell*, vol. 117, no. 3, pp. 279-280.
- Londono-Vallejo, J.A. 2004, "Telomere length heterogeneity and chromosome instability. [Review] [81 refs]", *Cancer letters*, vol. 212, no. 2, pp. 135-144.
- Londono-Vallejo, J.A., Der-Sarkissian, H., Cazes, L., Bacchetti, S. & Reddel, R.R. 2004, "Alternative lengthening of telomeres is characterized by high rates of telomeric exchange", *Cancer research*, vol. 64, no. 7, pp. 2324-2327.
- Londono-Vallejo, J.A., DerSarkissian, H., Cazes, L. & Thomas, G. 2001, "Differences in telomere length between homologous chromosomes in humans", *Nucleic acids research*, vol. 29, no. 15, pp. 3164-3171.

- Londoño-Vallejo, J.A. 2008, "Telomere instability and cancer", *Biochimie*, vol. 90, no. 1, pp. 73-82.
- Lopes, J., Ribeyre, C. & Nicolas, A. 2006, "Complex Minisatellite Rearrangements Generated in the Total or Partial Absence of Rad27/hFEN1 Activity Occur in a Single Generation and Are Rad51 and Rad52 Dependent", *Mol. Cell. Biol.*, vol. 26:, pp. 6675--6689.
- Lopes, J., Debrauwere, H., Buard, J. & Nicolas, A. 2002, "Instability of the human minisatellite CEB1 in rad27Delta and dna2-1 replication-deficient yeast cells", *The EMBO journal*, vol. 21, no. 12, pp. 3201-3211.
- Lopez-Beltran, A., Scarpelli, M., Montironi, R. & Kirkali, Z. 2006, "2004 WHO classification of the renal tumors of the adults", *Eur Urol*, vol. 49, pp. 798-805.
- Lundblad, V. 2002, "Telomere maintenance without telomerase. [Review] [60 refs]", *Oncogene*, vol. 21, no. 4, pp. 522-531.
- Lundblad, V. & Blackburn, E.H. 1993, "An alternative pathway for yeast telomere maintenance rescues est1- senescence", *Cell*, vol. 73, no. 2, pp. 347-360.
- Lydeard JR, FAU - Jain, S., Jain S, FAU - Yamaguchi, M., Yamaguchi M, FAU - Haber, J.E. & Haber JE "Break-induced replication and telomerase-independent telomere maintenance require Pol32.", - *Nature*.2007 Aug 16;448(7155):820-3.Epub 2007 Aug 1., , no. 1476-4687 (Electronic).
- Maleki, S., Cederberg, H. & Rannug, U. 2002, "The human minisatellites MS1, MS32, MS205 and CEB1 integrated into the yeast genome exhibit different degrees of mitotic instability but are all stabilised by RAD27", *Current genetics*, vol. 41, no. 5, pp. 333-341.
- Marcand, S., Buck, S.W., Moretti, P., Gilson, E. & Shore, D. 1996, "Silencing of genes at nontelomeric sites in yeast is controlled by sequestration of silencing factors at telomeres by Rap 1 protein", *Genes & development*, vol. 10, no. 11, pp. 1297-1309.
- Marcand, S., Gilson, E. & Shore, D. 1997, "A Protein-Counting Mechanism for Telomere Length Regulation in Yeast", *Science*, vol. 275, no. 5302, pp. 986-990.
- Marciniak, R.A., Cavazos, D., Montellano, R., Chen, Q., Guarente, L. & Johnson, F.B. 2005, "A novel telomere structure in a human alternative lengthening of telomeres cell line", *Cancer research*, vol. 65, no. 7, pp. 2730-2737.
- Maringele, L. & Lydall, D. 2005, "The PAL-mechanism of chromosome maintenance: causes and consequences", *Cell cycle (Georgetown, Tex.)*, vol. 4, no. 6, pp. 747-751.
- Maringele, L. & Lydall, D. 2004, "EXO1 plays a role in generating type I and type II survivors in budding yeast", *Genetics*, vol. 166, no. 4, pp. 1641-1649.
- Maringele, L. & Lydall, D. 2004, "Telomerase- and recombination-independent immortalization of budding yeast", *Genes & development*, vol. 18, no. 21, pp. 2663-2675.
- Maringele, L. & Lydall, D. 2002, "EXO1-dependent single-stranded DNA at telomeres activates subsets of DNA damage and spindle checkpoint pathways in budding yeast yku70Delta mutants", *Genes & development*, vol. 16, no. 15, pp. 1919-1933.
- Maser, R.S. & DePinho, R.A. 2002, "Connecting Chromosomes, Crisis, and Cancer", *Science*, vol. 297, no. 5581, pp. 565-569.

- Mathieu, N., Pirzio, L., Freulet-Marriere, M.A., Desmaze, C. & Sabatier, L. 2004, "Telomeres and chromosomal instability", *Cellular and Molecular Life Sciences*, vol. 61, no. 6, pp. 641-656.
- Matsuura, A. 2005, "Role of ATM-related proteins in the assembly of telomere replication proteins]. [Review] [51 refs", *Seikagaku - Journal of Japanese Biochemical Society*, vol. 77, no. 3, pp. 233-240.
- May, C.A., Jeffreys, A.J. & Armour, J.A. 1996, "Mutation rate heterogeneity and the generation of allele diversity at the human minisatellite MS205 (D16S309)", *Human molecular genetics*, vol. 5, no. 11, pp. 1823-1833.
- May, C.A., Tamaki, K., Neumann, R., Wilson, G., Zagars, G., Pollack, A., Dubrova, Y.E., Jeffreys, A.J. & Meistrich, M.L. 2000, "Minisatellite mutation frequency in human sperm following radiotherapy", *Mutation research*, vol. 453, no. 1, pp. 67-75.
- Mayer, U., Nischt, R., Poschl, E., Mann, K., Fukuda, K., Gerl, M., Yamada, Y. & Timpl, R. 1993, "A single EGF-like motif of laminin is responsible for high affinity nidogen binding", *The EMBO journal*, vol. 12, no. 5, pp. 1879-1885.
- McCarroll, R.M. & Fangman, W.L. 1988, "Time of replication of yeast centromeres and telomeres", *Cell*, vol. 54, no. 4, pp. 505-513.
- McCarroll, S.A., Huett, A., Kuballa, P., Chilewski, S.D., Landry, A., Goyette, P., Zody, M.C., Hall, J.L., Brant, S.R., Cho, J.H., Duerr, R.H., Silverberg, M.S., Taylor, K.D., Rioux, J.D., Altshuler, D., Daly, M.J. & Xavier, R.J. 2008, "Deletion polymorphism upstream of IRGM associated with altered IRGM expression and Crohn's disease", *Nature genetics*, vol. 40, no. 9, pp. 1107-1112.
- McClintock, B. 1939, "The behavior in successive nuclear divisions of a chromosome broken at meiosis", *Proc. Natl. Acad. Sci.*, vol. 25, pp. 405-416.
- McCord, R.A. & Broccoli, D. 2008, "Telomeric chromatin: Roles in aging, cancer and hereditary disease", *Mutation Research/Fundamental and Molecular Mechanisms of Mutagenesis*, vol. 647, no. 1-2, pp. 86-93.
- McEachern MJ, FAU - Blackburn, E.H. & Blackburn EH "Cap-prevented recombination between terminal telomeric repeat arrays (telomere CPR) maintains telomeres in *Kluyveromyces lactis* lacking telomerase.", - *Genes Dev.*1996 Jul 15;10(14):1822-34., , no. 0890-9369 (Print).
- McEachern MJ, FAU - Haber, J.E. & Haber JE "Break-induced replication and recombinational telomere elongation in yeast.", - *Annu Rev Biochem.*2006;75:111-35., , no. 0066-4154 (Print).
- Melissa A. Dunham, Axel A. Neumann, Clare L. Fasching & Roger R. Reddel 2000, "Telomere maintenance by recombination in human cells", *Nature Genetics*, vol. 26, pp. 447-450.
- Mendez-Bermudez, A., Hills, M., Pickett, H.A., Phan, A.T., Mergny, J.L., Riou, J.F. & Royle, N.J. 2009, "Human telomeres that contain (CTAGGG)_n repeats show replication dependent instability in somatic cells and the male germline", *Nucleic acids research*, .
- Meyer-Lindenberg, A., Nichols, T., Callicott, J.H., Ding, J., Kolachana, B., Buckholtz, J., Mattay, V.S., Egan, M. & Weinberger, D.R. 2006, "Impact of complex genetic variation in COMT on human brain function", *Molecular psychiatry*, vol. 11, no. 9, pp. 867-77, 797.
- Michishita E, FAU - McCord, R.A., McCord RA, FAU - Berber, E., Berber E, FAU - Kioi, M., Kioi M, FAU - Padilla-Nash, H., Padilla-Nash H, FAU - Damian, M., Damian M, FAU - Cheung, P., Cheung P, FAU - Kusumoto, R., Kusumoto R, FAU - Kawahara, T.L.A., Kawahara TL,

- FAU - Barrett, J.C., Barrett JC, FAU - Chang, H.Y., Chang HY, FAU - Bohr, V.A., Bohr VA, FAU - Ried, T., Ried T, FAU - Gozani, O., Gozani O, FAU - Chua, K.F. & Chua KF "SIRT6 is a histone H3 lysine 9 deacetylase that modulates telomeric chromatin.", - *Nature*. 2008 Mar 27;452(7186):492-6. Epub 2008 Mar 12., , no. 1476-4687 (Electronic).
- Miller, K.M., Ferreira, M.G. & Cooper, J.P. 2005, "Taz1, Rap1 and Rif1 act both interdependently and independently to maintain telomeres", *EMBO Journal*, vol. 24, no. 17, pp. 3128-3135.
- Miosge, N., Holzhausen, S., Zelent, C., Sprysch, P. & Herken, R. 2001, "Nidogen-1 and nidogen-2 are found in basement membranes during human embryonic development", *Histochem J*, vol. 33, pp. 523-530.
- Miosge, N., Sasaki, T. & Timpl, R. 2002, "Evidence of nidogen-2 compensation for nidogen-1 deficiency in transgenic mice", *Matrix Biol*, vol. 21, pp. 611-621.
- Mohaghegh, P., Karow, J.K., Brosh Jr, R.M., Jr, Bohr, V.A. & Hickson, I.D. 2001, "The Bloom's and Werner's syndrome proteins are DNA structure-specific helicases", *Nucleic acids research*, vol. 29, no. 13, pp. 2843-2849.
- Momparler, R.L. & Bovenzi, V. 2000, "DNA methylation and cancer", *Journal of cellular physiology*, vol. 183, no. 2, pp. 145-154.
- Monckton, D.G., Neumann, R., Guram, T., Fretwell, N., Tamaki, K., MacLeod, A. & Jeffreys, A.J. 1994, "Minisatellite mutation rate variation associated with a flanking DNA sequence polymorphism", *Nature genetics*, vol. 8, no. 2, pp. 162-170.
- Monckton, D.G., Tamaki, K., MacLeod, A., Neil, D.L. & Jeffreys, A.J. 1993, "Allele-specific MVR-PCR analysis at minisatellite D1S8", *Human Molecular Genetics*, vol. 2, no. 5, pp. 513-519.
- Moretti, P., Freeman, K., Coodly, L. & Shore, D. 1994, "Evidence that a complex of SIR proteins interacts with the silencer and telomere-binding protein RAP1", *Genes & development*, vol. 8, no. 19, pp. 2257-2269.
- Morla, M., Busquets, X., Pons, J., Sauleda, J., MacNee, W. & Agusti, A.G.N. 2006, "Telomere shortening in smokers with and without COPD", *European Respiratory Journal*, vol. 27, no. 3, pp. 525-528.
- Moyzis, R.K., Buckingham, J.M., Cram, L.S., Dani, M., Deaven, L.L., Jones, M.D., Meyne, J., Ratliff, R.L. & Wu, J.R. 1988, "A highly conserved repetitive DNA sequence, (TTAGGG)_n, present at the telomeres of human chromosomes", *Proceedings of the National Academy of Sciences of the United States of America*, vol. 85, no. 18, pp. 6622-6626.
- Mueller, M.M. & Fusenig, N.E. 2004, "Friends or foes - bipolar effects of the tumour stroma in cancer", *Nat Rev Cancer*, vol. 4, pp. 839-849.
- Mueller, O., Lightfoot, S. & Schroeder, A. 2004, "RNA Integrity Number (RIN) - Standardization of RNA Quality Control", *Agilent Technologies*, .
- Muller, H.J. 1938, "The remaking of chromosomes", *Collecting Net*, vol. 8, pp. 182-198.
- Multani, A.S. & Chang, S. 2007, "WRN at telomeres: implications for aging and cancer", *Journal of Cell Science*, vol. 120, no. 5, pp. 713-721.
- Munoz, P., Blanco, R., Flores, J.M. & Blasco, M.A. 2005, "XPF nuclease-dependent telomere loss and increased DNA damage in mice overexpressing TRF2 result in premature aging and cancer", *Nature genetics*, vol. 37, no. 10, pp. 1063-1071.

- Muntoni A, FAU - Neumann, A.A., Neumann AA, FAU - Hills, M., Hills M, FAU - Reddel, R.R. & Reddel RR "Telomere elongation involves intra-molecular DNA replication in cells utilizing alternative lengthening of telomeres.", - *Hum Mol Genet.* 2009 Mar 15;18(6):1017-27.Epub 2008 Dec 18., , no. 1460-2083 (Electronic).
- Muntoni, A. & Reddel, R.R. 2005, "The first molecular details of ALT in human tumor cells", *Human molecular genetics*, vol. 14, no. SUPPL. 2, pp. R191-R196.
- Muntoni, A., Neumann, A.A., Hills, M. & Reddel, R.R. 2008, "Telomere elongation involves intra-molecular DNA replication in cells utilizing Alternative Lengthening of Telomeres", *Hum.Mol.Genet.*, .
- Murnane, J.P., Sabatier, L., Marder, B.A. & Morgan, W.F. 1994, "Telomere dynamics in an immortal human cell line", *EMBO Journal*, vol. 13, no. 20, pp. 4953-4962.
- Murphy, R.M., Watt, K.K., Cameron-Smith, D., Gibbons, C.J. & Snow, R.J. 2003, "Effects of creatine supplementation on housekeeping genes in human skeletal muscle using real-time RT-PCR", *Physiol Genomics*, vol. 12, pp. 163-174.
- Murray, J., Buard, J., Neil, D.L., Yeramian, E., Tamaki, K., Hollies, C. & Jeffreys, A.J. 1999, "Comparative Sequence Analysis of Human Minisatellites Showing Meiotic Repeat Instability", *Genome Research*, vol. 9, pp. 130--136.
- Murray, M.J. & Lessey, B.A. 1999, "Embryo implantation and tumor metastasis: common pathways of invasion and angiogenesis", *Semin Reprod Endocrinol*, vol. 17, pp. 275-290.
- Murshed, M., Smyth, N., Miosge, N., Karolat, J., Krieg, T., Paulsson, M. & Nischt, R. 2000, "The absence of nidogen 1 does not affect murine basement membrane formation", *Mol Cell Biol*, vol. 20, pp. 7007-7012.
- Nabetani, A., Yokoyama, O. & Ishikawa, F. 2004, "Localization of hRad9, hHus1, hRad1, and hRad17 and caffeine-sensitive DNA replication at the alternative lengthening of telomeres-associated promyelocytic leukemia body", *Journal of Biological Chemistry*, vol. 279, no. 24, pp. 25849-25857.
- Nabetani, A. & Ishikawa, F. 2008, "Unusual telomeric DNAs in human telomerase-negative immortalized cells", *Mol.Cell.Biol.*, .
- Nagaraju, G., Odate, S., Xie, A. & Scully, R. 2006, "Differential regulation of short- and long-tract gene conversion between sister chromatids by Rad51C", *Molecular and cellular biology*, vol. 26, no. 21, pp. 8075-8086.
- Nakamura, Y., Leppert, M., O'Connell, P., Wolff, R., Holm, T., Culver, M., Martin, C., Fujimoto, E., Hoff, M. & Kumlin, E. 1987, "**Variable number of tandem repeat (VNTR) markers for human gene mapping**", *Science*, , pp. 1616-1622.
- Natarajan, S. & McEachern, M.J. 2002, "Recombinational Telomere Elongation Promoted by DNA Circles", *Molecular and cellular biology*, vol. 22, no. 13, pp. 4512-4521.
- Neumann, A.A. & Reddel, R.R. 2002, "Telomere maintenance and cancer - Look, no telomerase", *Nature Reviews.Cancer*, vol. 2, no. 11, pp. 879-884.
- Ng LJ, FAU - Cropley, J.E., Cropley JE, FAU - Pickett, H.A., Pickett HA, FAU - Reddel, R.R., Reddel RR, FAU - Suter, C.M. & Suter CM 2009, "Telomerase activity is associated with an increase in DNA methylation at the proximal subtelomere and a reduction in telomeric transcription.", - *Nucleic Acids Res.* 2009 Mar;37(4):1152-9.Epub 2009 Jan 7., , no. 1362-4962 (Electronic).

- Ng LJ, FAU - Cropley, J.E., Cropley JE, FAU - Pickett, H.A., Pickett HA, FAU - Reddel, R.R., Reddel RR, FAU - Suter, C.M. & Suter CM "Telomerase activity is associated with an increase in DNA methylation at the proximal subtelomere and a reduction in telomeric transcription.", - *Nucleic Acids Res.*2009 Mar;37(4):1152-9.Epub 2009 Jan 7., , no. 1362-4962 (Electronic).
- Nikitina, T. & Woodcock, C.L. 2004, "Closed chromatin loops at the ends of chromosomes", *Journal of Cell Biology*, vol. 166, no. 2, pp. 161-165.
- Nishihara, H. & Okada, N. 2008, "Retroposons: genetic footprints on the evolutionary paths of life", *Methods in molecular biology (Clifton, N.J.)*, vol. 422, pp. 201-225.
- Nishihara, H., Terai, Y. & Okada, N. 2002, "Characterization of novel Alu- and tRNA-related SINEs from the tree shrew and evolutionary implications of their origins", *Molecular biology and evolution*, vol. 19, no. 11, pp. 1964-1972.
- Nishimura, M., Yaguti, H., Yoshitsugu, H., Naito, S. & Satoh, T. 2003, "Tissue distribution of mRNA expression of human cytochrome P450 isoforms assessed by high-sensitivity real-time reverse transcription PCR", *Yakugaku Zasshi*, vol. 123, pp. 369-375.
- Nishiyama, R., Qi, L., Tsumagari, K., Weissbecker, K., Dubeau, L., Champagne, M., Sikka, S., Nagai, H. & Ehrlich, M. 2005, "A DNA repeat, NBL2, is hypermethylated in some cancers but hypomethylated in others", *Cancer biology & therapy*, vol. 4, no. 4, pp. 440-448.
- Nomiyama, H., Egami, K., Wada, N., Tou, K., Horiuchi, M., Matsusaki, H., Miura, R., Yoshie, O. & Kukita, T. 2005, "Identification of genes differentially expressed in osteoclast-like cells", *Journal of interferon & cytokine research : the official journal of the International Society for Interferon and Cytokine Research*, vol. 25, no. 4, pp. 227-231.
- Nosek J, FAU - Rycovska, A., Rycovska A, FAU - Makhov, A.M., Makhov AM, FAU - Griffith, J.D., Griffith JD, FAU - Tomaska, L. & Tomaska L "Amplification of telomeric arrays via rolling-circle mechanism.", - *J Biol Chem.*2005 Mar 18;280(11):10840-5.Epub 2005 Jan 18., , no. 0021-9258 (Print).
- Ogino, H., Nakabayashi, K., Suzuki, M., Takahashi, E., Fujii, M., Suzuki, T. & Ayusawa, D. 1998, "Release of Telomeric DNA from Chromosomes in Immortal Human Cells Lacking Telomerase Activity", *Biochemical and biophysical research communications*, vol. 248, no. 2, pp. 223-227.
- Ohl, F., Jung, M., Radonic, A., Sachs, M., Loening, S.A. & Jung, K. 2006, "Identification and validation of suitable endogenous reference genes for gene expression studies in human bladder cancer", *J Urol*, vol. 175, pp. 1915-1920.
- Ohl, F., Jung, M., Xu, C., Stephan, C., Rabien, A., Burkhardt, M., Nitsche, A., Kristiansen, G., Radonic, A. & Jung, K. 2005, "Gene expression studies in prostate cancer tissue: which reference gene should be selected?", *J Mol Med*, vol. 83, pp. 1014-1024.
- Old, J.M., Heath, C., Fitches, A., Thein, S.L., Jeffreys, A.J., Petrou, M., Modell, B. & Weatherall, D.J. 1986, "Meiotic recombination between two polymorphic restriction sites within the beta globin gene cluster", *Journal of medical genetics*, vol. 23, no. 1, pp. 14-18.
- Olovnikov, A. M. 1971. "[Principle of marginotomy in template synthesis of polynucleotides]." *Dokl Akad Nauk SSSR* vol. 201(6), pp. 1496-1499.
- Olovnikov, A.M. 1973, "A theory of marginotomy. The incomplete copying of template margin in enzymic synthesis of polynucleotides and biological significance of the phenomenon", *Journal of theoretical biology*, vol. 41, no. 1, pp. 181-190.

- Opresko P.L., Otterlei M., Graakjaer J., Bruheim P., Dawut L., Kolvraa S., May A., Seidman M.M. & Bohr V.A. 2004, "The Werner syndrome helicase and exonuclease cooperate to resolve telomeric D loops in a manner regulated by TRF1 and TRF2.", *Molecular Cell*, vol. 6, pp. 14763--74.
- Opresko, P.L., Mason, P.A., Podell, E.R., Lei, M., Hickson, I.D., Cech, T.R. & Bohr, V.A. 2005, "POT1 stimulates RecQ helicases WRN and BLM to unwind telomeric DNA substrates", *Journal of Biological Chemistry*, vol. 280, no. 37, pp. 32069-32080.
- Ottaviani, A., Gilson, E. & Magdinier, F. 2008, "Telomeric position effect: From the yeast paradigm to human pathologies?", *Biochimie*, vol. 90, no. 1, pp. 93-107.
- Ouyang, K.J., Woo, L.L. & Ellis, N.A. 2008, "Homologous recombination and maintenance of genome integrity: cancer and aging through the prism of human RecQ helicases", *Mechanisms of ageing and development*, vol. 129, no. 7-8, pp. 425-440.
- Paeschke, K., Simonsson, T., Postberg, J., Rhodes, D. & Lipps, H.J. 2005, "Telomere end-binding proteins control the formation of G-quadruplex DNA structures in vivo", *Nature Structural & Molecular Biology*, vol. 12, no. 10, pp. 847-854.
- Pardo, B. & Marcand, S. 2005, "Rap1 prevents telomere fusions by nonhomologous end joining", *EMBO Journal*, vol. 24, no. 17, pp. 3117-3127.
- Parenteau, J. & Wellinger, R.J. 2002, "Differential Processing of Leading- and Lagging-Strand Ends at *Saccharomyces cerevisiae* Telomeres Revealed by the Absence of Rad27p Nuclease", *Genetics*, vol. 162, no. 4, pp. 1583-1594.
- Parenteau, J. & Wellinger, R.J. 1999, "Accumulation of Single-Stranded DNA and Destabilization of Telomeric Repeats in Yeast Mutant Strains Carrying a Deletion of RAD27", *Mol.Cell.Biol.*, vol. 19, no. 6, pp. 4143-4152.
- Parsons, R., Li, G.M., Longley, M.J., Fang, W.H., Papadopoulos, N., Jen, J., de la Chapelle, A., Kinzler, K.W., Vogelstein, B. & Modrich, P. 1993, "Hypermutability and mismatch repair deficiency in RER+ tumor cells", *Cell*, vol. 75, no. 6, pp. 1227-1236.
- Paulsson, M. 1987, "Noncollagenous proteins of basement membranes", *Collagen and related research*, vol. 7, no. 6, pp. 443-461.
- Pennarun, G., Granotier, C., Gauthier, L.R., Gomez, D., Hoffschir, F., Mandine, E., Riou, J.F., Mergny, J.L., Mailliet, P. & Boussin, F.D. 2005, "Apoptosis related to telomere instability and cell cycle alterations in human glioma cells treated by new highly selective G-quadruplex ligands", *Oncogene*, vol. 24, no. 18, pp. 2917-2928.
- Perou, C.M., Moore, K.J., Nagle, D.L., Misumi, D.J., Woolf, E.A., McGrail, S.H., Holmgren, L., Brody, T.H., Dussault, B.J., Jr, Monroe, C.A., Duyk, G.M., Pryor, R.J., Li, L., Justice, M.J. & Kaplan, J. 1996, "Identification of the murine beige gene by YAC complementation and positional cloning", *Nature genetics*, vol. 13, no. 3, pp. 303-308.
- Perrem, K., Bryan, T.M., Englezou, A., Hackl, T., Moy, E.L. & Reddel, R.R. 1999, "Repression of an alternative mechanism for lengthening of telomeres in somatic cell hybrids", *Oncogene*, vol. 18, no. 22, pp. 3383-3390.
- Perrem, K., Colgin, L.M., Neumann, A.A., Yeager, T.R. & Reddel, R.R. 2001, "Coexistence of alternative lengthening of telomeres and telomerase in hTERT-transfected GM847 cells", *Molecular & Cellular Biology*, vol. 21, no. 12, pp. 3862-3875.
- Petrella, B.L., Lohi, J. & Brinckerhoff, C.E. 2005, "Identification of membrane type-1 matrix metalloproteinase as a target of hypoxia-inducible factor-2 alpha in von Hippel-Lindau renal cell carcinoma", *Oncogene*, vol. 24, pp. 1043-1052.

- Pfaffl, M.W. 2001, "A new mathematical model for relative quantification in real-time RT-PCR", *Nucleic acids research*, vol. 29, no. 9, pp. e45.
- Pfaffl, M.W., Tichopad, A., Prgomet, C. & Neuvians, T.P. 2004, "Determination of stable housekeeping genes, differentially regulated target genes and sample integrity: BestKeeper--Excel-based tool using pair-wise correlations", *Biotechnol Lett*, vol. 26, pp. 509-515.
- Pickett, H.A., Baird, D.M., Hoff-Olsen, P., Meling, G.I., Rognum, T.O., Shaw, J., West, K.P. & Royle, N.J. 2004, "Telomere instability detected in sporadic colon cancers, some showing mutations in a mismatch repair gene", *Oncogene*, vol. 23, no. 19, pp. 3434-3443.
- Pirzio, L.M., Pichierri, P., Bignami, M. & Franchitto, A. 2008, "Werner syndrome helicase activity is essential in maintaining fragile site stability", *J. Cell Biol.*, vol. 180, no. 2, pp. 305-314.
- Potts PR, FAU - Yu, H. & Yu H "The SMC5/6 complex maintains telomere length in ALT cancer cells through SUMOylation of telomere-binding proteins.", - *Nat Struct Mol Biol.* 2007 Jul;14(7):581-90. Epub 2007 Jun 24., , no. 1545-9993 (Print).
- Potts, P.R. & Yu, H. 2007, "The SMC5/6 complex maintains telomere length in ALT cancer cells through SUMOylation of telomere-binding proteins", *Nature structural & molecular biology*, vol. 14, no. 7, pp. 581-590.
- Prasad, R., Dianov, G.L., Bohr, V.A. & Wilson, S.H. 2000, "FEN1 Stimulation of DNA Polymerase beta Mediates an Excision Step in Mammalian Long Patch Base Excision Repair", *J. Biol. Chem.*, vol. 275, no. 6, pp. 4460-4466.
- Pryde FE, FAU - Louis, E.J. & Louis EJ "Limitations of silencing at native yeast telomeres.", - *EMBO J.* 1999 May 4;18(9):2538-50., , no. 0261-4189 (Print).
- Qiu, J., Qian, Y., Frank, P., Wintersberger, U. & Shen, B. 1999, "Saccharomyces cerevisiae RNase H(35) Functions in RNA Primer Removal during Lagging-Strand DNA Synthesis, Most Efficiently in Cooperation with Rad27 Nuclease", *Molecular and cellular biology*, vol. 19, no. 12, pp. 8361-8371.
- Radonic, A., Thulke, S., Mackay, I.M., Landt, O., Siegert, W. & Nitsche, A. 2004, "Guideline to reference gene selection for quantitative real-time PCR", *Biochem Biophys Res Commun*, vol. 313, pp. 856-862.
- Rasmussen, R. 2001, "Quantification on the LightCycler", *Rapid Cycle Real-time PCR, Methods and Applications*, , pp. 21-34.
- Reddel, R.R. 2003, "Alternative lengthening of telomeres, telomerase, and cancer", *Cancer letters*, vol. 194, no. 2, pp. 155-162.
- Reddel, R.R., Bryan, T.M. & Murnane, J.P. 1997, "Immortalized cells with no detectable telomerase activity. A review. [Review] [61 refs]", *Biochemistry-Russia*, vol. 62, no. 11, pp. 1254-1262.
- Redon, R., Ishikawa, S., Fitch, K.R., Feuk, L., Perry, G.H., Andrews, T.D., Fiegler, H., Shaper, M.H., Carson, A.R., Chen, W., Cho, E.K., Dallaire, S., Freeman, J.L., Gonzalez, J.R., Gratacos, M., Huang, J., Kalaitzopoulos, D., Komura, D., MacDonald, J.R., Marshall, C.R., Mei, R., Montgomery, L., Nishimura, K., Okamura, K., Shen, F., Somerville, M.J., Tchinda, J., Valsesia, A., Woodwark, C., Yang, F., Zhang, J., Zerjal, T., Zhang, J., Armengol, L., Conrad, D.F., Estivill, X., Tyler-Smith, C., Carter, N.P., Aburatani, H., Lee, C., Jones, K.W., Scherer, S.W. & Hurles, M.E. 2006, "Global variation in copy number in the human genome", *Nature*, vol. 444, no. 7118, pp. 444-454.

- Richard, G.F. & Dujon, B. 2006, "Molecular evolution of minisatellites in hemiascomycetous yeasts", *Mol. Biol. Evol.*, vol. 23, pp. 189-202.
- Richard, G.F. & Dujon, B. 2000, "Mini- and microsatellite expansions: the recombination connection", *EMBO Rep.*, vol. 1, pp. 122-126.
- Riches, L.C., Lynch, A.M. & Gooderham, N.J. 2008, "Early events in the mammalian response to DNA double-strand breaks", *Mutagenesis*, vol. 23, no. 5, pp. 331-339.
- Robinson, K., Asawachaicharn, N., Galloway, D.A. & Grandori, C. 2009, "c-Myc accelerates S-Phase and requires WRN to avoid replication stress", *PLoS one*, vol. 4, no. 6, pp. e5951.
- Rodriguez, J., Frigola, J., Vendrell, E., Risques, R., Fraga, M.F., Morales, C., Moreno, V., Esteller, M., Capella, G., Ribas, M. & Peinado, M.A. 2006, "Chromosomal Instability Correlates with Genome-wide DNA Demethylation in Human Primary Colorectal Cancers", *Cancer research*, vol. 66, no. 17, pp. 8462-9468.
- Roos-van Groningen, M., Eikmans, M., Baelde, H.J., de, H.E. & Bruijn, J.A. 2004, "Improvement of extraction and processing of RNA from renal biopsies", *Kidney Int*, vol. 65, pp. 97-105.
- Roskelley, C.D. & Bissell, M.J. 2002, "The dominance of the microenvironment in breast and ovarian cancer", *Semin Cancer Biol*, vol. 12, pp. 97-104.
- Roth, J. & Zuber, C. 1990, "Immunoelectron microscopic investigation of surface coat of Wilms tumor cells. Dense lamina is composed of highly sialylated neural cell adhesion molecule", *Lab Invest*, vol. 62, pp. 55-60.
- Rousseau, T., Peyret, C., Zerbib, M., Thiounn, N., Flam, T. & Debre, B. 1994, "Circumstances of the detection of kidney cancer. Current part of accidental discoveries", *J Urol (Paris)*, vol. 100, pp. 189-195.
- Royle, N.J., Hill, M.C. & Jeffreys, A.J. 1992, "Isolation of telomere junction fragments by anchored polymerase chain reaction.", *Proceedings. Biological Sciences/The Royal Society*, vol. 247(1318), pp. 57--67.
- Royle, N.J., Baird, D.M. & Jeffreys, A.J. 1994, "A subterminal satellite located adjacent to telomeres in chimpanzees is absent from the human genome.", *Nature Genetics*, vol. 6(1), pp. 52--6.
- Royle, N.J., Clarkson, R.E., Wong, Z. & Jeffreys, A.J. 1988, "Clustering of hypervariable minisatellites in the proterminal regions of human autosomes", *Genomics*, vol. 3, no. 4, pp. 352-360.
- Royle, N.J., Foxon, J., Jeyapalan, J.N., Mendez-Bermudez, A., Novo, C.L., Williams, J. & Cotton, V.E. 2008, "Telomere length maintenance--an ALternative mechanism", *Cytogenetic and genome research*, vol. 122, no. 3-4, pp. 281-291.
- Royle, N.J., Mendez-Bermudez, A., Gravani, A., Novo, C., Foxon, J., Williams, J., Cotton, V. & Hidalgo, A. 2009, "The role of recombination in telomere length maintenance", *Biochemical Society transactions*, vol. 37, no. Pt 3, pp. 589-595.
- Saharia, A. & Stewart, S.A. 2009, "FEN1 contributes to telomere stability in ALT-positive tumor cells", *Oncogene*, vol. 28, pp. 1162-1167.
- Saharia, A., Guittat, L., Crocker, S., Lim, A., Steffen, M., Kulkarni, S. & Stewart, S.A. 2008, "Flap Endonuclease 1 Contributes to Telomere Stability", *Current Biology*, vol. 18, no. 7, pp. 496-500.

- Samadashwily, G.M., Raca, G. & Mirkin, S.M. 1997, "Trinucleotide repeats affect DNA replication in vivo", *Nature genetics*, vol. 17, no. 3, pp. 298-304.
- Sarthy J, Bae NS, Scrafford J & Baumann P "Human RAP1 inhibits non-homologous end joining at telomeres.", - *EMBO J.2009 Sep 17.*, , no. 1460-2075 (Electronic).
- Savage, S.A., Stewart, B.J., Eckert, A., Kiley, M., Liao, J.S. & Chanock, S.J. 2005, "Genetic variation, nucleotide diversity, and linkage disequilibrium in seven telomere stability genes suggest that these genes may be under constraint", *Human mutation*, vol. 26, no. 4, pp. 343-350.
- Schaetzlein, S., Kodandaramireddy, N.R., Ju, Z., Lechel, A., Stepczynska, A., Lilli, D.R., Clark, A.B., Rudolph, C., Kuhnel, F., Wei, K., Schlegelberger, B., Schirmacher, P., Kunkel, T.A., Greenberg, R.A., Edelmann, W. & Rudolph, K.L. 2007, "Exonuclease-1 deletion impairs DNA damage signaling and prolongs lifespan of telomere-dysfunctional mice", *Cell*, vol. 130, no. 5, pp. 863-877.
- Scheel, C. & Poremba, C. 2002, "Telomere lengthening in telomerase-negative cells: The ends are coming together", *Virchows Archiv*, vol. 440, no. 6, pp. 573-582.
- Scheel, C., Schaefer, K.L., Jauch, A., Keller, M., Wai, D., Brinkschmidt, C., van Valen, F., Boecker, W., Dockhorn-Dworniczak, B. & Poremba, C. 2001, "Alternative lengthening of telomeres is associated with chromosomal instability in osteosarcomas", *Oncogene*, vol. 20, no. 29, pp. 3835-3844.
- Schlotterer, C. & Tautz, D. 1992, "Slippage synthesis of simple sequence DNA", *Nucleic acids research*, vol. 20, no. 2, pp. 211-215.
- Schmid, H., Cohen, C.D., Henger, A., Irrgang, S., Schlondorff, D. & Kretzler, M. 2003, "Validation of endogenous controls for gene expression analysis in microdissected human renal biopsies", *Kidney Int*, vol. 64, pp. 356-360.
- Schmittgen, T.D. & Zakrajsek, B.A. 2000, "Effect of experimental treatment on housekeeping gene expression: validation by real-time, quantitative RT-PCR", *J Biochem Biophys Methods*, vol. 46, pp. 69-81.
- Schmoeckel, C., Stolz, W., Sakai, L.Y., Burgeson, R.E., Timpl, R. & Krieg, T. 1989, "Structure of basement membranes in malignant melanoma and nevocytic nevi", *J Invest Dermatol*, vol. 92, pp. 663-668.
- Schoeftner, S. & Blasco, M.A. 2008, "Developmentally regulated transcription of mammalian telomeres by DNA-dependent RNA polymerase II", *Nature Cell Biology*, vol. 10.
- Schouten, J.P., McElgunn, C.J., Waaijer, R., Zwiijnenburg, D., Diepvens, F. & Pals, G. 2002, "Relative quantification of 40 nucleic acid sequences by multiplex ligation-dependent probe amplification", *Nucleic acids research*, vol. 30, no. 12, pp. e57.
- Schroeder, A., Mueller, O., Stocker, S., Salowsky, R., Leiber, M., Gassmann, M., Lightfoot, S., Menzel, W., Granzow, M. & Ragg, T. 2006, "The RIN: an RNA integrity number for assigning integrity values to RNA measurements", *BMC Mol Biol*, vol. 7, pp. 3.
- Schymeinsky, J., Nedbal, S., Miosge, N., Poschl, E., Rao, C., Beier, D.R., Skarnes, W.C., Timpl, R. & Bader, B.L. 2002, "Gene structure and functional analysis of the mouse nidogen-2 gene: nidogen-2 is not essential for basement membrane formation in mice", *Mol Cell Biol*, vol. 22, pp. 6820-6830.
- Sebat, J., Lakshmi, B., Troge, J., Alexander, J., Young, J., Lundin, P., Maner, S., Massa, H., Walker, M., Chi, M., Navin, N., Lucito, R., Healy, J., Hicks, J., Ye, K., Reiner, A., Gilliam, T.C., Trask, B., Patterson, N., Zetterberg, A. & Wigler, M. 2004, "Large-Scale Copy

- Number Polymorphism in the Human Genome", *Science*, vol. 305, no. 5683, pp. 525-528.
- Seger, Y.R., García-Cao, M., Piccinin, S., Cunsolo, C.L., Doglioni, C., Blasco, M.A., Hannon, G.J. & Maestro, R. 2002, "Transformation of normal human cells in the absence of telomerase activation", *Cancer Cell*, vol. 2, no. 5, pp. 401-413.
- Sengstag, C. & Wurgler, F.E. 1994, "DNA recombination induced by aflatoxin B1 activated by cytochrome P450 1A enzymes", *Molecular carcinogenesis*, vol. 11, no. 4, pp. 227-235.
- Shapiro, M.I. 1972, "Conversion of 11,17,21-trihydroxy-4-pregnene-3,20-dione-4-14 C to 3,11,17,21-tetrahydroxy-5-pregnen-20-one-14 C by reversal of the 3-hydroxysteroid dehydrogenase-isomerase reactions", *Steroids*, vol. 20, no. 6, pp. 669-680.
- Sharma, A., Awasthi, S., Harrod, C.K., Matlock, E.F., Khan, S., Xu, L., Chan, S., Yang, H., Thammavaram, C.K., Rasor, R.A., Burns, D.K., Skiest, D.J., Van Lint, C., Girard, A.M., McGee, M., Monnat, R.J., Jr & Harrod, R. 2007, "The Werner syndrome helicase is a cofactor for HIV-1 long terminal repeat transactivation and retroviral replication", *The Journal of biological chemistry*, vol. 282, no. 16, pp. 12048-12057.
- Sharma, S., Sommers, J.A. & Brosh, R.M., Jr 2008, "Processing of DNA replication and repair intermediates by the concerted action of RecQ helicases and Rad2 structure-specific nucleases", *Protein and Peptide Letters*, vol. 15, no. 1, pp. 89-102.
- Shay, J.W. & Wright, W.E. 1989, "Quantitation of the frequency of immortalization of normal human diploid fibroblasts by SV40 large T-antigen", *Experimental cell research*, vol. 184, no. 1, pp. 109-118.
- Shay, J.W., Wright, W.E. & Werbin, H. 1991, "Defining the molecular mechanisms of human cell immortalization", *Biochimica et Biophysica Acta (BBA) - Reviews on Cancer*, vol. 1072, no. 1, pp. 1-7.
- Sherwood, D.R., Butler, J.A., Kramer, J.M. & Sternberg, P.W. 2005, "FOS-1 promotes basement-membrane removal during anchor-cell invasion in *C. elegans*", *Cell*, vol. 121, pp. 951-962.
- Shigeeda, N., Uchida, M., Barrett, J.C. & Tsutsui, T. 2003, "Candidate chromosomal regions for genes involved in activation of alternative lengthening of telomeres in human immortal cell lines", *Experimental gerontology*, vol. 38, no. 6, pp. 641-651.
- Shlien, A., Tabori, U., Marshall, C.R., Pienkowska, M., Feuk, L., Novokmet, A., Nanda, S., Druker, H., Scherer, S.W. & Malkin, D. 2008, "Excessive genomic DNA copy number variation in the Li-Fraumeni cancer predisposition syndrome", *Proceedings of the National Academy of Sciences of the United States of America*, vol. 105, no. 32, pp. 11264-11269.
- Silver, N., Best, S., Jiang, J. & Thein, S.L. 2006, "Selection of housekeeping genes for gene expression studies in human reticulocytes using real-time PCR", *BMC Mol Biol*, vol. 7, pp. 33.
- Silverman, J., Takai, H., Buonomo, S.B., Eisenhaber, F. & de Lange, T. 2004, "Human Rif1, ortholog of a yeast telomeric protein, is regulated by ATM and 53BP1 and functions in the S-phase checkpoint", *Genes & development*, vol. 18, no. 17, pp. 2108-2119.
- Smith, G., Taylor-Kashton, C., Dushnicky, L., Symons, S., Wright, J. & Mai, S. 2003, "c-Myc-induced extrachromosomal elements carry active chromatin", *Neoplasia (New York, N.Y.)*, vol. 5, no. 2, pp. 110-120.

- Smogorzewska, A. & de Lange, T. 2004, "Regulation of telomerase by telomeric proteins. [Review] [213 refs]", *Annual Review of Biochemistry*, vol. 73, pp. 177-208.
- Smogorzewska, A. & de Lange, T. 2002, "Different telomere damage signaling pathways in human and mouse cells", *EMBO Journal*, vol. 21, no. 16, pp. 4338-4348.
- Smogorzewska, A., van Steensel, B., Bianchi, A., Oelmann, S., Schaefer, M.R., Schnapp, G. & de Lange, T. 2000, "Control of human telomere length by TRF1 and TRF2", *Molecular & Cellular Biology*, vol. 20, no. 5, pp. 1659-1668.
- Sobin, L.H. & Wittekind, C. 2002, *TNM classification of malignant tumours*, vol. 6th ed., pp. 184-187.
- Sokolsky, T. & Alani, E. 2000, "EXO1 and MSH6 are high-copy suppressors of conditional mutations in the MSH2 mismatch repair gene of *Saccharomyces cerevisiae*", *Genetics*, vol. 155, no. 2, pp. 589-599.
- Spangenberg, C., Winterpacht, A., Zabel, B.U. & Löbber, R.W. 1998, "Cloning and Characterization of a Novel Gene (TM7SF1) Encoding a Putative Seven-Pass Transmembrane Protein That Is Upregulated during Kidney Development", *Genomics*, vol. 48, no. 2, pp. 178-185.
- Stagno D'Alcontres, M., Mendez-Bermudez, A., Foxon, J.L., Royle, N.J. & Salomoni, P. 2007, "Lack of TRF2 in ALT cells causes PML-dependent p53 activation and loss of telomeric DNA", *The Journal of cell biology*, vol. 179, no. 5, pp. 855-867.
- Stavropoulos, D.J., Bradshaw, P.S., Li, X., Pasic, I., Truong, K., Ikura, M., Ungrin, M. & Meyn, M.S. 2002, "The bloom syndrome helicase BLM interacts with TRF2 in ALT cells and promotes telomeric DNA synthesis", *Human molecular genetics*, vol. 11, no. 25, pp. 3135-3144.
- Stead, J.D. & Jeffreys, A.J. 2000, "Allele diversity and germline mutation at the insulin minisatellite", *Human molecular genetics*, vol. 9, no. 5, pp. 713-723.
- Stewart, S.A. 2005, "Telomere maintenance and tumorigenesis: an "ALT"ernative road", *Current Molecular Medicine*, vol. 5, no. 2, pp. 253-257.
- Sun, B., Chen, M., Hawks, C.L. & Hornsby, P.J. 2005, "Immortal ALT⁺ human cells do not require telomerase reverse transcriptase for malignant transformation", *Cancer research*, vol. 65, no. 15, pp. 6512-6515.
- Sundquist WI, FAU - Klug, A. & Klug A "Telomeric DNA dimerizes by formation of guanine tetrads between hairpin loops.", - *Nature*.1989 Dec 14;342(6251):825-9., , no. 0028-0836 (Print).
- Sussel, L., Vannier, D. & Shore, D. 1995, "Suppressors of defective silencing in yeast: effects on transcriptional repression at the HMR locus, cell growth and telomere structure", *Genetics*, vol. 141, no. 3, pp. 873-888.
- Sutter, N.B., Scalzo, D., Fiering, S., Groudine, M. & Martin, D.I.K. 2003, "Chromatin insulation by a transcriptional activator", *Proceedings of the National Academy of Sciences of the United States of America*, vol. 100, no. 3, pp. 1105-1110.
- Swanson, C., Saintigny, Y., Emond, M.J. & Monnat Jr., R.J. 2004, "The Werner syndrome protein has separable recombination and survival functions", *DNA Repair*, vol. 3, no. 5, pp. 475-482.
- Szabo, A., Perou, C.M., Karaca, M., Perreard, L., Quackenbush, J.F. & Bernard, P.S. 2004, "Statistical modeling for selecting housekeeper genes", *Genome Biol*, vol. 5, pp. R59.

- Szilard, R.K. & Durocher, D. 2006, "Telomere Protection: An Act of God", *Current Biology*, vol. 16, no. 14, pp. R544-R546.
- Taggart, A.K., Teng, S.C. & Zakian, V.A. 2002, "Est1p as a cell cycle-regulated activator of telomere-bound telomerase", *Science*, vol. 297, no. 5583, pp. 1023-1026.
- Takai, H., Smogorzewska, A. & de Lange, T. 2003, "DNA Damage Foci at Dysfunctional Telomeres", *Current Biology*, vol. 13, no. 17, pp. 1549-1556.
- Tamaki, K., May, C.A., Dubrova, Y.E. & Jeffreys, A.J. 1999, "Extremely complex repeat shuffling during germline mutation at human minisatellite B6.7", *Human molecular genetics*, vol. 8, no. 5, pp. 879-888.
- Tamaki, K., Monckton, D.G., MacLeod, A., Allen, M. & Jeffreys, A.J. 1993, "Four-state MVR-PCR: increased discrimination of digital DNA typing by simultaneous analysis of two polymorphic sites within minisatellite variant repeats at D1S8", *Human molecular genetics*, vol. 2, no. 10, pp. 1629-1632.
- Tanaka, H., Mendonca, M.S., Bradshaw, P.S., Hoelz, D.J., Malkas, L.H., Meyn, M.S. & Gilley, D. 2005, "DNA damage-induced phosphorylation of the human telomere-associated protein TRF2", *Proceedings of the National Academy of Sciences of the United States of America*, vol. 102, no. 43, pp. 15539-15544.
- Tang, B., Li, Y.N. & Kruger, W.D. 2000, "Defects in methylthioadenosine phosphorylase are associated with but not responsible for methionine-dependent tumor cell growth", *Cancer research*, vol. 60, no. 19, pp. 5543-5547.
- Tarsounas, M., Munoz, P., Claas, A., Smiraldi, P.G., Pittman, D.L., Blasco, M.A. & West, S.C. 2004, "Telomere maintenance requires the RAD51D recombination/repair protein", *Cell*, vol. 117, no. 3, pp. 337-347.
- Tarsounas, M. & West, S.C. 2005, "Recombination at mammalian telomeres: an alternative mechanism for telomere protection and elongation. [Review] [27 refs]", *Cell Cycle*, vol. 4, no. 5, pp. 672-674.
- Telenius, H., Clark, J., Marcus, E., Royle, N., Jeffreys, A.J., Ponder, B.A. & Mathew, C.G. 1990, "Minisatellite DNA profiles: rapid sample identification in linkage analysis", *Human heredity*, vol. 40, no. 2, pp. 77-80.
- Temime-Smaali, N., Guittat, L., Wenner, T., Bayart, E., Douarre, C., Gomez, D., Giraud-Panis, M.J., Londono-Vallejo, A., Gilson, E., Amor-Gueret, M. & Riou, J.F. 2008, "Topoisomerase IIIalpha is required for normal proliferation and telomere stability in alternative lengthening of telomeres", *The EMBO journal*, vol. 27, no. 10, pp. 1513-1524.
- Teng, S.C., Chang, J., McCowan, B. & Zakian, V.A. 2000, "Telomerase-independent lengthening of yeast telomeres occurs by an abrupt Rad50p-dependent, Rif-inhibited recombinational process", *Molecular cell*, vol. 6, no. 4, pp. 947-952.
- Teng, S.C., Chen, Y.Y., Su, Y.N., Chou, P.C., Chiang, Y.C., Tseng, S.F. & Wu, K.J. 2004, "Direct activation of HSP90A transcription by c-Myc contributes to c-Myc-induced transformation", *Journal of Biological Chemistry*, vol. 279, no. 15, pp. 14649-14655.
- Thellin, O., Zorzi, W., Lakaye, B., De, B.B., Coumans, B., Hennen, G., Grisar, T., Igout, A. & Heinen, E. 1999, "Housekeeping genes as internal standards: use and limits", *J Biotechnol*, vol. 75, pp. 291-295.
- Tilman G, FAU - Lorient, A., Lorient A, FAU - Van Beneden, A., Van Beneden A, FAU - Arnoult, N., Arnoult N, FAU - Londono-Vallejo, J.A., Londono-Vallejo JA, FAU - De Smet, C., De Smet C, FAU - Decottignies, A. & Decottignies A "Subtelomeric DNA hypomethylation is

- not required for telomeric sister chromatid exchanges in ALT cells.", - *Oncogene*.2009 Apr 9;28(14):1682-93.Epub 2009 Mar 2., , no. 1476-5594 (Electronic).
- Timpl, R. & Brown, J.C. 1996, "Supramolecular assembly of basement membranes", *Bioessays*, vol. 18, pp. 123-132.
- Tishkoff, D.X., Filosi, N., Gaida, G.M. & Kolodner, R.D. 1997, "A Novel Mutation Avoidance Mechanism Dependent on *S. cerevisiae* RAD27 Is Distinct from DNA Mismatch Repair", *Cell*, vol. 88, no. 2, pp. 253-263.
- Tokutake, Y., Matsumoto, T., Watanabe, T., Maeda, S., Tahara, H., Sakamoto, S., Niida, H., Sugimoto, M., Ide, T. & Furuichi, Y. 1998, "Extra-Chromosomal Telomere Repeat DNA in Telomerase-Negative Immortalized Cell Lines", *Biochemical and biophysical research communications*, vol. 247, no. 3, pp. 765-772.
- Tomaska L, FAU - Nosek, J., Nosek J, FAU - Makhov, A.M., Makhov AM, FAU - Pastorakova, A., Pastorakova A, FAU - Griffith, J.D. & Griffith JD "Extragenomic double-stranded DNA circles in yeast with linear mitochondrial genomes: potential involvement in telomere maintenance.", - *Nucleic Acids Res*.2000 Nov 15;28(22):4479-87., , no. 1362-4962 (Electronic).
- Tricarico, C., Pinzani, P., Bianchi, S., Paglierani, M., Distante, V., Pazzagli, M., Bustin, S.A. & Orlando, C. 2002, "Quantitative real-time reverse transcription polymerase chain reaction: normalization to rRNA or single housekeeping genes is inappropriate for human tissue biopsies", *Anal Biochem*, vol. 309, pp. 293-300.
- Tsai, Y.L., Tseng, S.F., Chang, S.H., Lin, C.C. & Teng, S.C. 2002, "Involvement of replicative polymerases, Tel1p, Mec1p, Cdc13p, and the Ku complex in telomere-telomere recombination", *Molecular & Cellular Biology*, vol. 22, no. 16, pp. 5679-5687.
- Tseng, S.F., Chang, C.Y., Wu, K.J. & Teng, S.C. 2005, "Importin KPNA2 is required for proper nuclear localization and multiple functions of NBS1", *Journal of Biological Chemistry*, vol. 280, no. 47, pp. 39594-39600.
- Tsumagari, K., Qi, L., Jackson, K., Shao, C., Lacey, M., Sowden, J., Tawil, R., Vedanarayanan, V. & Ehrlich, M. 2008, "Epigenetics of a tandem DNA repeat: chromatin DNaseI sensitivity and opposite methylation changes in cancers", *Nucleic acids research*, vol. 36, no. 7, pp. 2196-2207.
- Tsutsui, T., Kumakura, S., Tamura, Y., Tsutsui, T.W., Sekiguchi, M., Higuchi, T. & Barrett, J.C. 2003, "Immortal, telomerase-negative cell lines derived from a Li-Fraumeni syndrome patient exhibit telomere length variability and chromosomal and minisatellite instabilities", *Carcinogenesis*, vol. 24, no. 5, pp. 953-965.
- Turaga, R.V., Massip, L., Chavez, A., Johnson, F.B. & Lebel, M. 2007, "Werner syndrome protein prevents DNA breaks upon chromatin structure alteration", *Aging cell*, vol. 6, no. 4, pp. 471-481.
- Turri, M.G., Cuin, K.A. & Porter, A.C. 1995, "Characterisation of a novel minisatellite that provides multiple splice donor sites in an interferon-induced transcript", *Nucleic acids research*, vol. 23, no. 11, pp. 1854-1861.
- Ulaner, G.A., Hoffman, A.R., Otero, J., Huang, H.-., Zhao, Z., Mazumdar, M., Gorlick, R., Meyers, P., Healey, J.H. & Ladanyi, M. 2004, "Divergent patterns of telomere maintenance mechanisms among human sarcomas: Sharply contrasting prevalence of the alternative lengthening of telomeres mechanism in Ewing's sarcomas and osteosarcomas", *Genes, chromosomes & cancer*, vol. 41, no. 2, pp. 155-162.
- Ulaner, G.A., Hu, J.F., Vu, T.H., Giudice, L.C. & Hoffman, A.R. 1998, "Telomerase activity in human development is regulated by human telomerase reverse transcriptase (hTERT)

- transcription and by alternate splicing of hTERT transcripts", *Cancer research*, vol. 58, no. 18, pp. 4168-4172.
- Ulaner, G.A., Huang, H.Y., Otero, J., Zhao, Z., Ben-Porat, L., Satagopan, J.M., Gorlick, R., Meyers, P., Healey, J.H., Huvos, A.G., Hoffman, A.R. & Ladanyi, M. 2003, "Absence of a telomere maintenance mechanism as a favorable prognostic factor in patients with osteosarcoma", *Cancer research*, vol. 63, no. 8, pp. 1759-1763.
- Ulazzi, L., Sabbioni, S., Miotto, E., Veronese, A., Angusti, A., Gafa, R., Manfredini, S., Farinati, F., Sasaki, T., Lanza, G. & Negrini, M. 2007, "Nidogen 1 and 2 gene promoters are aberrantly methylated in human gastrointestinal cancer", *Molecular Cancer*, vol. 6, no. 1, pp. 17.
- Usui T. 1998, "Complex formation and functional versatility of Mre11 of budding yeast in recombination. ", *Cell*, vol. 95, pp. 705-716.
- van Overbeek, M. & de Lange, T. 2006, "Apollo, an Artemis-Related Nuclease, Interacts with TRF2 and Protects Human Telomeres in S Phase", *Current Biology*, vol. 16, no. 13, pp. 1295-1302.
- van Steensel, B., Smogorzewska, A. & de Lange, T. 1998, "TRF2 Protects Human Telomeres from End-to-End Fusions", *Cell*, vol. 92, no. 3, pp. 401-413.
- Vandesompele, J., De Preter, K., Pattyn, F., Poppe, B., Van Roy, N., De Paepe, A. & Speleman, F. 2007, "GeNorm software manual, last update on March 13, 2007", .
- Vandesompele, J., De Preter, K., Pattyn, F., Poppe, B., Van Roy, N., De Paepe, A. & Speleman, F. 2002, "Accurate normalization of real-time quantitative RT-PCR data by geometric averaging of multiple internal control genes", *Genome Biol*, vol. 3, pp..
- Vanin, E.F. 1985, "Processed pseudogenes: characteristics and evolution", *Annual Review of Genetics*, vol. 19, pp. 253-272.
- Varley, H., Pickett, H.A., Foxon, J.L., Reddel, R.R. & Royle, N.J. 2002, "Molecular characterization of inter-telomere and intra-telomere mutations in human ALT cells", *Nature genetics*, vol. 30, no. 3, pp. 301-305.
- Vega, L.R., Mateyak, M.K. & Zakian, V.A. 2003, "Getting to the end: telomerase access in yeast and humans", *Nature Reviews Molecular Cell Biology*, vol. 4, pp. 948-959.
- Vega, A., Barros, F., Leonart, M.E., Ramon y Cajal, S. & Carracedo, A. 2001, "HRAS1 minisatellite alleles in colorectal carcinoma: relationship to microsatellite instability", *Anticancer Research*, vol. 21, no. 4A, pp. 2855-2860.
- Veldman T, FAU - Liu, X., Liu X, FAU - Yuan, H., Yuan H, FAU - Schlegel, R. & Schlegel R "Human papillomavirus E6 and Myc proteins associate in vivo and bind to and cooperatively activate the telomerase reverse transcriptase promoter.", - *Proc Natl Acad Sci U S A*.2003 Jul 8;100(14):8211-6.Epub 2003 Jun 23., , no. 0027-8424 (Print).
- Venter, J.C., Adams, M.D., Myers, E.W., Li, P.W., Mural, R.J., Sutton, G.G., Smith, H.O., Yandell, M., Evans, C.A., Holt, R.A., Gocayne, J.D., Amanatides, P., Ballew, R.M., Huson, D.H., Wortman, J.R., Zhang, Q., Kodira, C.D., Zheng, X.H., Chen, L., Skupski, M., Subramanian, G., Thomas, P.D., Zhang, J., Gabor Miklos, G.L., Nelson, C., Broder, S., Clark, A.G., Nadeau, J., McKusick, V.A., Zinder, N., Levine, A.J., Roberts, R.J., Simon, M., Slayman, C., Hunkapiller, M., Bolanos, R., Delcher, A., Dew, I., Fasulo, D., Flanigan, M., Florea, L., Halpern, A., Hannenhalli, S., Kravitz, S., Levy, S., Mobarry, C., Reinert, K., Remington, K., Abu-Threideh, J., Beasley, E., Biddick, K., Bonazzi, V., Brandon, R., Cargill, M., Chandramouliswaran, I., Charlab, R., Chaturvedi, K., Deng, Z., Francesco, V.D., Dunn, P., Eilbeck, K., Evangelista, C., Gabrielian, A.E., Gan, W., Ge, W., Gong, F., Gu, Z., Guan, P., Heiman, T.J., Higgins, M.E., Ji, R., Ke, Z., Ketchum,

- K.A., Lai, Z., Lei, Y., Li, Z., Li, J., Liang, Y., Lin, X., Lu, F., Merkulov, G.V., Milshina, N., Moore, H.M., Naik, A.K., Narayan, V.A., Neelam, B., Nusskern, D., Rusch, D.B., Salzberg, S., Shao, W., Shue, B., Sun, J., Wang, Z.Y., Wang, A., Wang, X., Wang, J., Wei, M., Wides, R., Xiao, C., Yan, C., Yao, A., Ye, J., Zhan, M., Zhang, W., Zhang, H., Zhao, Q., Zheng, L., Zhong, F., Zhong, W., Zhu, S.C., Zhao, S., Gilbert, D., Baumhueter, S., Spier, G., Carter, C., Cravchik, A., Woodage, T., Ali, F., An, H., Awe, A., Baldwin, D., Baden, H., Barnstead, M., Barrow, I., Beeson, K., Busam, D., Carver, A., Center, A., Cheng, M.L., Curry, L., Danaher, S., Davenport, L., Desilets, R., Dietz, S., Dodson, K., Doup, L., Ferreira, S., Garg, N., Gluecksmann, A., Hart, B., Haynes, J., Haynes, C., Heiner, C., Hladun, S., Hostin, D., Houck, J., Howland, T., Ibegwam, C., Johnson, J., Kalush, F., Kline, L., Koduru, S., Love, A., Mann, F., May, D., McCawley, S., McIntosh, T., McMullen, I., Moy, M., Moy, L., Murphy, B., Nelson, K., Pfannkoch, C., Pratts, E., Puri, V., Qureshi, H., Reardon, M., Rodriguez, R., Rogers, Y., Romblad, D., Ruhfel, B., Scott, R., Sitter, C., Smallwood, M., Stewart, E., Strong, R., Suh, E., Thomas, R., Tint, N.N., Tse, S., Vech, C., Wang, G., Wetter, J., Williams, S., Williams, M., Windsor, S., Winn-Deen, E., Wolfe, K., Zaveri, J., Zaveri, K., Abril, J.F., Guigo, R., Campbell, M.J., Sjolander, K.V., Karlak, B., Kejariwal, A., Mi, H., Lazareva, B., Hatton, T., Narechania, A., Diemer, K., Muruganujan, A., Guo, N., Sato, S., Bafna, V., Istrail, S., Lippert, R., Schwartz, R., Walenz, B., Yooseph, S., Allen, D., Basu, A., Baxendale, J., Blick, L., Caminha, M., Carnes-Stine, J., Caulk, P., Chiang, Y., Coyne, M., Dahlke, C., Mays, A.D., Dombroski, M., Donnelly, M., Ely, D., Esparham, S., Fosler, C., Gire, H., Glanowski, S., Glasser, K., Glodek, A., Gorokhov, M., Graham, K., Gropman, B., Harris, M., Heil, J., Henderson, S., Hoover, J., Jennings, D., Jordan, C., Jordan, J., Kasha, J., Kagan, L., Kraft, C., Levitsky, A., Lewis, M., Liu, X., Lopez, J., Ma, D., Majoros, W., McDaniel, J., Murphy, S., Newman, M., Nguyen, T., Nguyen, N., Nodell, M., Pan, S., Peck, J., Peterson, M., Rowe, W., Sanders, R., Scott, J., Simpson, M., Smith, T., Sprague, A., Stockwell, T., Turner, R., Venter, E., Wang, M., Wen, M., Wu, D., Wu, M., Xia, A., Zandieh, A. & Zhu, X. 2001, "The Sequence of the Human Genome", *Science*, vol. 291, no. 5507, pp. 1304-1351.
- Vergnaud, G. & Denoeud, F. 2000, "Minisatellites: mutability and genome architecture", *Genome research*, vol. 10, no. 7, pp. 899-907.
- Verstrepen, K.J., Jansen, A., Lewitter, F. & Fink, G.R. 2005, "Intragenic tandem repeats generate functional variability", *Nat Genet*, vol. 37, pp. 986-990.
- Wang J, FAU - Xie, L.Y., Xie LY, FAU - Allan, S., Allan S, FAU - Beach, D., Beach D, FAU - Hannon, G.J. & Hannon GJ "Myc activates telomerase.", - *Genes Dev.*1998 Jun 15;12(12):1769-74., , no. 0890-9369 (Print).
- Wang SS, FAU - Pluta, A.F., Pluta AF, FAU - Zakian, V.A. & Zakian VA "DNA sequence analysis of newly formed telomeres in yeast.", - *Prog Clin Biol Res.*1989;318:81-9., , no. 0361-7742 (Print).
- Wang Y, FAU - Patel, D.J. & Patel DJ "Solution structure of the human telomeric repeat d[AG3(T2AG3)3] G-tetraplex.", - *Structure.*1993 Dec 15;1(4):263-82., , no. 0969-2126 (Print).
- Wang, H., Xing, J., Grover, D., Hedges, D.J., Han, K., Walker, J.A. & Batzer, M.A. 2005, "SVA elements: a hominid-specific retroposon family", *Journal of Molecular Biology*, vol. 354, no. 4, pp. 994-1007.
- Wang, J.C.Y., Warner, J.K., Erdmann, N., Lansdorp, P.M., Harrington, L. & Dick, J.E. 2005, "Dissociation of telomerase activity and telomere length maintenance in primitive human hematopoietic cells", *Proceedings of the National Academy of Sciences of the United States of America*, vol. 102, no. 40, pp. 14398-14403.
- Wang, R.C., Smogorzewska, A. & de Lange, T. 2004, "Homologous recombination generates T-loop-sized deletions at human telomeres", *Cell*, vol. 119, no. 3, pp. 355-368.

- Wang, S., Wang, M., Yin, S., Fu, G., Li, C., Chen, R., Li, A., Zhou, J., Zhang, Z. & Liu, Q. 2008, "A novel variable number of tandem repeats (VNTR) polymorphism containing Sp1 binding elements in the promoter of XRCC5 is a risk factor for human bladder cancer", *Mutation Research/Fundamental and Molecular Mechanisms of Mutagenesis*, vol. 638, no. 1-2, pp. 26-36.
- Watson, J.D. & CRICK, F.H. 1952, "Molecular structure of nucleic acids; a structure for deoxyribose nucleic acid.", *Nature*, vol. 171, pp. 737-738.
- Watson, J. D. 1972. "Origin of concatemeric T7 DNA." *Nat New Biol* vol. 239(94), pp.197-201
- Wei, K., Clark, A.B., Wong, E., Kane, M.F., Mazur, D.J., Parris, T., Kolas, N.K., Russell, R., Hou, H., Jr, Kneitz, B., Yang, G., Kunkel, T.A., Kolodner, R.D., Cohen, P.E. & Edelman, W. 2003, "Inactivation of Exonuclease 1 in mice results in DNA mismatch repair defects, increased cancer susceptibility, and male and female sterility", *Genes & development*, vol. 17, no. 5, pp. 603-614.
- Weiner, A.M., Deininger, P.L. & Efstratiadis, A. 1986, "Nonviral retroposons: genes, pseudogenes, and transposable elements generated by the reverse flow of genetic information", *Annual Review of Biochemistry*, vol. 55, pp. 631-661.
- Wei-Qin Jiang, Ze-Huai Zhong, Jeremy D. Henson, Axel A. Neumann, Andy C.-M. Chang & Roger R. Reddel 2005, "Suppression of Alternative Lengthening of Telomeres by SP100-mediated sequestration of the MRE11/RAD50/NBS1 complex", *Mol. Cell Bio.*, vol. 25, pp. 2708-2721.
- Weisenberger, D.J., Velicescu, M., Cheng, J.C., Gonzales, F.A., Liang, G. & Jones, P.A. 2004, "Role of the DNA methyltransferase variant DNMT3b3 in DNA methylation", *Molecular cancer research : MCR*, vol. 2, no. 1, pp. 62-72.
- Wellinger RJ, FAU - Wolf, A.J., Wolf AJ, FAU - Zakian, V.A. & Zakian VA "Origin activation and formation of single-strand TG1-3 tails occur sequentially in late S phase on a yeast linear plasmid.", - *Mol Cell Biol*.1993 Jul;13(7):4057-65., , no. 0270-7306 (Print).
- Wilhelm Palm, Titia de Lange 2008, "How Shelterin Protects Mammalian Telomeres", *Annual Review of Genetics*, vol. 42, pp. 301-334--334.
- Wiltzius, J.J., Hohl, M., Fleming, J.C. & Petrini, J.H. 2005, "The Rad50 hook domain is a critical determinant of Mre11 complex functions", *Nature structural & molecular biology*, vol. 12, no. 5, pp. 403-407.
- Wiren, M., Silverstein, R.A., Sinha, I., Walfridsson, J., Lee, H.-., Laurenson, P., Pillus, L., Robyr, D., Grunstein, M. & Ekwall, K. 2005, "Genomewide analysis of nucleosome density histone acetylation and HDAC function in fission yeast", *EMBO Journal*, vol. 24, no. 16, pp. 2906-2918.
- Wong Z, Wilson V, Patel I, Povey S & Jeffreys AJ. 1987, "Characterization of a panel of highly variable minisatellites cloned from human DNA.", *Ann Hum Genet*, vol. 51, pp. 269-288.
- Wong, Z., Wilson, V., Jeffreys, A.J. & Thein, S.L. 1986, "Cloning a selected fragment from a human DNA 'fingerprint': isolation of an extremely polymorphic minisatellite", *Nucleic acids research*, vol. 14, no. 11, pp. 4605-4616.
- Wright, W.E. & Shay, J.W. 2005, "Telomere biology in aging and cancer", *Journal of the American Geriatrics Society*, vol. 53, no. 9, pp. S292-S294.
- Wu G, FAU - Lee, W.H., Lee WH, FAU - Chen, P.L. & Chen PL "NBS1 and TRF1 colocalize at promyelocytic leukemia bodies during late S/G2 phases in immortalized telomerase-negative cells. Implication of NBS1 in alternative lengthening of telomeres.", - *J Biol Chem*.2000 Sep 29;275(39):30618-22., , no. 0021-9258 (Print).

- Wu, C., Chung, A.E. & McDonald, J.A. 1995, "A novel role for alpha 3 beta 1 integrins in extracellular matrix assembly", *J Cell Sci*, vol. 108 (Pt 6), pp. 2511-2523.
- Wu, G., Jiang, X., Lee, W.-. & Chen, P.-. 2003, "Assembly of functional ALT-associated promyelocytic leukemia bodies requires nijmegen breakage syndrome 1", *Cancer research*, vol. 63, no. 10, pp. 2589-2595.
- Wu, L. & Levine, A.J. 1997, "Differential regulation of the p21/WAF-1 and mdm2 genes after high-dose UV irradiation: p53-dependent and p53-independent regulation of the mdm2 gene", *Molecular medicine (Cambridge, Mass.)*, vol. 3, no. 7, pp. 441-451.
- Wu, M.Y., Eldin, K.W. & Beaudet, A.L. 2008, "Identification of chromatin remodeling genes Arid4a and Arid4b as leukemia suppressor genes", *Journal of the National Cancer Institute*, vol. 100, no. 17, pp. 1247-1259.
- Wyman, A.R. & White, R. 1980, "A highly polymorphic locus in human DNA.", *Proceedings of the National Academy of Sciences of the United States of America*, vol. 77, pp. 6754--6758.
- Xu D, FAU - Dwyer, J., Dwyer J, FAU - Li, H., Li H, FAU - Duan, W., Duan W, FAU - Liu, J. & Liu JP "Ets2 maintains hTERT gene expression and breast cancer cell proliferation by interacting with c-Myc.", - *J Biol Chem*.2008 Aug 29;283(35):23567-80.Epub 2008 Jun
- Yamamoto, T., Tamaki, K., Kojima, T., Uchihi, R., Katsumata, Y. & Jeffreys, A.J. 1994, "DNA typing of the D1S8 (MS32) locus by rapid detection minisatellite variant repeat (MVR) mapping using polymerase chain reaction (PCR) assay", *Forensic science international*, vol. 66, no. 1, pp. 69-75.
- Yandava, C.N., Gastier, J.M., Pulido, J.C., Brody, T., Sheffield, V., Murray, J., Buetow, K. & Duyk, G.M. 1997, "Characterization of Alu repeats that are associated with trinucleotide and tetranucleotide repeat microsatellites", *Genome research*, vol. 7, no. 7, pp. 716-724.
- Yang, M.H., Chiang, W.C., Chou, T.Y., Chang, S.Y., Chen, P.M., Teng, S.C. & Wu, K.J. 2006, "Increased NBS1 expression is a marker of aggressive head and neck cancer and overexpression of NBS1 contributes to transformation", *Clinical Cancer Research*, vol. 12, no. 2, pp. 507-515.
- Yeager, T.R., Neumann, A.A., Englezou, A., Huschtscha, L.I., Noble, J.R. & Reddel, R.R. 1999, "Telomerase-negative immortalized human cells contain a novel type of promyelocytic leukemia (PML) body", *Cancer research*, vol. 59, no. 17, pp. 4175-4179.
- Yehezkel S, FAU - Segev, Y., Segev Y, FAU - Viegas-Pequignot, E., Viegas-Pequignot E, FAU - Skorecki, K., Skorecki K, FAU - Selig, S. & Selig S "Hypomethylation of subtelomeric regions in ICF syndrome is associated with abnormally short telomeres and enhanced transcription from telomeric regions.", - *Hum Mol Genet*.2008 Sep 15;17(18):2776-89.Epub 2008 Jun 16., , no. 1460-2083 (Electronic).
- Yi, X.Y., Wayner, E.A., Kim, Y. & Fish, A.J. 1998, "Adhesion of cultured human kidney mesangial cells to native entactin: role of integrin receptors", *Cell Adhes Commun*, vol. 5, pp. 237-248.
- Yu, S., Mangelsdorf, M., Hewett, D., Hobson, L., Baker, E., Eyre, H.J., Lapsys, N., Le Paslier, D., Doggett, N.A., Sutherland, G.R. & Richards, R.I. 1997, "Human chromosomal fragile site FRA16B is an amplified AT-rich minisatellite repeat", *Cell*, vol. 88, no. 3, pp. 367-374.

- Yuan, J., Takahashi, A., Masumori, N., Itoh, N. & Tsukamoto, T. 2006, "Peroxisome proliferator-activated receptor gamma is frequently underexpressed in renal cell carcinoma", *Int J Urol*, vol. 13, pp. 265-270.
- Zaffaroni, N., Villa, R., Pastorino, U., Cirincione, R., Incarbone, M., Alloisio, M., Curto, M., Pilotti, S. & Daidone, M.G. 2005, "Lack of telomerase activity in lung carcinoids is dependent on human telomerase reverse transcriptase transcription and alternative splicing and is associated with long telomeres", *Clinical cancer research : an official journal of the American Association for Cancer Research*, vol. 11, no. 8, pp. 2832-2839.
- Zahler AM, FAU - Williamson, J.R., Williamson JR, FAU - Cech, T.R., Cech TR, FAU - Prescott, D.M. & Prescott DM "Inhibition of telomerase by G-quartet DNA structures.", - *Nature.1991 Apr 25;350(6320):718-20.*, , no. 0028-0836 (Print).
- Zakian, V.A. 1995, "Telomeres: beginning to understand the end. [Review] [147 refs]", *Science*, vol. 270, no. 5242, pp. 1601-1607.
- Zaug AJ, FAU - Podell, E.R., Podell ER, FAU - Cech, T.R. & Cech TR "Human POT1 disrupts telomeric G-quadruplexes allowing telomerase extension in vitro.", - *Proc Natl Acad Sci U S A.2005 Aug 2;102(31):10864-9.Epub 2005 Jul 25.*, , no. 0027-8424 (Print).
- Zellinger, B., Akimcheva, S., Puizina, J., Schirato, M. & Riha, K. 2007, "Ku Suppresses Formation of Telomeric Circles and Alternative Telomere Lengthening in Arabidopsis", *Molecular cell*, vol. 27, no. 1, pp. 163-169.
- Zeng, S. & Yang, Q. 2009, "The MUS81 endonuclease is essential for telomerase negative cell proliferation", *Cell cycle (Georgetown, Tex.)*, vol. 8, no. 14, pp. 2157-2160.
- Zhao Y, FAU - Wang, S., Wang S, FAU - Popova, E.Y., Popova EY, FAU - Grigoryev, S.A., Grigoryev SA, FAU - Zhu, J. & Zhu J "Rearrangement of upstream sequences of the hTERT gene during cellular immortalization.", - *Genes Chromosomes Cancer.2009 Nov;48(11):963-74.*, , no. 1098-2264 (Electronic).
- Zheng, L., Huifang, D., Zhou, M., Li, M., Singh, P., Qiu, J., Tsark, W., Huang, Q., Kernstine, K., Zhang, X., Lin, D. & Shen, B. 2007, "Fen1 mutations result in autoimmunity, chronic inflammation and cancers", *Nature Medicine*, vol. 13, pp. 812 - 819-- 819.
- Zheng, L., Zhou, M., Chai, Q., Parrish, J., Xue, D., Patrick, S.M., Turchi, J.J., Yannone, S.M., Chen, D. & Shen, B. 2005, "Novel function of the flap endonuclease 1 complex in processing stalled DNA replication forks", *EMBO reports*, vol. 6, pp. 83-89--89.
- Zhu J, FAU - Wang, H., Wang H, FAU - Bishop, J.M., Bishop JM, FAU - Blackburn, E.H. & Blackburn EH "Telomerase extends the lifespan of virus-transformed human cells without net telomere lengthening.", - *Proc Natl Acad Sci U S A.1999 Mar 30;96(7):3723-8.*, , no. 0027-8424 (Print).
- Zhu, X.D., Kuster, B., Mann, M., Petrini, J.H. & de Lange, T. 2000, "Cell-cycle-regulated association of RAD50/MRE11/NBS1 with TRF2 and human telomeres", *Nature genetics*, vol. 25, no. 3, pp. 347-352.
- Zhu, X.D., Niedernhofer, L., Kuster, B., Mann, M., Hoeijmakers, J.H. & de Lange, T. 2003, "ERCC1/XPF removes the 3' overhang from uncapped telomeres and represses formation of telomeric DNA-containing double minute chromosomes", *Molecular cell*, vol. 12, no. 6, pp. 1489-1498.